TECHNISCHE UNIVERSITÄT MÜNCHEN
Fakultät für Chemie
Lehrstuhl für Bauchemie

Investigations on the very first nucleation and growth of early cement hydrate phases

Markus Philipp Schönlein

Vollständiger Abdruck der von der Fakultät für Chemie der Technischen Universität München zur Erlangung des akademischen Grades eines

Doktors der Naturwissenschaften (Dr. rer. nat.)

genehmigten Dissertation.

Vorsitzender:	Univ.-Prof. Dr. Klaus Köhler
Prüfer der Dissertation:	1. Univ.-Prof. Dr. Johann P. Plank
	2. apl. Prof. Dr. Anton Lerf

Die Dissertation wurde am 16.05.2019 bei der Technischen Universität München eingereicht und durch die Fakultät für Chemie am 11.07.2019 angenommen.

TECHNISCHE UNIVERSITÄT MÜNCHEN
Fakultät für Chemie
Lehrstuhl für Bauchemie

Investigations on the very first nucleation and growth of early cement hydrate phases

Markus Philipp Schönlein

Vollständiger Abdruck der von der Fakultät für Chemie der Technischen Universität München zur Erlangung des akademischen Grades eines

Doktors der Naturwissenschaften (Dr. rer. nat.)

genehmigten Dissertation.

Vorsitzender:	Univ.-Prof. Dr. Klaus Köhler
Prüfer der Dissertation:	1. Univ.-Prof. Dr. Johann P. Plank
	2. apl. Prof. Dr. Anton Lerf

Die Dissertation wurde am 16.05.2019 bei der Technischen Universität München eingereicht und durch die Fakultät für Chemie am 11.07.2019 angenommen.

Acknowledgments

First and foremost I would like to express my deep gratitude to my academic teacher and supervisor **Prof. Dr. Johann Peter Plank** for admitting me to the Chair for Construction Chemistry and providing this challenging and highly interesting research subject, his continuous support, the many interesting discussions and consultations that contributed to the success of my PhD project, but also for enabling me to present at international conferences and to participate on two parabolic flight campaigns and being given the rare opportunity to experience the state of zero gravity.

My great appreciation also goes to Deutsches Zentrum für Luft- und Raumfahrt (DLR) for financing our parabolic flight experiments. I would like to thank especially Dr. Ulrike Friedrich and Dr. Rainer Forke for their support. In this regard, many thanks go to the whole team of Novespace, France, especially to Frédéric Gai, Nicolas Courtioux and Anne-Clotilde Duchesne for the friendly atmosphere during our stays in Bordeaux, as well as for their support and guidance during the parabolic flight campaigns.

I would like to express further my gratitude to Dr. Markus Meier for his introduction into the organization of parabolic flight campaigns and the experimental procedure under microgravity and for his company on the long road trips to Bordeaux, where the campaigns took place. Furthermore, I want to thank Dr. Lei Lei for her advice and support which contributed significantly to the success of the parabolic flight campaigns.

Similar gratitude goes to Dr. Sevil Weinkauf and her team and Dr. Oksana Storcheva for their support with TEM measurements and MAS-NMR measurements.

Very special thanks I want to address also to Dr. Nan Zou who introduced me into the LDH-chemistry and to Dr. Vipasri Kanchanason for the many interesting discussions on C-S-H formation.

A special thanks goes to the colleagues of my laboratory Mouala Moumin, Stefanie Gruber, Dr. Julia Pickelmann, Huiqun Li, Claudia Chomyn, Nicolas Ewert and Johannes Paas for all the scientific discussions and non-scientific conversations, the collegiality and the great working atmosphere.

Moreover, I want to thank all my current and former colleagues at the Chair of Construction Chemistry, namely, Dr. Tobias Kornprobst, Dr. Stefan Baueregger, Dr. Alex Lange, Dr. Thomas Hurnaus, Dr. Johanna de Reese, Dr. Salami Taye Oyewoli, Dr. Constantin Tiemeyer, Dr. Ahmad Habbaba, Manuel Ilg, Timon Echt, Thomas Pavlitschek, Somruedee Klaithong, Johannes Stecher, My Linh Vo, Maike Müller and Michael Spörl.

My thanks go also to the non-scientific colleagues at the chair, especially to our secretaries Anke Kloiber and Jingnu Liu for their support in all administrative and organisational topics and Dagmar Lettrich for her support in chemical analysis and experiments.

Last but not least, a very big thank you to my parents Hans and Veronika for the possibility of this education, their continuous unrestricted support during my studies, for their backup in all my decisions and their great motivation and encouragement at any time!

List of articles

This thesis is based on the three published scientific research papers:

Journal Articles with Peer-Review:

1) Schönlein M., Plank J.
   Influence of PCE kind and dosage on ettringite crystallization performed under terrestrial and microgravity conditions
   Journal of the American Ceramic Society, 101, 2018, 8, 3575 - 3584

2) Schönlein M., Plank J.
   A TEM study on the very early crystallization of C-S-H in the presence of polycarboxylate superplasticizers: Transformation from initial C-S-H globules to nanofoils
   Cement and Concrete Research 106, 2018, 33 – 39

3) Plank J., Schönlein M., Kanchanason V.
   Study on the early crystallization of calcium silicate hydrate (C-S-H) in the presence of polycarboxylate superplasticizers
   Journal of Organometallic Chemistry 869, 2018, 227 - 232

Further conference contributions without Peer-Review:

4) Plank J., Schönlein M., Meier M. R., Lei L.
   Cement hydration under microgravity conditions on parabolic flights
   2nd International Conference on the Chemistry of Construction Materials (ICCCM), Munich (Germany), October 10-12, 2016, GDCh-Monographie 50, 137-140.

5) Plank J., Spörl M., Schönlein M.
   Untersuchungen zur Umwandlung von globulärem in folienartiges C-S-H während der Frühphase der C-S-H-Nukleation
   Tagung der GDCh-Fachgruppe Bauchemie, September 18-20, Weimar (Germany), GDCh-Monographie 52, 2017, 84-87.

6) Plank J., Schönlein M.

Study on the early crystallization of C-S-H in the presence of polycarboxylate superplasticizers

2nd International Conference on Polycarboxylate Superplasticizers (PCE 2017), Garching (Germany), September 27 – 28, 2017, Conference proceedings, p. 271 – 278

List of Abbreviations

0 *g*	Zero gravity
1 *g*	Terrestrial gravity
a	Acceleration
A	*Arrhenius* constant (pre-exponential factor)
Å	Ångström (1 Å = 10^{-10} m)
AA	Acrylic acid
AFS	Acetone-formaldehyde-sulfite polycondensate
AMPS	2-acrylamido-2-methylpropane sulfonic acid
APEG	α-allyl-ω-methoxypoly(ethyleneglycol)
BNS	Sulfonated *β*-naphthalene formaldehyde polycondensate
bwoc	By weight of cement
c	Concentration
cm	Centimeter
Δ	Delta (difference)
DLR	Deutsches Zentrum für Luft- und Raumfahrt e.V.
DP	Degree of polymerization
EO	Ethylene oxide
ESEM	Environmental Scanning Electron Microscope
DLS	Dynamic light scattering
G	*F*ree Enthalpy
G_1	Volume energy
G_2	Surface energy
g	Gravitational acceleration
g	Gram
GPC	Gel permeation chromatography
H	Enthalpy
HEMAP	2-(methacryloyloxy)ethylphosphate
IA	Itaconic acid
IPEG	Isoprenyl polyethylenglycol ether
ISS	International Space Station

J	Rate of nucleation
kB	*Boltzmann*'s constant
L	Litre
LDH	Layered double hydroxide
m	Meter
m	Mass
MAA	Methacrylic acid
MAS NMR	Magic-angle spinning nuclear magnetic resonance
MCL	Mean chain length
MFS	Melamine formaldehyde sulfite polycondensate
µ g	Microgravity
µeq/g	Measure for the charge density per 1 g polymer
mL	Milliliter
μ	chemical potential
$\Delta\mu$	Supersaturation
µm	Micrometer
mm	Millimeter
M_n	Number average molecular weight
MPEG	Methoxy poly(ethyleneglycol)
M_w	Weight average molecular weight
nm	Nanometer
OPC	Ordinary Portland Cement
PCE	Polycarboxylate ether
PDI	Polydispersity index
r	Radius
r*	Critical radius for nucleation
rpm	Rounds per minute
SEM	Scanning electron microscope
σ	Specific surface energy
s	Second
SCPS	Synthetic cement pore solution
θ	Diffraction angle

TEM	Transmission electron microscope
TG-MS	Thermogravimetry coupled with a mass spectrometer
TGA	Thermogravimetric analysis
TOC	Total organic carbon
UHPC	Ultra high performance concrete
V	Volume
V_m	Molecular volume
wt.	Weight
w/c ratio	Water-to-cement ratio (per weight)
w/s ratio	Water-to-solid ratio (per weight)
XRD	X-Ray diffraction

Cement chemistry notation

Notation	Chemical formula	Mineral name
C	CaO	Calcium oxide
S	SiO_2	Silicon dioxide
A	Al_2O_3	Aluminium oxide
F	Fe_2O_3	Iron oxide
H	H_2O	Water
$\bar{S}$	SO_3	Sulfur trioxide
C_3S	$Ca_3(SiO_4)O$	Tricalcium oxy silicate
C_2S	$Ca_2(SiO_4)$	Dicalcium silicate
C_3A	$Ca_9(Al_6O_{18})$	Tricalcium aluminate
C_4AF	$Ca_4Al_2Fe_2O_{10}$	Tetracalcium alumino ferrite
$C\bar{S}$	$CaSO_4$	Calcium sulfate
$C_3A \cdot 3C\bar{S} \cdot H_{32}/AF_t$	$[Ca_3Al(OH)_6]_2(SO_4)_3 \cdot 26\ H_2O$	Ettringite
$C_3(A,F) \cdot 3C\bar{S} \cdot H_{32}/AF_t$	$[Ca_3(Al,Fe)(OH)_6]_2(SO_4)_3 \cdot 26\ H_2O$	Iron ettringite
$C_3A \cdot C\bar{S} \cdot H_{12}/AF_m$	$[Ca_2Al(OH)_6](SO_4)_{0.5} \cdot 9\ H_2O$	Monosulfate
C_4AH_x/AF_m	$[Ca_2Al(OH)_6](OH) \cdot x\ H_2O$	Monocalcium aluminate hydrate
$C_3A \cdot CaCl_2 \cdot H_{12}/AF_m$	$[Ca_2Al(OH)_6]Cl \cdot 2\ H_2O$	Friedel's Salt
C_3AH_6	$Ca_3Al_2[(OH)_4]_3$	Hydrogarnet
C-S-H	$Ca_5[Si_6O_{18}H_2] \cdot 8\ H_2O$	Tobermorite (1.4 nm)
	$Ca_9[Si_6O_{18}H_2(OH)_8] \cdot 6\ H_2O$	Jennite (1.05 nm)
CH	$Ca(OH)_2$	Calcium hydroxide / Portlandite

Table of contents

1. Introduction

Since the year 2014, cement production overtook crude oil and is since then the main industrial product of the world with an annual production volume of 4.1 bn. tons (2017).[1] Although its invention goes back more than 2000 years ago, it is still the subject of intensive research. The reaction of cement with water, the so-called hydration, is a complex process of dissolution, precipitation, crystallization and surface-reactions of the various clinker phases. These clinkers consist of different silicates and aluminates which upon the addition of the mixing water result in a saturated solution of mainly calcium hydroxide, silicate and aluminate. From this solution, the cement hydrates precipitate and grow to a dense matrix exhibiting high compressive strength. The first hydrates form within seconds after addition of water and have only a size of several nanometers. The focus of this work is the study of the formation of these early hydrate phases.

While Ordinary Portland Cement (OPC), also defined as CEM I, presented for a very long time the only hydraulic binder used in mortar and concrete mixtures, many new classes of cement were established over the last years to reduce CO_2 emission during production. Nowadays, CEM II, a composite material of CEM I and up to 35% of ground granulated blast furnace slag, fly ash, limestone or pozzolanes, respectively, is the most widely used binder. Nonetheless, OPC still presents the most reactive hydraulic binder of the established cements and is responsible for the early strength development of mortars and concrete made of OPC blends.

A high early strength is of great industrial importance, because it decides when in a precast concrete plant a concrete slab for example can be demoulded and is ready for loading. This determines the time when the next working cycle in the construction process can be started. Currently, 28 days is regulated as the minimum curing time for most concretes. At low temperatures, this curing time is even more extended. An accelerated strength development is thus very beneficial as it saves a lot of labour costs and would allow a faster building process. Increased final strength of concrete provides also the possibility to cast new structural elements and meet thus the demands of modern architecture (see for example the Marina Bay Sands Hotel in **Figure 1**).

The strength of concrete is strongly depending on its porosity and thus on the microstructure of the hardened cement matrix. Reducing the water-to-cement ratio is one of the main measures to reduce porosity of mortars and concretes. This lever is applied in the case of ultra-high performance concretes which gained much popularity within the last years. But with less water present, the viscosity of concrete slurries increases significantly which reduces the workability tremendously. Especially for high-rise buildings and in oil well cementing, long pumping times are inevitable. There, adjustment of the desired rheology and maintaining it over the whole working time are key features in the application, as proper placing of the concrete plays a decisive role for its durability.

Figure 1: Marina Bay Sands Hotel in Singapore as an example for modern construction.[2]

Therefore, admixtures are used in almost every concrete formulation nowadays, particularly dispersing agents and retarders are very important to tailor the workability of the formulation for the application as needed. As dispersing agents, polycondensates and polycarboxylate ethers (PCEs) are very commonly used. Both types of polymers consist of a backbone possessing functional groups exhibiting anionic charges like from sulphites or carboxylic groups. Thus, they can adsorb onto the positively charged surfaces of cement clinkers and hydrates, hinder agglomeration of the particles and thus maintain the workability of concrete

slurries. C_3A presents the most reactive clinker phase in OPC and produces the first hydrates, namely ettringite and monosulfate. Therefore, the interaction of these minerals with the various kinds of admixtures is the key to tailor workability.

But the aluminates in the clinker present only a minor part of OPC compared to the silicates C_3S and C_2S. Their main hydration product is called calcium silicate hydrate, short C-S-H. It determines the microstructure of hardened cement and is thus mainly responsible for the strength development of cement. However, its structure and composition are still the focus of many investigations. C-S-H can exhibit different morphologies from an amorphous gel consisting of many disordered C-S-H foils to long fibres possessing a high degree of crystallinity, depending on the Ca/Si ratio, the content of silicate and the distribution of Ca-OH and Si-OH.[3] C-S-H is of special interest, as it is believed to be the primary binding phase in the cement matrix, keeping all other hydrates together as a whole.[4] To further improve the strength development of C-S-H and thus of cement, it is of fundamental importance to get more insight into the evolvement of its structure, especially in the presence of the above mentioned cement admixtures.

The nature of a material, whether it is crystalline or amorphous, is generally determined by the reaction conditions during its nucleation process and the following early crystallization. Nucleation occurs when a certain supersaturation of ions is given. Then, nuclei can form and grow. If a nucleus reaches a critical size where the volume energy is higher than the surface energy, it is stable. Further growth is then determined by the transportation of ions to the surface of the nucleus. In the presence of polymers, crystal growth can be hindered due to blockage of the surfaces or sequestration of ions or, like in nature, polymers can help to form so-called mesocrystals which are consisting of stable aggregates.[5] These mesocrystals are then assembled by continued attachment to a crystalline structure.

While crystallization experiments under terrestrial gravity conditions often leads to crystals exhibiting more defects, due to the faster mass transport caused by convection, crystallization in the absence of gravity, e.g. on the International Space Station (ISS) or on parabolic flights, was used by some researchers to get more information on defect-free structures and compositions of crystals, because there, generally crystals where shown to exhibit higher purity

and less defects. In the past, the focus of crystallization experiments under microgravity conditions was strongly directed towards proteins. The limited mass transport was used to obtain protein crystals with a more homogeneous size distribution and less defects which resulted in a successful structural analysis of numerous organic molecules which was not possible under terrestrial gravity.[6-7] Crystallization experiments of inorganic salts in microgravity on the other hand were quite scarce so far.

Nonetheless, crystallization experiments under microgravity conditions have proven to be a powerful tool to get more insight into nucleation and crystallization processes and was thus used within this work to study the crystal growth of different cement hydrates and to reveal interactions between cement hydrates and admixtures during early cement hydration. Previous studies by our group have shown that ettringite crystal size and morphology are influenced by the absence of convection, too. There, generally smaller, but more abundant ettringite crystals were found.[8] Synthetic ettringite, precipitated from aqueous solutions of $Ca(NO_3)_2$ and $Al_2(SO_4)_3$ in the presence of PCEs confirmed the findings of the short-term hydration experiments with OPC and further showed that especially the anionicity of the polymers plays a significant role during nucleation and crystal growth of ettringite.[9]

As mentioned before, application of organic admixtures like polymers is getting more and more popular in the construction industry, because it allows tuning of the workability of cementitious slurries. Therefore, it is of great importance to gain more knowledge on the influence of the various kinds of admixtures on the nucleation and crystallization of cement hydrate phases to evaluate their impact on the microstructure of hardened cement and hence on the mechanical properties of concrete. But understanding the interaction between admixtures and cement is not only beneficial for predicting the workability and durability of formulations, it can as well reveal levers to tailor admixtures for different kinds of cements and make them more efficient.

2. Aim and scope of this thesis

To meet the increasing demands regarding workability and mechanical properties, the use of admixtures like e.g. superplasticizers or retarders is inevitable. Although Portland cement is one of the most used industrial products, its interactions with additives during hydration still bears many questions. This work aims to give a better understanding of these interactions.

In a first series of experiments within this research, the hydration of C_3A in the presence of retarders was investigated. Upon hydration, besides ettringite C_3A forms so-called hydrocalumite-type Layered Double Hydroxides (LDHs) which consist of stacked positively charged inorganic sheets. Some organic polymers, e.g. dispersing agents like PCEs and polycondensates, have already been reported to intercalate into the interlayer space and thus lose their dispersing effect.[10-12] However, no literature has so far reported on the intercalation of retarding admixtures during cement hydration and the stability of such inorganic-organic host-guest structures. Here, the intercalation ability of two chemically different retarder molecules based on co-polymers of acrylic acid (AA) and 2-acrylamido-2-methylpropane sulfonic acid (AMPS) and itaconic acid (IA) and AMPS, respectively, into LDHs formed during the hydration of C_3A as well as the stability of the obtained inorganic-organic composite materials was studied. These findings are of great importance as upon intercalation, a loss of the retarding effect of these co-polymers is to be expected and consequently a higher dosage of retarders must be used to obtain a similar retarding effect. Furthermore, if the obtained composite materials possess a low stability, i.e. the polymers are released by anion exchange e.g. with sulfates present in the concrete slurry during the hydration process, they might be used as admixtures themselves to obtain a delayed retarding effect in special applications like oil-well cementing, where long pumping times and consequently extended times of high fluidity are necessary to place the cement.

The scope of the second part of this research is the investigation of the ability of nanoparticles of calcium aluminate hydrates to accelerate cement hydration, especially that of C_3A, as a seeding agent. Calcium chloride is probably the most prominent hardening accelerator, but it was found that the use of chlorides in concrete increases the risk of corrosion of structural reinforcement bars. Thus, the search for a similarly effective alternate admixture is the topic of

many studies.[13-15] Calcium formate, $Ca(HCOO)_2$, for example, is a popular alternative, but its acceleration within the first days is less compared to that of $CaCl_2$. Meanwhile, the approach of using C-S-H nanoparticles as seeding agent for C_3S and C_2S hydration has proven to be very efficient and has moved from laboratory research to industrial application.[16] Although the amount of C_3A in commercial OPC is significantly less than that of silicate clinkers, it possesses higher reactivity and determines the set behaviour of cement. Within this work, calcium aluminate hydrate, namely the AF_m phase C_4AH_x with formate, $HCOO^-$, as anion, was chosen as a potential seeding material for the aluminate clinker hydration. In the literature, all reported attempts for a facile synthesis of the Ca_2Al-formate-LDH via co-precipitation which allows easy industrial upscaling were not successful.[17-19] Because an economic and industrially applicable synthesis route is mandatory for the practical use of a Ca_2Al-formate-LDH, an up-scalable preparation method by co-precipitation was developed. The obtained Ca_2Al-formate-LDH was characterized and the potential as hardening accelerator and its accelerating mechanism was assessed on mortars prepared with different commercial OPC samples.

The third part of this work focuses on the early hydration processes, i.e. the nucleation and crystallization of early hydrate phases, especially of ettringite which is very crucial not only for the workability, but also for the final microstructure of concrete and thus has a great impact on the performance of mortars and concretes. It has been shown in previous studies that PCEs have a high affinity for aluminate hydrates, especially for C_4AH_x and ettringite.[11-12, 20-21] While these studies have rather focused on the adsorbed amount of polymer over very long reaction times of 2 – 24 h, the aim of this study is to investigate the impact on the ettringite nucleation and crystal growth in the first seconds of hydration.

To get a better understanding of the nucleation and crystal growth, short-term hydration of OPC samples was performed in the absence and presence of convection. Different commercial OPC samples as well as OPC admixed with different types of dispersing agents were studied. The influence on ettringite crystal growth and morphology was assessed in dependence of the side chain length, the anionic charge density and dosage of MPEG-based PCE comb polymers. Additionally, different kinds of polycondensates and a polyphosphate comb polymer were admixed to OPC and the ettringite crystals obtained were investigated.

As Portland cement is a very complex binder which contains many different phases, simplified model systems consisting of blends of C_3A and C_4AF, respectively, with 15 % of calcium sulfate hemihydrate and 5 % gypsum were hydrated in synthetic cement pore solution to gain more insight into the different reactivities of the two aluminate clinkers with respect to ettringite formation. Besides the crystallization of ettringite, the impact of the absence and presence of gravity on the nucleation and crystal growth of AF_m phases was of special interest in this work. In the case of sulfate depletion during OPC hydration, the formation of the AF_m phase monosulfate (also referred to as monosulfo aluminate), $[Ca_2Al(OH)_6](SO_4)_{0.5} \cdot 9\ H_2O$, is thermodynamically favoured. The crystallization of monosulfate was studied under both gravity conditions by hydration of neat C_3A clinker with a saturated calcium sulfate hemihydrate solution. When no sulfate ions are present anymore in the cement pore solution, formation of C_4AH_x takes place, another AF_m phase, having OH^- as counterbalancing anions in the interlayer space instead of SO_4^{2-}. Synthesis was performed by hydration of the neat C_3A phase in a saturated $Ca(OH)_2$ solution. The obtained hydrate phases were studied by XRD analysis and SEM imaging regarding their morphology and the amount formed.

The last part of this research was dedicated to give more insight into the nucleation and crystal growth of C-S-H. Here, the structure and composition of synthetic C-S-H obtained by flash precipitation of aqueous solutions of $Ca(NO_3)_2$ and Na_2SiO_3 in the absence and presence of PCE was studied. At first, the influence of the pH value on C-S-H size and morphology in the absence and presence of convection was studied via TEM imaging and dynamic light scattering. During this study it was found that the type of PCE seems to alter the formation of C-S-H and - most surprisingly - a globular morphology instead of the well-known foils was obtained. Thus, the interactions between C-S-H globules and chemically different types of PCEs, namely IPEG-, MPEG- and APEG-PCEs, were investigated more thoroughly, especially regarding the nanostructure of the C-S-H-PCE composites formed. Based on these findings, a mechanism for the very early interaction between precipitated C-S-H and PCE superplasticizers is proposed. Finally, nucleation and crystal growth of synthetic C-S-H in the absence and presence of two MPEG-PCEs possessing low and high anionic charge beyond the first seconds were studied by TEM imaging, ^{29}Si MAS NMR spectroscopy and heat flow calorimetry.

3. Theoretical background and state of the art

3.1. Portland cement composition and hydration

Portland cement clinker presents a mixture of phases and generally consists of four main clinker phases, namely alite (C_3S), belite (C_2S), tricalcium aluminate (C_3A) and calcium aluminoferrite (C_4AF). It is obtained by calcination of a raw mix which contains mainly limestone ($CaCO_3$) as CaO source and clays and marl as silicate and aluminate sources in a rotating cement kiln at approximately 1450°C, where the raw materials are converted into calcium oxide CaO, silicon dioxide (silica) SiO_2, aluminum oxide (alumina) Al_2O_3 and iron oxide Fe_2O_3. Finally, sulfate carriers, e.g. gypsum, hemihydrate or anhydrite are added to control the hydration of the highly reactive tricalcium aluminate clinker.[22]

The reaction of cement with water is called hydration. It is a complex process of many different chemical reactions that take place in parallel and successively. Hydration of cement can already occur in humid air, but for complete hydration of the cement, sufficient amounts of water must be added. The water/cement ratio (w/c ratio) affects the rheology of the paste, the progress of hydration and finally the properties of the hardened hydrated cement. Immediately after mixing with water, the suspension exhibits a paste consistency and is called “fresh cement paste”. As hydration progresses, the cement paste “sets”, meaning that it suddenly loses its original plasticity and transforms to a solid material with barely measurable strength. Subsequently, hydration continues and a dense cement matrix forms based on intergrowing hydrate phases. This part of hydration is called “hardening”, because the compressive strength of the cement matrix now is measurable and increases over time with decreasing porosity, i.e. with progressing hydrate formation.[23]

The main hydration products are calcium silicate hydrate (C-S-H), portlandite ($Ca(OH)_2$), tricalciumaluminate (ferrite) hydrate (mineralogically called ettringite), a so-called “AF_t phase”, and monocalciumaluminates (AF_m), e.g. C_4AH_x or $C_4A\bar{S}H_{12}$.

The hydration mechanism can be divided into the following stages:[22-24]

- Pre-induction period
- Induction (Dormant) period
- Acceleration period
- Post-acceleration or Deceleration period
- Final hydration (Diffusion) period

In the following, the single stages of the hydration of Portland cement are elaborated in more detail:

Pre-induction period

Upon addition of water, the clinker phases, mainly C_3A and C_3S, and sulfates immediately start to dissolve and supply the liquid phase rapidly with ions like e.g. Ca^{2+}, SO_4^{2-}, $Al(OH)_4^-$. Alkali sulfates present in Portland cement completely dissolve during this period, while calcium sulfate only dissolves until the liquid phase is saturated. This initial dissolution can be detected via heat flow calorimetry by a first heat release. Tricalcium silicate dissolution soon stops due to precipitation of an amorphous C-S-H-gel which forms a low permeable layer on the surface of the C_3S phases and impedes further dissolution. The fraction of hydrated C_3S in the pre-induction period is about 2 – 10 per cent. The C_2S phase stays almost inert during the initial hydration. In contrast, the calcium aluminates have a turnover between 5 and 25 per cent and lead to precipitation of ettringite crystals, the AF_t phase, on the surface of cement.[23-24]

Induction period

During the induction period the rate of hydration slows down (and hence the released heat decreases), because of the fast precipitation of hydrate phases on the clinker surfaces which prevents further dissolution. The concentration of $Ca(OH)_2$ in the liquid phase at this point reaches its maximum and declines subsequently. The SO_4^{2-} ions consumed by ettringite formation are immediately replaced by further dissolution of calcium sulfate and thus the concentration is kept nearly constant.[22-23]

Acceleration period

The acceleration period starts when the low permeable layers covering the clinker surfaces are decomposed or broken up by osmosis.[22] During this period, the heat generated by cement hydration reaches is maximum. Hydration of calcium silicates, C_3S and C_2S, accelerates and the formation of a "second-stage" C-S-H occurs.[24] The reactivity of the C_3S phase is still dominant over that of the C_2S. Besides C-S-H, also a noticeable amount of crystalline portlandite, $Ca(OH)_2$, precipitates. Calcium sulfate dissolves completely and ettringite is formed until the SO_4^{2-} concentration starts to decrease.[22-23]

Post-acceleration period

The post-acceleration period is marked by a decrease in heat release due to decelerating hydration as the amount of non-reacted clinker phases declines. The silicate hydration still continues and the contribution of C_2S to the formation of C-S-H increases with time. The decreasing SO_4^{2-} ion concentration in the pore solution leads to a recrystallization of formed ettringite together with unreacted C_3A and C_4AF to form monosulfate.[23]

Final hydration period

During the first periods, cement hydration is dominated by fast surface reactions. In the final hydration period, all ongoing hydration reactions are diffusion-controlled due to the already dense cement hydrate layers on the surface of the cement particles and come slowly to an end. After the hydration process has been completed, ageing of the formed hydrates may take place. This is characterized by polycondensation of SiO_4 tetrahedra leading to an increase in the average chain length of C-S-H phases.[24]

Figures 2 and **3** show the consumption of the various clinker phases and the corresponding formation of hydrate phases as described above:

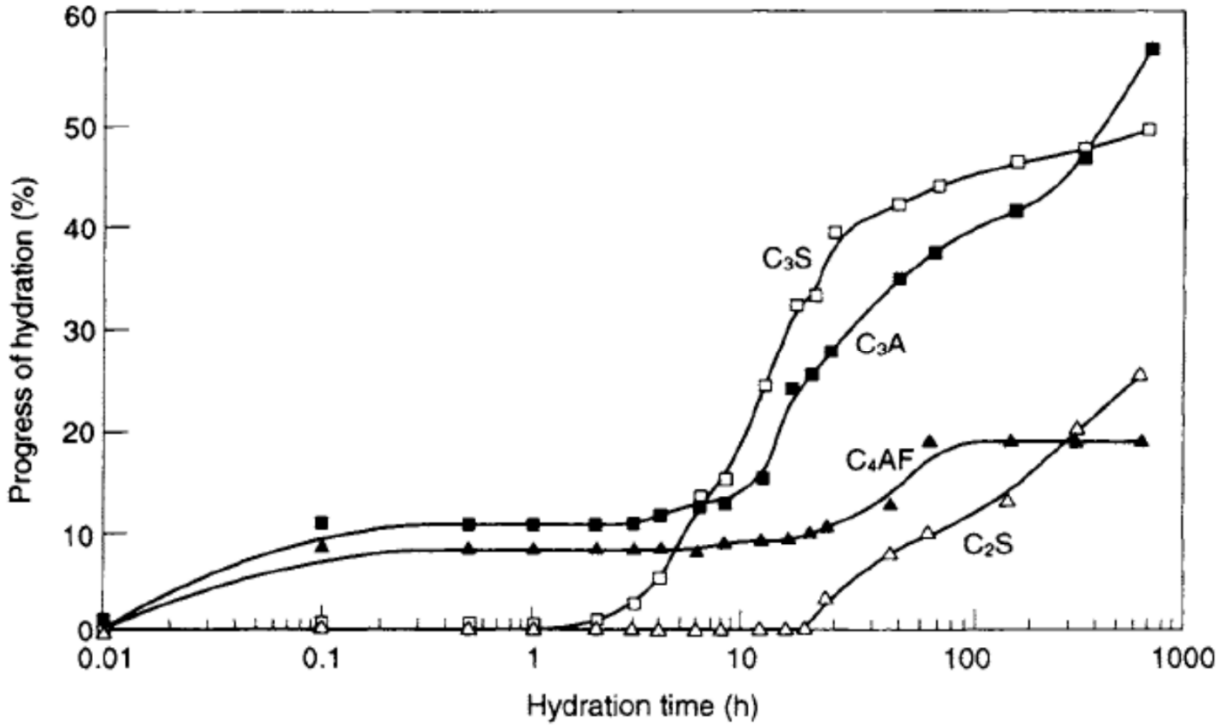

Figure 2: Consumption of clinker phases during hydration of an ordinary Portland cement.[23]

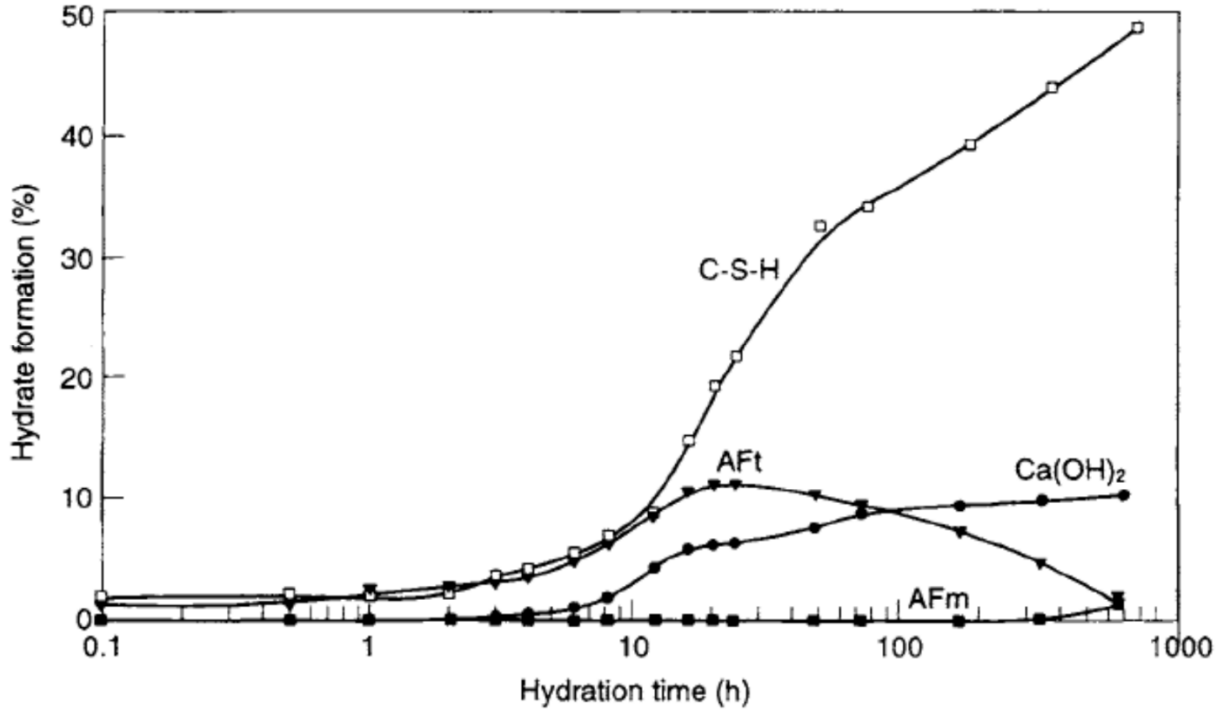

Figure 3: Formation of cement hydrate phases during hydration of an ordinary Portland cement.[23]

The reaction kinetics of the hydration differ depending on the cement constituents and with time. In the following, the main reactions of the various phases are described in more detail.

Silicate reactions:

Tricalcium silicate, or chemically more precisely known as tricalcium oxysilicate, is the main constituent of Portland cement and plays a major role in the setting and hardening of cement. In the following, the knowledge on its hydration as presented in current literature is described. It will be shown later on that experiments performed during this thesis suggest a partial revision of the current model for C_3S hydration. Its hydration can be divided in similar stages as those defined for Portland cement. The hydration reaction of silicates is rather complex and still not fully understood. The resulting amorphous C-S-H gel can be of variable composition, thus for its reaction only a general equation can be provided:[24]

$$3\ CaO \cdot SiO_2 + x\ H_2O \rightarrow \underset{\text{C-S-H phase}}{y\ CaO \cdot SiO_2 \cdot (y-(3-x))\ H_2O} + \underset{\text{Portlandite}}{(3-y)\ Ca(OH)_2} \qquad \text{Equ. 1}$$

Equation 1: Reaction of C_3S with water.[25]

C_3S possesses a very high dissolution rate that exceeds the rate of transportation of dissolved ions away from the clinker surface. This leads to an oversaturation of the cement suspension with regard to C-S-H causing a rapid precipitation of C-S-H gel on the C_3S surface, forming a low permeable layer. Subsequently, the dissolution of C_3S and thus its hydration is slowed down until the layer decomposes. During the acceleration stage, the rate of hydration appears to be mainly controlled by the dissolution rate of non-hydrated C_3S. The ions dissolve into the pore solution and precipitate as C-S-H in the bulk solution. This reaction is accompanied by precipitation of crystalline portlandite. In the following, the hydration rate decreases and becomes diffusion-controlled until it ends due to the consumption of C_3S or in case of low w/c ratios due to a lack of space for C-S-H and CH precipitation.[23]

The C_2S phase reacts similarly to C_3S, but with a significantly extended induction period and generally more slowly. The C-S-H formed exhibits similar morphology to that from the C_3S phase. Thus, only the amount of portlandite formed is less during the hydration of C_2S, compared to that of C_3S.[24]

$$2\ CaO{\cdot}SiO_2 + x\ H_2O \rightarrow y\ CaO{\cdot}SiO_2{\cdot}(y\text{-}(2\text{-}x))H_2O + (2\text{-}y)\ Ca(OH)_2 \qquad \text{Equ. 2}$$

C-S-H phase Portlandite

Equation 2: Reaction of C_2S with water.[25]

Aluminate reactions in the presence of high sulfate concentration:

C_3A constitutes the most reactive clinker phase in the Portland cement system. As mentioned before, sulfate carriers are added to the cement to control the hydration of the aluminate phases. Thus, the hydration products of C_3A and C_4AF are strongly dependent on the amount of sulfates present. In the presence of an excess of SO_4^{2-} ions the main hydration product is ettringite. C_3A hydration starts with a high initial dissolution accompanied by significant liberation of heat followed by a dormant period initiated by a protective layer of ettringite covering the clinker surface.[23, 26]

$$C_3A + 3\ C\bar{S}H_2 + 26\ H \rightarrow C_3A \cdot 3\ C\bar{S} \cdot 32\ H \qquad \text{Equ. 3}$$

Ettringite, AF_t

Equation 3: Reaction of C_3A with gypsum and water.[23]

The composition of C_4AF may vary between $C_2(A_{0.7}, F_{0.3})$ and $C_2(A_{0.3}, F_{0.7})$.[23] Generally, the reactivity of the C_4AF phase is comparable to that of C_3A, but decreases with increasing iron content.[27] A similar reaction to that of C_3A takes place when C_4AF hydrates in the presence of sulfate yielding the so-called iron ettringite and 2 (A,F) · 3 H, a mixture consisting of $Al(OH)_3$ and $Fe(OH)_3$.[24, 28] During early hydration of C_4AF, iron-free ettringite is formed. Only at later stages of hydration, iron ettringite was detected.

$$3\ C_4AF + 12\ C\bar{S}H_2 + 110\ H \rightarrow 4\ [C_3(A,F) \cdot 3\ C\bar{S} \cdot 32] + 2\ [(A,F) \cdot 3\ H] \qquad \text{Equ. 4}$$

Iron ettringite, AF_t

Equation 4: Reaction of C_4AF with gypsum and water.[23, 29]

Over the course of hydration, the SO_4^{2-} concentration in the pore solution decreases and with unreacted aluminate the AF_t phases transform through dissolution and recrystallization into the AF_m phases calcium aluminate monosulfate and calcium aluminate ferrite monosulfate. This

process is accompanied by a second heat maximum and represents the end of the induction period and the beginning of the acceleration stage.[23]

$$2\ C_3A + C_3A \cdot 3\ C\bar{S} \cdot 32\ H + 4\ H_2O \rightarrow C_3A \cdot C\bar{S} \cdot 12\ H \quad \text{Equ. 5}$$

Ettringite, AF_t Monosulfate, AF_m

Equation 5: Reaction of Ettringite and C_3A to monosulfate.[24]

$$3\ C_4AF + 4\ [C_3(A,F) \cdot 3\ C\bar{S} \cdot 32\ H] + 14\ H_2O \rightarrow 6\ [C_3(A,F) \cdot C\bar{S} \cdot 12\ H] + 2\ [(A,F) \cdot 3\ H] \quad \text{Equ. 6}$$

Ettringite, AF_t Monosulfate, AF_m

Equation 6: Reaction of iron ettringite and C_4AF to monosulfate.[24]

Additionally to the transformation of ettringite to monosulfate, a direct reaction of C_3A to monosulfate or C_4AH_x phases may occur.

Aluminate reactions in the presence of low sulfate concentration:

The direct reaction of C_3A or C_4AF to AF_m phases can occur initially because of a low SO_4^{2-} content in the cement, e.g. because of slow dissolution rate of the kind of calcium sulfate, or during the course of hydration when most of the SO_4^{2-} ions have already been consumed by the formation of AF_t phases.

$$C_3A + C\bar{S}H_2 + 10\ H_2O \rightarrow C_3A \cdot C\bar{S} \cdot 12\ H \quad \text{Equ. 7}$$

Monosulfate, „AFm“

Equation 7: Reaction of C_3A with gypsum and water.[23]

Aluminate reactions in the absence of sulfate:

In the absence of sulfate, C_3A reacts instantly to calcium aluminate hydrates exhibiting a hexagonal plate morphology which arrange like a card house and thus bridge the distances between cement grains. This leads to a sudden setting of the cement paste. For the calcium aluminate hydrates of the formula C_4AH_x, different species have been identified comprising different amounts of water, e.g. C_4AH_{13} and C_4AH_{19}.[23-24]

$$2\ C_3A + x\ H_2O \rightarrow C_4AH_x + C_2AH_8 \qquad \text{Equ. 8}$$

Equation 8: Reaction of C_3A with water.

As C_4AH_x and C_2AH_8 present only metastable phases, they convert over time to the thermodynamically stable, cubic mineral hydrogarnet (C_3AH_6).

$$C_4AH_{13} + C_2AH_8 \rightarrow 2\ C_3AH_6 + 9\ H_2O \qquad \text{Equ. 9}$$

Equation 9: Conversion of metastable calcium aluminate hydrates to hydrogarnet.

Usually, during the hydration of Portland cement sufficient Ca^{2+} ions are available in the pore solution, thus C_4AH_x hydrates are formed exclusively while formation of C_2AH_8 is not observed.

Calcium aluminate ferrite hydrates to metastable calcium aluminate ferrite hydrates that subsequently transform over time to iron-containing hydrogarnet.

$$2\ C_4AF + 16\ H \rightarrow C_4(A,F)H_{13} + 2\ C_2(A,F) + (A,F)H_3 \qquad \text{Equ. 10}$$

Equation 10: Reaction of C_4AF with water.

$$2\ C_4(A,F)H_{13} + 2\ C_2(A,F) \rightarrow 4\ C_3(A,F)H_6 + 2\ H \qquad \text{Equ. 11}$$

Equation 11: Conversion of metastable calcium aluminate ferrite to iron-containing hydrogarnet.

3.1.1. Structure and composition of calcium silicate hydrates

Calcium silicate hydrate is not only a promising precursor for biomedical applications in drug delivery and bone tissue engineering, foremost it is the main product in the hydration of ordinary Portland cement. [30-33] C-S-H is formed during the hydration of tricalcium and dicalcium silicate (C_3S and C_2S) and is known to exhibit a Ca/Si ratio in the range from 0.7 to approximately 2.0. Below a Ca/Si ratio of 0.7, amorphous silica will be present and above 1.45 – 1.60, increased amounts of portlandite were found.[34] At the beginning of cement hydration, C_3S dissolves and releases calcium, silicon and hydroxide ions into the water. The dissolution

of C_3S stops when a critical supersaturation with respect to C-S-H is reached and first C-S-H precipitates exhibiting a significantly lower Ca/Si ratio than in C_3S.[35] An earlier study by *Garrault* et al. has shown that C-S-H nucleation occurs mainly heterogeneously and the C_3S clinker is the most favored nucleation site.[36] The calcium silicate hydrates formed during hydration are extremely fine-grained and exhibit a low crystalline order, so they are often also designated as C-S-H gel. The crystal growth of C-S-H is the main driver of the acceleration period during cement hydration. Two distinct growth modes have been found for C-S-H, namely parallel and perpendicular to the clinker surface. The growth rate is determined by the concentration of Ca^{2+} ions. Growth parallel to the clinker surface leading to a high surface coverage occurs at low lime concentration, while perpendicular growth is enhanced at high Ca^{2+} concentrations.[37-38]

Its structural properties are still subject to many investigations due to its amorphous character and the varying Ca/Si ratio. Generally, C-S-H macroscopically exhibits a foil-like morphology during the beginning of hydration. These foils present precursors for C-S-H needles to which they convert over time (see **Figure 4**). The interlocking of these C-S-H needles is considered the main reason for the development of the high strength of concrete.[24-25]

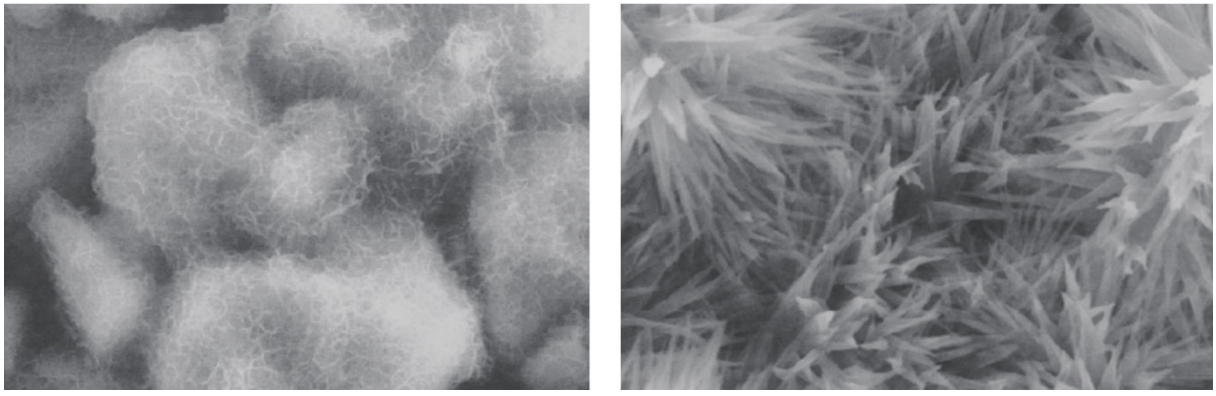

Figure 4: C-S-H foils with ~ 20 nm diameter formed from C_3S hydrated for 140 minutes (left) and ~ 2 mm long C-S-H needles obtained after 360 days of hydration of C_2S (right). Magnifications: 8,000x and 16,000x. After *Stark*.[24]

On the nanoscale, C-S-H possesses a disordered layered structure made of linear silicate chains in the so-called "*dreierketten*" arrangement, analogous to that of tobermorite (Ca/Si = 0.8 - 1.5) or jennite (Ca/Si = 1.5 - 2.0).[39] The structural elements of 1.4 nm tobermorite are chains of $[SiO_4]^{4-}$ tetrahedra and distorted double layers of Ca^{2+} and O^{2-} ions with the

composition $[CaO_2]^{2-}$ (see **Figure 5**). The structural components of jennite are described as distorted $[CaO_2]^{2-}$ double layers and $[SiO_4]^{4-}$ tetrahedra chains, too, where every second silicate chain is replaced by a series of OH^- ions. While *Taylor* found two different types of C-S-H which he denoted by C-S-H(I) and C-S-H(II), where the phase transition takes place around Ca/Si = 1.5, *Nonat*, *Grutzeck* and *Stade* found several indications that suggest another phase transition at a low Ca/Si ratio of 1.0.[29, 40-42]

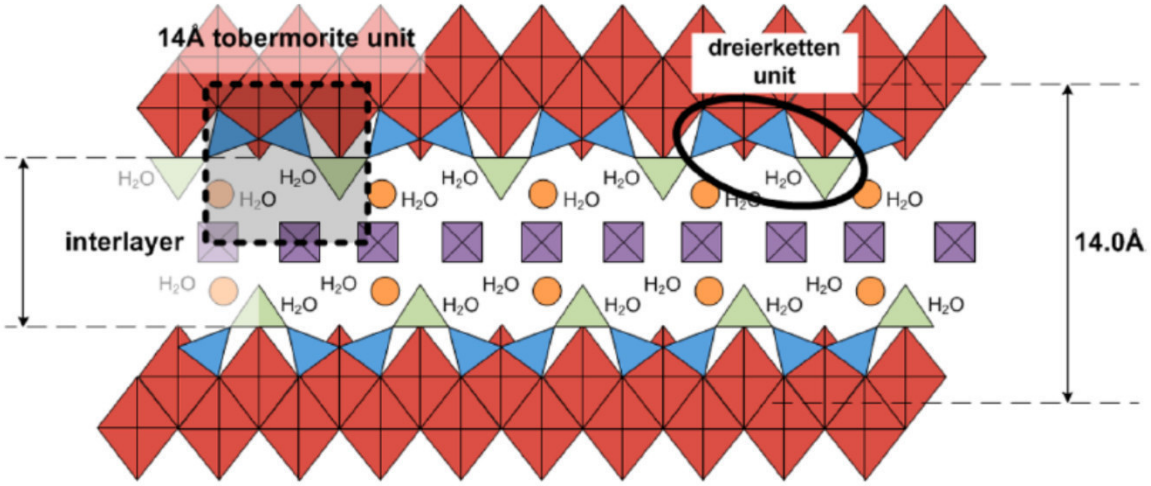

Figure 5: Schematic representation of a sublattice of 1.4 nm tobermorite. Paired and bridging tetrahedra are represented by blue and green triangles, respectively, intralayer calcium, charge-balancing alkali cations and interlayer protons and/or calcium ions by red diamonds, orange circles and purple squares, respectively, from *Myers*.[43]

As described in section 3.1., C-S-H forms a dense metastable layer that impedes further dissolution of the clinker and causes the induction period. Therefore, the structure and morphology of C-S-H formed very early during cement hydration is of special interest.[37, 44] Furthermore, the reasons for the end of the induction period, i.e. for the decomposition of the initial C-S-H layer, are still under debate.

In this work, the early formation of C-S-H phases at a Ca/Si ratio of 1.0 in the presence of different polycarboxylate ether (PCE) superplasticizers is studied. At this Ca/Si ratio, formation of 1.4 nm tobermorite occurs which consists of infinite linear chains of silica tetrahedra. These silicate chains are connected to Ca-O sheets in an alternating sandwich-like arrangement stabilized by charge-balancing cations and water in the interlayer region. Solid-state nuclear

magnetic resonance (SS NMR) spectroscopy, especially ^{29}Si MAS NMR and other instrumental techniques, e.g. infrared-spectroscopy or X-ray powder diffraction, have been used in the last decades to obtain a more clear image of the C-S-H microstructure. For pure C-S-H, a decrease of the silicate chain length with increasing Ca/Si ratio was found.[45] Whereas at high Ca/Si ratios of 1.7, mainly silicate dimers and calcium hydroxide is present.[46]

As the demands for concrete rise concerning strength, durability and workability, almost every formulation nowadays contains organic admixtures. Among the most important admixtures for concrete are superplasticizers which allow good workability even at low w/c ratios. Their most effective representatives are polycarboxylate ethers possessing a comb-like structure with strong carboxylate anchor groups in the backbone and long polyethylene oxide side chains. As these admixtures can induce changes to the nanostructure of C-S-H which has ultimately a huge impact on the mechanical properties of concrete, it is of greatest interest to understand these organic/inorganic interactions on a molecular level.[47]

So far, there have not been many reports on the interactions of polymers with calcium silicate hydrates. *Matsuyama* and *Young* have investigated the ability of several anionic polymers, e.g. poly(acrylic acid) and poly(methacrylic acid), to intercalate into the C-S-H interlayer. They found that at Ca/Si ratios < 1.0 almost no intercalation takes place. Only poly(acrylic acid) led to an interlayer expansion in this case.[48] The interaction of polyethylene glycols with C-S-H was studied by *Beaudoin* et al.. By ^{29}Si MAS NMR spectroscopy they found an increase of the degree of polymerization (DP) for silicate chains (Q^2/Q^1 ratio) in the presence of organic additives which increases with the dosage of the polymers.[49] The interactions of calcium silicate hydrates with polymeric dispersants was also studied by *Popova* et al..[50] A melamine formaldehyde sulfite and a “small molecule” based superplasticizer consisting of polyalkylene oxide chain with a phosphonic acid as anchor group were studied at different Ca/Si ratios between 0.66 and 1.50 and no significant change in the structure of C-S-H was found. In another study by *Cappelletto* et al., ^{29}Si MAS NMR spectroscopy was used in order to understand the interactions between different methacrylate ester (MPEG)-based polycarboxylate superplasticizers and C-S-H formed by the hydration of tricalcium silicate (C_3S) over 40 days. On the one hand, organic additives delayed the hydration of C_3S, i.e. more unreacted monosilicate (Q^0) was found in the presence of MPEG-PCEs. But, on the other

hand, C-S-H formed in PCE solution possessed a higher degree of polymerization compared to the one obtained in pure water. Surprisingly, they found an increase of DP with increasing charge density of PCE and a lower reactivity of C_3S for PCEs with short and few side chains.[51]

These studies show that the structure of C-S-H can undergo significant changes, depending on the type of additive. To our knowledge, there is no study on the effect of chemically different types of polycarboxylate ethers, particularly during the early C-S-H formation. Therefore, it is of special interest to investigate the impact of isoprenyl ether (IPEG)- and allyl ether (APEG)-based PCEs which consist of different monomers on the nanostructure of C-S-H and to compare the resulting structures to those of MPEG-PCEs.

3.1.2. Layered Double Hydroxides

The family of layered double hydroxides has been studied extensively for a wide range of applications including catalysts, catalyst supports, adsorbents, bio-organic nanohybrids and anion exchangers.[52-53] The most famous LDH is probably the mineral hydrotalcite: $[Mg_6Al_2(OH)_{16}](CO_3) \cdot 4\ H_2O$. Due to the structural resemblance of LDH to this mineral they are often called hydrotalcite-like compounds. The basic structure of LDHs (see scheme in **Figure 6**) can be derived from a cadmium iodide type layered hydroxide, e.g. brucite ($Mg(OH)_2$). The brucite structure consists of divalent metal cations that are surrounded almost octahedrally by hydroxide anions. A single layer is formed by edge-sharing of these octahedral units. By stacking of these layers on top of each other, the three-dimensional structure evolves.[54] The LDH structure can now be derived by substitution of a fracture of the divalent cations by trivalent cations, introducing an overall positive charge into the layers. The positive charges of the layers are counterbalanced by anions intercalated in the interlayers. Thus, LDHs can also be seen as antitypes to clay minerals which consist of negatively charged inorganic layers and interlayer cations.

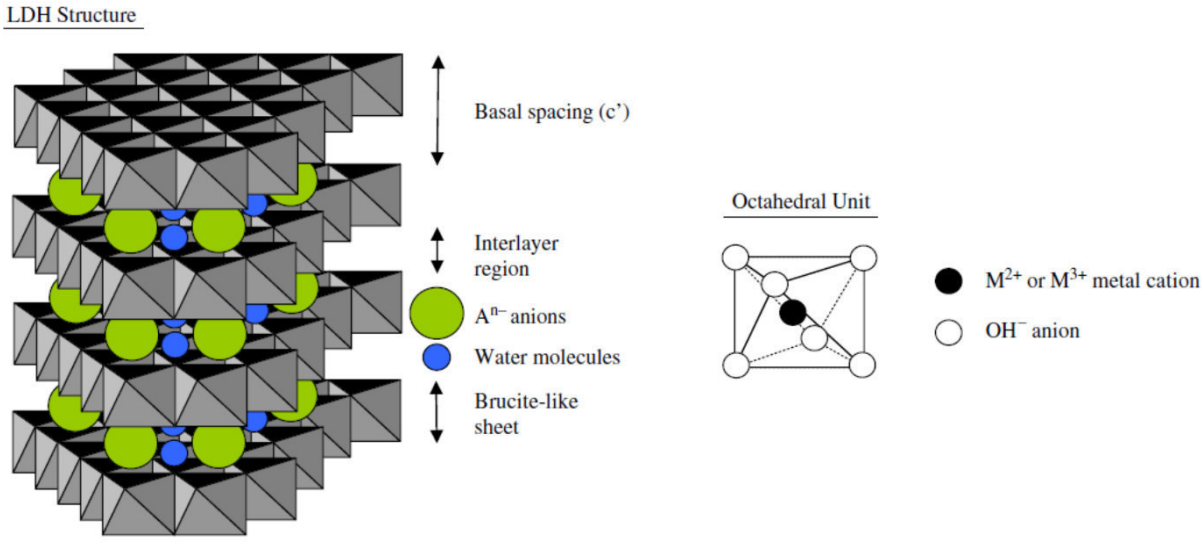

Figure 6: Schematic representation of the LDH structure after *Goh*.[55]

The general composition of LDHs can be formulated as $[M^{II}_{1-x}M^{III}_{x}](OH)_2^{x+}(A^{n-})_{x/n}\cdot y\,H_2O$, where M^{II} can be a divalent cation like Zn^{2+}, Ni^{2+}, Ca^{2+} or Mn^{2+} and M^{III} a trivalent cation like e.g. Al^{3+}, Ga^{3+} or Fe^{3+}. The anions compensating the positively charged hydroxide layers can range from small inorganic ones such as Cl^-, NO_3^-, CO_3^{2-} and SO_4^{2-}, up to large biopolymers or polyelectrolytes exhibiting negative charges like e.g. polycarboxylates. Additionally, water molecules are often present in the interlayers, too. While the bonds within the layers are covalent, the stacking is held together by weaker forces of electrostatic nature, like hydrogen bonding and Van-der-Waals attractions.[56-57] Thus, the population of the interlayers with anions and water leads to increased layer-to-layer distances compared to brucite (c_0 = 0.4766 nm).[54] The relatively weak bonding between the host layers gives LDHs a high anion exchange capacity. Furthermore, the type of anion and the amount of water molecules present in the interlayer galleries of the LDH determine the distance between the layers, the so-called basal spacing.

Over the years, many different synthesis methods have been established for the preparation of LDHs. The most commonly used methods are the following:[58-59]

1) Coprecipitation
2) Rehydration or Reconstruction method
3) Ion-exchange method
4) Hydrothermal methods

In the following, the methods 1 - 3 will be explained in more detail due to their relevance within this work. The most frequently used one is probably coprecipitation from aqueous solutions as it is most suitable for upscaling in order to produce large quantities. It further allows direct incorporation of the desired anions into the interlayers which makes it the method of choice for incorporation of larger organic anions. To precipitate two different types of cations simultaneously, the synthesis has to be carried out under supersaturation conditions. This is commonly achieved by adjusting the pH to the value where the most soluble hydroxide precipitates, or higher. Different methods have been developed using coprecipitation to synthesize LDHs, namely: Coprecipitation at high or low supersaturation, the urea hydrolysis method and a method comprising separate nucleation and aging steps. A synthesis at high supersaturation is performed by addition of a solution consisting of a mixture of M^{2+}/M^{3+} salts to an alkaline solution holding the anion. This can lead to impurities of $M(OH)_2$ and $M(OH)_3$ and low crystallinity of the LDH due to the high amount of crystallization nuclei formed. Thus, to obtain a pure and highly crystalline LDH, precipitation at low supersaturation is the method of choice. Here, mixed solutions of the divalent and trivalent metal salts are slowly added into a reactor holding the solution containing the anion. Additionally, a base (commonly NaOH) is added dropwise to keep the pH value in the reactor constant at the desired value where both metal salts precipitate. Due to the diluted solutions compared to coprecipitation at high supersaturation, the rate of crystal growth is higher than the rate of nuclei formation which favours formation of highly crystalline LDHs.[58, 60] More information on the other coprecipitation methods can be found in the literature.[58]

Another method to synthesize LDHs is the rehydration which is based on the so-called structural “memory-effect”. By calcination at 500 - 800°C LDHs are transformed to mixed metal

oxides. Upon dispersion of those mixed metal oxide precursors into water, they absorb water to re-form the hydroxide layers and incorporate anions and water into the interlayer galleries. The main advantage of this method is the absence of anions from metal salts which can compete with the desired anions for the intercalation. This is especially useful when large organic molecules like e.g. graphene or enzymes which often possess only a low anionic charge are supposed to be intercalated.[61-62]

LDHs can be further prepared by the ion-exchange method. This technique is especially useful for example when the anion or the metal cations are not stable in alkaline media or in case there are any favoured direct reactions between one of the cations and the anion. Then, a preformed LDH containing an anion with rather low affinity to the positively charged layers is dispersed in a solution holding the desired anion. The intercalated anion will then be gradually replaced by the dissolved anion based on its higher affinity for the positive main layers. It was found that the ion-exchange in LDH is determined mainly by the electrostatic interactions between the anion and the positively charged hydroxide layers. The free-energy involved in the changes of hydration is less decisive.[63-64] The affinity of the most common inorganic anions towards the positively charged host-sheets is as follows:[65]

$$CO_3^{2-} \gg SO_4^{2-} \gg OH^- > F^- > Cl^- > Br^- > NO_3^- > I^-$$

The low affinity of the nitrate anion for the hydroxide layers and the good availability of nitrate metal salts makes it very popular as anion of precursor LDHs for the ion-exchange synthesis. Carbonate possesses the highest affinity of all anions for the host sheets due to its small size and the divalent anionic charge. Consequently, Carbonate-LDHs are often found as impurity after synthesis due to the uptake of atmospheric CO_2 into the interlayer galleries. Thus, it is necessary to perform all synthesis methods in a CO_2-free atmosphere, e.g. in a nitrogen atmosphere.

3.1.3. Structure and composition of calcium aluminate hydrates

In cement chemistry, the hydration products of tricalcium aluminate (C_3A) and tetracalcium aluminoferrite (C_4AF) are mainly hexagonal layered materials of the hydrocalumite-type, e.g. $[Ca_2Al(OH)_6](OH) \cdot 6\ H_2O$ (cement chemistry notation: C_4AH_{19}) or $[Ca_2Al(OH)_6](OH) \cdot 3\ H_2O$ (cement chemistry notation: C_4AH_{13}) which are called AF_m phases.[29] In the presence of sulfate, another AF_m phase, the so-called monosulfate ($[Ca_2Al(OH)_6](SO_4)_{0.5} \cdot 3\ H_2O$) is formed. Its structure is presented in **Figure 7**. Besides these layered calcium aluminate hydrates, so-called AF_t phases are forming in the presence of an excess of e.g. SO_4^{2-} ions. The most prominent representative of these phases is ettringite (trisulfate) with the empirical formula $[Ca_3Al(OH)_6 \cdot 12\ H_2O]_2(SO_4)_3 \cdot 2\ H_2O$.

3.1.3.1. Structure and composition of AF_m compounds

The structure and composition of AF_m phases is analogous to that of the mineral hydrocalumite ($[Ca_2Al(OH)_6]Cl \cdot 2\ H_2O$). Therefore, they are also referred to as hydrocalumite-type LDHs. Like the hydrotalcite-based layered double hydroxides, the AF_m phases consist of positively charged $[Ca_2Al(OH)_6]^+$ layers with OH^-, Cl^- or SO_4^{2-} anions balancing the overall charge. The overall formula of hydrocalumite-based LDHs can thus be written as $[Ca_2M(OH)_6]^+(A^{n-}_{1/n}) \cdot x\ H_2O$ (M represents a trivalent metal cation and A the interlayer anion).[66] In contrast to other LDHs, in hydrocalumites the calcium ions are not positioned in the centre of an octahedra but are seven-fold coordinated, with half of the calcium ions being shifted upwards along the *c* axis and half down. Besides the six hydroxyl groups they are coordinated to a water molecule in the interlayer to which they are shifted.[54]

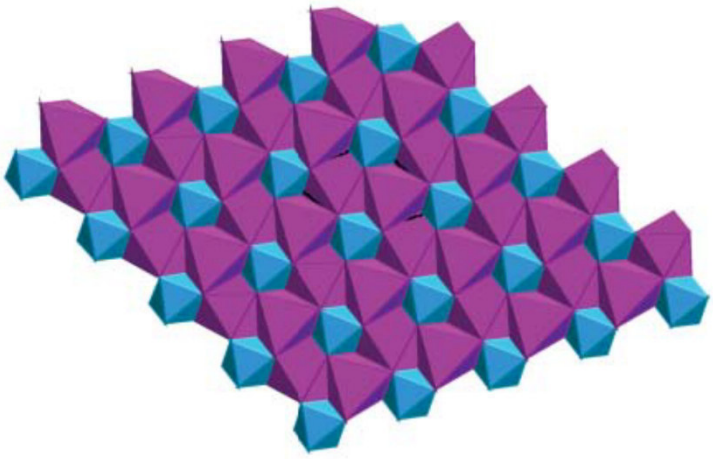

Figure 7: Schematic representation of the structural arrangement of metal cations and their coordination in a layer of monosulfate, $[Ca_2Al(OH)_6]SO_4 \cdot 3\ H_2O$ in the *ab* plane. Blue = Al^{3+} and violet Ca^{2+}.After *Khan*.[67]

The hydrocalumite-type LDHs have drawn much attention in cement chemistry over the last years due to their interaction with cement admixtures. Several studies have shown that Portland cements with a high amount of tricalcium aluminate can interact with superplasticizers which are a key admixture, especially for ultra-high performance concrete.[68-70] A study by *Plank* et al. revealed that comb-like polycarboxylate ether superplasticizers can intercalated into the hydrocalumite-type LDH framework during rehydration of the C_3A phase. The polymers used possessed side chains with repeating ethylene oxide units in the range of 4.5 to 45 units. The successful intercalation of the different polycarboxylates was evidenced by increased basal spacings in the range of 1.15 nm to 4.27 nm, compared to 0.87 nm found for the corresponding NO_3-LDH. The organic part of these LDHs was found to be in the range of 29 – 53 wt.-%.[71] In a further study of our group, the intercalation of more complex superplasticizers was investigated. Comb- and star-shaped polymers with different backbone and side chain lengths were synthesized and intercalated via rehydration of C_3A. The side chain lengths varied between 2 nm and 25.2 nm. While an increase of the gallery height from 1.97 nm to 4.37 nm could be observed for the Ca_2Al-PCE-LDHs containing PCEs with 7 to 34 ethylene oxide units in the side chain, lower gallery heights of 3.54 nm and 3.68 nm for 90 and 70 EO units were found. Comparison of the polymer characteristics and the gallery heights found revealed different conformations of the polymers in the interlayers, namely brush-like vs. perpendicular arrangement of the side-chains.[72]

Besides polycarboxylate ethers, another class of dispersing agents for cement has been reported to be suitable to intercalate into hydrocalumite-type LDHs, namely polycondensates. In contrast to PCEs, polycondensates are linear polymers that are often functionalized with sulfonate groups, thus introducing a negative charge. *Raki* et al. reported on the preparation of a Ca_2Al-NO_3-LDH by coprecipitation and successful intercalation of naphthalene sulfonic acid and nitrobenzoic acid into the Ca_2Al-LDHs via anion exchange. They suggest a higher affinity of the polymers towards the inorganic host sheets than the nitrate anion.[73]

Furthermore, an acetone-formaldehyde-sulfonate polycondensate, a sulfanilic acid-phenol-formaldehyde polycondensate and different melamine-sulfonate-formaldehyde polycondensates have been successfully intercalated into Ca_2Al-LDH by rehydration, as reported by our group in the literature.[11-12, 21] All these studies have proven that even complex organic polymers used as cement admixtures strongly interact with aluminate hydrates and can lose their dispersing effect due to intercalation. The obtained inorganic-organic host-guest composites have also shown great stability compared to the Ca_2Al-OH-LDH as there was no transformation of the Ca_2Al-LDHs into the thermodynamically favoured C_3AH_6 observed on samples aged for 60 days.[72] These composites have further been proposed as potential slow-release admixtures, i.e. the composites release the intercalated dispersing agents slowly over time via anion exchange with sulfate ions which are present in every type of concrete formulation for setting control.[11, 21] Thus the rheology could be maintained over a longer period of time. So far, there is no report in the literature that sulfate ions can exchange such large polymers and release them. Such a slow release additive would be especially interesting for oil well cementing where very long pumping times are required and thus the rheology needs to be maintained until the cement is completely placed. Therefore, retarding molecules which delay the setting of concrete and thus keep the slurry fluid are of special interest for such slow-release composites.

Within this study, two different commercial retarding agents were added to the mixing water and Ca_2Al-LDHs were prepared via rehydration. The obtained composites were characterized by XRD, IR, SEM, TGA and elemental analysis. In a next step, the obtained composites were subjected to anion exchange with sulfate ions and the affinity of the polymers to the LDH matrix was evaluated. Finally, the Ca_2Al-retarder-LDHs were added as admixtures to a cement paste

and their delayed retardation was studied by heat flow calorimetry. In a further study, a synthesis method for a Ca_2Al-formate-LDH via co-precipitation was developed and its potential as an accelerator for cement hydration, especially for C_3A, was investigated in strength tests of mortars and via in-situ XRD and heat flow calorimetry of cement admixed with the Ca_2Al-formate-LDH.

3.1.3.2. Structure and composition of ettringite

Ettringite is probably the first reaction product during cement hydration and occurs instantaneously within the first seconds after addition of water. Like all AF_t phases, it crystallizes in the form of needles. The pre-requisite for its formation is an excess of sulfate ions which are present in every common cement formulation to control the setting behaviour. Then, the formation of ettringite is favoured over the formation of monosulfate.

The crystal structure of ettringite consists of cylindrical pillars that are oriented parallel to the *c* axis of the crystal (see **Figure 8**). Four of these pillars form a rhombus. Along the *c* axis of a pillar, $Al(OH)_6$ units are alternating with CaO_8 polyhedrons where the Al^{3+} ions and the Ca^{2+} ions are bridged by shared OH^- ions. One column has basically the formula $[Ca_3Al(OH)_6 \cdot 12\ H_2O]_2^+$. In the voids between the pillars, also referred to as channels, SO_4^{2-} ions are situated balancing the charges of the pillars. Additionally, the channels contain water molecules.[29, 74-75] The channels between the pillars can also take up CO_3^{2-}, OH^- or Cl^- instead of sulfate, thus producing tricarbonate, trihydroxide and trichloride, respectively. Furthermore, the Al^{3+} ions can be replaced by Fe^{3+} ions or other trivalent cations, e.g. Mn^{3+} or Cr^{3+}.[22]

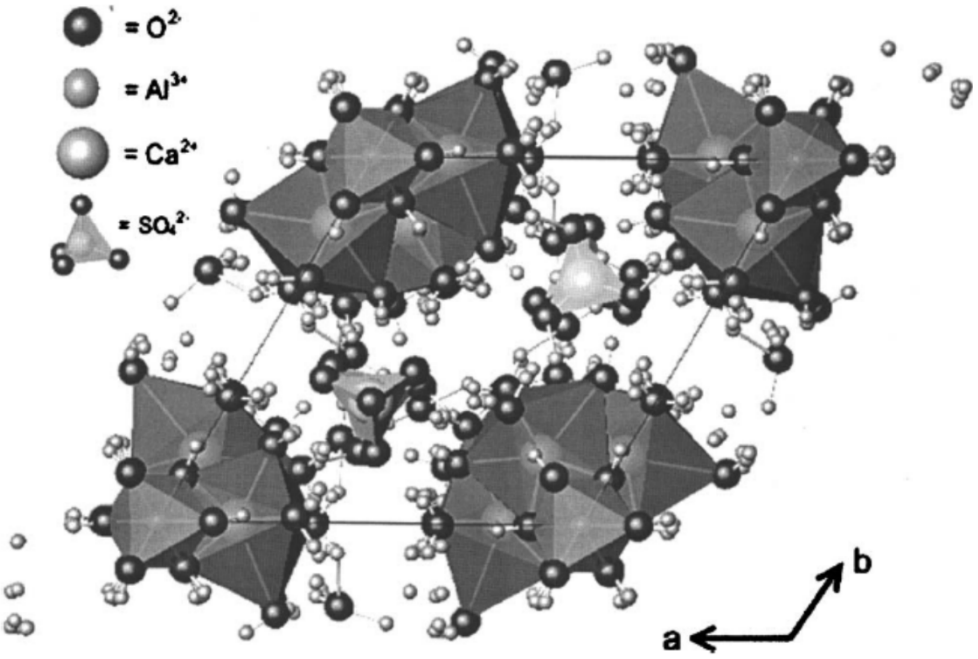

Figure 8: Unit cell of hexagonal ettringite (projection along *c axis*).[76]

Compared to other cement hydrates, ettringite contains a high amount of water. The decomposition starts at temperatures above 60°C and normal ambient humidity. Upon contact with moisture, ettringite takes up water again. This process can occur without changing the morphology of ettringite.[22]

In contrast to temperature and moisture, the chemical environment, e.g. the pH and the ions present in the pore solution, can exert a significant change on the crystal morphology of ettringite. It was found that increasing the pH from 9.5 to 12.5, the aspect ratio, i.e. the ratio of crystal length to diameter, of ettringite crystals decreased.[77] A study by *Kreppelt* et al. showed that using an extracted cement pore solution exhibiting a pH > 13 with c(SO_4^{2-}) being 14 g/L and c(Ca^{2+}) being 0.77 g/L, respectively, formation of ettringite with low aspect ratio can be observed within 24 h. With artificial pore solution (pH = 12.5, c(SO_4^{2-}) = 1 g/L and c(Ca^{2+}) = 1.36 g/L) rather slender crystals were found.[78]

As the charge balancing anions are situated within the channels between the pillars, the crystal surface possesses a positive charge. This fact and the early formation during cement hydration makes ettringite prone for interactions with negatively charged cement admixtures. It has been reported that ettringite presents the main adsorption site for superplasticizers.[20, 79]

Furthermore, it was found by *Lange* and *Plank* that cements rich in tricalcium aluminate show significant incompatibility with PCE superplasticizers due to their fast formation of nanosized ettringite crystals.[80] But not only the effectiveness of the PCEs is affected by these interactions. Cement hydration in general was found to be delayed in the presence of PCE superplasticizers. The influence of the addition of superplasticizers on the nucleation and crystal growth of ettringite has already been proven in several studies. The retarding effect of PCEs on the aluminate hydration can be attributed either to sequestration of Ca^{2+} ions from the pore solution, leading to a lower rate of precipitation of cement hydrates, or to the adsorption on the cement hydrates and thus inhibiting their growth.[81] As the size and morphology of cement hydrates are decisive for the microstructure in hardened cement and thus for its mechanical properties, it is of fundamental importance to understand the impact of cement admixtures on cement hydrate formation.[82]

A study by *Cody* et al. revealed that most carboxylic acids, such as e.g. acetic acid, do not influence the formation of synthetic ettringite, except for those that are effective calcium chelators, like citric, tartaric or gluconic acid. These delayed both nucleation and crystal growth.[83] In a previous study by *Plank* et al. several PCEs possessing different specific anionic charge amounts were investigated regarding their impact on synthetic ettringite formed by flash precipitation from aqueous solutions of $Ca(OH)_2$ and $Al_2(SO_4)_3$.[9] Generally, PCEs lead to a reduced crystal size, with their effect depending considerably on their anionicity. The aspect ratio of the obtained smaller crystals did not change which suggests that the polymer did not only adsorb on the side faces of the hexagonal prismatic ettringite crystals, but also on the top and bottom faces, inhibiting crystal growth in all directions.

As explained in chapter 3.1., cement hydration constitutes a very complex interplay of various processes. Thus, observations made on the crystallization of synthetic ettringite are not necessarily representative for the interactions of those admixtures with cement hydrates in an actual cementitious system, where different ion concentrations are present. In a simplified binder system of C_3A and $CaSO_4$, *Dalas* et al. showed that the impact of PCEs on ettringite formation is dependent on the type of PCE. While in the presence of two PCEs differing by their anionic charge density, ettringite precipitation was generally slowed down during the first 2 h of hydration. This effect increased with increasing charge density of the polymer and with

increasing PCE dosage. Furthermore, it was found that in the presence of PCEs the specific surface area of the ettringite crystals increased significantly within the first 5 minutes which suggests that more abundant, but smaller crystals were formed compared to hydration in the absence of superplasticizers. This effect decreased over the following two hours which suggests that already instantaneously after addition of the mixing water a strong interaction between ettringite and PCEs occurs.[84] Further studies on short-term hydration of Portland cement (CEM I 42.5 R and CEM I 42.5 N) containing low amount of tricalcium aluminate clinker in the presence of PCEs (dosage = 0.05 % bwoc) under terrestrial and microgravity conditions have shown that PCEs influence the formation of ettringite already within the first 10 seconds of hydration.[8, 85] There, larger crystals exhibiting higher aspect ratios were reported in the presence of PCEs, especially under terrestrial gravity conditions.

Regarding the limited amount of information on the nucleation and crystal growth of ettringite in cement paste as well as on its interactions with dispersing agents, namely polycarboxylate ethers and polycondensates, within the first seconds of hydration, the objective of this work was to provide a better understanding of its early hydration. Therefore, the nucleation and crystal growth of ettringite in simplified model mixes of C_3A and C_4AF with $CaSO_4$ hemihydrate in the absence and presence of convection, as well as that of different commercial Portland cement samples (CEM I 52.5 N and CEM I 42.5 R) was studied. Additionally, the impact of polycondensates, polycarboxylate ethers and a novel phosphate comb polymer on the size and morphology of ettringite crystals formed during this short-term hydration was studied. As polycarboxylate ethers present the most important class of industrially applied dispersing agents, the impact of different side chain lengths, anionic charge density and dosages was investigated.

3.2. Admixtures for cement

Nowadays, Portland cement still is considered as the most important binder in the construction industry and is used for many different types of applications ranging from casting simple slabs towards oil well cementing deep below the surface of the earth. Admixtures allow tuning of the fresh or hardened properties or both of concrete by chemical or physical means to obtain the desired optimum properties for each application on the jobsite. There is a broad range of admixtures, the most common classes are: dispersing agents, retarding agents, accelerating agents and stabilizing agents. Within this work, the first four classes are relevant and are introduced in the following.

3.2.1. Dispersing agents for cement

Dispersing agents can be divided into two categories. Plasticizers or liquefiers are dispersing agents that act by electrostatic repulsion (see chapter 3.1.2.) and allow reduction of water between 5 – 10 L/m³ concrete, whereas superplasticizers are even more efficient admixtures that lead to a very high reduction of the viscosity of the concrete slurry via strong electrostatic or electrosteric repulsion. Lignosulfonate is probably the only remaining plasticizer that is produced and used in higher amounts today, especially in Russia.[86] Representatives for superplasticizers are mainly polycondensates and polycarboxylate ethers.

3.2.1.1. Polycondensates

The first type of superplasticizers used as cement dispersant were polycondensates back in the 1960s. Based on melamine, the German company *SKW Trostberg AG* invented the melamine formaldehyde sulfite (MFS) polycondensate, while almost at the same time in Japan *Kao Soap* invented the sulfonated *β*-naphthalene formaldehyde (BNS) polycondensate (chemical structure of the two polymers are shown in **Figure 9**).[25] The invention of these polycondensate-type superplasticizers created a huge hype in the construction industry as applicators realized the very important role of admixtures in concrete formulations.

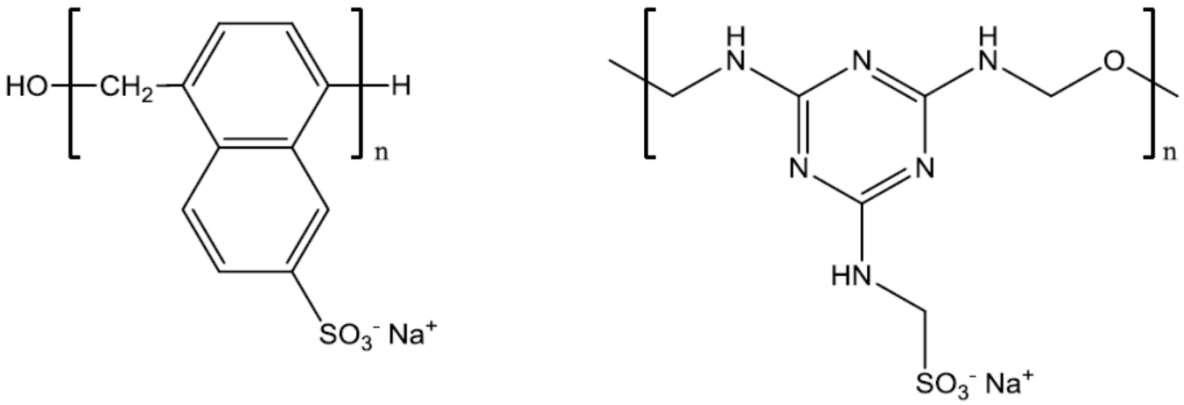

Figure 9: Molecular structure of a sulfonated β-naphthalene formaldehyde polycondensate (left) and a melamine formaldehyde sulfite polycondensate (right).

Approximately 20 years later, in 1981, *SKW Trostberg AG* developed a new polycondensate based on an aldol condensation of the cheap raw materials acetone, formaldehyde and sulfite, the so-called acetone formaldehyde sulfite (AFS) superplasticizer.

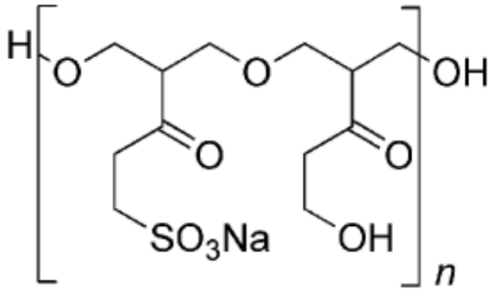

Figure 10: Molecular structure of an acetone formaldehyde sulfite polycondensate.

The AFS polycondensates usually possess a very distinct red colour which limits their popularity. But AFS poylcondensates have also great advantages, e.g. their good compatibility with cellulose ethers, stability at higher temperatures in oil well cementing and good performance in saline environment.[87]

Despite their individual advantages, all these polycondensates exhibit several disadvantages, too. Among the main disadvantages is their free formaldehyde content and their limited dispersing ability at low water-to-cement ratios. Furthermore, they tend to lose their plasticizing ability already approximately one hour after mixing.[25] All these disadvantages encouraged

researchers to develop new types of superplasticizers which led to the invention of the class of polycarboxylate ethers.

3.2.1.2. Polycarboxylate ethers

The invention of this new generation of superplasticizers can be dated back to the early 1980s by the Japanese company *Nippon Shokubai*. Polycarboxylate ethers (PCEs) are comb polymers consisting of a negatively charged backbone and, most commonly, uncharged side chains, e.g. of polyethylene glycol. Nowadays, there exists a broad range of types of PCEs synthesized from various monomers. By variation of the backbone length, the side chain length and the number of anionic charges within the backbone, PCE comb polymers can be tailored specifically to different applications. Thus, it is possible to obtain a good dispersing effect up to 4 hours and even at w/c ratios below 0.35 with a CEM I type cement. Moreover, PCEs have been tailored to exhibit compatibility with alternative binders, like e.g. fly ash, or limestone or calcined clay blended cements. In the following, the classes of PCEs relevant for this work are described in more detail.

MPEG-type PCEs

MPEG-PCEs belong to the first generation of PCEs and consist of acrylic or methacrylic acid and ω-methoxy poly(ethylene glycol) methacrylate ester (MPEG-MAA) macromonomer. Generally, they can be synthesized via the industrially favoured free radical co-polymerization of both monomers in the presence of a chain-transfer agent or via grafting of a ω-methoxy poly(ethylene glycol) via esterification onto an existing polymethacrylic acid backbone. While the grafting approach commonly leads to a more equal distribution of side chains along the backbone, in the free radical process homopolymerization of the methacrylic acid is likely to occur, leading to a high molecular by-product. Free radical co-polymerization also produces a gradient distribution of the side chains along the backbone due to the different reactivity of the monomers, but can be performed at much less harsh conditions and allows good control of the length of the PCE backbone. PCEs exhibiting a gradient distribution of side chains have further shown good sulfate resistance, as the long side chain-free anionic parts of the backbone possess high adsorption capacity on cement particles. The use of acrylic acid as monomer

has the disadvantage that the ester bond to the side chain is easily hydrolysable and is prone to decompose in alkaline media such as in cement paste. Therefore, mainly methacrylic acid is used today.

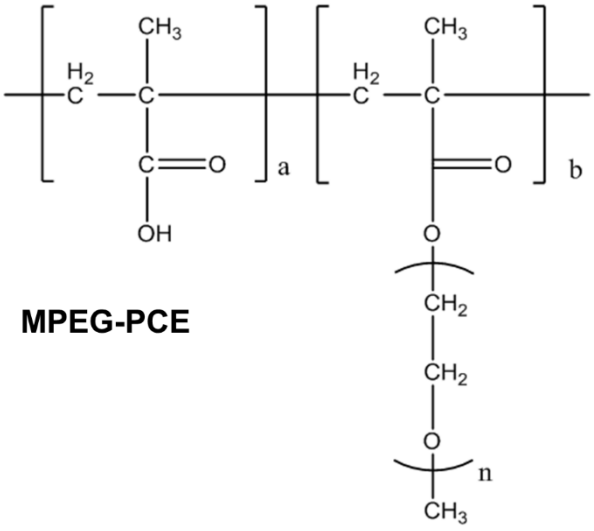

Figure 11: Molecular structure of MPEG-PCEs synthesized from methacrylic acid and MPEG-MAA macromonomer.

APEG-PCEs

The APEG-PCEs are presenting the second generation of PCEs. They are prepared by free radical co-polymerization of α-allyl-ω-methoxy poly(ethylene glycol) (APEG) macromonomers and maleic acid anhydride. In some cases, small additions of styrene are used instead of maleic acid anhydride. By using these monomers, the drawback of homopolymerization of monomers could be eliminated. Because a thermodynamically favoured HOMO-LUMO interaction between the two monomers can only occur in an alternating order in the backbone, APEG-PCEs exhibit always a very homogenous distribution of side chains.[88] This strictly alternating arrangement leaves less freedom in tailoring these PCEs regarding anionicity and only the side chain length can be varied. An advantage of these PCEs is the connection of the polyethylene glycol to the polymer backbone via a robust ether bond which makes the side chains completely resistant towards hydrolysis in alkaline media.

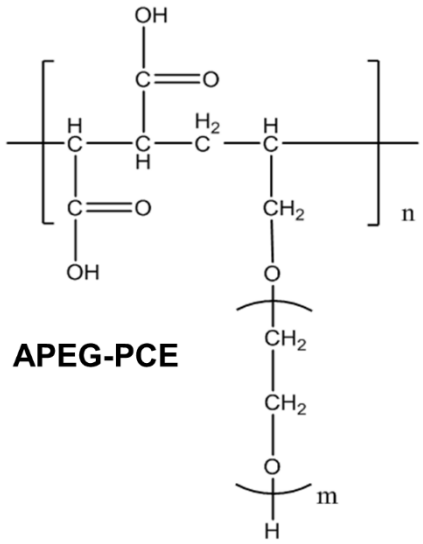

Figure 12: Molecular structure of APEG-PCEs synthesized from maleic acid anhydride and an APEG macromonomer.

IPEG-PCEs

One of the latest innovations in the PCE design are the isoprenyl ether based PCEs, shortly IPEG-PCEs. They are very widespread produced and used in Asia, especially in China. Like the other PCE types they are synthesized via free radical co-polymerization. As monomers, isoprenyl oxy poly(ethylene glycol) macromonomer and acrylic acid are used. Compared to the previously described PCEs, the synthesis in aqueous medium is facile, because of the high reactivity of the isoprenyl ether. The side chains are linked to the backbone by an ether bond comparable to that in APEG-PCEs which makes this class of PCEs stable towards hydrolysis in cement paste, too. Additionally, IPEG-PCEs possess a very high dispersing effectiveness compared to the other classes and thus require lower dosages to obtain the desired rheology of the concrete slurry. Like MPEG-PCEs, this class can be tailored regarding anionicity, backbone and side chain length and allows thus versatile application. [88] The disadvantage of this type of PCE is in bulk material an elimination reaction of the isoprenyl ether to isoprene, glycol and water during storage which can lead to impurities that affect the synthesis or the performance of the obtained product.[89]

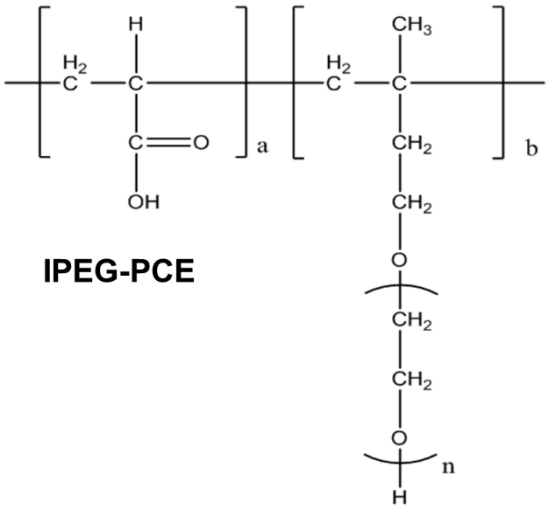

Figure 13: Molecular structure of IPEG-PCEs synthesized from acrylic acid and an IPEG macromonomer.

Phosphated comb polymer

Recently, it has been shown that phosphonate anchor groups possess a higher affinity towards positively charged particles than carboxylate groups present in conventional PCEs.[90] Thus, many researchers focused over the last years on the incorporation of phosphonate or phosphate groups into linear polycondensates or comb polymers.[90-93] It was found that particularly phosphate containing polymers have a good sulfate resistance and a high dispersing effectiveness at low w/c ratios. The synthesis of phosphated comb polymers is generally more complex due to the poor availability of suitable monomers which have often to be synthesized in a first step. *Stecher* et al. successfully prepared phosphate comb polymers from 2-(methacryloyloxy)-ethylphosphate (HEMAP) exhibiting structures similar to the well-known MPEG-PCEs (see **Figure 14**). [93] The obtained comb polymers exhibit a longer slump retention than conventional MPEG-PCEs, especially at lower w/c ratios, and increase the flowability of the cement paste.

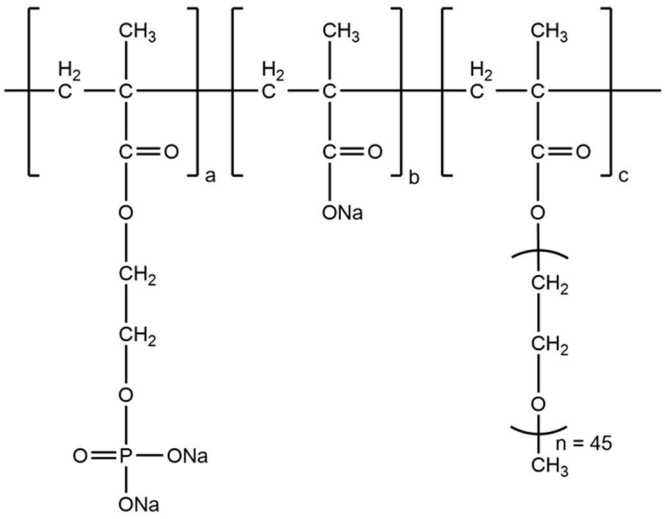

Figure 14: Molecular structure of a comb-polymer containing carboxylate and phosphate groups after *Stecher.* [93]

3.2.1.3. Mode of action of dispersing agents

Cement particles possess a very inhomogeneous composition of different silicates and aluminates (see chapter 3.1.). Upon mixing with water, the particles thus exhibit different surface charges, depending on the kind of phase present at the surface. Silicate phases exhibit a negative charge and aluminate phases a positive charge. Therefore, cement particles tend to agglomerate and flocculate which leads to a high viscosity and low workability of the slurry. By adding dispersing agents to the formulation, agglomeration of cement particles is inhibited or at least delayed, depending on the setting time of the cement. *Yoshioka* et al. and *Plank* et al. have demonstrated that anionic polymers have a high affinity for the aluminate phases and their hydrates which present the first hydration products.[20, 79] Especially ettringite which forms within the first seconds of hydration is a preferred adsorption site for superplasticizers, due to its high positive surface charge.[80, 94] Thus, anionic polymers are the most effective dispersing agents, as they can adsorb on the educts as well as on the products of cement hydration and prevent agglomeration. As explained before, there are different types of dispersing agents that can prevent attraction of cement particles via two different mechanisms, namely the electrostatic and the steric repulsion mechanism.[95]

Cement dispersion via electrostatic repulsion is based on the repulsion between equally charged particles. As mentioned above, cement particles possess different local surface charges related to the kind of clinker phase present at the particle surface. Negatively charged, linear polymers can adsorb onto the positively charged sites on the surface of cement particles and thus induce an overall negative charge which leads to repulsion of the particles (see **Figure 15**).

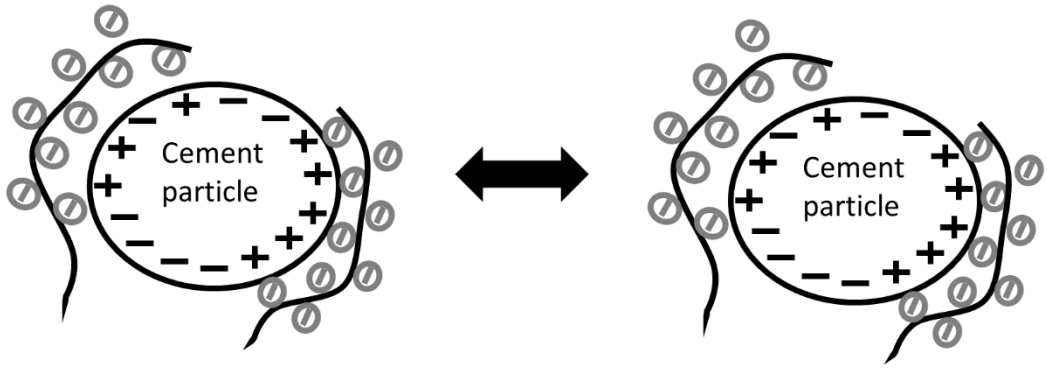

Figure 15: Schematic representation of the adsorptive mode of action of polycondensate superplasticizers via electrostatic repulsion.

The adsorption can also be mediated by Ca^{2+} ions coordinated to the negatively charged sites.[91] Hence, the adsorption process of the polymers is determined by the charge density of the polymers and the capability to coordinate with Ca^{2+} ions. In the presence of sulfate ions, a competitive adsorption to the positively charged sites on the cement particles and cement hydrates occurs which can impact the performance of superplasticizers.[96]

Polycarboxylate ether comb polymers can adsorb on the positively charged sites of cement particles and calcium aluminate hydrates, too. Additionally, they possess hydrophilic side chains which extend into the space between the particles and thus can sterically hinder the agglomeration of particles (see **Figure 16**). Many studies reported that PCEs possessing a high anionic charge density exhibit high adsorption and good initial dispersing effect but a short slump retention. PCEs exhibiting low anionic charge density, on the other hand, showed low adsorption capability and thus low initial dispersing effect, but long slump retention.[97-99] These different behaviours make the latter types of PCEs suitable for application in ready-mixed

concrete, while those with short slump retention, but high initial dispersion are preferably used in precast concrete.[25, 100]

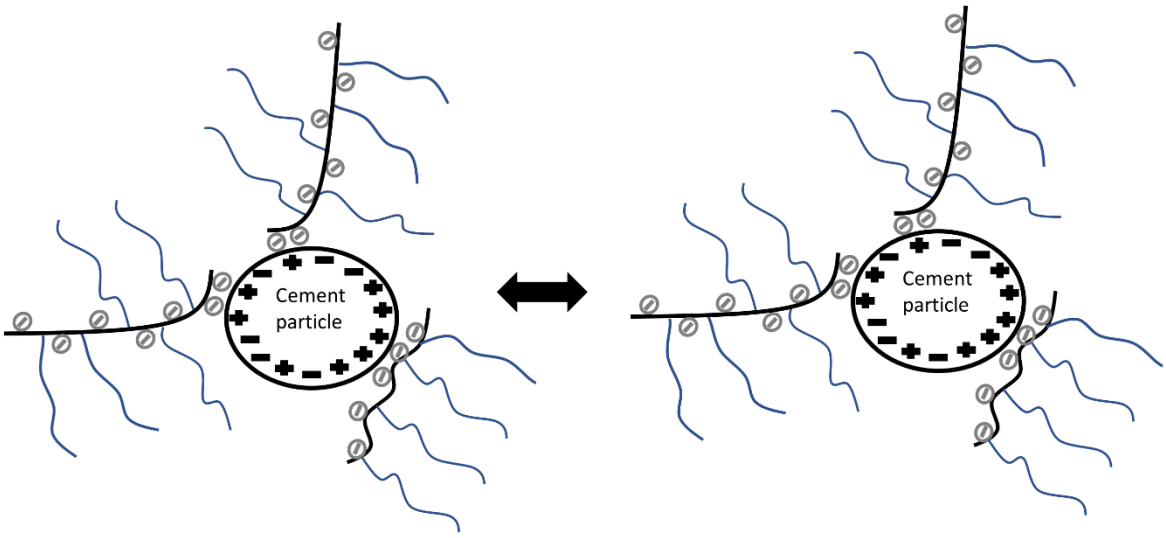

Figure 16: Schematic representation of the adsorptive mode of action of polycarboxylate superplasticizers via electrostatic and steric repulsion.

A key factor for the adsorption capability is the molecular structure of the PCE which depends on the density of anionic charges and the length and distribution of side chains along the backbone (linear or gradient).[25, 91, 99] It was found that the dispersing effectiveness of a PCE is further determined by its adsorbed layer thickness (ALT).[100-102] With increasing side chain length, the adsorbed layer thickness and thus the dispersing effectiveness of a PCE increases, assuming that the surface of particles is fully covered by PCE. Moreover, *Flatt* et al. reported that the conformation of the PCE in solution correlates with its ALT and thus with the steric hindrance of polymers.[103-104] *Shu* et al. investigated the impact of methyl groups from methacrylic acid monomers in the backbone on the solution conformation of PCEs in aqueous solution and cement pore solution and the resulting ALT.[105] It was found that PCEs containing a high backbone methyl group content exhibited less shrinkage in cement pore solution due to steric hindrance which exposed more carboxylic groups. This led to a high initial adsorbed amount, but lower ALT than PCEs containing more acrylic acid instead of methacrylic acid in the backbone (see **Figure 17**). These findings suggest a different adsorption behaviour between MPEG- and IPEG-PCEs with similar molar ratios of methacrylic acid or acrylic acid to macromonomer in the backbone.

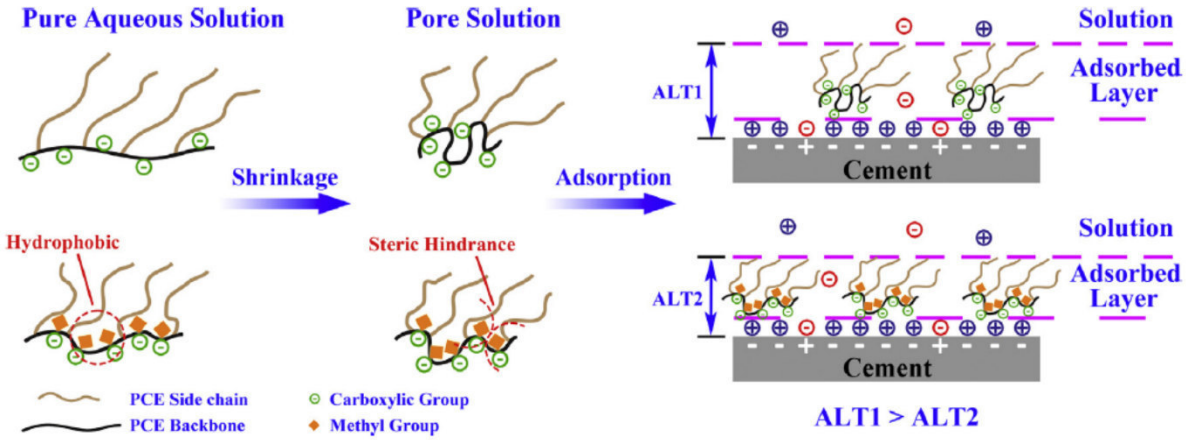

Figure 17: Impact of the methyl group in the backbone of PCEs on the adsorbed layer thickness (ALT) on cement, according to *Shu*.[105]

PCEs have not only been found to be very effective dispersing agents, they can as well retard cement hydration, depending on their molecular structure.[78, 81] Here, three different mechanisms are generally discussed:

a) Non-adsorbed PCEs present in the pore solution of a cement paste can complex Ca^{2+} ions and sequestrate these from the pore solution, delaying thus the silicate and the aluminate reaction.
b) Adsorption of the superplasticizer on cement hydrates, especially on ettringite and AF_m phases, hinders ion transport to the nucleation sites on the crystal surface and thus inhibits the growth of cement hydrates.
c) The adsorption of PCEs on unhydrated cement clinker particles prevents dissolution of the clinker which as a result leads to undersaturation of the pore solution and thus delays the precipitation of hydrate phases.

All these findings underline the importance of the molecular structure of PCEs and its impact on their performance. However, the dispersing effectiveness of PCEs is unmatched in cement chemistry and the big variety of types of PCEs and the high degree of freedom in raw material selection and synthesis allow tailoring of superplasticizers to the application needed.

3.2.2. Retarding admixtures for cement hydration and mode of action

Retarders are generally added to a concrete formulation when a long workability is required, like in oil well cementing. Furthermore, they are very useful for low carbon concrete systems, e.g. when sludge technology is used to produce sludge water in ready-mix concrete plants.[106] Usually, retarding admixtures reduce the solubility of cement clinker phases. Some admixtures can react e.g. with dissolved ions and form precipitates on the surface of cement grains. By formation of a low permeable layer, further dissolution is impeded.[107] Within this work, the latter kind of retarding admixtures is of special interest. Until today, a broad range of organic (sugars, carboxylic acids) and inorganic (zinc oxide, phosphates) as well as synthetic retarders (AMPS®-itaconic acid co-polymer) is known.[108-110] The most commonly used retarders are hydroxylic acids, saccharide derivatives and lignosulfonates.

Young revealed already quite early the four principle mechanisms of retarders: Adsorption, precipitation, complexation and nucleation control. In the “adsorption theory”, the retarder adsorbs onto the surface of an unhydrated cement particle and presents thus a barrier for water to get in contact with the clinker.[111] In the second mechanism, precipitation of the retarder in the cement paste leads to the formation of a semipermeable protective layer on the surface of cement particles. This layer prevents diffusion of water to the cement surface and hence dissolution of the clinkers. Due to high osmotic pressure, these layers can burst, upon which the cement hydration continues.[112] The mode of action via complexation involves already dissolved Ca^{2+} ions which are chelated by the retarder which is in this case mostly a carboxylic acid. Thus, Ca^{2+} ions are sequestrated from the cement pore solution which leads to a slower rate of precipitation of the early cement hydrates, such as ettringite, and slower crystal growth rates of already existing hydrates. The precipitates formed may also contribute to the “precipitation mechanism” as explained before.[113] Last, but not least, retarders can poison nucleation of initial nuclei of cement hydrates, e.g. of $Ca(OH)_2$ which presents the precursor for C-S-H formation, by occupation of the reactive sites on the nuclei and thus inhibiting their growth.[114-115]

The actual modes of action of industrial retarders are for most of the classes unclear, as they often act via a combination of the above described mechanisms. Recently, *Bishop* et al.

proposed a fifth mechanism for cement hydration, the so-called dissolution-precipitation-mechanism.[116] Here, the retarding admixture enhances dissolution of the clinker phases and subsequently forms low permeable precipitates with the dissolved ions. This was found to be the mode of action for organic phosphonic acids that have a high affinity to complex Ca^{2+} ions.

As mentioned above, small inexpensive molecules like citric acid, tartaric acid or gluconic acid which present excellent calcium chelators are most commonly used. In oil well cementing, where often temperatures above 100°C are present, these kinds of retarders are not sufficiently effective. Here, synthetic co-polymers that exhibit high temperature resistance are applied. 2-acrylamido-2-methylpropane sulfonic acid (AMPS) has proven to be a very effective monomer for preparation of such high temperature-stable co-polymers. Furthermore, *Zhang* et al. revealed a quite linear correlation between dosage and retardation time of cement hydration for these polymers.[117] It was found by *Tiemeyer* et al. that an AMPS-co-itaconic acid polymer exerts excellent cement retardation via complexation and chelation of Ca^{2+} ions via carboxylic groups and donor atoms present in AMPS. While most retarders act via a combination of at least two mechanisms, e.g. adsorption and complexation, this synthetic co-polymer retards cement hydration solely via complexation, hence indicating exceptionally high calcium binding capacity.[109]

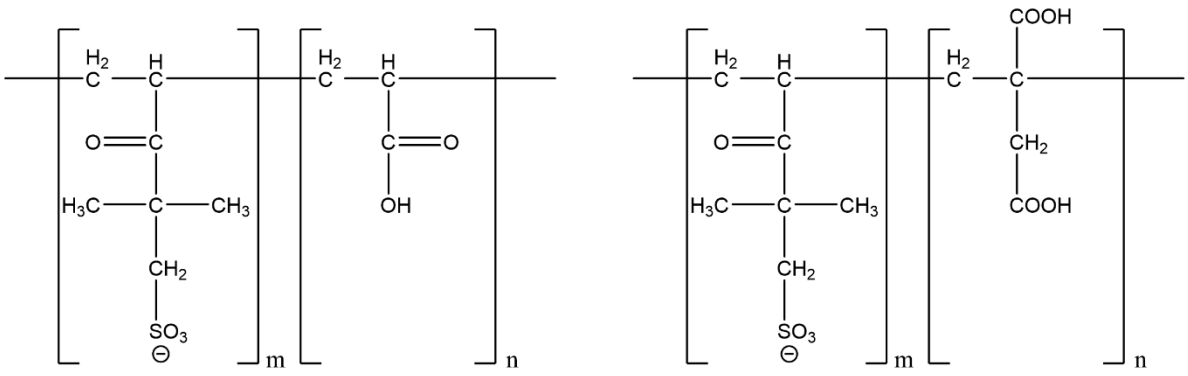

Figure 18: Molecular structures of retarder co-polymers synthesized from AMPS and acrylic acid (left) and AMPS and itaconic acid (right).

3.2.2.1. Accelerating admixtures for cement hydration and mode of action

Accelerating admixtures for cement can be generally divided into set accelerating and hardening accelerating admixtures which are defined as follows:[118]

- Set accelerators are defined as admixtures which decrease the time to commencement of the transition from the plastic state to stiffness of a concrete mix.
- Hardening accelerators are admixtures that are used in concrete mixtures to increase the rate of cement hydration and thus development of early strength of concrete with or without affecting the setting time.

While accelerators affecting simply the setting of mortars or concretes find only limited application in practice, like e.g. for plugging of water leaks in tunnels or basements, the latter group of admixtures is of special importance for concreting in cold climate conditions and pre-cast concrete fabrication. But especially nowadays, where the use of blended cements becomes more and more common to reduce CO_2 emission during cement clinker production, hardening accelerators are needed more than ever. Generally, the effect of setting and hardening accelerators is strongly depending on the composition of the cement used. Thus, there is a variety of these admixtures ranging from soluble inorganic salts like e.g. halogenides, nitrates, silicates and aluminates, to organic salts like calcium formate or acetate and organic compounds like triethanolamine (TEA) or triisopropanolamine (TIPA).[13, 107, 119-120] Amines are usually used in combination with other accelerators and only rarely as a single admixture.

Setting accelerators are usually alkalis which promote the dissolution of the silicate and aluminate phase by interfering with the C_3A-gypsum reaction.[107] Accelerators for hardening alter the rate of hydration of the C_3S phase, leading to increased formation of C-S-H phases during early hydration. It was found that inorganic salts are most effective in acceleration of the C_3S dissolution. A screening revealed that the kind of both, anion and cation, plays a significant role. There accelerating ability decreases in the following order:[29, 121]

Anions: $Br^- \approx Cl^- > SCN^- > I^- > NO_3^- > ClO_4^-$

Cations: $Ca^{2+} > Sr^{2+} > Ba^{2+} > Li^+ > K^+ > Na^+ \approx Cs^+ > Rb^+$

This study clearly suggests that calcium chloride is an effective hardening accelerator. Indeed, it has been the most commonly used accelerator over decades, because of its good availability, high efficiency and low cost. Calcium chloride is known to accelerate both the hydration of C_3S as well as the reaction between C_3A and $CaSO_4 \cdot 2\ H_2O$.[122-124] This leads to the formation of increased amounts of C-S-H phases, $Ca(OH)_2$ and ettringite which contribute to a denser microstructure and thus increase compressive and flexural strengths. The acceleration of C_2S during the early hydration was found to be quite minor compared to that of C_3S.[119] While all these observations where made on pure pastes of the clinkers, the accelerating mechanism in the Portland cement system is yet not fully understood. Still, it is proposed that the C_3S phase is most affected by the presence of $CaCl_2$. Between C_3A and $CaCl_2$, no reaction during the early hydration was found in the presence of gypsum. Only after complete reaction to ettringite, the so-called Friedel's salt, a calcium hydrochloroaluminate ($3\ CaO \cdot Al_2O_3 \cdot CaCl_2 \cdot 10\ H_2O$) was detected. However, the reaction between C_3A and gypsum appears to be accelerated by the presence of $CaCl_2$ and the following reaction sequence is suggested:[107, 123]

First, complete reaction of C_3A to ettringite takes place, without any consumption of $CaCl_2$:

$$C_3A + 3\ CaSO_4 + 32\ H_2O \rightarrow C_3A \cdot 3\ CaSO_4 \cdot 32\ H_2O \qquad \text{Equ. (12)}$$

As soon as gypsum and other sulfate sources are consumed the reaction of $CaCl_2$ and C_3A to Friedel's salt takes place:

$$CaCl_2 + C_3A + 10\ H_2O \rightarrow C_3A \cdot CaCl_2 \cdot 10\ H_2O \qquad \text{Equ. (13)}$$

Upon consumption of $CaCl_2$, transformation of ettringite to monosulfate occurs:

$$C_3A \cdot 3\ CaSO_4 \cdot 32\ H_2O + 2\ C_3A \cdot Ca(OH)_2 \cdot 12\ H_2O \rightarrow$$
$$3\ C_3A \cdot CaSO_4 \cdot 12\ H_2O + 20\ H_2O + 2\ Ca(OH)_2 \qquad \text{Equ. (14)}$$

Furthermore, it has been shown that the presence of $CaCl_2$ leads to a higher surface area of cement pastes and a reduced porosity of mortars.[119] However, salts of chlorides were found to promote the risk of corrosion of steel bars in reinforced concrete which led to a ban of this

admixture. This finding renewed the interest for new efficient chloride-free hardening accelerators.

Calcium formate, calcium nitrate/nitrite and TEA were found to be suitable chloride-free replacements as setting-accelerators.[14, 125] While calcium nitrate only accelerates setting and as a result leads to a minor strength increase, the other two calcium salts and TEA have also been found to be good hardening accelerators for concrete.[107, 118, 125] In pure C_3S pastes, $Ca(HCOO)_2$ and $Ca(NO_2)_2$ increase the degree of hydration, but less effective than $CaCl_2$.[118] It was proposed that the small formate ions can diffuse through the precipitated layers covering C_3S and C_2S particles and thus accelerate dissolution of the silicate phases and consequently precipitation of $Ca(OH)_2$.[14, 126] For calcium nitrites, reports on the mode of action are lacking despite its widespread use, but based on its rather good solubility a similar accelerating mechanism than for nitrate can be assumed. Despite its high effectiveness and low cost, it suffers one big disadvantage compared to other admixtures, namely its toxicity.

Triethanolamine has been commonly used, especially in combinations with other accelerators, as TEA solely accelerates C_3A dissolution by interaction with aluminium and can even retard C_3S dissolution at dosages above 0.5 % bwoc.[13, 107] Thus, mixtures of calcium nitrate and TEA or TIPA were investigated and have proven to be good accelerators for the development of early strength and shortening of the setting time.[13]

The development of chloride-free accelerating admixtures with favorable cost/performance ratio is still a challenge.[118] More recently, seeding materials like C-S-H nanoparticles and Ca-Al-LDHs have gained much attention for the application as hardening accelerators. The addition of seeding materials is supposed to lower the energy barrier of the formation of cement hydration products which accelerates their precipitation and thus furthers dissolution of the cement clinker (more details on the mechanism of nucleation and crystal growth are described in section 3.3.).[127-128] *Xu* et al. have investigated Ca_2Al-Cl-LDHs as admixtures to increase the development of early strength of cement by acceleration of the C_3A hydration. It was found that dosages between 1 – 5 % bwoc led to an increase of compressive strength of up to 70 % within the first 24 hours. The increase in strength development decreases over time and final strength after 28 days of mortars comprising this admixture is comparable to neat mortar

formulations.[120] XRD analysis revealed further an increased amount of C-S-H gel present in the mortars comprising Ca_2Al-Cl-LDH as admixture. As it is rather unlikely that the hexagonal calcium aluminate hydrate acts as nucleation site for the disordered C-S-H gel, *Xu* et al. proposed a similar mechanism for the acceleration of the Ca_2Al-Cl-LDH like for $CaCl_2$, namely by diffusion of the chloride anions through the semi-permeable layer blocking C_3S dissolution. This mechanism requires an anion exchange of the intercalated chloride ions by e.g. sulfate ions present in the cement pore solution. Because free chloride ions can induce corrosion of steel, this type of accelerator is not suitable for application in reinforced concrete.

C-S-H nanoparticles, on the other hand, have shown to increase not only the early strength of mortars after 16 h up to 80 % already at dosages of 0.35 % bwoc, but also provide increased final strength which is rather uncommon for accelerators.[35, 129-131] Furthermore, it has been reported that C-S-H nanoparticles can increase the development of early strength of cements blended with fly ash, slag or calcined clay. Here, acceleration of the pozzolanic reaction by formation of increased amounts of portlandite and hemicarbonate were found.[130, 132] C-S-H nanoseeds can be synthesized via different methods: The synthesis by co-precipitation from calcium salts and sodium metasilicate is probably the most common method, but also syntheses via pozzolanic reaction between $Ca(OH)_2$ and SiO_2 and by a sol-gel approach have been reported. *BASF* has introduced polymer-stabilized C-S-H seeds into the market under the tradename *X-Seed*® in 2011.[133-134]

3.3. Nucleation und Crystal growth

The formation of a crystal is based on two essential steps. In the first, most critical step, a stable nucleus needs to be formed which involves physical as well as chemical processes. Physical processes during nucleation comprise e.g. crystallization and condensation processes or phase transitions in a solid phase etc. Chemical processes include heterogeneous reactions, for example.[135] In the second step, the stable nucleus grows to a crystal involving transportation processes of building units to the growth sites and connection of these units to the nucleus or crystal, respectively.

3.3.1. Nucleation

Nucleation is defined as the series of atomic or molecular processes by which the atoms or molecules of a reactant phase rearrange into a cluster of the product phase large enough as to have the ability to grow irreversibly to a macroscopically larger size.[136] The cluster is defined as "nucleus" or, if the above mentioned critical size is reached, a "critical nucleus". This arrangement of atoms or molecules can occur via two different pathways, namely primary and secondary nucleation. When primary nucleation occurs spontaneously from a liquid phase (solution or melt) or a gas phase, then the nucleation mechanism is called homogeneous. If nucleation is initiated by foreign particles, the nucleation is called heterogeneous. Secondary nucleation, on the other hand, is induced by crystals of the same substance and is especially applied in industrial processes.[135]

3.3.1.1. Homogeneous nucleation

The pre-requisite or driving force, respectively, for nucleation is supersaturation which is defined as the difference in chemical potential of a molecule in solution and that in the bulk of a crystal phase.[136] In homogeneous supersaturated solutions, nuclei of a new phase appear randomly and will decompose again until a nucleus reaches sufficient energy to form a stable new phase, the so-called "critical nuclei". The formation of a critical nucleus involves basically changes of two types of enthalpies: ΔG_1, representing the volume energy of the new phase, and ΔG_2, the surface energy which results from the built-up interface due to the growing of the nuclei:[135]

$$\Delta G = \Delta G_1 + \Delta G_2 \qquad \text{Equ. (15)}$$

Here, the overall volume energy ΔG_1 is negative, because the free enthalpy is lowered compared to the initial state. This relates to the reduction in entropy when a transition from an unstable state, e.g. from a liquid or gas phase to a stable, solid state occurs. Assuming a spherical droplet, ΔG_1 and ΔG_2 can be expressed as follows:[135-136]

$$\Delta G_1 = - (4\pi r^3 / 3V_m) \Delta\mu \qquad \text{Equ. (16)}$$

where V_m is the molecular volume and r the radius of the droplet and μ the chemical potential

$$\Delta G_2 = 4\pi r^2\sigma \qquad \text{Equ. (17)}$$

where σ is the surface tension of the infinitely large liquid

Combining the above equations, we get for ΔG:

$$\Delta G = -(4\pi r^3 / 3V_m)\,\Delta\mu + 4\pi r^2\sigma \qquad \text{Equ. (18)}$$

The surface of the initial nucleus is generally significantly higher than its volume, owed to its small size. Hence, the surface energy is the decisive component when it comes to the overall change in free enthalpy during formation of a nucleus.[135-136]

The relation between the surface energy and the volume energy, respectively, and the radius of a nucleus are schematically represented in **Figure 19**.

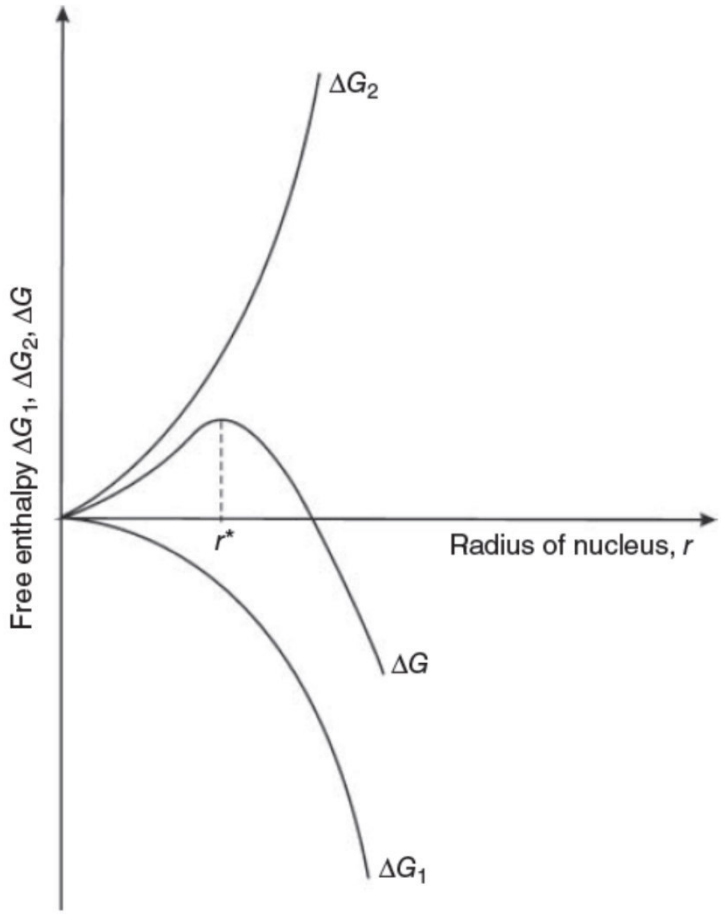

Figure 19: Free enthalpy as a function of the radius of a nucleus. ΔG = total free enthalpy, ΔG_1 = volume energy and ΔG_2 = surface energy.[135]

The total free enthalpy ΔG increases with increasing radius of the nucleus until a maximum value r* is reached. Nuclei with a size below a radius of r* are unstable and will decompose again. Those nuclei, so-called “critical nuclei”, obtaining a radius r > r* are stable and can grow, as the total free enthalpy decreases.

The value for r* can be expressed as follows:

$$r^* = 2\sigma V / \Delta\mu \qquad \text{Equ. (19)}$$

It was found that the critical radius for nucleation r* (and the value for ΔG*) decreases with increasing supersaturation, i.e. the probability that nucleation occurs in a given system increases the higher the supersaturation within the system.[136-137]

The rate of nucleation which is defined as the number of nuclei formed per unit time per unit volume can be expressed by considering the Arrhenius equation:[136]

$$J = A \exp(-\Delta G^*/kT) \qquad \text{Equ. (20)}$$

where A is depending on the degree of supersaturation

By plotting J versus the supersaturation (see **Figure 20**) it can be seen that the rate of nucleation is basically zero until a critical degree of supersaturation is reached, where a strong increase in the rate of nucleation occurs.

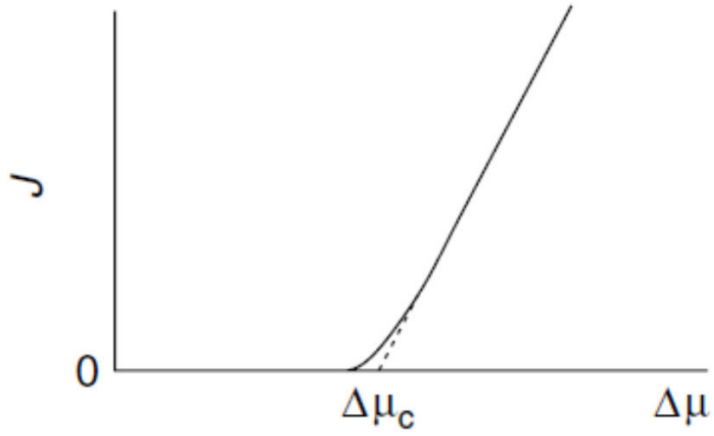

Figure 20: Nucleation rate as a function of supersaturation ($\Delta\mu_c$ indicating critical supersaturation).[136]

As a consequence, the degree of supersaturation is decisive for the number of nuclei formed. At low supersaturation, less nuclei are formed than at high supersaturation.

3.3.1.2. Heterogeneous nucleation

In contrast to homogeneous nucleation, formation of nuclei via heterogeneous nucleation takes place on a substrate. Such substrates can be reactor walls or impurity particles during the course of homogeneous nucleation or special substrate crystals. As can be seen from equations 18 and 19, both ΔG^* and r^* strongly depend on the surface tension σ. It was further shown that foreign substrates lead to a decrease in σ and thus to a decrease of r^* and subsequently of ΔG^* at constant supersaturation.[137] This means that in the presence of a foreign substrate, nucleation is more favourable as the surface free energy is reduced. Moreover, the value of critical supersaturation is depending on σ, too. Hence, a decrease in σ leads to a decrease in $\Delta\mu_c$ which determines the beginning of the exponential increase in the rate of nucleation. Consequently, at low supersaturation conditions heterogeneous nucleation is more viable than homogeneous nucleation.[136] When the best match between the nucleus and the foreign substrate is achieved, the reduction in surface tension will be the highest. This state only occurs when both the foreign substrate and the crystallizing nucleus are the same which is referred to as secondary nucleation. [136]

Finally, during crystallization from a supersaturated solution always both pathways, homogeneous and heterogeneous nucleation, will occur. The influence of impurities can be reduced by strict control of the cleanliness of the reactor vessel and purity of the raw materials, but heterogeneous nucleation on reactor walls will always occur under normal gravity. In cementitious systems, where crystallization from a supersaturated solution occurs, of course both homogeneous and heterogeneous nucleation take place. The different clinker phases dissolve and very fast the first nuclei form in the supersaturated cement pore solution and crystals of the various cement hydrate phases precipitate. Thus, critical nuclei can be formed on already existing crystals of the same hydrate phase, on different hydrate phases or on the unhydrated cement grains that are still present in the pore solution, too. The detailed mechanism is still unknown yet. The *Johnson-Mehl-Avrami-Kolmogorov* (JMAK) model

assumes that nuclei are randomly distributed throughout the pore solution, while recent findings suggest that nucleation primarily occurs on cement particles. The latter model is mostly referred to as the BNG model (boundary nucleation and growth).[138-139]

3.3.2. Crystal growth

Upon formation of a critical nucleus, the following step according to the classical crystallization theory is growth of the nucleus to a macroscopic crystal. As previously mentioned, this occurs via transportation of growth units, e.g. atoms, ions or molecules to the crystal sites and attachment of the units onto the existing crystal. The first process is the transport process and the latter process is called surface process. The rate of crystal growth is determined by the slowest process and can thus be either transport-controlled or surface-controlled.[136]

3.3.2.1. Attachment of growth units

Models for crystal growth, i.e. for the attachment of growth units to an existing crystal, are based on considerations of the crystal surface and the various types of surface sites, like e.g. smooth surface, edges, defects, etc. Probably the most commonly used model provided by *Volmer*, *Kossel* and *Stranski* assumes that the crystal surface consists of cubic units that form layers of monoatomic height and that the different surface sites have distinct binding energies.[140-142] Calculation of these site-specific binding energies required the following three assumptions:[135]

- The crystal is surrounded by a nutrient, a melt, a solution, or a vapour phase.
- The crystal does not comprise any impurities nor exhibit lattice defects.
- The forces between the atoms are Coulomb forces for ions and van der Waals forces for homopolar crystals.

Figure 21 depicts the possible processes involved in *Kossel*'s model of crystal growth and shows the corresponding binding energies:

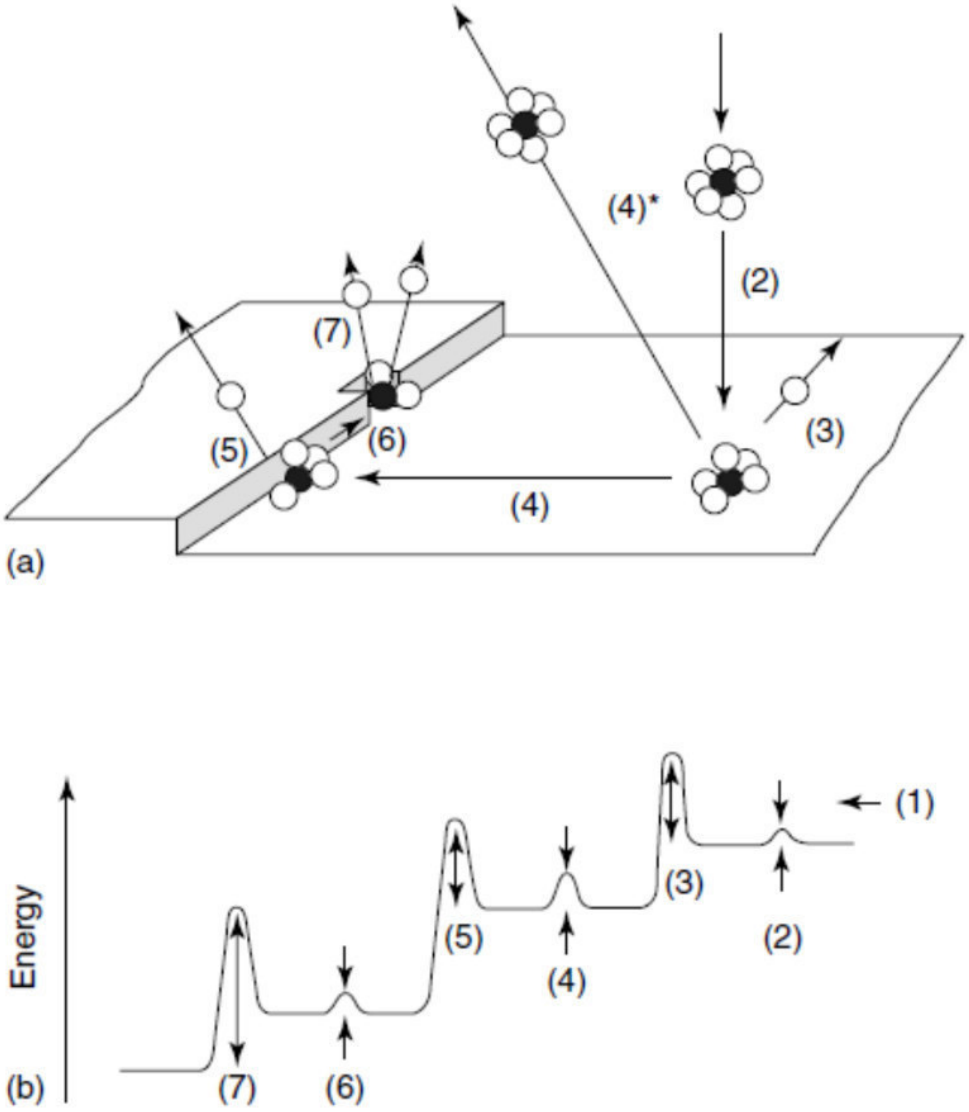

Figure 21: **(a)** Schematic representation of processes involved in the crystal growth: (1) Transport of solute to a position near the crystal surface; (2) diffusion through boundary layer; (3) adsorption on crystal surface; (4) diffusion over surface; (4*) desorption from the surface; (5) attachment to a step or edge; (6) diffusion along the step or edge; (7) incorporation into a kink site or step vacancy. **(b)** Associated energy changes for the processes depicted in (a).[136]

According to this model, growth units attached to the plain surface, also referred to as terrace, form one bond to the crystal, units attached to steps and kinks will form two and three bonds. Thus, kink sites offer the most stable configuration, but also require the most energy.[136] Growth can generally proceed by layer-growth according to *Kossel*'s model, but depending on the

surface roughness which correlates with the degree of supersaturation, it can also proceed via spiral or interlaced spiral growth, birth and spread growth or adhesive growth.[135-136]

3.3.2.2. Transportation of growth units

For the attachment of growth units as described within section 3.3.2.1., transportation of the growth units from the nutrient or bulk solution to the boundary zone between the crystal and the liquid phase is necessary. Transportation in liquid phases can occur via *Brownian* motion or by convection. For convective flows within nutrients many different origins have been identified, like e.g. *Buoyancy*-driven convection can be caused by either gradients in temperature or concentration in the nutrient. Differences in temperature and concentration within the liquid phase can subsequently trigger *Marangoni* convection which is driven by gradients in the surface tension at liquid/liquid or liquid/gas interfaces. Other artificially introduced forces that may lead to convection are e.g. rotation of the crystal, electrodynamic convection, external magnetic fields or vibrational convection.[135]

The diffusion of growth units through the boundary layer requires a certain amount of energy, as depicted in **Figure 21**. This energy constitutes of the enthalpy for the phase transition, e.g. sublimation or melting, and the kinetic barrier of the incorporation of the growth unit into the crystal.[135] The kinetic barrier is dependent on the type of the ambient medium (vapour, solution, melt).

3.3.3. Classical nucleation theory vs. crystallization by particle attachment

Nucleation and crystal growth as described in the previous sections all refer to the classical nucleation theory and the so-called terrace-ledge-kink model of crystal growth which was proposed at the beginning of the 20th century. Again, crystallization requires the formation of a nucleus by addition of precritical clusters (that are considered unstable) where the volume energy of the nucleus overcomes the unfavourable surface energy. This type of nucleus is referred to as critical or postcritical nucleus. As soon as such a postcritical nucleus exists,

crystal growth proceeds until a macroscopic crystal is formed. Although this theory is based on monomer-to-monomer additions of rather simple chemical species, it is still viable to successfully describe more complex crystallizations like e.g. *Giuffre*'s study on polysaccharides controlling calcite nucleation or *Petsev*'s investigation of the crystallization of ferritin and apoferritin, two proteins possessing identical shells but having different molecular masses.[143-144]

However, until today, several phenomena have been reported that could not be explained satisfactorily by the classical crystallization pathway. For example, the microstructure and habits of biomineral crystals, the unusual mineralogical and textural patterns of many minerals or the nucleation of amorphous phases that nucleate at concentrations far below those predicted by the classical theory.[145-147] Recent studies have proposed the role of stable clusters in nucleation.[148-149] This concept was confirmed by *Gebauer* et al. who were able to detect the presence of stable precritical clusters with approximately 2 nm diameter before nucleation of calcium carbonate commenced and suggested that they grow by coalescence.[150] Similar pathways were found for the crystallization of the biominerals calcium phosphate and calcium oxalate.

According to the new cluster theory which is meanwhile referred to as non-classical crystallization or crystallization by particle attachment (CPA), precritical clusters are formed out of atoms, ions or molecules. These precritical clusters aggregate and form thus a postcritical nucleus that does not necessarily possess a crystalline structure, but can be of amorphous nature. Over time, a crystalline phase forms within the postcritical nucleus and finally the crystalline phase grows to a bulk crystal (see **Figure 22**).

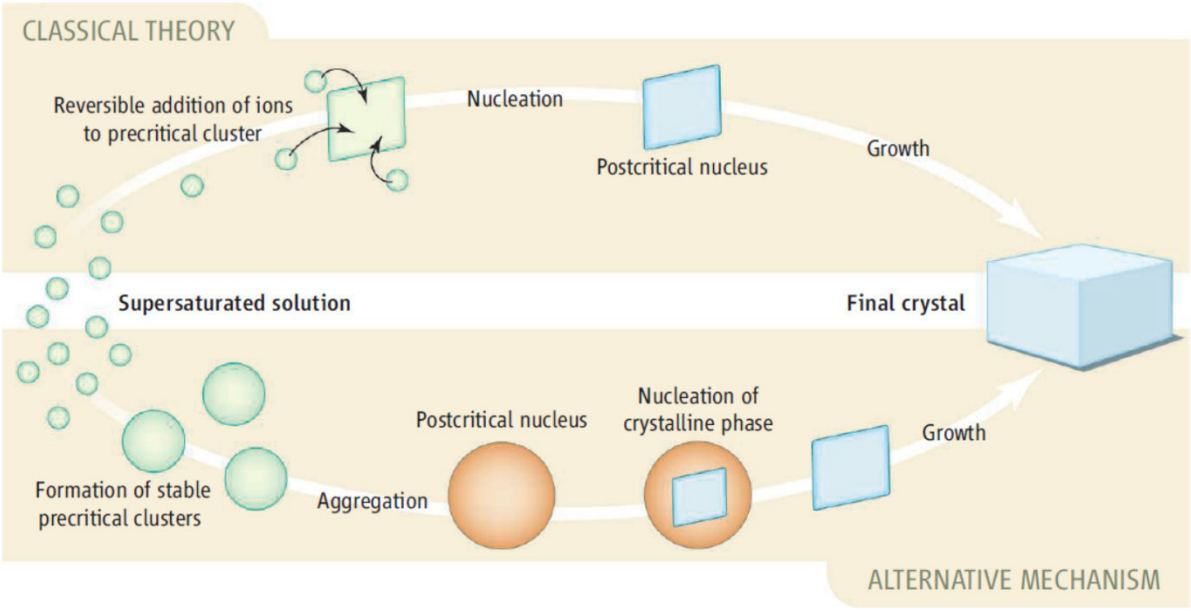

Figure 22: Schematic representation of the fundamental differences in crystallization via the classical theory vs. the new alternative mechanism via particle attachment.[151]

The precritical clusters were found to be not limited to a specific structure, but can exhibit many different unique morphologies like multi-ion complexes, oligomers, nanoparticles of liquid, amorphous or crystalline character or even small nanocrystals (see **Figure 23**). To include all these different types, the precritical clusters are nowadays more broadly defined as particles or precursors.[5]

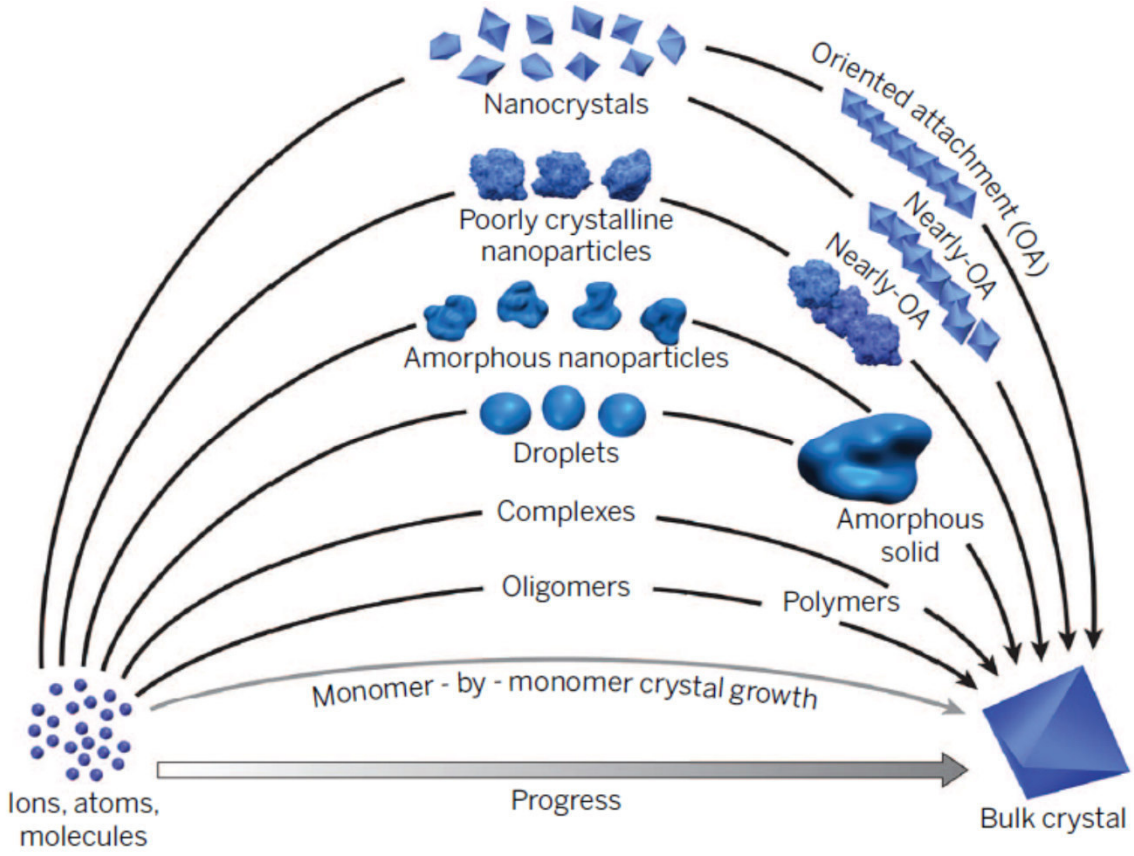

Figure 23: Schematic illustration of different types of precritical clusters according to the non-classical crystallization theory.[5]

Nucleation of these particles is, in contrast to the classical theory, not necessarily governed by the degree of supersaturation. According to the classical theory, in the presence of low supersaturation the free-energy barrier is relatively high and thus the generation of a critical nucleus is quite rare. Consequently, the probability that a critical nucleus formed will meet another nucleus is low and growth will most likely follow the pathway of monomer-by-monomer addition of the classical theory. With increasing supersaturation, the free-energy barrier decreases, and precursors are formed in higher amount. These can then grow (or shrink) by exchanging monomers with other particles or through occasional collision or coalescence events. In the case where the degree of supersaturation reaches the point at which the free-energy barrier is equal to the thermal energy (k_BT), the solution undergoes spinodal decomposition and an abundance of particles will evolve, and crystal growth is dominated by collision and coalescence with other particles. The free-energy landscape as described by the classical theory does not exhibit any features that would explain the existence of multiple particles during nucleation.[5]

The non-classical crystallization theory states that variations of the free-energy barrier depend on the shape and magnitude of particles. This allows formation of particles of particular sizes or morphologies that are thermodynamically favoured if a local minima in the free-energy landscape is present.[5]

Another very interesting type of complex assembly pathway is the formation of thermodynamically metastable bulk phases which are subsequently replaced by more stable phases.[147] Here, a metastable solid phase nucleates because it is thermodynamically favoured considering its lower free-energy barrier compared to the nucleation of the stable phase. Nucleation of the stable phase occurs then either heterogeneously on or in the metastable solid phase or via a homogeneous mechanism in the surrounding solution. This leads subsequently to dissolution or recrystallization of the metastable phase into the stable phase. This pathway is generally referred to as the *Ostwald-Lussac* rule of stages or the *Ostwald* step rule.[5] This has often been reported for the calcium carbonate system.[152-154] There, nucleation of amorphous nanoparticles that are initially hydrated occurs. These nanoparticles are stable in bulk in dry conditions, but start to crystallize under humid conditions or upon heating with the release of water.[152]

Until today, there are still only very few examples known where the formation of such stable precursors have been unequivocally demonstrated and most of the investigations on CPA are based on observations of crystals that have already passed the transformation from the solvated state to the crystalline phase.[5]

The post-nucleation growth of nuclei formed by CPA differs also to a certain extent from the classical theory. Growth of particles can occur, for example, via *Ostwald* ripening, molecular attachment, cluster attachment, amorphous addition, oriented attachment or recrystallization. Whether CPA dominates over monomer-by-monomer addition is dependent on numerous factors associated with the free-energy landscape and the kinetics of the system. While monomer-by-monomer addition is governed by *Brownian* movement and *van der Waals* forces, for inorganic nanoparticles in close proximity *Coulombic* and *Lewis* acid/base interactions predominate, thereby guiding the interacting particles to find energetically favourable crystallographic orientations for attachment.[5]

While the non-classical nucleation theory is viable to provide explanations for different phenomena that go beyond the classical theory, there are still many open questions regarding the nanoscale physics and chemistry at the interface zone between particles that control alignment and attachment. Moreover, the size dependency of surface energy, solvation energy and phase stability is still unknown.[5] With today's limitations, mainly in analytics but also in modelling, a competitive pathway of both nucleation and growth theories cannot be outruled and both theories have to be considered when crystallization of a material is investigated.

3.3.4. Crystal growth in the absence of gravity

In order to describe the impact of the absence of gravity on crystal growth, the main aspects of nucleation and crystal growth are briefly summed up:

- Nucleation is initiated by supersaturation.

- The higher the degree of supersaturation, the more nuclei are formed.

- Crystal growth consists of two steps: transportation of growth units from the bulk solution through *Brownian* movement, convection or electrostatic interactions to the crystal surface and attachment of the growth unit to the crystal surface.

- With increasing supersaturation of the nutrient, the growth rate increases.

Based on the rather limited amount of experiments performed in the absence of gravity compared to terrestrial crystallization experiments, many processes are still unclear until today. In the following, the main observations during crystallization in the absence of gravity and their consequence are summed up.

In the absence of gravity or in the state of microgravity, convection in the solution is supressed. This limits mass and heat transport within a solution mainly to *Brownian* movement, i.e. crystallization under microgravity conditions will be diffusion-controlled. Crystallization of

calcium phosphate in microgravity by *Lundager Madsen* et al. revealed strong supersaturation gradients in the solution which are most likely a consequence of the limited mass transport.[155] Furthermore, the elimination of flow-induced hydrodynamic forces which may cover weak mechanical forces acting on and between growing crystallites are eliminated.[156]

These observations lead to the conclusion that nucleation will not occur randomly throughout the solution, but locally where high supersaturation is given. Moreover, the absence of convection will lead to a transport-controlled crystal growth which will subsequently be the rate determining step during crystallization processes in the absence of gravity. At this point it has to be mentioned that most of the previous experiments regarding the crystallization of inorganic crystals under micro or zero gravity conditions are rather contradictory. For example, *Lundager Madsen* et al. performed crystallization of hydroxy apatite (HAP) in a long-term experiment from solutions of $CaCl_2$ and KH_2PO_4/K_2HPO_4 over the period of five months. The crystals obtained from the 0 *g* experiment were bigger in size compared to those from a comparable terrestrial experiment. This was attributed to the high supersaturation gradients which at first lead to less nuclei, but allow controlled growth of crystals in the low supersaturated areas over this long period.[155, 157] Crystallization experiments with various inorganic salts, e.g. $BaSO_4$, $Mn(OH)_2$ and $Hg(Cl)_2$, by *Frates* et al. on a space shuttle mission resulted in smaller crystals under 0 *g* compared to those under 1 *g*. Besides, differences in the morphologies of the crystals were found.[158] Further examples for crystallization experiments in the absence of gravity can be found elsewhere.[159] While most of the previous experiments were performed by mixing of two aqueous solutions, there are only a few reports (see section 3.1.3.2.) on cement hydration where a solid is combined with an aqueous solution and thus supersaturation is supplied by dissolution of the solid prior to nucleation. Additionally, the influence of organic additives, i.e. of polyelectrolytes, during crystallization of an inorganic material leaves still many open questions. This work shall give more insight into the early nucleation and crystallization processes occurring in the absence and presence of convection and admixtures.

4. Materials and Methods

4.1. Materials

4.1.1. Cements and clinker phases

Within this work, following commercial cement samples were used: API Class G (Lengerich plant) manufactured by Dyckerhoff (Wiesbaden) while CEM I 32.5 R (Rohrdorf plant) and CEM I 52.5 N (Milke ® "Classic", Geseke plant) were supplied by HeidelbergCement AG (Heidelberg). CEM I 42.5 R (Allmendingen plant) was manufactured by SchwenkZement KG (Ulm). Following, the composition of the different commercial OPC samples are displayed:

Table 1: Phase composition of the commercial CEM I samples, as determined by quantitative XRD analysis using *Rietveld* refinement.

Phases	**API Class G**	**CEM I 32.5 R**	**CEM I 42.5 R**	**CEM I 52.5 N**
C_3S, m	59.30	53.93	58.83	53.95
C_2S, m	19.50	16.69	17.01	26.54
C_3A, c	0.30	5.12	3.61	3.26
C_3A, o	1.40	4.73	1.60	4.24
C_4AF, o	14.10	8.57	9.43	2.44
Free lime, *Franke*	0.10	-	0.09	0.36
Free lime, *Rietveld*	0.10	0.97	0.06	0.14
Periclase	-	2.06	0.66	0.03
Anhydrite	-	2.15	1.83	2.63
Hemihydrate *	0.20	2.00	0.27	1.20
Dihydrate *	4.60	-	2.42	0.03
Calcite	0.40	3.04	2.80	3.59
Quartz	0.10	0.90	0.36	1.16
Arcanite	-	0.80	1.04	0.46
Sum	**100.10**	**100.97**	**100,02**	**100,04**

* determined via thermogravimetry

The aluminate phases C_3A (cubic) and C_4AF (orthorhombic, $Ca_2Al_xFe_{1-x}$ with x = 0.5 (idealized)) were synthesized as described elsewhere.[160] The raw materials $CaCO_3$ (ACS reagent, > 99.0 %) and Fe_2O_3 (> 99.995 % trace metal basis) were purchased from Merck KGaA (Darmstadt, Germany) and Al_2O_3 (> 99.9 % metals basis) from Alfa-Aesar (Karlsruhe, Germany).

For the blends of C_3A (cubic) and C_4AF (orthorhombic), $CaSO_4 \cdot ½\ H_2O$ (purum, > 98 %) purchased from Merck KGaA (Darmstadt, Germany) and $CaSO_4 \cdot 2\ H_2O$ (99 %) from Alfa Aesar (Karlsruhe, Germany) were used. The blends consisted of a mixture of 80 wt.-% aluminate phase (C_3A_C or C_4AF, respectively), 15 wt.-% $CaSO_4 \cdot ½\ H_2O$ and 5 wt.-% $CaSO_4 \cdot 2\ H_2O$.

4.1.2. Polycarboxylate ethers

Different PCE superplasticizers were used to study their effect on nucleation and crystal growth. Basically, three different types of PCEs were used, namely methacrylate ester (MPEG) based, isoprenyl ether (IPEG) based and allyl ether (APEG) based PCEs. For MPEG- and IPEG-PCEs the first number in the nomenclature represents the number of ethylene oxide (EO) units in the side chain, while the second number refers to the molar ratio of the acrylic or methacrylic acid monomer to the polyglycol macromonomer. For example, MPEG-23PC6 has 23 repeating EO units in the side chain and a molar ratio of methacrylic acid to methacrylate ester macromonomer of 6:1. All polymers were synthesized via aqueous free radical co-polymerization as described in the literature.[161] The molecular structure of the different types of PCEs and their compositions are displayed in **Figure 24**.

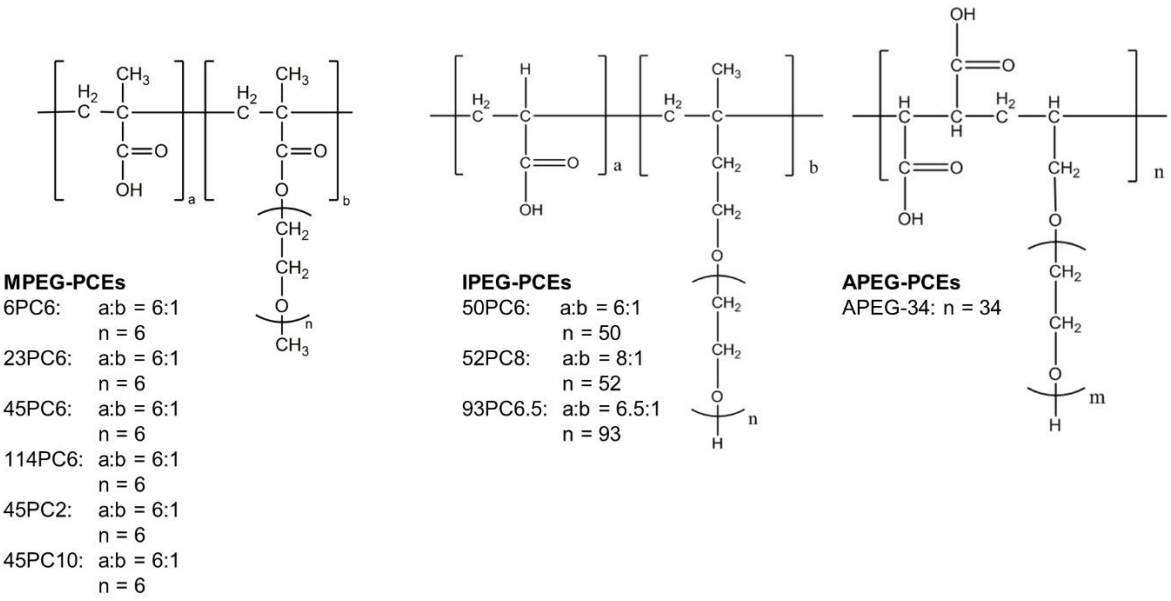

Figure 24: Molecular structures of the PCE samples used in this study. MPEG-based PCE (left), IPEG-based PCE (mid), APEG-based PCE (right).

The novel phosphate comb polymer MPEG-45PC-P3 was synthesized from 2-(methacryloyloxy)ethylphosphate (HEMAP) and MPEG-ester macromonomer in the molar ratio 3:1 as described elsewhere.[93] The obtained comb polymer possessed an actual ratio of HEMAP : MPEG macromonomer of 1.5:1.

The synthesized polymers were characterized by gel permeation chromatography (GPC) with a *Waters 2695* separation module possessing a refracturing index detector (2414 RI, Waters, Eschborn) and a three-angle light scattering detector (Dawn EOS, Wyatt Technology, Santa Barbara, USA). The specific anionic charge density of the polymers was determined by polyelectrolyte titration in a streaming current charge detector (Mütek Analytic PCD 03 pH) at pH 12.5 (adjusted with NaOH). The molecular properties of the different PCEs used are summed up in **Table 2**.

Table 2: Molecular properties of the different PCE superplasticizers.

Superplasticizer sample	Conversion of macromonomer [%]	M_w [g mol^{-1}]	M_n [g mol^{-1}]	PDI (M_w/M_n)	Specific anionic charge amount @ pH = 12.5 [µeq g^{-1}]
MPEG-6PC6	96	15.600	6.500	2.4	4.900
MPEG-23PC6	93	24.000	11.900	2.3	4.200
MPEG-45PC6	90	28.500	16.000	1.8	3.600
MPEG-114PC6	89	69.800	36.300	1.9	1.000
MPEG-45PC2	89	30.500	18.000	1.7	1.500
MPEG-45PC10	90	18.900	10.600	1.8	5.000
IPEG-50PC6	84	99.800	38.400	2.6	3.000
IPEG-52PC8	87	24.000	12.000	2.0	3.200
IPEG-93PC6.5	100	33.100	13.100	2.5	2.100
APEG-34	83	60.000	20.000	3.0	1.700
MPEG-45PC-P3	100	62.800	32.200	1.9	1.630

4.1.3. Polycondensates

As melamine-based polycondensate sample Melment® F10 and as naphthalene-based polycondensate sample Melcret® 500F was used, both were purchased from BASF Construction Polymers GmbH (Trostberg, Germany). The acetone-formaldehyde-sulfite polycondensate was synthesized as described elsewhere.[162]

The specific anionic charge amount of the polycondensates was determined by polyelectrolyte titration in a streaming current charge detector (Mütek Analytic PCD 03 pH) in synthetic cement pore solution (SCPS).[163]

Table 3: Specific anionic charge amounts of polycondensate superplasticizer samples.

	MFS	BNS	AFS
Specific anionic charge amount in SCPS [µeq g^{-1}]	1980	2530	4060

4.1.4. Retarding admixtures

The retarders SCR-100™, a co-polymer based on acrylic acid (AA) and 2-acrylamido-2-methylpropane sulfonic acid (AMPS) with a molar ratio of 1:1, and the retarder SCR-500™, a co-polymer of itaconic acid (IA) and AMPS in the molar ratio 0.32:1, were purchased from Halliburton.

Both retarders were characterized analogous to the PCEs as described in chapter 4.1.2. The molecular properties of these co-polymers are summarized in **Table 4**. **Figure 25** displays the molecular structures of the two co-polymers.

Table 4: Molecular properties of the two retarder polymers studied.

Retarder sample	M_w [g mol^{-1}]	M_n [g mol^{-1}]	PDI (M_w/M_n)	Specific anionic charge amount @ pH = 12.5 [µeq g^{-1}]
AA/AMPS co-polymer	73.000	46.000	1.6	8.100
IA/AMPS co-polymer	180.000	110.000	1.6	4.200

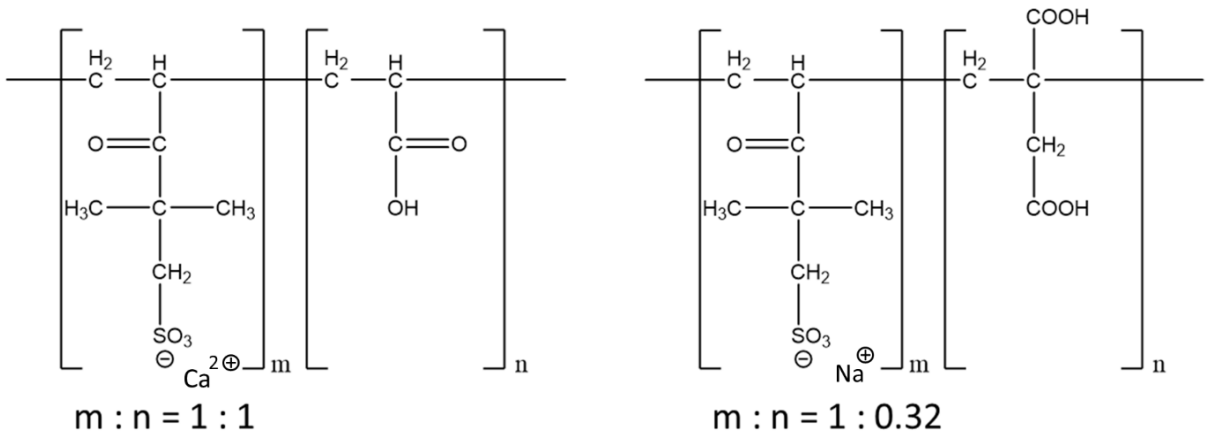

Figure 25: Molecular structures of the retarder co-polymers AMPS-co-acrylic acid (left) and AMPS-co-itaconic acid (right).

4.2. Experimental methods

Within this work, Layered Double Hydroxides were synthesized via two different routes: Rehydration and co-precipitation. Ca_2Al-retarder-LDHs were exclusively prepared via rehydration of cubic tricalcium aluminate (C_3A_C) in the presence of the co-polymers while Ca_2Al-formate-LDH was prepared via rehydration and co-precipitation.

4.2.1. Synthesis of Ca_2Al-retarder-LDHs via rehydration

In a typical synthesis, 1.3 g of the co-polymer were dissolved in 100 mL of decarbonized water and stirred under nitrogen for 2 hours to degas. After addition of 1 g C_3A_C, the suspension was stirred for 48 h in an ice bath under nitrogen atmosphere. The product was recovered by centrifugation, washed with decarbonized water and freeze-dried under vacuum.

4.2.2. Synthesis of Ca_2Al-formate-LDH via rehydration

For the synthesis via rehydration, 100 mL of decarbonized water were stirred under nitrogen for 2 hours to degas. After addition of 0.767 g of $Ca(HCOO)_2$ (BioUltra, ≥ 99 %, Merck KGaA, Darmstadt) and stirring until it was dissolved, 1.59 g C_3A_c were added. The suspension was stirred for 48 h in an ice bath under nitrogen atmosphere. The product was recovered by centrifugation, washed with decarbonized water and dried in a desiccator.

4.2.3. Synthesis of Ca_2Al-formate-LDH via co-precipitation

Preparation via co-precipitation consists of three steps:

1. Synthesis of freshly precipitated aluminum hydroxide.
2. Synthesis of aluminum formate.
3. Precipitation of Ca_2Al-formate-LDH.

Aluminum hydroxide was prepared by dissolution of 58.52 g $Al(NO_3)_3 \cdot 9\ H_2O$ (p.a., Merck KGaA, Darmstadt, Germany) in decarbonized water. While stirring, 32.3 g of a 25 wt.-% solution of NH_3 (p.a., Merck KGaA, Darmstadt, Germany) are added dropwise. The white precipitate is centrifuged and washed with decarbonized water.

Aluminum formate was prepared by dropwise addition of 0.468 mol of formic acid (≥ 98 % puriss. p.a., Merck KGaA, Darmstadt, Germany) to a suspension of freshly precipitated aluminium hydroxide (0.156 mol). The mixture was stirred until complete formation of $Al(HCOO)_3$. To this solution, 0.312 mol $Ca(HCOO)_2$ dissolved in 250 mL decarbonized water were added. In another flask, 0,78 mol NaOH (pellets, Merck KGaA, Darmstadt, Germany) were dissolved in 500 mL decarbonized water.

In a three-neck-flask, 100 mL decarbonized water were flushed with nitrogen for 1 hour and the pH was adjusted to 12.5. Then the formate salt solution and the sodium hydroxide solution were added dropwise via peristaltic pumps with a flow rate of 0.5-1 mL/min. The pH of the mixture is adjusted to 12.5 over the whole time. After complete addition of the solutions, the reaction mixture is stirred for 2 hours and then aged overnight. The precipitated Ca_2Al-formate-LDH is recovered by centrifugation, washed 3 times with decarbonized water and freeze-dried under vacuum.

4.2.4. Short-term hydration of cement under terrestrial and microgravity conditions

The experimental setup for conducting the experiments onboard as well as under terrestrial conditions consists of three syringes (BD Discardit II 20 mL, Becton Dickinson, Franklin Lakes, New Jersey, USA) connected via a three-way valve. One syringe (#1) serves as the reaction container. It is loaded with 5 g cement in the beginning. The reaction container was further equipped with a cellulose filter (MN520, thickness 1.5 mm, Macherey-Nagel, Düren, Germany) to hold back cement particles when separating the pore solution after 10 seconds of hydration. The next syringe (#2) is filled with 6 mL water (including PCE, 1 mL dead volume). Thus, the water-to-cement ratio in the reaction container was 1.0. The third syringe (#3) contains 10 mL acetone to stop the hydration. The hydration was started by injecting the mixing water from

syringe #1 into the reaction container (#2) holding the cement sample. Proper mixing of water and cement was ensured by shaking the reaction container three times. Then, the paste was hydrated for 10 s followed by filtration of the cement pore solution into syringe #1. Subsequently, acetone was injected from syringe #3 into syringe #1 to stop the hydration. This method for ending the hydration of cement was already used in previous studies.[22, 164-165] After the hydration was stopped, the hydrated cement samples were recovered from the reaction container, crushed and dried overnight in an oven at 40°C to remove residual acetone. For the experiments under microgravity conditions, all syringes were loaded at the ground laboratories prior to each flight. The post-hydration treatment was conducted right after landing. All experiments were carried out three times to confirm the results.

4.2.5. Short-term hydration of clinker phases and blends under terrestrial and microgravity conditions

The experiments with clinker phases and their blends were performed using the same equipment and following the same procedure as in the short-term hydration experiments with cement.

For the preparation of the AF_m phase C_4AH_x, 0.149 g C_3A_C were loaded into syringe #1 and syringe #2 was loaded with 11 mL (including 1 mL dead volume) of a saturated $Ca(OH)_2$ solution.

Monosulfoaluminate ($[Ca_2Al(OH)_6] \cdot ½(SO_4) \cdot 6 H_2O$) was prepared by loading syringe #1 with 0.149 g C_3A_C and syringe #2 with 11 mL of a saturated $CaSO_4 \cdot ½ H_2O$ solution (including 1 mL dead volume), yielding a molar ratio of $C_3A/CaSO_4 = 1$.

For the hydration of C_3A_C and C_4AF_O blended with sulfate carriers a water-solid ratio of 1.0 was applied. The blends consist of mixtures as described in chapter 4.1.1. Syringe #1 was loaded with 2 g of the blend, while syringe #2 was loaded with 3 mL synthetic cement pore solution (including 1 mL dead volume) prepared as described elsewhere.[163]

Hydration was stopped in all experiments by addition of acetone from syringe #3. The hydrated samples were recovered from the syringes, crushed and dried overnight in an oven at 40°C. All experiments were carried out three times to confirm the results.

4.2.6. Synthesis of Calcium Silicate Hydrates via flash precipitation

Synthetic C-S-H was prepared by flash precipitation from aqueous solutions of $Ca(NO_3)_2 \cdot 4\ H_2O$ (PanReac AppliChem, Germany) and $Na_2SiO_3 \cdot 5\ H_2O$ (VWR Prolabo BDH Chemicals, Germany) with a Ca/Si ratio of 1.0. PCEs were pre-dissolved in the $Ca(NO_3)_2$ solution. NaOH (Merck KGaA, Darmstadt, Germany) was used to adjust the pH. More details on the experimental procedure can be found in chapter 5.6. The same experimental setup was used for experiments under terrestrial and microgravity conditions.

4.3. Parabolic flights

Cement hydration experiments under microgravity conditions were conducted during a parabolic flight campaign initiated by Deutsches Zentrum für Luft- und Raumfahrt (DLR, German Aerospace Center) onboard an Airbus A 300 aircraft operated by Novespace (Paris, France). A characteristic flight pattern for a parabola is presented in **Figure 26**. At the beginning, the aircraft starts ascending (crew announcement “pull up”) from an altitude of ~ 6000 m to ~ 8500 m, during which period a maximum gravity of 1.8 to 1.9 *g* occurs in the cabin. When an angle of inclination of 47° is reached (“injection”), the transition from 1.5 *g* to μ *g* takes place within a couple of seconds. The following ~ 22 seconds of microgravity conditions are used to conduct the experiments. Afterwards, the plane descends to an angle of inclination of 42°. Then, the command “pull out” is given and the microgravity phase is over. The subsequent acceleration period is accompanied by a rise of gravity of up to 1.8 *g* in the cabin. Due to some continuing acceleration phenomena from e.g. air maelstroms impacting the aircraft during performance of the parabola, it is not possible to reach the condition of absolute zero gravity. Thus, the gravitational forces acting on the experimental setup during this period which are in the range of 10^{-2}-10^{-3} *g*, are called microgravity throughout this work.

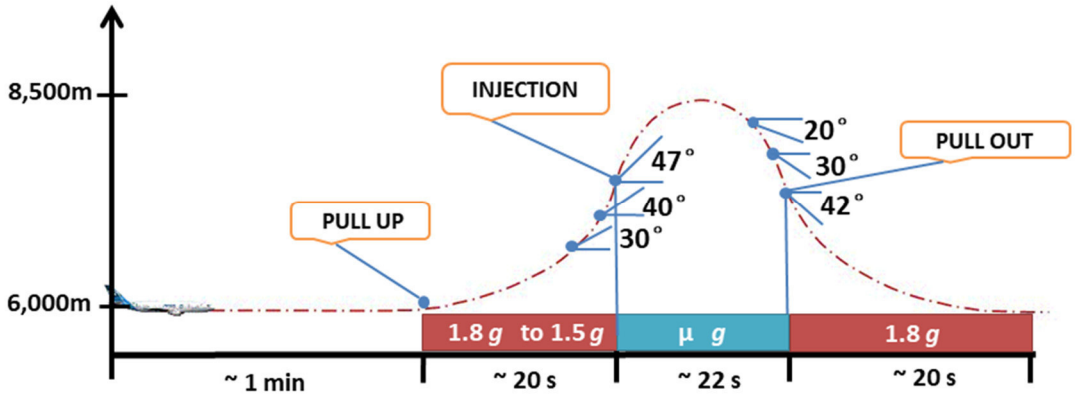

Figure 26: Trajectory performed by the aircraft and gravity conditions in the cabin when flying a parabola, after Lei.[85]

Further details about the experimental design onboard the aircraft can be found in previous literature from our group.[159]

4.4. Analytical methods

4.4.1. X-ray diffraction

XRD patterns were collected in the range of 0.5 – 60° 2θ using an *AXS D8 Advance* instrument (Bruker, Corp., Billerica, Massachusetts, USA) with a *Bragg-Brentano* geometry and Cu Kα source (30 kV, 35 mA). For in-situ measurements, the cement paste was filled into the sample holder and covered by Kapton® foil to prevent evaporation of the mixing water.

4.4.2. Scanning electron microscopy

SEM micrographs were collected on a *FEI XL 30 FEG* environmental scanning electron microscope equipped with an EDX detector at an accelerating voltage of 4 kV at a working distance of 7.5 mm and a tilt angle of 20°. Samples were prepared by applying a conductive carbon paint (Planocarbon N 650, Plano GmbH, Wetzlar, Germany) on the sample stub to fix the cement particles.

For the evaluation of ettringite crystals, from each sample 30 representative images from different areas were collected at a magnification of 40,000 x. For each system, ~ 200 ettringite crystals were analyzed. The lengths and diameters of the ettringite crystals formed were then measured with the *XL Doku* software (version 3.1, Soft Imaging System GmbH, Münster, Germany) and the arithmetical mean values and standard deviation were calculated.

The statistical significance of the obtained mean values was evaluated by performing a two-tailored t-test for two independent random samples. A significance level of 5 % and 1 %, respectively, was chosen, i.e. the mean values differ significantly with a probability of error of 5 % or 1 %, respectively.

Elemental analysis of C-S-H phases was performed via EDX measurement on 50 random spots of each sample to obtain a representative composition and the average value was calculated for the Ca/Si molar ratio.

4.4.3. Transmission electron microscopy

TEM micrographs were collected with a *JEM 2010* microscope (JEOL, Eching, Germany) equipped with a LaB_6 cathode. Acetone suspensions of the prepared C-S-H samples were placed on a carbon-coated copper grid.

4.4.4. Dynamic Light Scattering

Particle sizes were determined via dynamic light scattering (DLS) of C-S-H phases dispersed in acetone. Measurements were performed at 25°C on a *Zetasizer Nano ZS* apparatus from Malvern Instruments (Workestershire, United Kingdom). Each sample was equilibrated for 10 seconds in the cell, measured 100 times and the average value was calculated.

4.4.5. Thermogravimetric analysis

TGA was conducted using a *NETZSCH STA409PC Luxx* system (Netzsch GmbH & Co KG, Selb, Germany) equipped with a mass spectrometer for weight loss investigation. Samples were heated up to 800°C with a heating rate of 10°C/min under air.

4.4.6. Fourier-Transformed Infrared Spectroscopy

Infrared-spectra were collected on a FT-IR spectrometer (*Bruker Vertex 70 FT IR*, Bruker, Corp., Billerica, Massachusetts, USA) equipped with an ATR diamond cell.

4.4.7. ^{29}Si MAS NMR Spectroscopy

Solid-state MAS NMR measurements were conducted on a *Bruker Advance 300 MHz* instrument (Bruker Corp., Billerica, Massachusetts, USA) that was operated at a frequency of 59.63 MHz. Samples were packed into a 7 mm zirconia rotor and spinned at a frequency of 5 kHz. All spectra were obtained with a pulse width of 6 µs and a repetition time of D 1 – 45 s. Tetrakis(trimethylsilyl)silane (Sigma-Aldrich Chemie GmbH, Taufkirchen, Germany) was used as external standard.

4.4.8. Heat Flow Calorimetry

Calorimetric studies were performed on a *TAM-Air* isothermal heat conduction calorimeter equipped with an admix-ampoule set from Thermometric, Järfälla, Sweden.

For analysis of the heat flow of Portland cement, in a typical procedure 4 g of cement were placed in the glass ampoule together with the solid admixture, and the syringe was loaded with the mixing water according to the desired w/c ratio. Upon injection of the mixing water, the cement paste was stirred for one minute and then the heat flow was recorded over time.

For heat flow measurements of C-S-H prepared by flash precipitation, an aqueous solution of $Na_2SiO_3 \cdot 5\ H_2O$ was placed in the glass ampoule and the syringes were loaded with an aqueous solution of $Ca(NO_3)_2 \cdot 4\ H_2O$ holding the PCE superplasticizer. Upon injection of the $Ca(NO_3)_2$/PCE solution, the bulk solution was stirred for one minute by the admix-ampoule device and the heat flow was recorded subsequently. More information on the experimental details can be found in chapter 5.6.

4.4.9. Compressive and flexural strength of mortars

Mechanical properties of mortars were tested using an instrument from Toni-Technik (Berlin, Germany). Mortar prisms (160 mm x 40 mm x 40 mm) were prepared according to DIN EN 450 (DIN EN 196 T1) from a mixture of 450 g of a commercial OPC sample, 225 g water and 1.35 kg sand. After 24 h in the mould at 20 ± 1°C and 90% r.h., prisms were demoulded and cured under water at 20°C for 27 days.

5. Results and Discussion

5.1. Structure and composition of LDHs synthesized by rehydration of C_3A in the presence of retarders

Concrete mixtures nowadays often contain organic admixtures to adjust the properties of the concrete, such as rheology or workability time, to the application needed. Especially in oil well cementing, where long pumping times are unavoidable, the use of cement retarders is common to ensure extended periods of high fluidity of the cement slurry. Depending on cement composition and the type of additive, a loss of the desired property of the slurry can occur during the working time. This is mainly attributed to the hydration products of C_3A which is known to be the most reactive phase. Upon reaction with water it leads to the formation of hydrocalumite-type Layered Double Hydroxides, such as $[Ca_2Al(OH)_6](OH) \cdot 13\ H_2O$, or in the presence of sulfates to $[Ca_2Al(OH)_6](SO_4)_{0.5} \cdot 9\ H_2O$, the so-called monosulfate. As has been explained before (see section 3.1.3.1.), this LDH structure consists of positively charged metal hydroxide sheets balanced by intercalated negatively charged ions or molecules. During hydration, polymers exhibiting an anionic charge can intercalate into the positively charged layers of such LDHs and thus these polymers cannot interact with the surface of cement particles and dissolved ions, e.g. Ca^{2+}, which can result in a loss of workability of the slurry.

Within this work, the interaction of two commercially available, chemically different retarder polymers possessing anionic charge, with cubic C_3A was investigated. In a first step, the two retarders were intercalated into Hydrocalumite-type LDH by rehydration of pure C_3A_C. The obtained inorganic-organic composites were characterized by XRD, TGA, IR and elemental analysis to prove successful incorporation of the polymers into the inorganic host structure.

The collected XRD patterns of the obtained rehydration products are displayed in **Figure 27**. The XRD pattern of Ca_2Al-IA/AMPS-LDH indicates a more disordered structure than the Ca_2Al-AA/AMPS-LDH which shows very sharp reflexes. Both composites show the typical (003) reflection of LDHs in the low 2θ° region which allows determination of the basal spacing between two hydroxide layers. The reflection of the (003) plane of Ca_2Al-IA/AMPS-LDH is at 5.2° 2θ and at 6.0° 2θ for Ca_2Al-AA/AMPS-LDH, respectively. The corresponding basal

spacings of the LDHs are 1.45 nm for the AA/AMPS-copolymer and 1.68 nm for the IA/AMPS co-polymer.

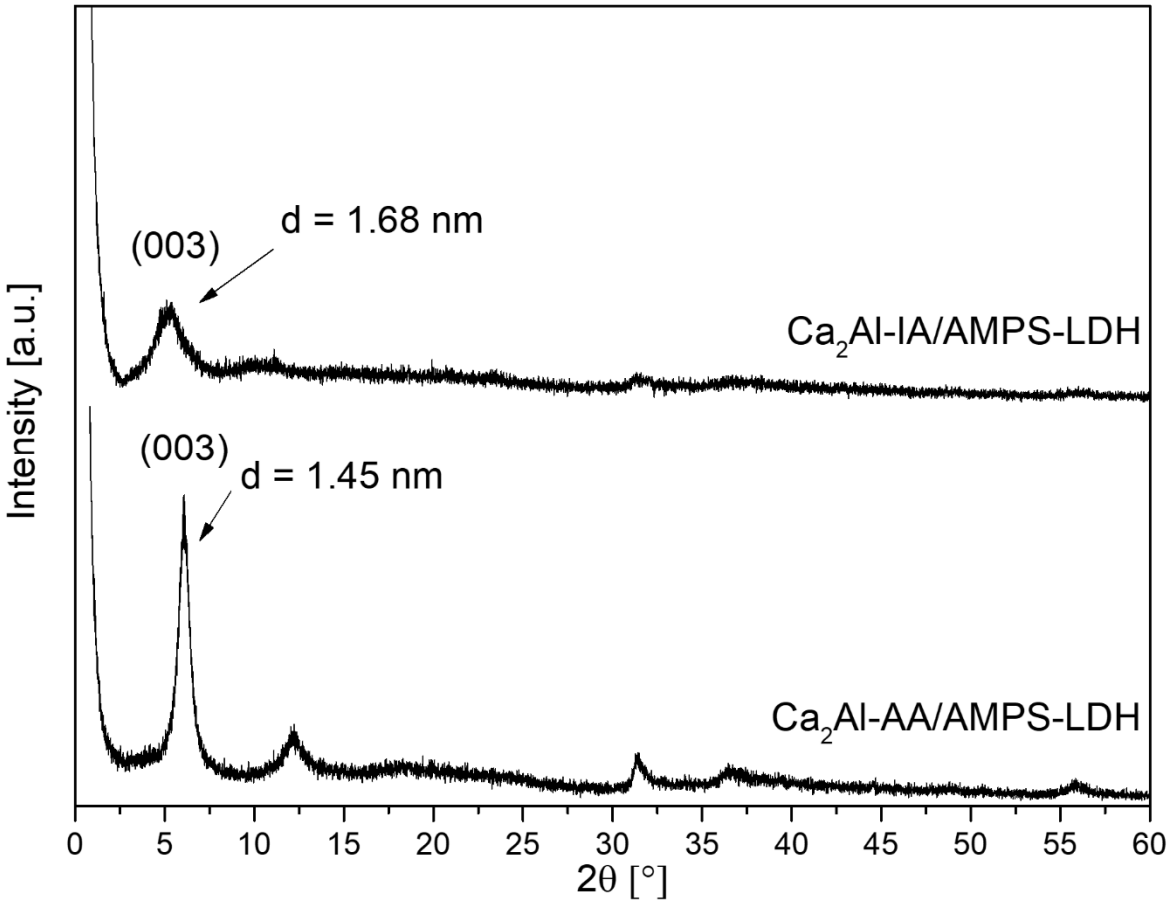

Figure 27: XRD patterns of Ca_2Al-AA/AMPS-LDH and Ca_2Al-IA/AMPS-LDH obtained by rehydration of C_3A_C in the presence of the co-polymers.

This indicates a successful intercalation of the retarder, considering the thickness of an inorganic layer being only 0.48 nm and the Ca_2Al-LDH with OH^- as anion having only a basal spacing of 0.8 nm.[21] Another reflection can be observed at 12° 2θ and can be assigned to the (006) plane. The reflections at 31° and 56° 2θ can be associated with the (*hk*0) and (0*k*0) reflections of the compound.

Because of the large steric size of the co-polymers, the characteristic reflections of the obtained LDHs are close to the signal of the primary beam of the XRD. Thus, small-angle X-ray diffraction (SAXS) and wide-angle X-ray diffraction (WAXS) measurements were performed to investigate the potential formation of LDHs possessing higher basal spacings

than those observed in conventional XRD. SAXS measurements did not reveal any reflections in the range from 0 - 2.5° 2 θ for both LDH compounds (see **Figure A1** and **Figure A2** in the appendix). The obtained WAXS-patterns are displayed in **Figure 28**.

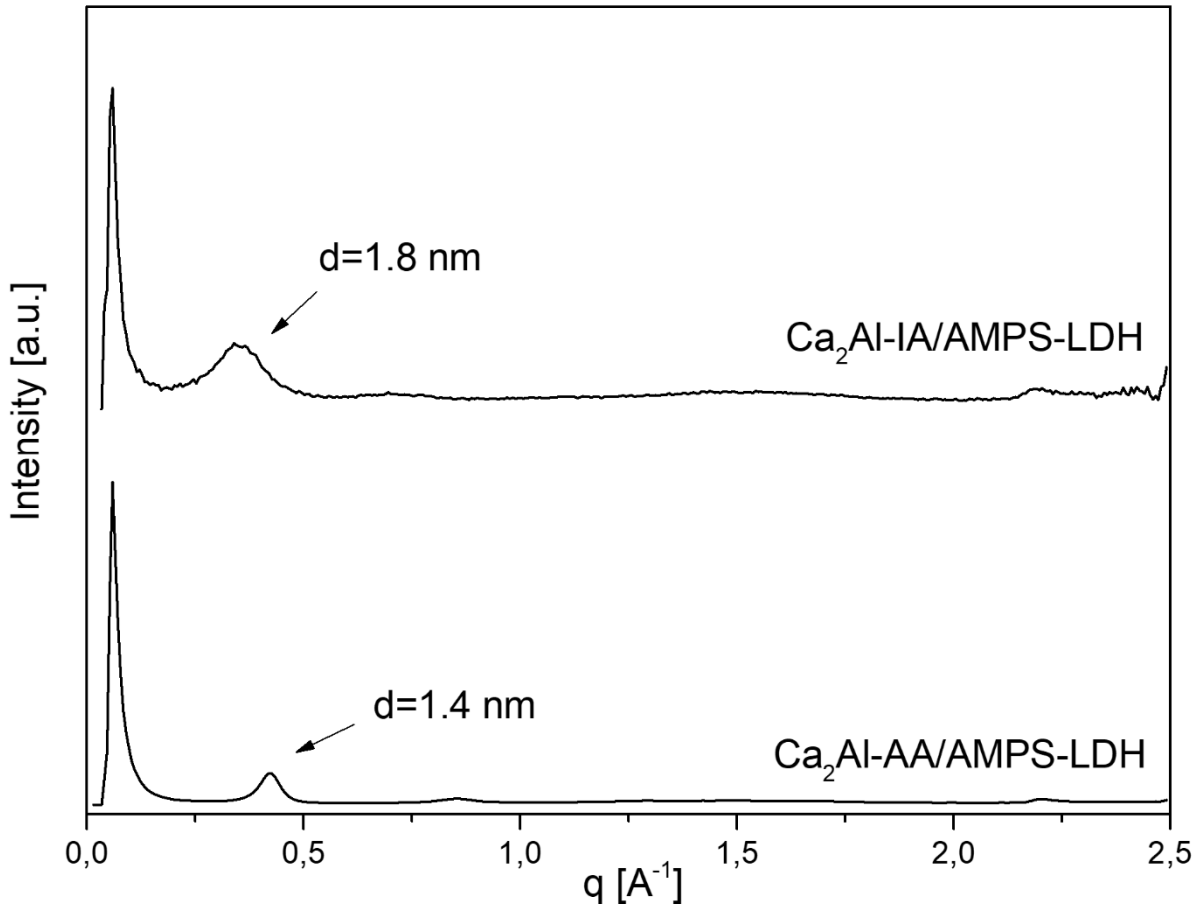

Figure 28: WAXS patterns of Ca_2Al-AA/AMPS-LDH and Ca_2Al-IA/AMPS-LDH obtained by rehydration of C_3A_C in the presence of the co-polymers.

From the WAXS pattern of the Ca_2Al-AA/AMPS-LDH, we can see a signal at 0.46 A^{-1} which corresponds to a d-value of 1.4 nm. This is in good correlation with the XRD pattern which produced a basal spacing of 1.45 nm. In the WAXS pattern of Ca_2Al-IA/AMPS-LDH, we can see a broad reflex at 0.34 A^{-1} which corresponds to a basal spacing of 1.8 nm. This is also in good agreement with the basal spacing of 1.68 nm as calculated from the XRD pattern.

The basal spacings of the Ca_2Al-retarder-LDHs as determined by XRD show an increase from 1.45 nm to 1.68 nm and from 1.5 nm to 1.8 nm for the WAXS-measurements, respectively, with increasing amount of AMPS present in the copolymer. The length of an AMPS side chain of the co-polymers is about 1 nm and 0.25 nm for acrylic acid, respectively. The molar ratio of

AA to AMPS in the retarder SCR-100© is 1:1. As AMPS has a length of approximately 1 nm and the $[Ca_2Al(OH)_6]^+$ layer 0.48 nm, the AA/AMPS co-polymer is most likely orientated comb-like in the interlayer space. SCR-500©, on the other hand, has a molar ratio of IA : AMPS = 1:3. The increase in basal spacing might thus be due to steric repulsion between the side chains leading to an opposite arrangement of AMPS and IA.

The IR-spectra for the retarder and the product are given in **Figure 29**. The IR spectrum of the pure Ca-AA/AMPS co-polymer displayed a N-H and O-H stretching band in the range from approximately 3,180 cm^{-1} to 3,500 cm^{-1}, a C-C stretching band at ~ 2,800 cm^{-1}, a C=O stretching band at 1,615 cm^{-1}, a N-H bending band at 1,562 cm^{-1} and S=O stretching bands at 1,411 cm^{-1}, 1,183 cm^{-1} and 1,033 cm^{-1}.

The spectrum of the inorganic-organic composite shows a strong absorption at 430 cm^{-1} and 540 cm^{-1} for the Ca-O and Al-O vibrations which can be attributed to the layered double hydroxide. Furthermore, S-O vibrations of the sulfonate group of AMPS can be found at approximately 1,050 cm^{-1}, 1,200 cm^{-1} and 1,400 cm^{-1}. The peak of N-H bending was detected at 1,525 cm^{-1} and the C=O stretching bond vibrations appeared at 1,630 cm^{-1}. The product shows also a very broad peak from 2,700 – 3,600 cm^{-1} which can be assigned to O-H, N-H and C-H vibrations. The spectrum of the retarder itself shows quite similar peaks, except for the inorganic part in the low wave length area. This indicates that the intercalation of the retarder into $[Ca_2Al(OH)_6]^+$ layers was successful. The peaks at ~2,350 cm^{-1} in the spectra can be assigned to carbonate.

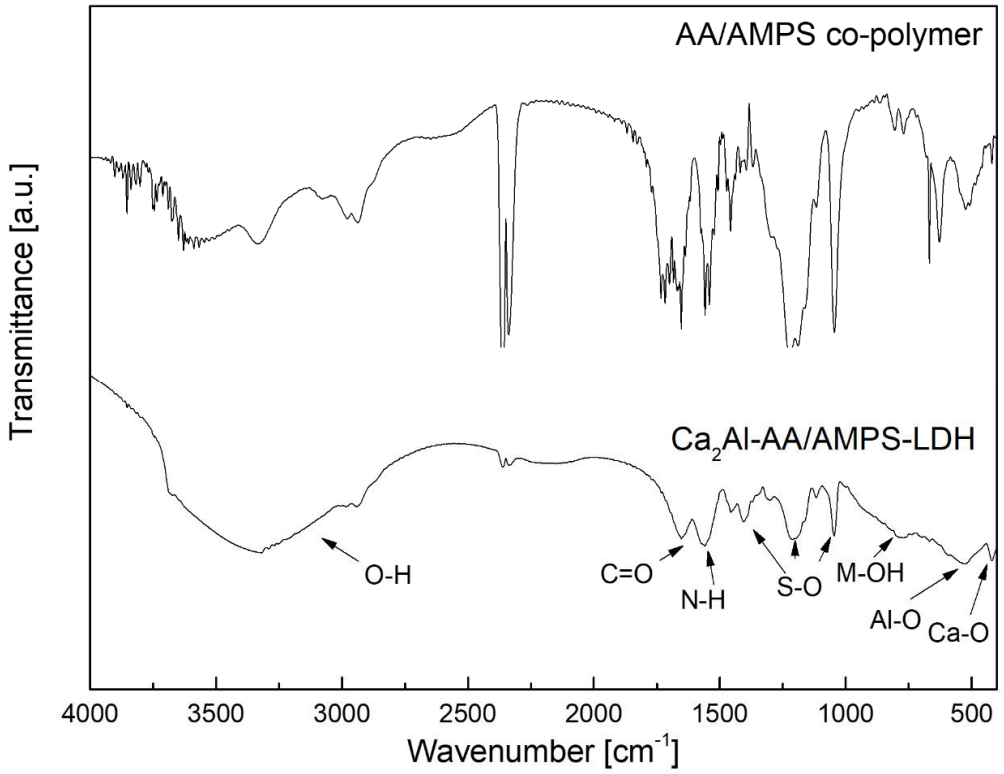

Figure 29: IR-spectra of the AA/AMPS co-polymer and of the Ca_2Al-AA/AMPS-LDH.

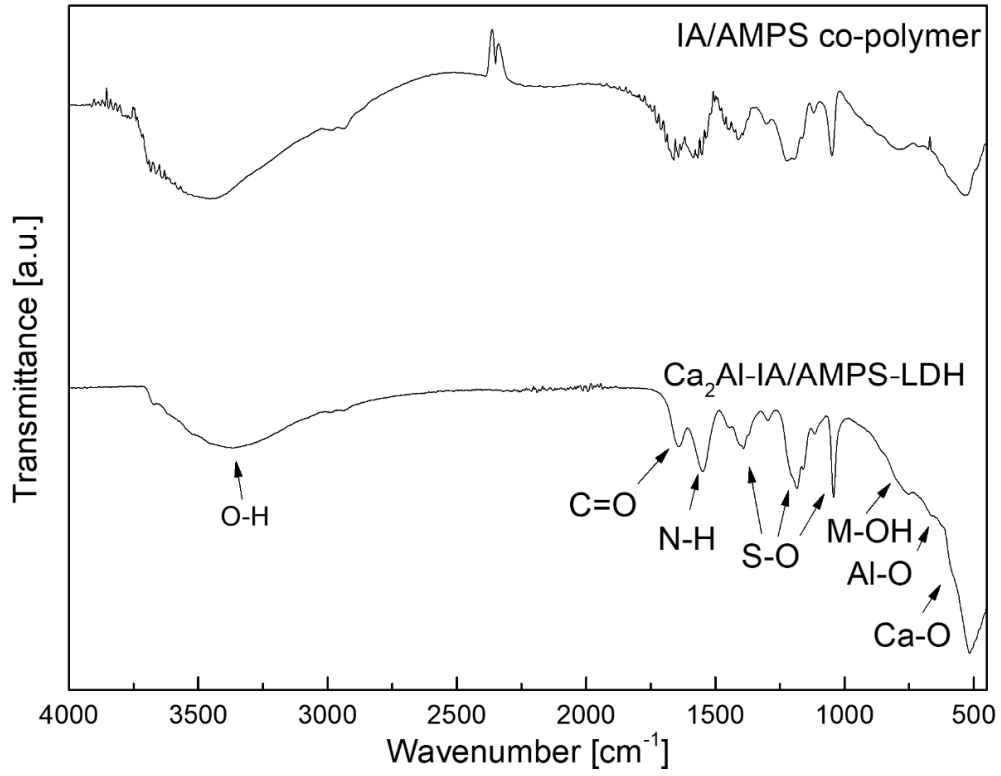

Figure 30: IR-spectra of the IA/AMPS co-polymer and of the Ca_2Al-IA/AMPS-LDH.

The IR spectrum of the LDH incorporating the IA/AMPS co-polymer shows similar absorptions like the Ca_2Al-AA/AMPS-LDH, suggesting successful intercalation of the co-polymer into the positively charged metal hydroxide layers. The IR spectrum of the organic-inorganic LDH-compound shows the C=O stretching band at 1,682 cm^{-1}, a N-H bending band at 1,564 cm^{-1}, the characteristic S=O stretching bands at 1,391 cm^{-1}, 1,186 cm^{-1} and 1,041 cm^{-1} of the IA/AMPS co-polymer as well as the Al-O and Ca-O vibration bands of the inorganic host structure. The broad peak from 2,800 cm^{-1} to approximately 3,700 cm^{-1} can be related to O-H, N-H and C-H vibrations originating from both the co-polymer and the LDH.

The reaction products were further investigated regarding their elemental composition, and the results are shown in **Table 5** and **Table 6**. From these results, the sum formulas of the LDHs where calculated. The calculations are based on the assumption that Al is the charge determining ion and is evenly incorporated in all LDH layers. For the intercalate with the AA/AMPS co-polymer with a molar ratio of 1:1 for AA/AMPS, it was found that the LDH layers exhibit a higher positive charge due to the lower ratio of Ca:Al of 1.8:1. The positive charge of the inorganic layer is, according to the masses found for the elements C, S and N which can be exclusively tied to the co-polymer, almost completely compensated by the negatively charged AA/AMPS molecule considering the two anionic groups per repetition unit.

Table 5: Elemental compositions of the AA/AMPS co-polymer (molar ratio 1:1) and of the Ca_2Al-AA/AMPS-LDH obtained by rehydration of cubic C_3A.

Sample	**Elemental composition**					
	C/wt.-%	H/wt.-%	S/wt.-%	N/wt.-%	Ca/wt.-%	Al/wt.-%
AA/AMPS co-polymer	37.7	5.0	10.1	4.4	12.6	-
Ca_2Al-AA/AMPS-LDH	15.19	4.75	4,05	1.71	16.3	6.2

	Organic part/wt.-%	**Calculated formula**
AA/AMPS co-polymer	87.4	$C_{10}H_{16}NSO_6Ca$
Ca_2Al-AA/AMPS-LDH	39.6	$Ca_{1.8}Al(OH)_6 \cdot (AA/AMPS)_{0.55}$

For the intercalation of the IA/AMPS co-polymer, the theoretical molar ratio of Ca:Al of 2:1 was found for the reaction product. Similar to the LDH comprising the retarder AA/AMPS, a complete balance of the positively charged hydroxide layers by the anionic co-polymer was found. The slight surplus of polymer detected in the elemental analysis most likely can be related to adsorbed IA/AMPS co-polymer.

Table 6: Elemental compositions of the pure IA/AMPS co-polymer (molar ratio 0.32:1) and of the Ca_2Al-IA/AMPS-LDH obtained by rehydration of cubic C_3A.

Sample	**Elemental composition**						
	C/wt.-%	H/wt.-%	S/wt.-%	N/wt.-%	Ca/wt.-%	Al/wt.-%	Na/wt.-%
IA/AMPS co-polymer	37.6	5.3	12.6	5.5	-	-	8.5
Ca_2Al-IA/AMPS-LDH	16.1	4.6	3.9	2.0	15.0	5.0	n.a.*

	Organic part/wt.-%	**Calculated formula**
IA/AMPS co-polymer	91.5	$C_{8.6}H_{14.24}NSO_{5.28}Na$
Ca_2Al-IA/AMPS-LDH	38.0	$Ca_2Al(OH)_6 \cdot (IA/AMPS)_{0.56}$

*not analysed

To investigate further the successful intercalation of the retarder molecules into the LDH layers, the obtained intercalation products were analysed by TG-MS up to 800°C. The ion flows of water and the decomposition products of the retarders (nitrogen oxide, carbon dioxide and nitrogen dioxide) were detected by mass spectrometry throughout the heating period. The spectrum for the Ca_2Al-AA/AMPS-LDH is displayed in **Figure 10**.

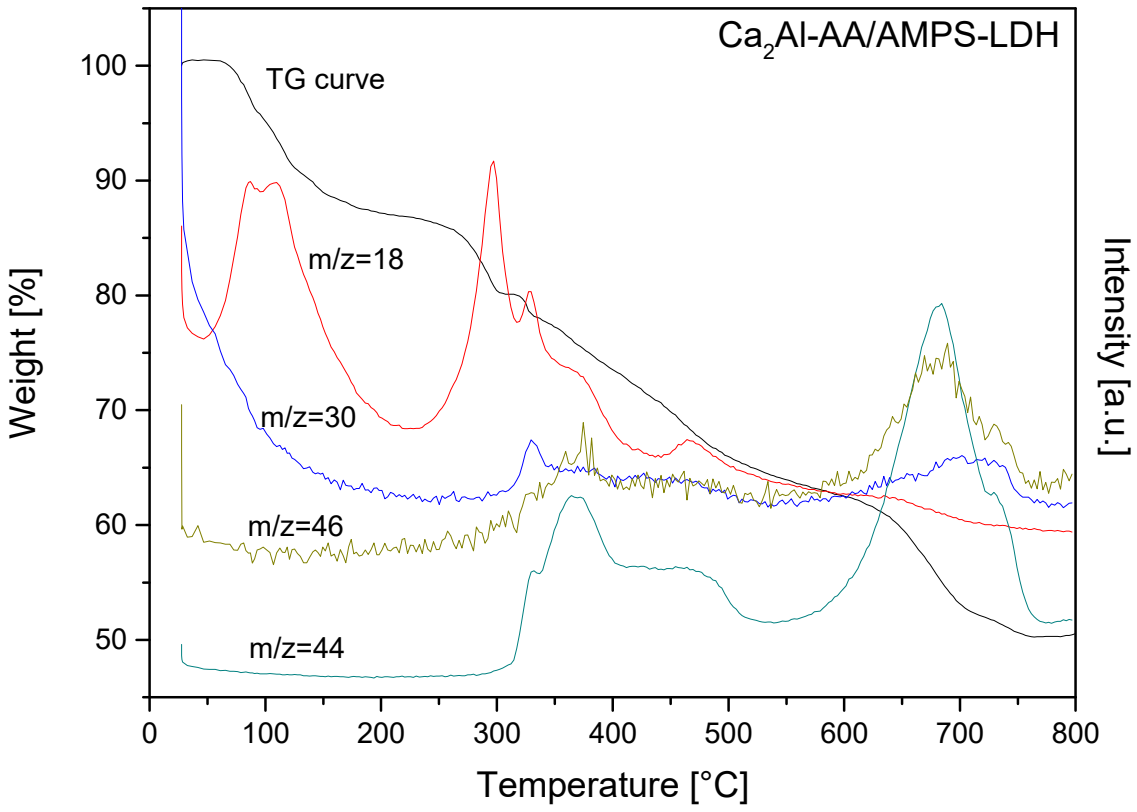

Figure 31: TG-MS spectrum of Ca_2Al-AA/AMPS-LDH showing mass loss (black), and mass spectrometry curves for H_2O (red), NO (blue), CO_2 (brown) and NO_2 (green).

As we can see from the TG-MS curve, the first mass loss begins at approximately 70°C and can be addressed to adsorbed water (13 wt.-%). From ~ 225 - 300°C, intercalated water is released which leads to a further weight loss (~ 6.5 wt.-%) of the LDH. From 300°C on, more water, carbon dioxide and nitrogen oxides are released due to decomposition of adsorbed AA/AMPS co-polymer (~ 9.5 wt.-%). Above 600°C, another step in the TG curve is observed and a large amount of carbon dioxide and nitrogen dioxide are detected (approximately 20 % weight loss). This indicates decomposition of the AA/AMPS co-polymer intercalated in the LDH interlayers. The total weight loss up to 800°C is 49.45 %. These results are in fair accordance with the elemental analysis which yielded an organic part of 33 wt.-% compared to ~ 30 wt.-% from TG MS.

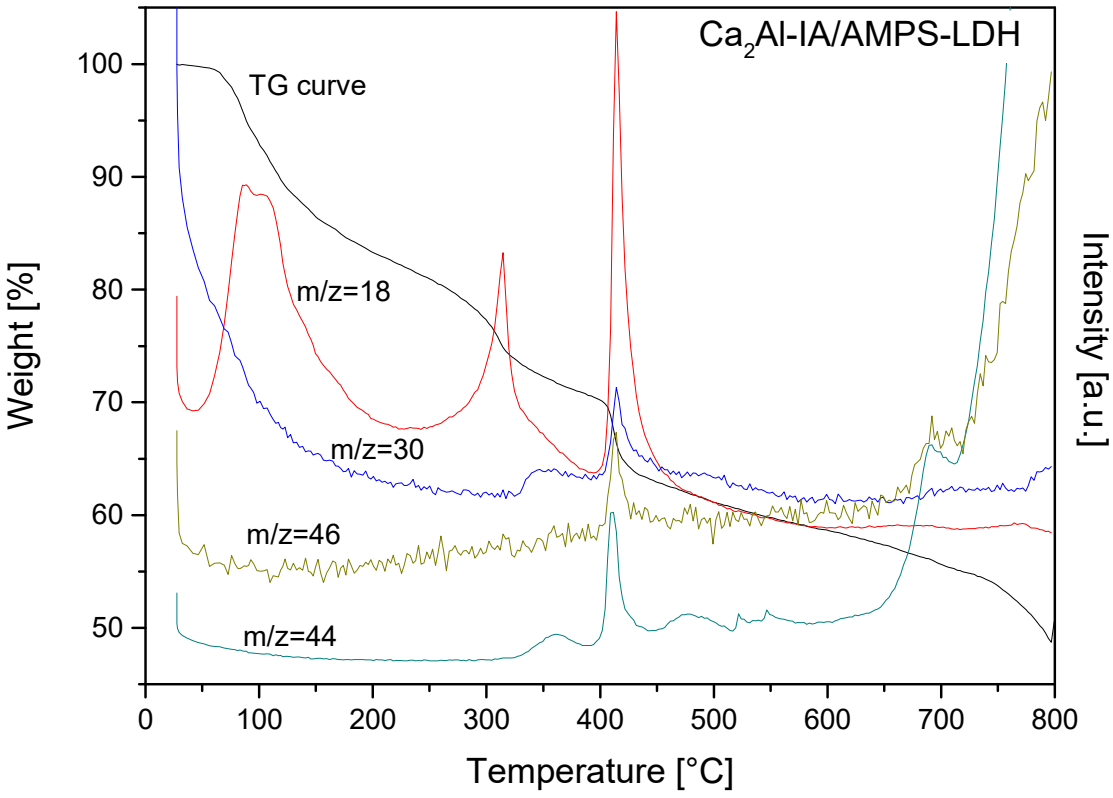

Figure 32: TG-MS spectrum of Ca_2Al-IA/AMPS-LDH showing mass loss (black), and mass spectrometry curves for H_2O (red), NO (blue), CO_2 (brown) and NO_2 (green).

The TG-MS spectrum of Ca_2Al-IA/AMPS-LDH shows a significant weight loss of 30 wt.-% up to 400°C, where ~ 27 wt.-% can be tied to released free, adsorbed and interlayer water and 3 wt.-% to carbon dioxide and nitrogen oxide as a result of the beginning decomposition of the adsorbed co-polymer. The water detected above 400°C is from the hydroxide layers. The CO_2, NO and NO_2 detected above 400°C signify the decomposition of the adsorbed IA/AMPS co-polymer. Decomposition of the intercalated co-polymer starts at 630°C and is not complete at 800°C. The weight loss above 630°C is approximately 10 %.

The TG-MS analysis of both organic-inorganic compounds shows two significantly different temperature regions where the co-polymers decompose. This suggests that a part of the co-polymer was successfully intercalated, while the rest of the co-polymers only adsorbed on the metal hydroxide layers. The intercalation of the co-polymers into the LDH structure protects the organic molecules by giving them a better thermal stability, similarly to observations made for other organo-ceramic materials.[166]

In a next step, the above characterized Retarder-LDHs were analysed regarding their stability towards an anion exchange with sulfate. As described above, due to their divalent negative charge and their small size SO_4^{2-} ions are one of the most attractive counterions for LDHs. Furthermore, sulfate was chosen because of its presence in the mixing water already from the first seconds of cement hydration, for its quick dissolution from sulfate sources like e.g. gypsum. The anion exchange with SO_4^{2-} ions was carried out for 24 h at two different concentrations equal to 100 % and 200 % of the anion exchange capacity (aec) of the Ca_2Al-LDHs each. The total organic carbon content in the supernatant of the anion exchange solution was determined which was then compared to the carbon content determined by elemental analysis. The results are shown in **Figure 33**. It was found that ~ 25 % of the AA/AMPS co-polymer was released from the LDH interlayers within 24 h at 100 % aec and more than 80 % at 200 % aec, while the IA/AMPS co-polymer showed superior interaction with positively charged LDH layers, as only 5.3 % were exchanged by SO_4^{2-} within 24 h at 100 % aec and 21.7 % at 200 % aec, respectively.

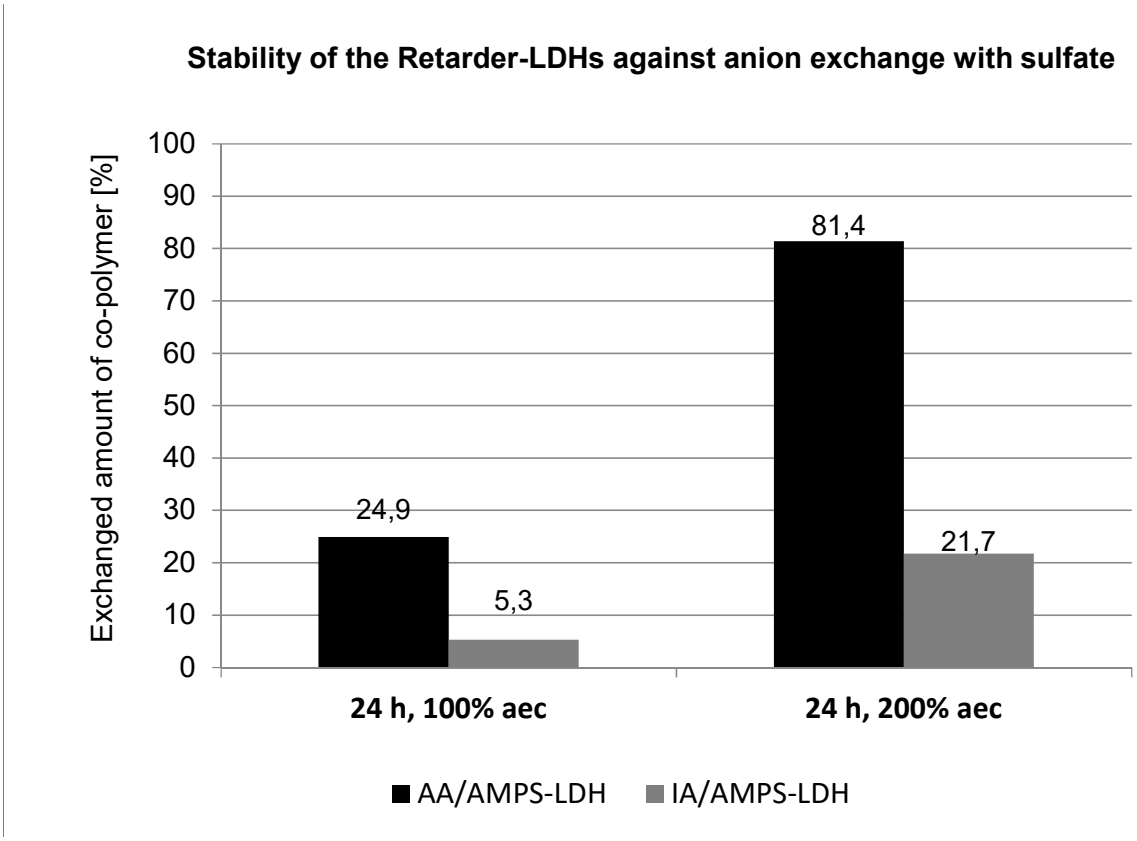

Figure 33: Amount of co-polymer replaced by SO_4^{2-} as determined from the TOC content of the supernatant after anion exchange for 24 h with sulfate concentrations according to 100 % and 200 % anion exchange capacity (aec) of the Ca_2Al-retarder-LDHs.

With regard to the anionic charge density of the co-polymers, these results are rather unexpected, as the AA/AMPS co-polymer possesses a charge density of 8,100 µeq g^{-1}, while the IA-AMPS co-polymer has only 4,200 µeq g^{-1}. The two retarding admixtures differ further in their molecular structure. An explanation for the low release of the IA/AMPS co-polymer might be its higher amount of SO_3^- anchor groups compared to the AA/AMPS co-polymer. As the anion exchange is mainly diffusion driven, it is also possible that the high molecular IA/AMPS-copolymer is just slightly immobilized in the LDH-interlayer, while the low molecular AA/AMPS co-polymer can easily diffuse out from the interlayer and is then replaced by SO_4^{2-}.

Both co-polymers have shown that they can readily intercalate into the metal hydroxide double layers, while the AA/AMPS interaction with the LDH is less strong than that of IA/AMPS and can thus be released again from the interlayers if sufficient SO_4^{2-} ions are present. This kind of interaction can significantly impact the effectiveness of a retarder, as it determines whether it can e.g. adsorb on cement particles or sequestrate Ca^{2+} ions, or if it is fixed in the interlayers of the hydration products of C_3A. To evaluate the correlation between the exchange capability with sulfate during cement hydration, the heat flow generated by the hydration of a commercial oil well cement in the presence of a Hydroxide-LDH, both Retarder-LDHs and the retarders themselves, respectively, was measured. The result is shown in **Figure 34**.

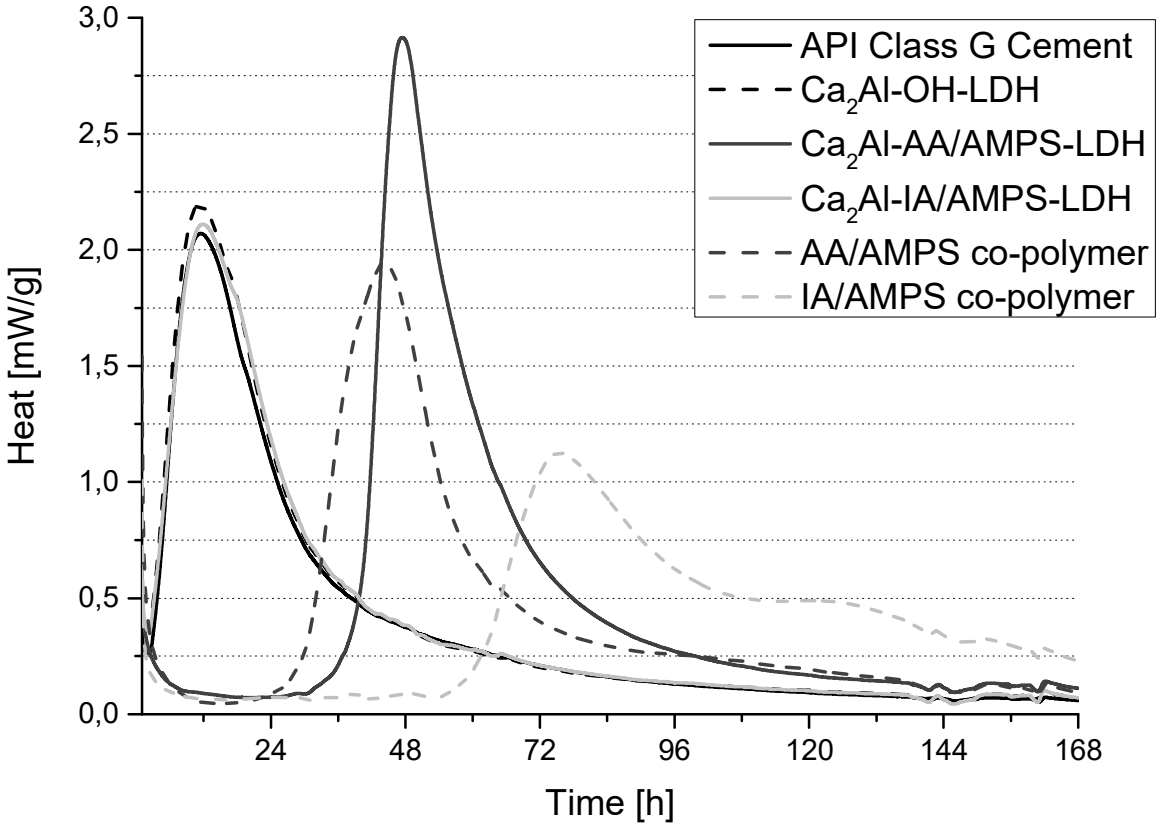

Figure 34: Heat flow calorimetry of a commercial API Class G oil well cement with a w/c ratio of 0.44 and admixed with 2% bwoc of Ca_2Al-OH-LDH, Ca_2Al-AA/AMPS-LDH, Ca_2Al-IA/AMPS-LDH and such dosages of AA/AMPS co-polymer or IA/AMPS co-polymer, as present in their respective LDH compounds.

It can be observed that the cement sample without additive as well as admixed with Hydroxide-LDH release the main heat of hydration within the first 24 hours. This shows that the LDH-structure itself does not possess a retarding effect on cement hydration. Both retarders impact significantly the beginning of the cement hydration, delaying it about ~ 24 h in the case of the AA/AMPS co-polymer and for roughly 50h for the IA/AMPS co-polymer, respectively.

The delay in the onset of the heat flow curves shows the strong retarding effect especially of the IA/AMPS co-polymer. Therefore, it is interesting to see that the LDH containing the IA/AMPS co-polymer shows a similar heat flow curve as the pure cement sample and the cement admixed with the Hydroxide-LDH sample containing no retarder. These results suggest that the IA/AMPS co-polymer is well intercalated in the LDH and immobilized during cement hydration which is in good agreement with the results of the anion exchange

experiments. The Ca_2Al-AA-AMPS-LDH admixture delays the beginning of cement hydration by approximately 30 h compared to 24 h for the pure retarder. This indicates that as was already found in the anion exchange experiments, the AA-AMPS co-polymer underwent anion exchange most likely with sulfate ions from the cement pore solution and thereupon the co-polymer was released from the LDH interlayers and was able to act as a retarder. The slightly later onset of the heat of hydration in this case can be addressed to the step-wise release of the retarder molecule from LDH interlayers as the anion exchange process is strongly diffusion driven. Despite its high anionic charge density, the pure AA/AMPS co-polymer exhibits less retarding effect compared to the IA/AMPS co-polymer. This might be attributed to partial intercalation of the AA/AMPS co-polymer at a later stage in cement hydrates and consequently a lower concentration of the co-polymer present in the cement paste causing less retardation.

5.2. Ca_2Al-formate-LDH as potential early-strength enhancer for cement

The hydration of Portland cement can be accelerated by various mechanisms described before. Within this section, the accelerating effect of Ca_2Al-formate-LDH nanoparticles as nucleation seeds for C_3A hydration was investigated. The rapid formation of nanosized ettringite during initial hydration leads to a strong deceleration of the hydration of C_3A.[23, 26] Transformation of ettringite to monosulfate is assumed to be one reason for the decomposition of the protective layer and beginning of the acceleration stage of cement hydration. By addition of a structural analogon of monosulfate to the neat cement, the initial formation of ettringite shall be prevented. The LDH structure should act as a nucleation seed for monosulfate and thus initiate directly the reaction of C_3A and gypsum to monosulfate. Another potential accelerating mechanism could be an earlier initiated and accelerated transformation of ettringite to monosulfate. Formate was chosen as an anion due to its known potential as an accelerator for C_3S and its compatibility with steel in reinforced concrete. *Iyi* et al. reported the preparation of Mg-Al-formate-LDH in the hydrated (basal spacing 1.1 nm) and dehydrated (basal spacing 0.78 nm) state via anion exchange from a Cl-LDH precursor.[18] In a study by *Gordijo* et al. formate-LDH was prepared via decarbonation of the Carbonate-LDH in a formamide-ethanol mixed solvent. The reported basal spacing is 0.76 nm which is corresponding to that of the Carbonate-LDH.[17] *Manohara* et al. have reported the synthesis of

a Ni-Al-formate-LDH by a homogeneous precipitation from a mixture of formamide and aqueous solutions of the metal nitrates in an autoclave at 150°C for 24h.[19]

Up to now, there has not been reported a successful synthetic approach for the preparation of Ca_2Al-formate-LDHs via conventional co-precipitation. This type of synthesis is crucial for a potential use of this kind of accelerator as the co-precipitation synthesis allows simple upscaling for an industrial use without applying high temperatures and the use of solvents. In the following, a facile synthesis of the Ca_2Al-formate-LDH via co-precipitation is reported. To verify the successful synthesis via co-precipitation, Ca_2Al-formate-LDH was prepared via rehydration as a reference and the products of both synthesis routes were characterized by XRD and SEM. The obtained Ca_2Al-formate-LDH was then admixed to mortars prepared from commercial Portland cement samples and the effect on the early strength of mortars was characterized by compressive and tensile strength. Additionally, the mechanism of acceleration was investigated by heat flow calorimetry and in-situ XRD measurements.

5.2.1. Ca_2Al-formate-LDH synthesized by rehydration vs. co-precipitation

Preparation of Ca_2Al-formate-LDH can be easily done by hydrating pure C_3A_C with an equimolar amount of $Ca(HCOO)_2$. The obtained product of the rehydration of C_3A with Calcium formate was characterized by XRD. The results are displayed in **Figure 35**. The d-value shows a basal spacing of 0.80 nm which is comparable to the basal spacing of 0.79 nm reported in the literature for Formate-LDHs synthesized via anion exchange. [18] The slightly increased d-value of 0.80 nm can be related to a higher amount of interlayer water molecules.

Attempts to prepare the Ca_2Al-formate-LDH from aqueous solutions of calcium and aluminum nitrates into a formate solution as well as precipitation from a $Ca(HCOO)_2$ and $Al(NO_3)_3$ solution were not successful, because of the competitive affinity of NO_3^- ions to the positively charged LDH main sheets, yielding always Ca_2Al-nitrate-LDH as by-product. Therefore, $Al(HCOO)_3$ was prepared from freshly precipitated $Al(OH)_3$ and formic acid. Finally, co-precipitation from aqueous solutions of $Ca(HCOO)_2$ and $Al(HCOO)_3$ yielded the desired Ca_2Al-formate-LDH.

The Ca_2Al-formate-LDH synthesized via the new facile co-precipitation route exhibits a basal spacing of 0.79 nm. Comparing the sharp signal of the (006) reflection from the rehydration product to the broader (006) reflection of the co-precipitated LDH, this suggests that the product from rehydration has either a more ordered structure or consists of bigger crystals than the one obtained by co-precipitation. In both cases, no other by-products, e.g. hydrogarnet or hydrocalumite, were found which makes the LDHs of both synthesis routes suitable for investigating their potential accelerating effect on cement hydration.

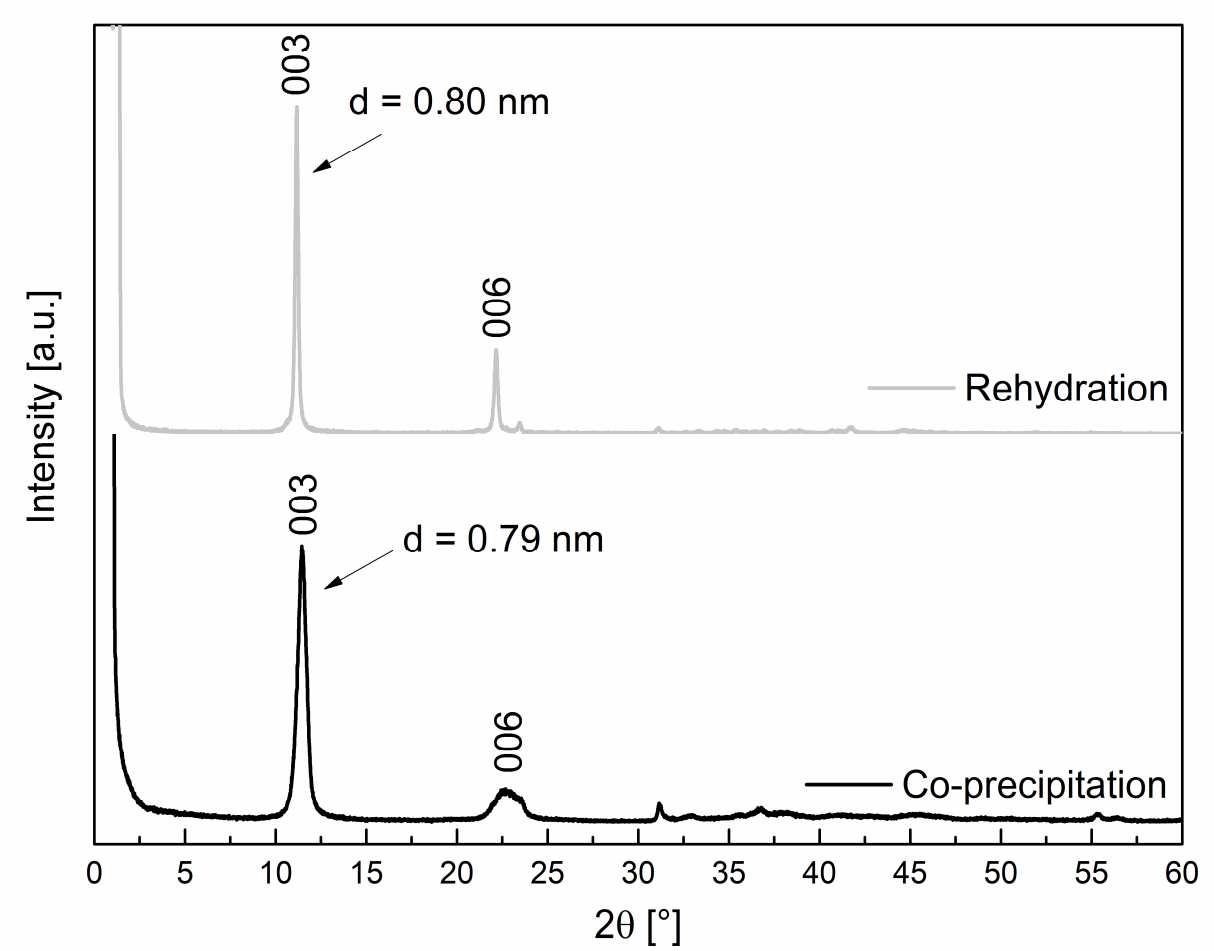

Figure 35: XRD patterns of Ca_2Al-formate-LDH prepared by rehydration (top) and co-precipitation (bottom).

The obtained precipitates were further analysed by SEM imaging (see **Figure 36**). Both Ca_2Al-Formate-LDHs exhibit an exfoliated flaky morphology which is typical for hydrocalumite-type LDHs incorporating organic anions.[12]

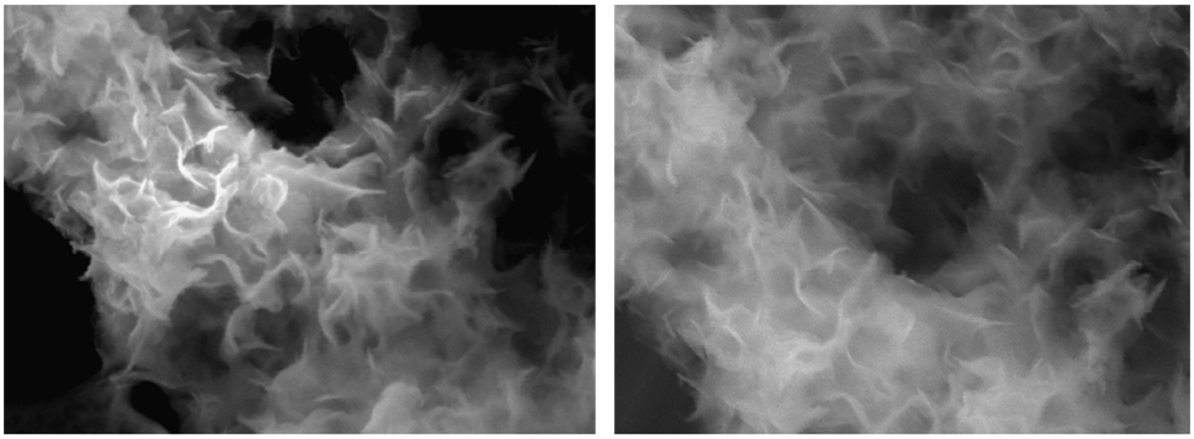

Figure 36: SEM images of Ca_2Al-formate-LDH synthesized by rehydration (left) and co-precipitation (right). Magnification: 40.000x.

5.2.2. Influence of Ca_2Al-formate-LDH admixture on the mechanical properties of mortars

For evaluation of the accelerating effect of Ca_2Al-formate-LDH on early cement hydration, the compressive and flexural strengths of three different mortar mixes after 16 and 24 hours were tested. The three mixes were based on commercial Portland cement samples possessing a fine (CEM I 52.5 R), a medium (CEM I 42.5 R) and a coarse (CEM I 32.5 R) clinker granulometry. Generally, cement hydration and thus strength development increases with increasing fineness of the cement particles.

Table 7: Phase composition of different cements as determined by Rietveld analysis.

Cement sample	C_3S, m [%]	C_2S, m [%]	C_3A, o [%]	C_3A, c [%]	C_4AF [%]	AH [%]	HH [%]	DH [%]	Sum of aluminate clinkers
CEM I 52.5 R	71.0	8.3	3.0	5.9	7.0	2.2	1.3	0.0	15.9
CEM I 42.5 R	57.6	12.7	1.8	7.4	6.7	2.3	2.7	0,7	15.9
CEM I 32.5 R	53.9	16.7	4.7	5.1	8.6	2.2	2.0	0.0	18.4

To find out whether the hydrocalumite-type structure incorporating the $HCOO^-$ ion enhances the hydration, mortar mixes admixed with the same amount of calcium formate as present in the Ca_2Al-formate-LDH and with a hydrocalumite-type LDH comprising OH^- as anion (Ca_2Al-hydroxide-LDH) were tested, too.

For the highly reactive cement CEM I 52.5 R, no increase in compressive strength compared to the reference could be observed for the mortars containing LDHs after 16 h and 24 h (see **Figure 37**). However, calcium formate led to an increase of compressive strength from 34.8 MPa to 38.0 MPa within 24 h. Consequently, the LDH phases tested here have no accelerating effect.

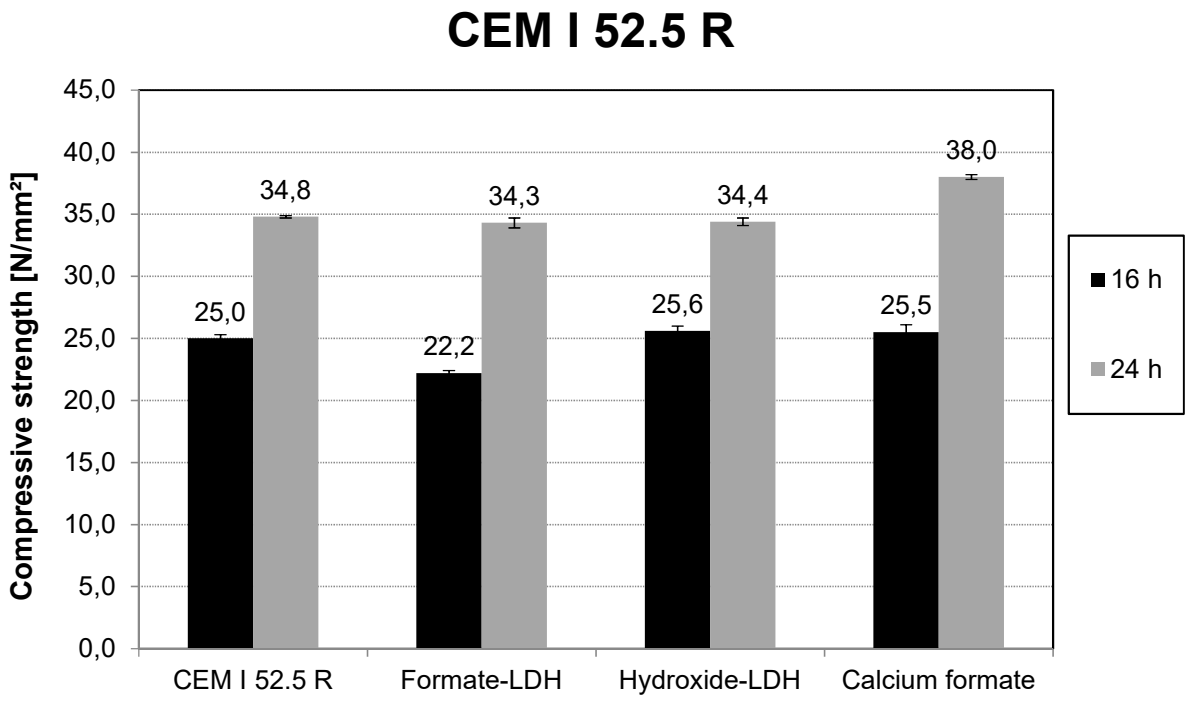

Figure 37: Compressive strength of mortars consisting of CEM I 52.5 R admixed with 2 % bwoc of Ca_2Al-formate-LDH, 0.7 % bwoc calcium formate (equivalent to the amount in 2 % Ca_2Al-formate-LDH) and 2 % bwoc Ca_2Al-hydroxide-LDH, after 16 or 24 hours.

Regarding the flexural strength, all admixtures resulted in slightly increased mechanical properties after 24 hours, while only calcium formate and the Hydroxide-LDH showed already an increase after 16 hours (see **Figure 38**).

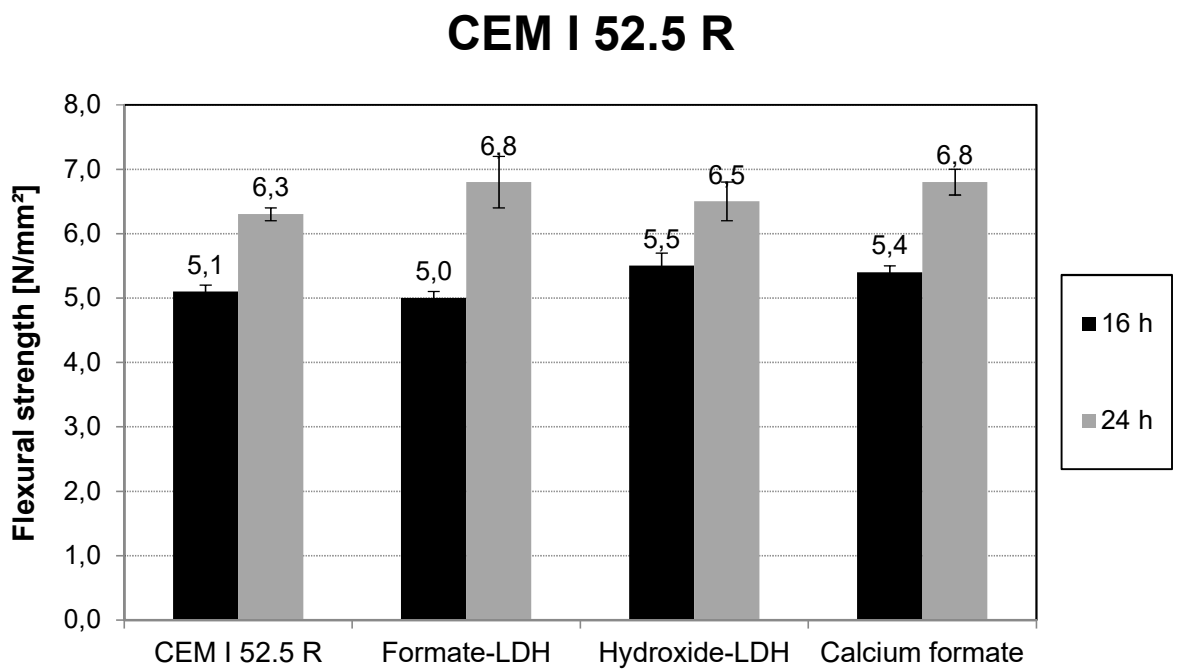

Figure 38: Flexural strength of the mortars consisting of CEM I 52.5 R admixed with 2 % bwoc of Ca_2Al-formate-LDH, 0.7 % bwoc calcium formate (equivalent to the amount in 2 % Ca_2Al-formate-LDH) and 2 % bwoc Ca_2Al-hydroxide-LDH, after 16 or 24 hours.

Testing of compressive and flexural strengths of the mortar consisting of CEM I 42.5 R showed that the samples admixed with Formate-LDH or calcium formate produced lower compressive strengths after 24 hours than the reference. Whereas the Hydroxide-LDH had a slightly accelerating effect on the early strength of the mortar (see **Figure 39**). The same trends were observed for the flexural strength values (see **Figure 40**). It can be concluded that this cement is slightly accelerated by the Hydroxide-LDH phase.

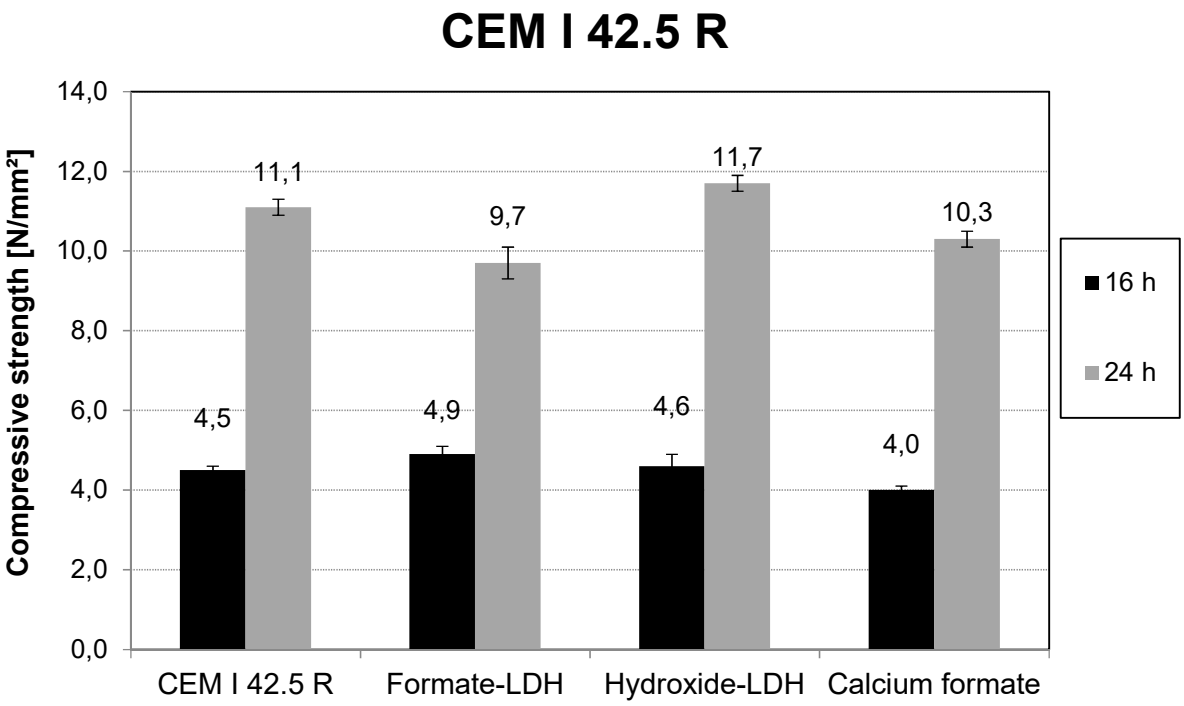

Figure 39: Compressive strength of the mortars consisting of CEM I 42.5 R admixed with 2 % bwoc of Ca_2Al-formate-LDH, 0.7 % bwoc calcium formate (equivalent to the amount in 2 % Ca_2Al-formate-LDH) and 2 % bwoc Ca_2Al-hydroxide-LDH, after 16 or 24 hours.

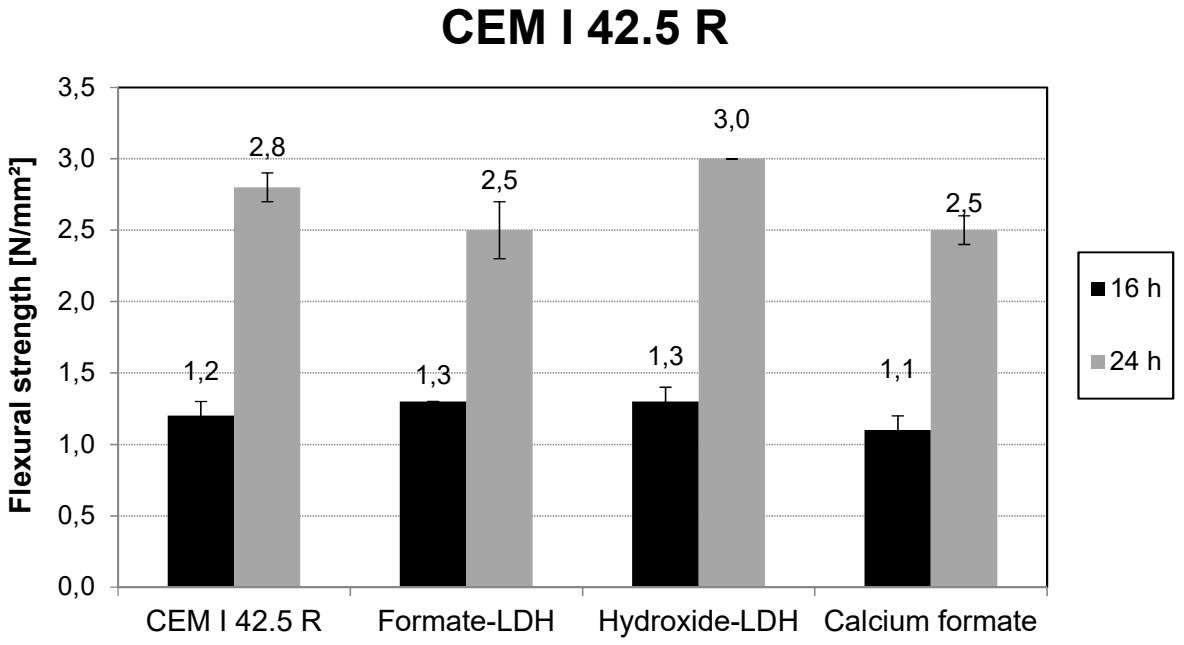

Figure 40: Flexural strength of the mortars consisting of CEM I 42.5 R admixed with 2 % bwoc of Ca_2Al-formate-LDH, 0.7 % bwoc Calcium formate (equivalent to the amount in 2 % Ca_2Al-formate-LDH) and 2 % bwoc Ca_2Al-Hydroxide-LDH, after 16 or 24 hours.

Interestingly, higher early strength of mortars admixed with hydrocalumite-type LDHs were observed with the coarse and thus low reactive CEM I 32.5 R, while the mortar admixed with equimolar amounts of $Ca(HCOO)_2$ only showed values comparable to the reference. This applies for the compressive strengths measured after 16 hours and especially after 24 hours.

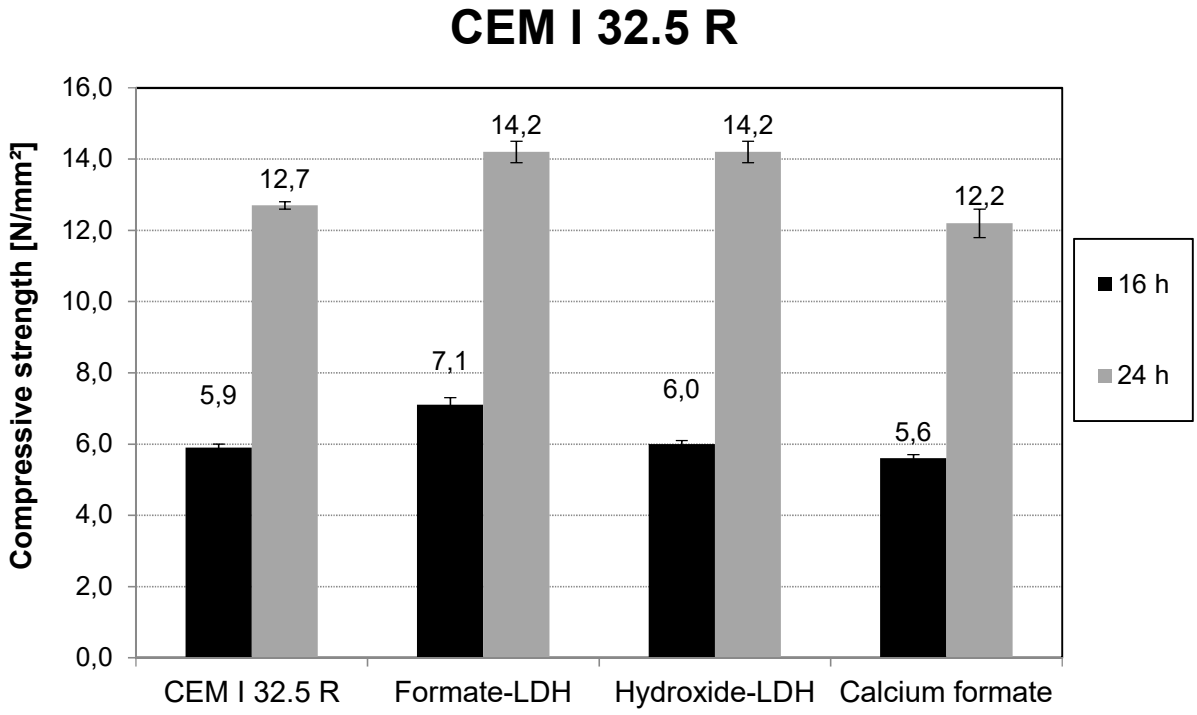

Figure 41: Compressive strength of the mortars consisting of CEM I 32.5 R admixed with 2 % bwoc of Ca_2Al-formate-LDH, 0.7 % bwoc Calcium formate (equivalent to the amount in 2 % Ca_2Al-formate-LDH) and 2 % bwoc Ca_2Al-Hydroxide-LDH, after 16 or 24 hours.

The same trend as for the compressive strength was observed for the flexural strength of mortars admixed with the hydrocalumite-type LDHs (see **Figure 42**). The overall higher values observed for the CEM I 32.5 R compared to mortars with CEM I 42.5 R or 52.5 R are due to its coarser particles size. It is well established that coarser cements which dissolve slower in water respond more pronounced to accelerating compounds. What is most significant here is that even a Formate-LDH accelerates substantially, while pure formate has no such effect on strength, as is known in the industry.

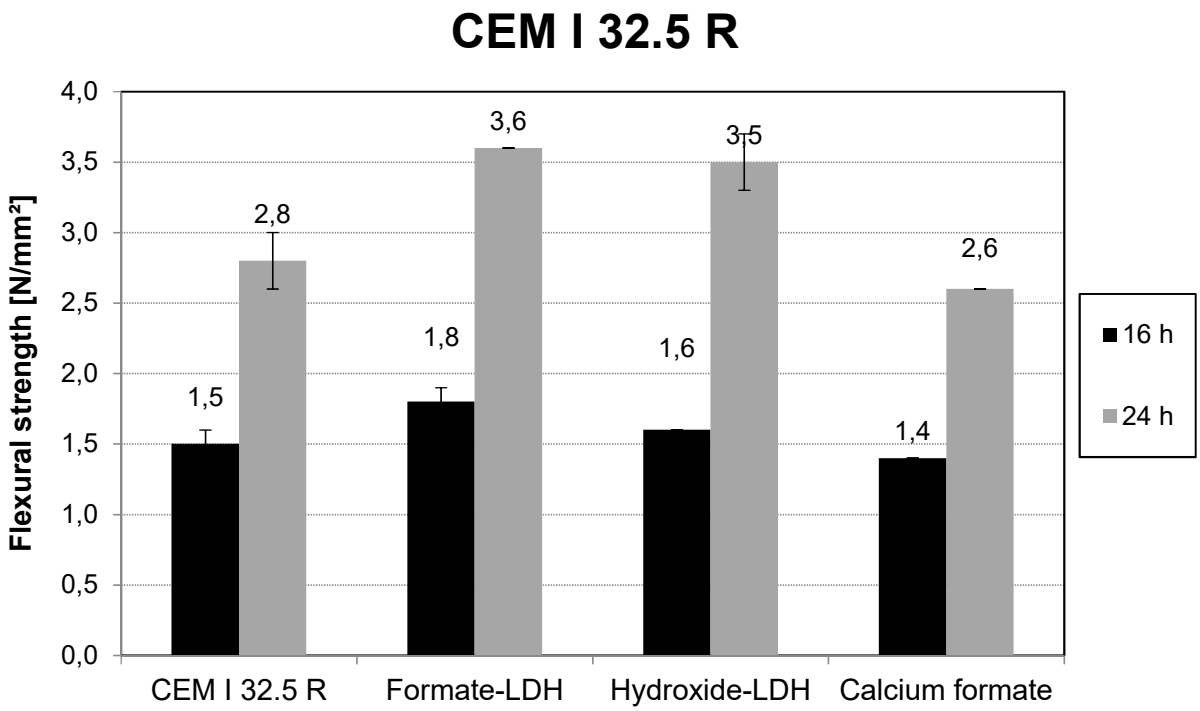

Figure 42: Flexural strength of the mortars consisting of CEM I 32.5 R admixed with 2 % bwoc of Ca_2Al-formate-LDH, 0.7 % bwoc Calcium formate (equivalent to the amount in 2 % Ca_2Al-formate-LDH) and 2 % bwoc Ca_2Al-Hydroxide-LDH, after 16 or 24 hours.

The results of the strength tests allow to conclude that hydrocalumite-type LDHs have an accelerating effect on cements exhibiting a coarse particle size. The low acceleration of the calcium formate can be explained by its different mode of action. This type of accelerator does not serve as a seeding material for AF_m phases like the LDH compounds, but it contributes Ca^{2+} and $HCOO^-$ ions which speed up dissolution of C_3S and the formation of C-S-H phases that occur mainly at a later stage during hydration (approximately 6 hours after mixing).[24, 118] This behaviour was observed in the compressive strengths reported by *Heikal* et al., too, where the accelerating effect of calcium formate after one day is not as pronounced as for example after seven days.[14]

Heat flow calorimetric measurements of the different cement samples admixed with Ca_2Al-HCOO-LDH and the equimolar amount of $Ca(HCOO)_2$ show only very minor differences in the heat of hydration during the first 12 h, compared to the reference (see **Figure 43**). A slightly higher heat of hydration was only detected for the samples admixed with calcium formate. This

experiment demonstrates that the heat flow released during cement hydration not necessarily represents the strength development as measured by crushing tests.

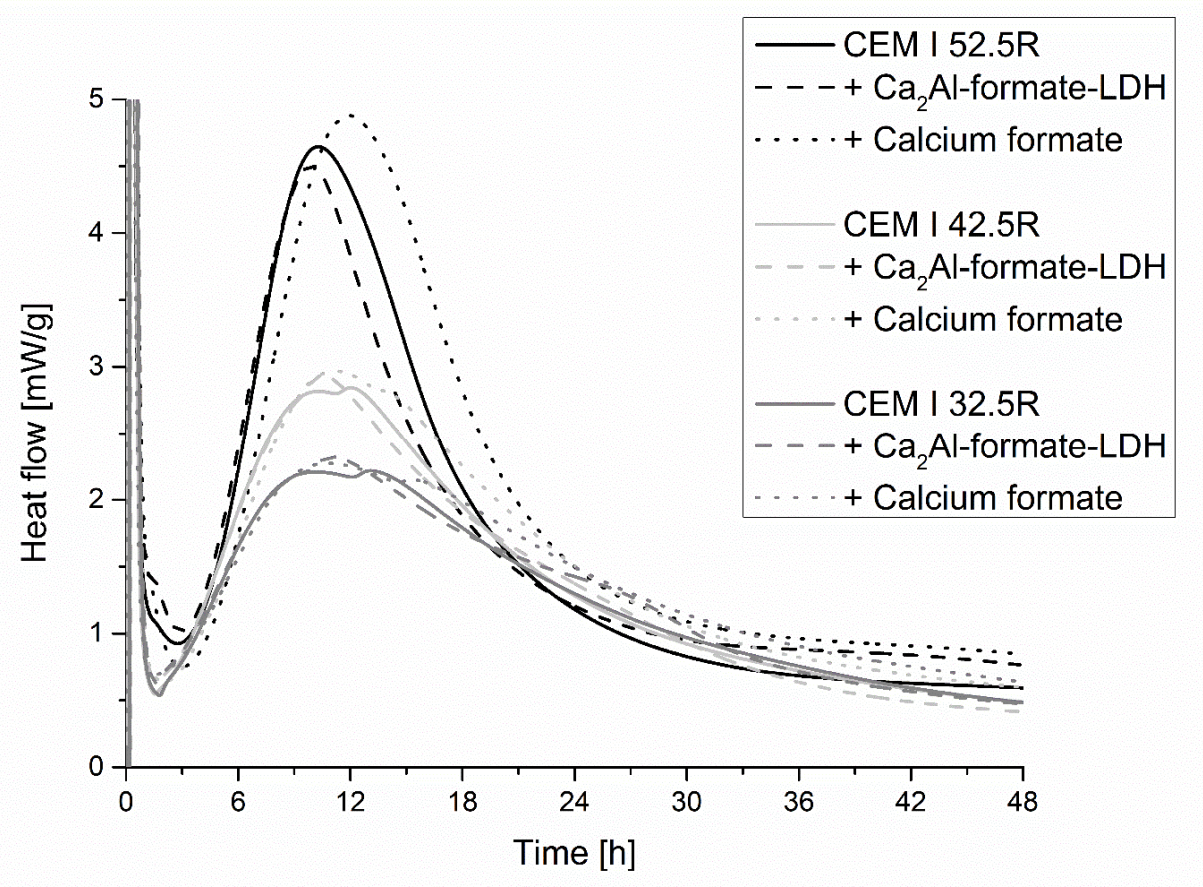

Figure 43: Heat of hydration of CEM I 52.5 R, CEM I 42.5 R and CEM I 32.5 R, admixed with 2% bwoc of Ca_2Al-HCOO-LDH and 0.7% bwoc Calcium formate (equivalent to the amount in 2% Ca_2Al-formate-LDH), at a w/c ratio of 0.5.

To obtain more insight into the accelerating effect of the Ca_2Al-HCOO-LDH on cement hydration, it was further investigated by in-situ XRD studies with pure CEM I 52.5 R cement at a w/c ratio of 0.5 which was used in the mortar tests. The patterns were collected over 72 hours and are given in the appendix (see **Figure A3 - A 6**). For a better illustration of the differences the in-situ XRD patterns in **Figures 44** and **45** only show the range from 28 - 36° 2θ.

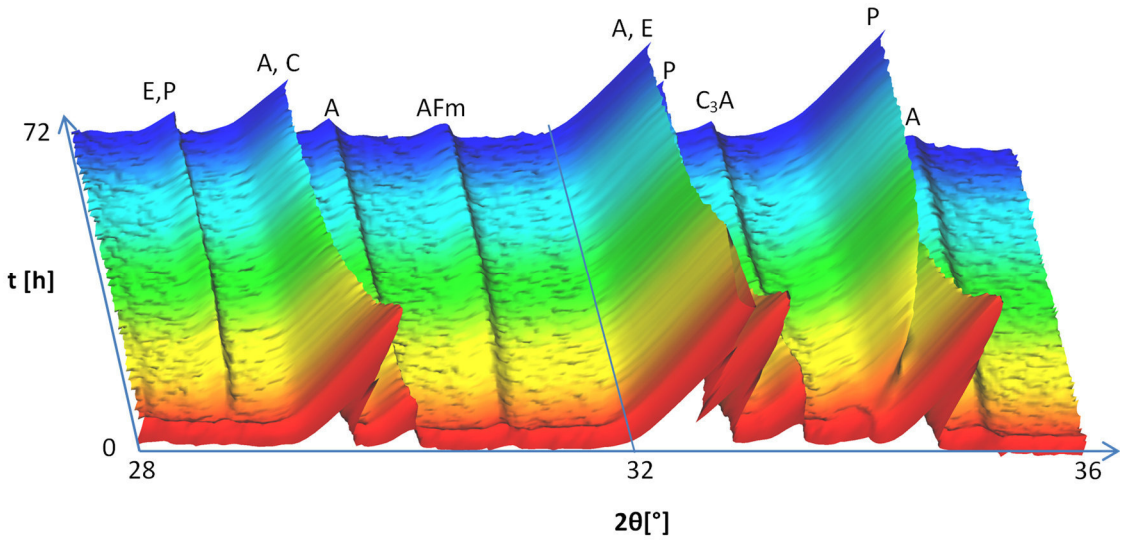

Figure 44: In-situ XRD pattern of CEM I 52.5 R mixed at w/c = 0.5. A = Alite, C = Calcite, E = Ettringite and P = Portlandite

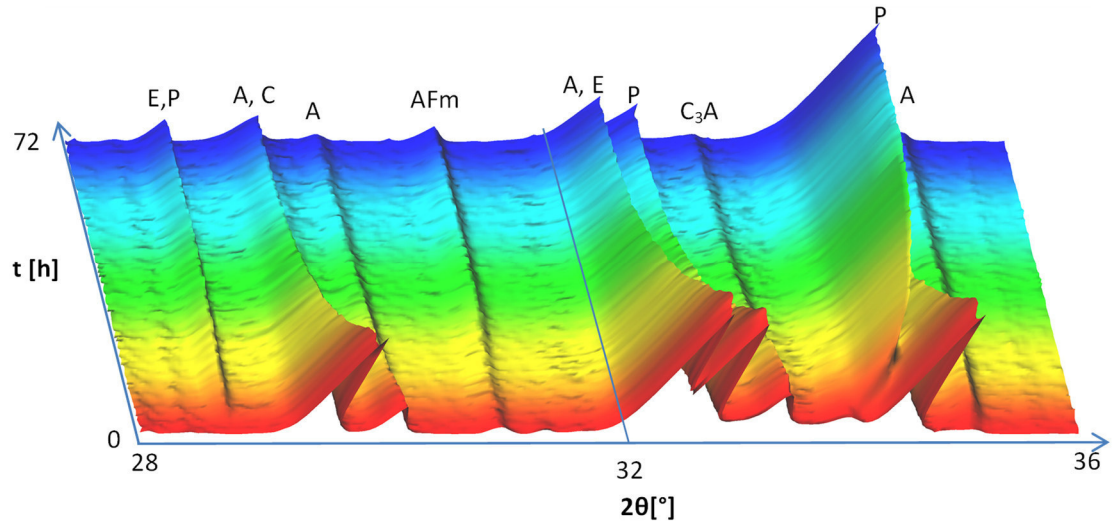

Figure 45: In-situ XRD pattern of CEM I 52.5 R mixed at w/c = 0.5 and holding 2 % bwoc Ca_2Al-HCOO-LDH. A = Alite, C = Calcite, E = Ettringite and P = Portlandite

The accelerating effect of the HCOO-LDH can be seen very clearly from the strong decline of the reflection of Alite in **Figure 45**, compared to **Figure 44**, especially in the first 24 hours. The reference mixture exhibits a longer induction period before the dissolution of C_3S starts, the main phase contributing to the final strength of Portland cement which produces C-S-H. Surprisingly, this could not be confirmed by heat flow calorimetry, where no increased heat release during the first 24 hours compared to the neat cement was observed.

5.3. Ettringite crystallization in OPC under terrestrial and microgravity conditions

Tricalcium aluminate is the most reactive clinker phase in OPC and influences significantly the setting and early strength of mortars. Therefore, it is of great interest to get insight into the crystal growth of its hydration products, namely ettringite and the AF_m phases like monosulfate or calcium aluminate hydrates. According to the classical nucleation theory, crystallization occurs in two main steps, namely nucleation and crystal growth. For nucleation, oversaturation of the solution is a pre-requisite. Once a nucleus has formed, crystal growth proceeds via transportation of growth units to the crystal surface and attachment of the growth units. In a cementitious system, upon addition of the mixing water dissolution of cement clinker phases leads to a supersaturation in the boundary zone between clinker and the bulk solution. First, precipitation of cement hydrates can then already occur in this boundary zone. The rest of the solved ions get transported away from the clinker surface into the bulk solution which decreases the concentration of ions near the clinker surface, thus leading to further dissolution of the clinker. Besides *Brownian* movement, convection is the main phenomenon driving transportation of ions in solution. In the absence of convection, ion transport is limited to *Brownian* movement and transportation of growth units becomes the rate-determining step of the crystallization process. Additionally, without convection supersaturation is reached earlier in the zone near the clinker surface due to slowed down mass transport away from the clinker. Thus, nucleation and precipitation processes start earlier under microgravity conditions. This was evidenced in previous studies from our group, where generally smaller but more abundant ettringite crystals were found in the absence of convection.[159]

In the following chapter, the very early crystallization of aluminate hydrates was studied under terrestrial gravity conditions as well as under microgravity. The experiments under microgravity conditions were performed on parabolic flights, with a special experimental setup, allowing hydration of cement for 10 s and subsequent stopping of the hydration reaction by addition of acetone at the end of the ~ 25 s of microgravity. Of special interest is the impact of superplasticizers which are present in almost every concrete formulation nowadays, and in particular the impact on the ettringite crystal growth of their molecular characteristics like the kind of their anionic anchor groups, their side chain length, their anionic charge density and

their dosage. The obtained crystals were characterized by XRD and SEM imaging regarding their morphology and crystal size.

5.3.1. Impact of the PCE side chain length on ettringite crystallization

In the following, commercial OPC samples, a CEM I 52.5 N and a CEM I 42.5 R, were hydrated for 10 s in the presence of different MPEG-PCEs under terrestrial and microgravity conditions. For the experiments a w/c ratio of 1.0 and a PCE dosage of 0.05 % bwoc was applied. The aim was to study the impact of the PCE side chain length on the ettringite crystal growth. Therefore, MPEG-PCEs with the same backbone comprising a molar ratio of acrylic acid to polyethylene glycol macromonomer of 6:1 were used. The side chain lengths varied from 6 ethylene oxide (EO) units up to 114.

Electron microscopic analysis showed clearly that the ettringite crystal size changes significantly in the presence of superplasticizers, compared to those in neat cement paste (see **Figure 46**). The ettringite crystals formed in the neat cement paste generally look very stocky, while those crystals obtained in the presence of PCEs appear longer, but slimmer. The different side chain lengths of the PCEs do not inflict a significant change in the morphology or size of the ettringite crystals. This observation was confirmed by measuring the crystal sizes (see **Figure 47** and **49**).

At 1 *g*, there is a significant change in both length and diameter of the ettringite crystals and thus in the aspect ratio between the crystals from neat cement paste and those from pastes containing admixture. While at µ *g*, in the presence of PCEs only a statistically significant change in the length, but not in the diameter of the crystals was observed, compared to the neat cement paste. Thus, the increasing aspect ratios observed for ettringite crystals recovered from hydration experiments admixed with PCE are statistically significant, too (see **Table 8**). Generally, the ettringite crystals formed under microgravity are smaller in size compared to the crystals formed under terrestrial condition.

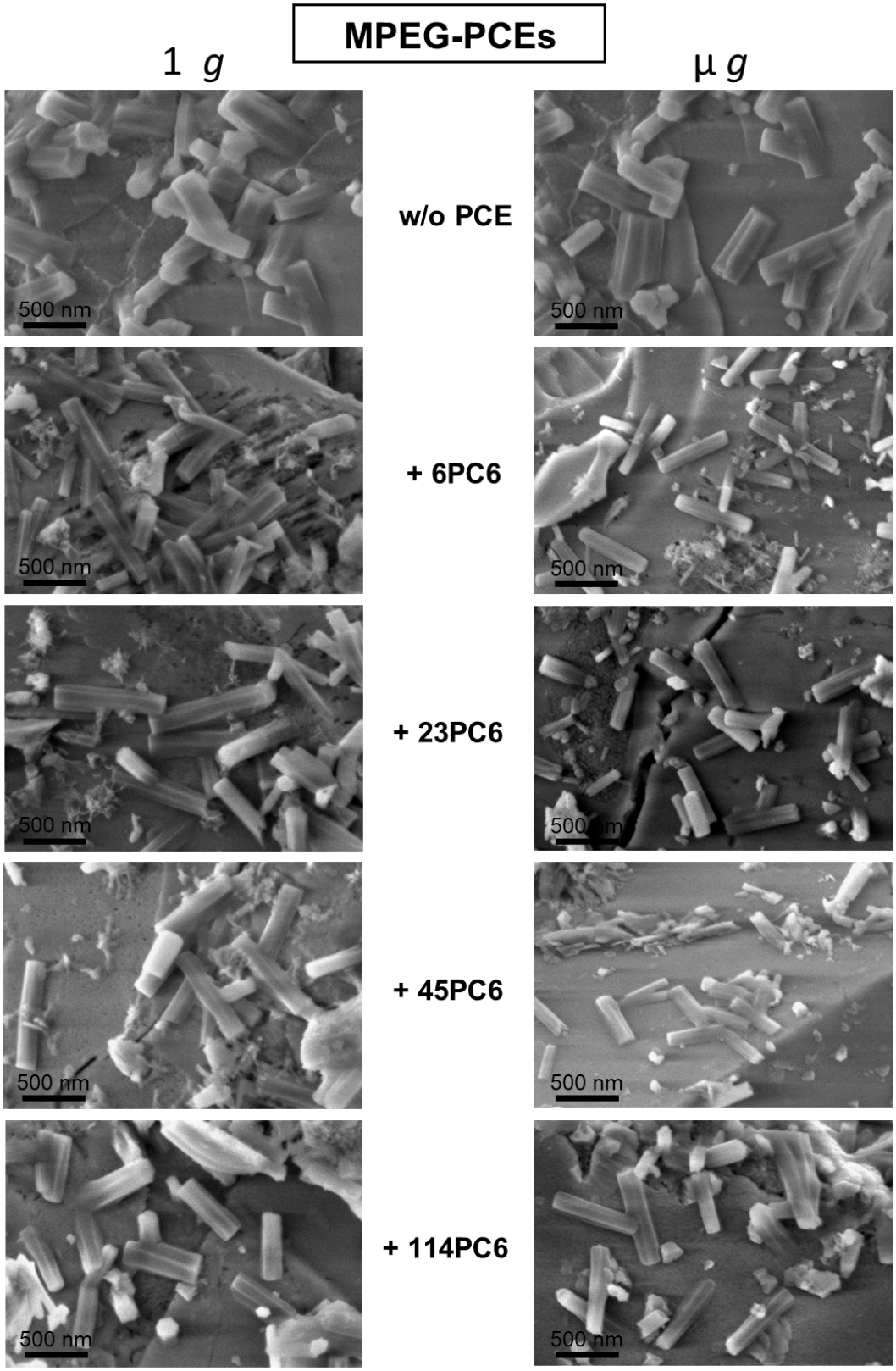

Figure 46: SEM images of CEM I 52.5 N sample hydrated for 10 s in the presence of 0.05 % bwoc MPEG-PCE samples with side chain lengths increasing from 6 to 114 ethylene oxide units under terrestrial (left) and microgravity (right) conditions. All images were collected at 40 k magnification.

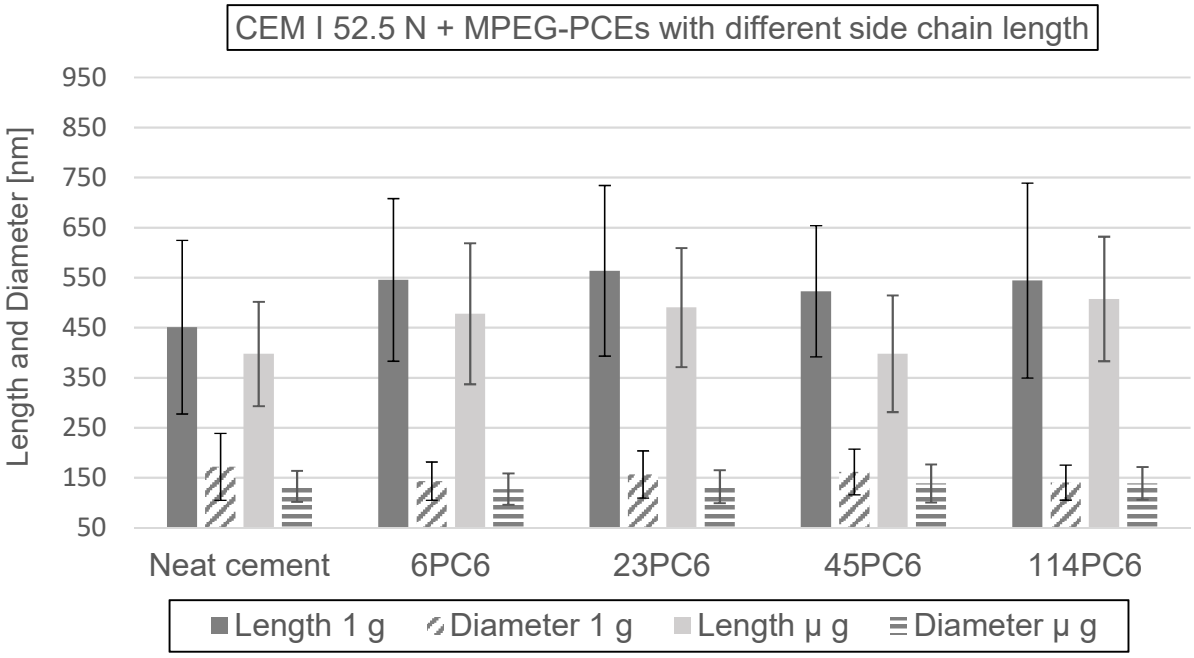

Figure 47: Average length and diameter of ettringite crystals obtained from CEM I 52.5 N admixed with 0.05 % bwoc MPEG-PCE samples possessing increasing side chain lengths from 6 to 114 ethylene oxide units, grown under terrestrial and microgravity conditions.

The increase in ettringite crystals lengths accompanied by a decrease in crystal diameter in the presence of PCE suggests that the PCEs adsorb rather on the lateral crystal faces than on the hexagonal top and bottom faces of the ettringite crystals. Thus, crystal growth along the *a* and *b* axis is inhibited by adsorbed polymer, while growth along the *c*-axis can proceed. Furthermore, under µ *g* condition this effect is much less pronounced (see **Table 8**), because there, crystal growth is generally slower.

Table 8: Average aspect ratios of ettringite crystals obtained from CEM I 52.5 N admixed with 0.05 % bwoc MPEG-PCE samples with side chain lengths increasing from 6 to 114 ethylene oxide units, grown under terrestrial and microgravity conditions.

Condition	Neat Cement	+ MPEG-PCE 6PC6	+ MPEG-PCE 23PC6	+ MPEG-PCE 45PC6	+ MPEG-PCE 114PC6
1 *g*	2.8 ± 1.0	3.9 ± 1.1	4.0 ± 1.4	3.4 ± 0.9	4.0 ± 1.3
µ *g*	3.1 ± 0.7	3.9 ± 1.3	3.8 ± 1.0	2.9 ± 0.6	3.7 ± 0.8

In another series of experiments, all PCEs were admixed to the CEM I 42.5 R sample and the ettringite crystals obtained under terrestrial and microgravity conditions after 10 s of hydration were analysed.

The ettringite crystals formed in the neat cement paste of CEM I 42.5 R appear to be larger in size, compared to those obtained from the hydration of CEM I 52.5 N (see **Figures 46** and **48**). This observation was also made for the samples containing PCE. This could be attributed to the more coarse cement particles which prolongs the time to reach oversaturation, or a different pH value resulting from the specific clinker composition of this cement. Furthermore, the ettringite crystals formed during hydration of this CEM I 42.5 R in the presence of MPEG-PCEs exhibit the same size and morphology as those from the neat cement paste, as is evident from the SEM images displayed in **Figure 48**.

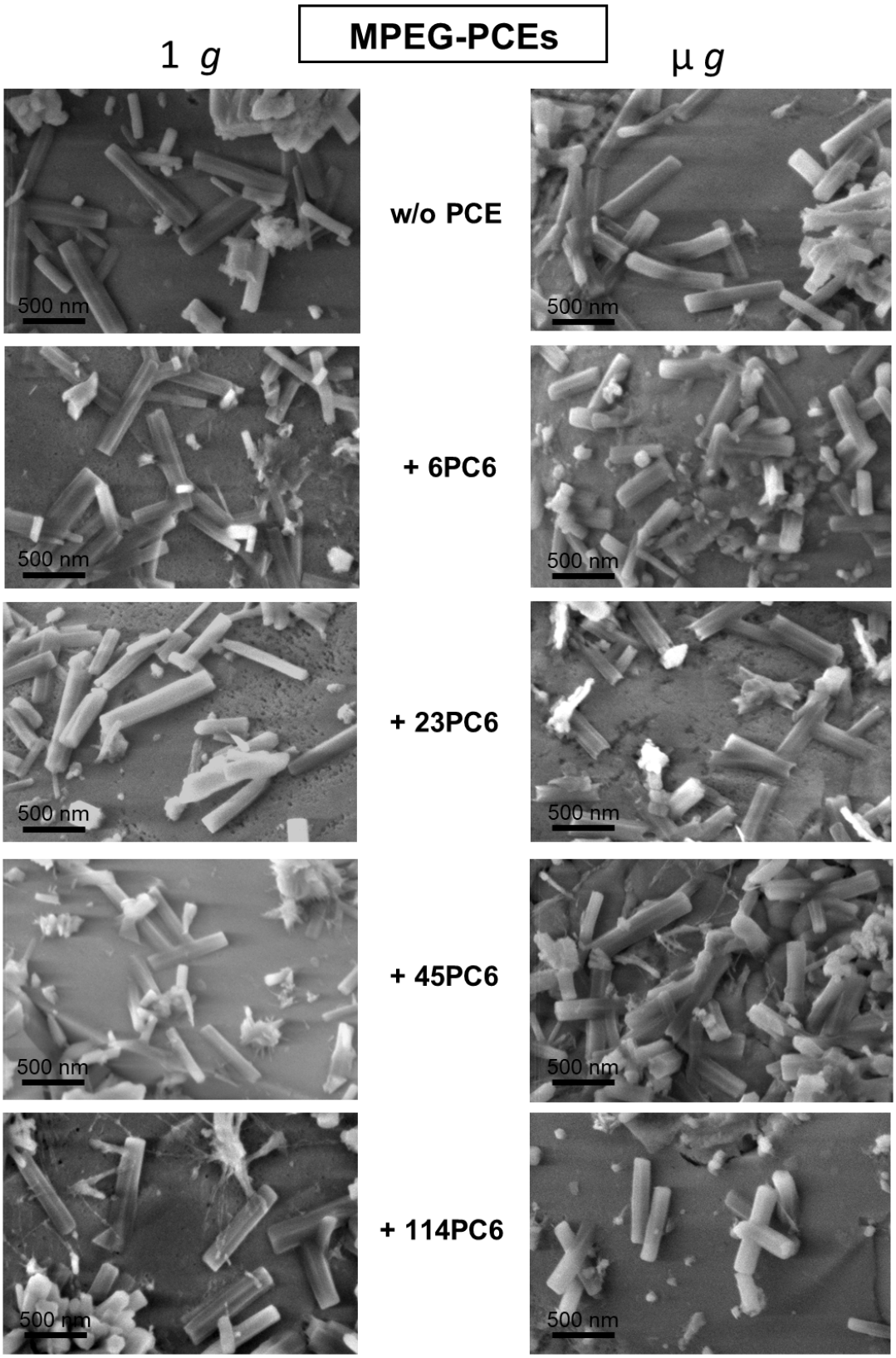

Figure 48: SEM images of CEM I 42.5 R sample hydrated for 10 s in the presence of 0.05 % bwoc MPEG-PCE samples with side chain lengths increasing from 6 to 114 ethylene oxide units under terrestrial (left) and microgravity (right) conditions. All images were collected at 40 k magnification.

The evaluation of ettringite crystal sizes confirmed these findings. Ettringite crystals formed during 10 s hydration of CEM I 42.5 R admixed with PCEs possessing different side chain lengths show no statistically significant trend regarding their crystal lengths or diameters, compared to the crystals from the neat cement paste. Furthermore, the calculated aspect ratios of the crystals range from 3.6 to 4.6 without a clear trend from the side chain lengths of the PCE samples (see **Figure 49** and **Table 9**). Interestingly, under microgravity conditions all PCE polymers produce ettringite crystals with relatively uniform aspect ratio (3.7 – 4.1).

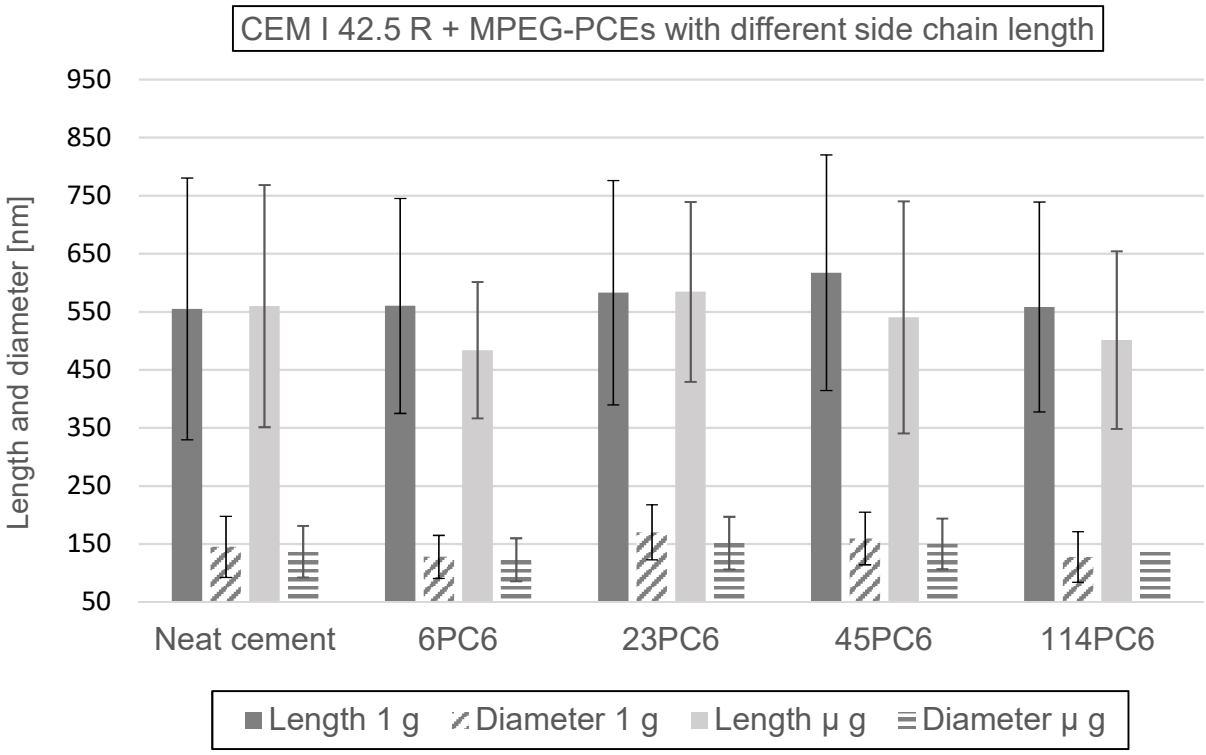

Figure 49: Average length and diameter of ettringite crystals obtained from CEM I 42.5 R admixed with 0.05 % bwoc MPEG-PCE samples possessing increasing side chain lengths from 6 to 114 ethylene oxide units, grown under terrestrial and microgravity conditions.

Table 9: Average aspect ratios of ettringite crystals grown under 1 *g* and μ *g* conditions on CEM I 42.5 R sample admixed with 0.05 % bwoc MPEG-PCE samples with side chain lengths increasing from 6 to 114 ethylene oxide units.

Condition	Neat Cement	+ MPEG-PCE 6PC6	+ MPEG-PCE 23PC6	+ MPEG-PCE 45PC6	+ MPEG-PCE 114PC6
1 *g*	3.9 ± 1.4	4.6 ± 1.5	3.6 ± 1.1	4.0 ± 1.2	4.6 ± 1.3
μ *g*	4.1 ± 1.3	4.0 ± 1.0	4.0 ± 1.1	3.7 ± 1.1	3.7 ± 1.5

Apparently, a PCE dosage of 0.05 % bwoc is too low to significantly inhibit ettringite crystal growth in cement samples containing a high amount of aluminates.

5.3.2. Impact of the anionic charge density of PCEs on ettringite crystallization

Polycarboxylate superplasticizers are negatively charged polymers that adsorb on positively charged cement particles or cement hydrates. Their adsorption capability is determined by their anionic charge density. This property can be adjusted during synthesis by varying the ratio of carboxylic acid monomers to macromonomers. As mentioned above, ettringite is known to present the main anchoring site for negatively charged superplasticizers. Therefore, it is of great interest to investigate the impact of the anionic charge density of PCEs on the crystal growth of ettringite during early hydration. For the experiments here, three different MPEG-PCE samples possessing an average side chain made of 45 EO units were chosen. The ratio of methacrylic acid to ω-methoxy poly(ethylene glycol) methacrylate ester was 2:1, 6:1 and 10:1, resulting in anionic charge densities of the polymers of 1,460 μeq/g, 3,630 μeq/g and 5,030 μeq/g for the polymers designated as 45PC2, 45PC6 and 45PC10, respectively. Again, the Portland cement samples CEM I 52.5 N and 42.5 R were admixed with a dosage of 0.05 % bwoc of the MPEG-PCEs and hydrated for 10 s under terrestrial and microgravity conditions. The impact of the anionic charge density of the polymers was evaluated by measurement of the ettringite crystal sizes found in the recovered hydrated cement samples.

For CEM I 52.5 N hydrated under terrestrial gravity, generally longer and slimmer ettringite crystals were found in the presence of PCEs, compared to those recovered from neat cement paste (see **Figure 50**). Furthermore, crystal size became even larger with increasing anionic charge density of the polymers. While the impact of MPEG-PCE samples 45PC2 and 45PC6 on ettringite crystal size was quite comparable, crystals obtained in the presence of the highly anionic MPEG-PCE sample 45PC10 were significantly larger in size. Additionally, the average crystal size determined under 1 *g* condition was larger compared to those obtained under microgravity conditions. This observation is in good agreement with the results presented in section 5.3.1. At µ *g*, a similar trend for the ettringite crystal size was found as under terrestrial conditions. Here, the presence of MPEG-PCE 45PC10 which possesses a particularly high anionic charge leads to very long and thin ettringite crystals (see **Figure 50**).

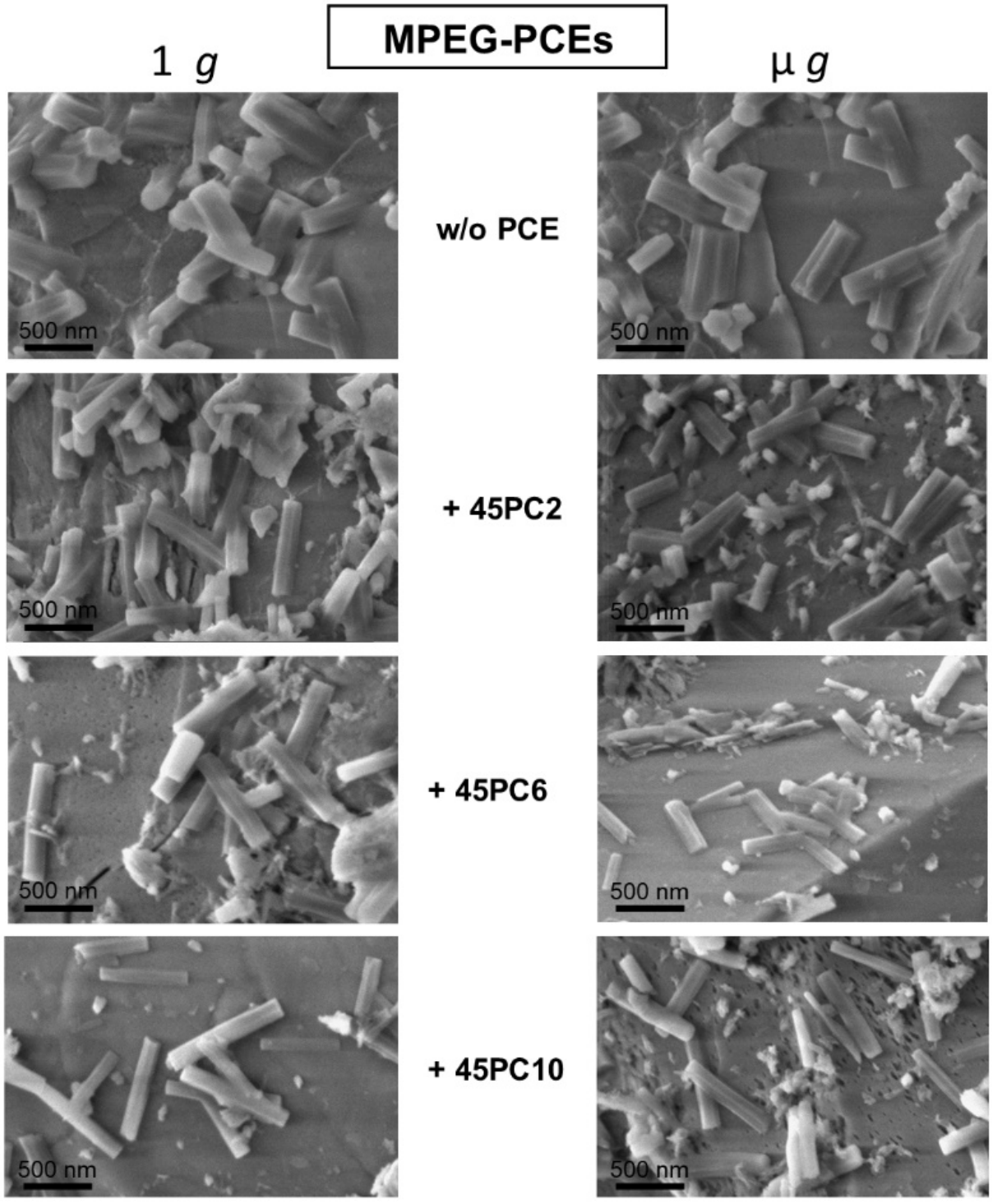

Figure 50: SEM images of CEM I 52.5 N sample hydrated for 10 s in the presence of 0.05 % bwoc MPEG-PCE samples 45PC2, 45PC6 and 45PC10 possessing increasing anionic charge density under terrestrial (left) and microgravity (right) conditions. All images were collected at 40 k magnification.

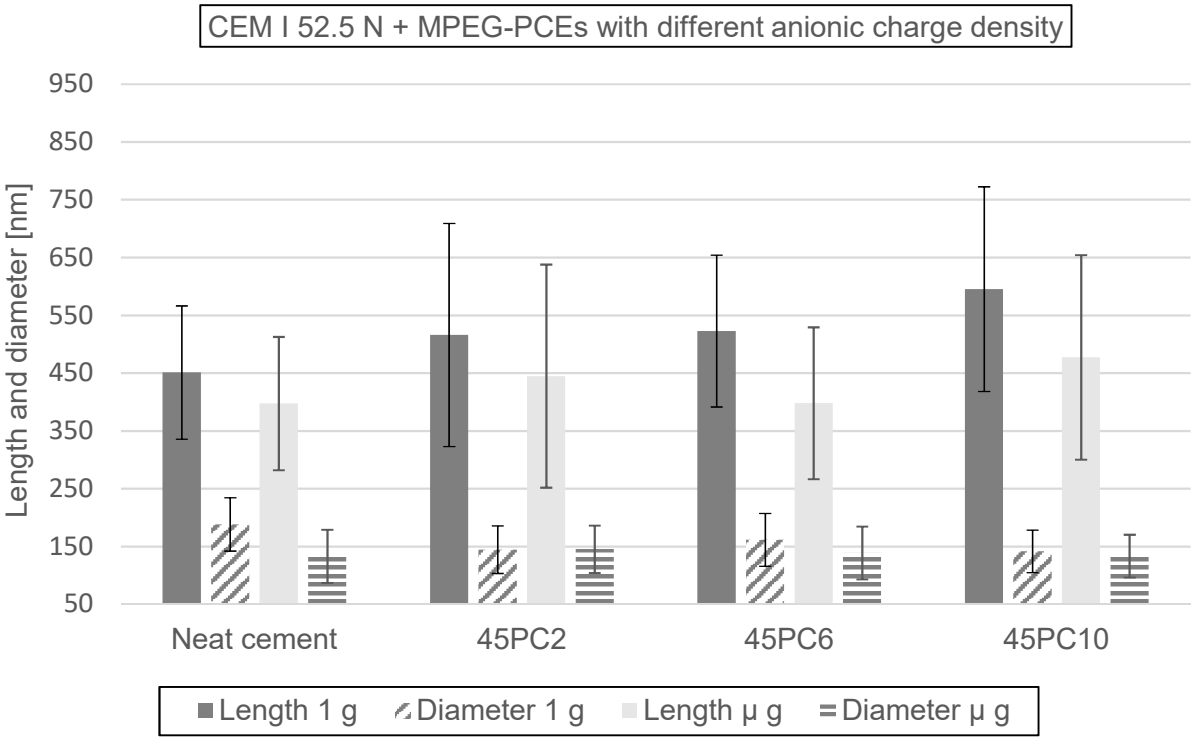

Figure 51: Average length and diameter of ettringite crystals obtained from CEM I 52.5 N admixed with 0.05 % bwoc MPEG-PCE samples 45PC2, 45PC6 and 45PC10 possessing increasing anionic charge density, grown under terrestrial and microgravity conditions.

Under both terrestrial and microgravity condition, MPEG-PCE 45PC10, possessing the highest anionic charge and thus the highest adsorption capacity of the PCEs tested produces ettringite crystals of very high aspect ratios of 4.3 and 3.7 for 1 *g* and µ *g*, respectively, compared to those found in neat cement paste (2.8 and 3.1 for 1 *g* and µ *g*; see **Table 10**).

Table 10: Average aspect ratios of ettringite crystals grown under 1 *g* and µ *g* conditions on CEM I 52.5 N admixed with 0.05 % bwoc MPEG-PCE samples 45PC2, 45PC6 and 45PC10 possessing increasing anionic charge density.

Condition	**Neat Cement**	**+ MPEG-PCE 45PC2**	**+ MPEG-PCE 45PC6**	**+ MPEG-PCE 45PC10**
1 *g*	2.8 ± 1.0	3.7 ± 1.2	3.4 ± 0.9	4.3 ± 1.1
µ *g*	3.1 ± 0.7	3.2 ± 0.8	2.9 ± 0.6	3.7 ± 1.0

These results show that at a dosage of only 0.05 % bwoc a highly anionic PCE can significantly alter the morphology of ettringite crystals within the first seconds of hydration. Crystal growth along the *a* and *b* axis of ettringite is inhibited, as can be seen from the decrease of the crystal diameter by approximately 40 nm for hydration under 1 *g*. Contrary, the crystal growth along the *c* axis is promoted which suggests a high affinity of the polymer to the lateral crystal faces, while the top and bottom faces stay free of polymer. Hence, crystal growth can proceed by ion transport to the end faces of the crystals.

Representative ettringite crystals obtained from short-term hydration of OPC sample CEM I 42.5 R admixed with MPEG-PCEs possessing different anionic charge are shown in **Figure 52**. An abundance of long crystals exhibiting the characteristic hexagonal prismatic shape of ettringite was found. As expected, in the presence of the sample 45PC2 which possesses the lowest anionic charge, the largest crystals with respect to length and diameter were found. With increasing anionic charge of the PCEs, present in the cement paste, lengths and diameters of the ettringite crystals decreased. This effect of the anionic charge of PCEs on ettringite crystal size has been observed before for samples hydrated at µ *g*, although once again there it is less pronounced due to the slower crystal growth under microgravity conditions.

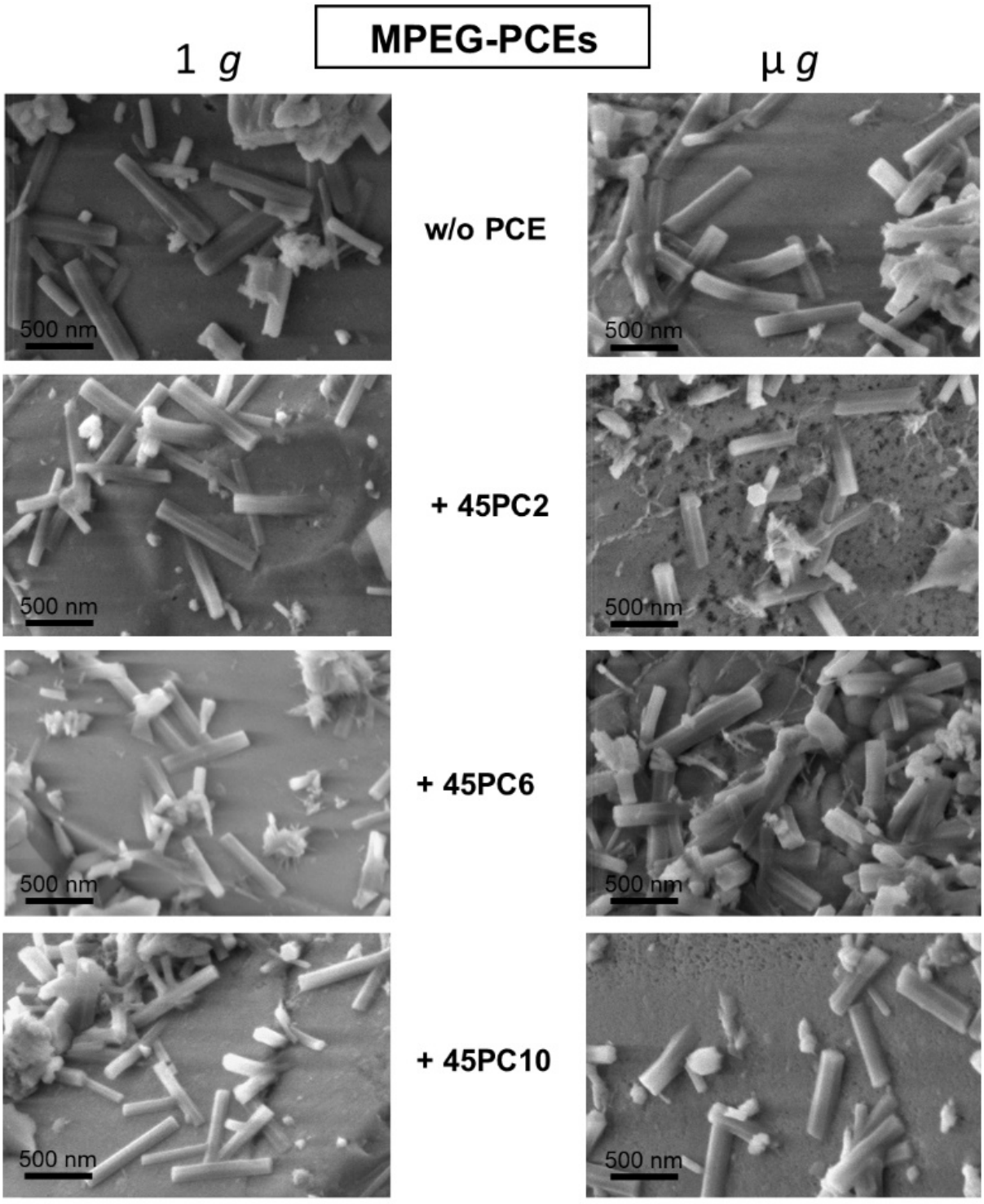

Figure 52: SEM images of CEM I 42.5 R sample hydrated for 10 s in the presence of 0.05 % bwoc MPEG-PCE samples 45PC2, 45PC6 and 45PC10 possessing increasing anionic charge density under terrestrial (left) and microgravity (right) conditions. All images were collected at 40 k magnification.

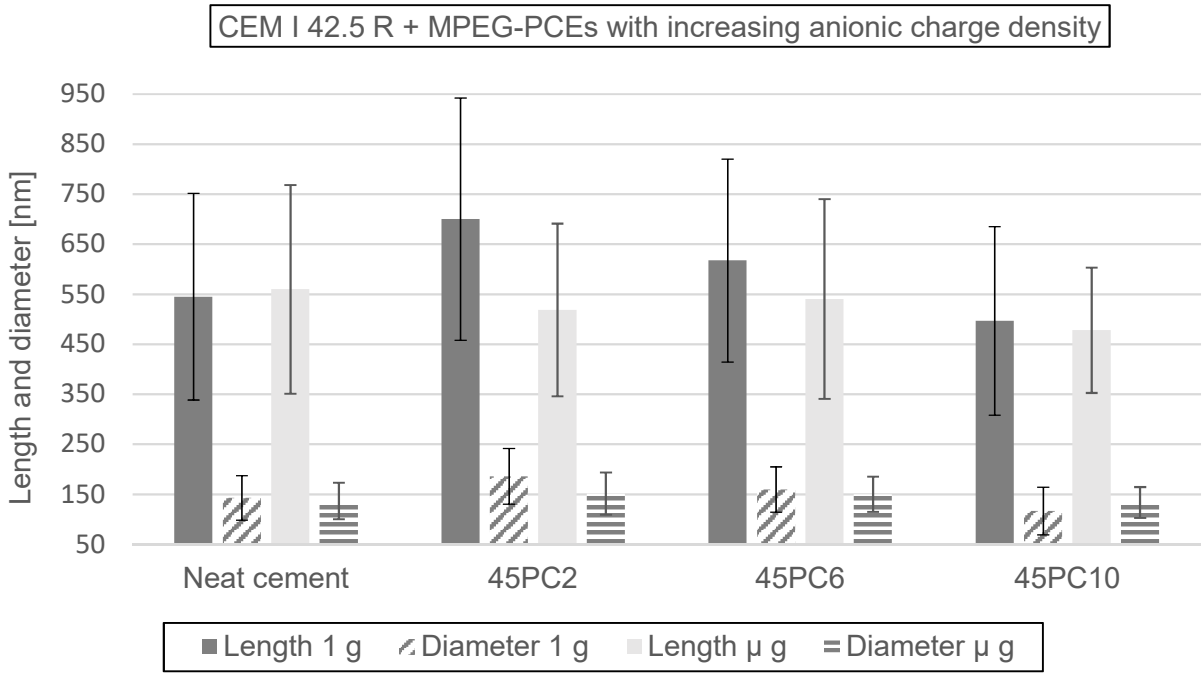

Figure 53: Average length and diameter of ettringite crystals obtained from CEM I 42.5 R admixed with 0.05 % bwoc MPEG-PCE samples 45PC2, 45PC6 and 45PC10 possessing increasing anionic charge density, grown under terrestrial and microgravity conditions.

The decrease of both crystal length and diameter is quite consistent for samples 45PC2 and 45PC6, as their aspect ratios are comparable (see **Table 11**). For the highly anionic sample 45PC10, however, a significant decrease in crystal diameter is observed which leads to a higher aspect ratio (4.5) of the ettringite crystals formed. This is in good agreement with the findings on the hydration of CEM I 52.5 N admixed with these PCEs. It supports the hypothesis of strong adsorption of highly anionic PCEs on the lateral faces of ettringite crystals.

Table 11: Average aspect ratios of ettringite crystals grown under 1 *g* and µ *g* conditions on CEM I 42.5 R admixed with 0.05 % bwoc MPEG-PCE samples 45PC2, 45PC6 and 45PC10 possessing increasing anionic charge density.

Condition	**Neat Cement**	**+ MPEG-PCE 45PC2**	**+ MPEG-PCE 45PC6**	**+ MPEG-PCE 45PC10**
1 *g*	3.9 ± 1.4	4.0 ± 1.4	4.0 ± 1.2	4.5 ± 1.7
µ *g*	4.1 ± 1.3	3.5 ± 1.0	3.7 ± 1.1	3.7 ± 1.0

5.3.3. Influence of PCE kind and dosage on ettringite crystallization performed under terrestrial and microgravity conditions

The previous investigations have revealed that a PCE dosage of 0.05 % bwoc already can impede ettringite crystal growth and alter the overall size and aspect ratio of ettringite crystals. Especially PCEs with a very long side chain, like MPEG-114PC6, and those exhibiting a high anionic charge density, e.g. MPEG-45PC10, led to ettringite crystals with an increased aspect ratio due to hindered crystal growth along the *a* and *b* axis.

In the following, the impact of two chemically different types of polycarboxylate ether comb-polymers, a MPEG-45PC6 and an IPEG-52PC8 possessing medium side chain lengths and anionic charges on early ettringite crystal growth as a function of their dosage is investigated under terrestrial and microgravity conditions. PCE dosages of 0 %, 0.05 %, 0.15 % and 0.25 % bwoc were applied. The amount of ettringite crystals formed was determined by X-ray analysis and the crystal size was evaluated by SEM imaging.

It was found that the presence of those PCEs leads generally to longer, but slimmer ettringite crystals. This effect became even more pronounced with increased PCE dosage (see **Figure 54**).

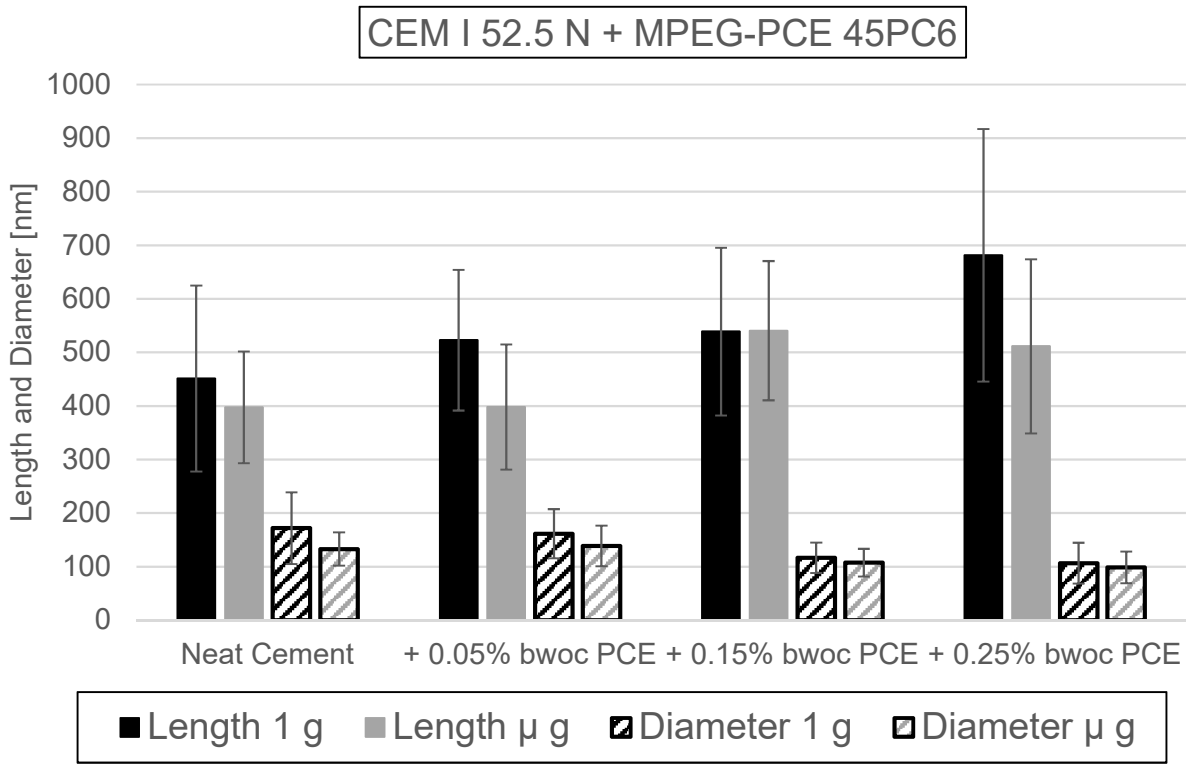

Figure 54: Average length and diameter of ettringite crystals obtained from CEM I 52.5 N admixed with different dosages of PCE sample MPEG-45PC6, hydrated under 1 *g* and µ *g* conditions, respectively, after[167].

SEM images of the formed ettringite crystals showed that at the high PCE dosage of 0.25 % bwoc, the crystals exhibited a needle-like morphology compared to the rather stocky crystals formed in the absence of PCE (see **Figure 55**). This effect manifests itself in the increasing aspect ratios of the ettringite crystals obtained at higher dosages.

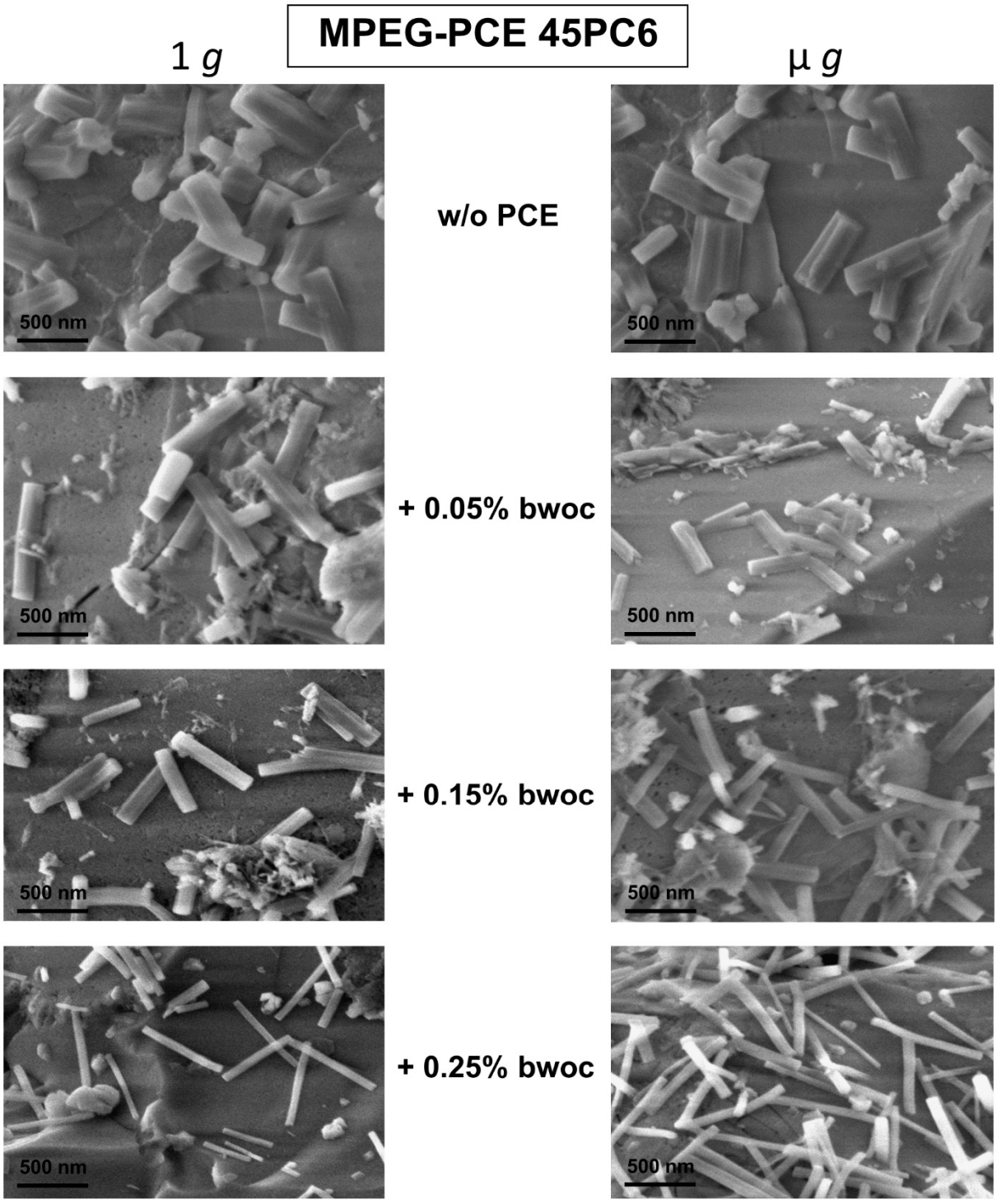

Figure 55: SEM images of CEM I 52.5 N sample hydrated for 10 s in presence of increasing dosages of PCE sample MPEG-45PC6 under terrestrial (left) and microgravity (right) conditions. All images were collected at 40.000 x magnification.

Moreover, the MPEG-based PCE had no influence on the amount of ettringite formed while cement hydrated in the presence of the IPEG-PCE sample formed significantly less ettringite crystals under microgravity conditions.

Furthermore, the ettringite crystals grown in the presence of the IPEG-PCE sample were generally larger in size compared to the crystals grown in the presence of the MPEG-PCE. Only few ettringite crystals exhibiting a needle-like morphology like in the case of the MPEG-PCE were found as evidenced by SEM images (see **Figure 56**).

With increasing PCE dosage the ettringite crystal length increased significantly, while the decrease in diameter was less pronounced (see **Figure 57**). Thus, similar aspect ratios were found for the ettringite crystals grown in the presence of these two chemically different PCEs.

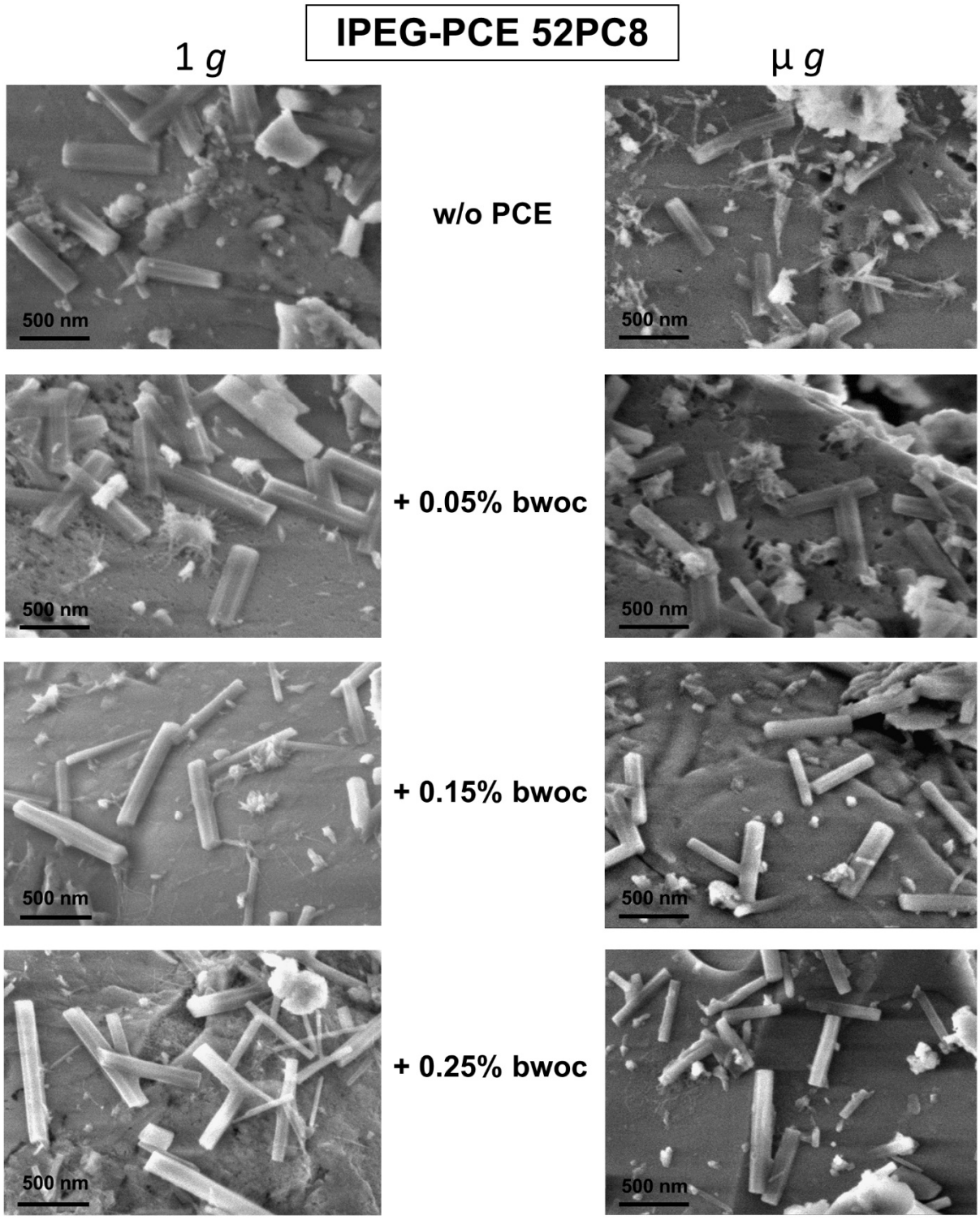

Figure 57: SEM images of CEM I 52.5 N sample hydrated for 10 s in presence of increasing dosages of PCE sample IPEG-52PC8 under terrestrial (left) and microgravity (right) conditions. All images were collected at 40.000 x magnification.

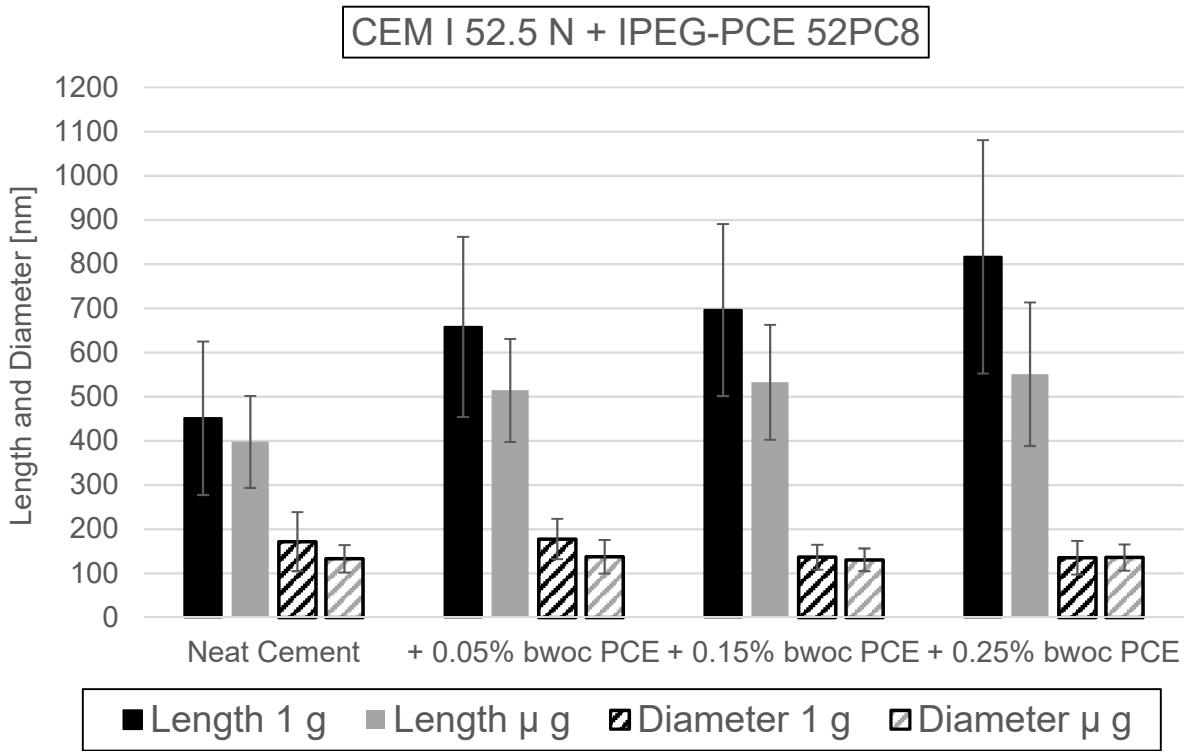

Figure 57: Average length and diameter of ettringite crystals obtained from CEM I 52.5 N admixed with different dosages of PCE sample IPEG-52PC8, hydrated under 1 *g* and µ *g* conditions, respectively, after[167].

The pronounced crystal growth along the *c* axis and the limited growth along the *a* and *b* axis suggests that the polymer adsorbs preferably on the lateral faces of the ettringite crystals than on the top and bottom faces.

Ettringite crystals grown under microgravity were again smaller in size than those grown under terrestrial gravity conditions. Additionally, it was found that the effect of the IPEG-PCE on the ettringite crystal growth was here nearby independent from the dosage of the PCE. Apparently, already a small dosage of this IPEG-PCE is sufficient to alter the nucleation and crystal growth of ettringite. This is in contrast to the experiments with the MPEG-PCE which requires higher dosages to gradually change the morphology of ettringite crystals. These results are presented in detail in the publication #1 which follows.

Finally, it was found that the inhibition of ettringite crystal growth by two chemically different superplasticizers is strongly related to their adsorption ability on cement hydrate surfaces. PCEs exhibiting a high affinity for the surface of ettringite crystals can cover the crystal surface

more densely, especially the lateral faces, and thus impede the transport of growth units to the crystal surface more effectively.

Publication #1

Influence of PCE kind and dosage on ettringite crystallization performed under terrestrial and microgravity conditions

M. Schönlein, J. Plank

Journal of the American Ceramic Society
Volume 101, Issue 8, August 2018, Pages 3575 - 3584

Received: 8 September 2017 | Accepted: 14 February 2018

DOI: 10.1111/jace.15513

ORIGINAL ARTICLE

Journal of the American Ceramic Society

Influence of PCE kind and dosage on ettringite crystallization performed under terrestrial and microgravity conditions

Markus Schönlein | **Johann Plank**

Chair for Construction Chemistry, Technische Universität München, Garching, Germany

Correspondence
Johann Plank, Chair for Construction Chemistry, Technische Universität München, Garching, Germany.
Email: sekretariat@bauchemie.ch.tum.de

Abstract

Early ettringite crystallization in the presence of 2 chemically different polycarboxylate superplasticizers was studied by hydrating a commercial portland cement (CEM I 52.5 N) for 10 seconds. It was found that the presence of polycarboxylate superplasticizers leads to ettringite crystals which are longer, yet slimmer (higher aspect ratio), compared with the crystals obtained from neat cement paste. This finding suggests that the polycarboxylate (PCE) polymers predominantly adsorb on the lateral faces of the hexagonal-prismatic crystals of ettringite. For the methacrylate-based PCE, this effect increases with increasing superplasticizer dosage, whereas for the IPEG-PCE, the effect achieved at a very low dosage (0.05%) is not altered when dosage increases. The behaviors of both PCE polymers can be explained by their different adsorption behavior, whereby the IPEG-PCE reached the saturated adsorbed amount at much lower dosage than the MPEG-PCE. Microgravity only has a minor effect on the growth of ettringite. There, generally smaller crystals are observed.

KEYWORDS

crystal growth, ettringite, microgravity, nucleation, portland cement, superplasticizer

1 | INTRODUCTION

The hydration of portland cement is a very complex process involving dissolution, precipitation, crystallization, and surface reactions of the various clinker phases. Tricalcium aluminate (C_3A) which is known to present the most reactive of all clinker phases upon hydration mainly produces ettringite and/or monosulfoaluminate, depending on the kind and content of sulfate species, for example, gypsum, hemihydrate or anhydrite. In portland cements the formation of ettringite occurs instantaneously, that is, within seconds after mixing with water, due to the rapid dissolution of significant amounts of Ca^{2+}, $Al(OH)_4^-$, and SO_4^{2-} ions into the pore solution. Such early formed ettringite not only contributes to the "green" strength of concrete, but it also significantly influences the consistency and workability of the cement paste.

Nowadays, concrete mixes routinely contain polycarboxylate (PCE) superplasticizers which present the most effective cement dispersants and allow high workability even at low water/cement ratios. The impact of these admixtures on the crystallization of cement hydrates is crucial as they affect not only the fluidity of the cement paste, but also the microstructure of hardened cement.[1] Heat calorimetric studies performed by Jansen et al[2] and Kreppelt et al[3] revealed that specific PCE polymers can significantly retard cement hydration. The retarding effect was attributed either to complexation of Ca^{2+} ions present in the pore solution, resulting in calcium depletion which delays the crystallization of cement hydrates, or to polymer adsorption on cement hydrates which inhibits their growth.[2] Yoshioka et al[4] and Plank et al[5] have shown that the main anchoring site for anionic superplasticizer polymers is ettringite due to its positively charged surface. It is therefore of fundamental importance to understand the

nucleation and early crystal growth mechanism of the latter in the presence of different kinds of superplasticizers.

Cody et al[6] have investigated the morphology of synthetic ettringite formed in the presence of a large number of different additives and concrete admixtures. Their study revealed that most carboxylic acids, such as, for example, acetic acid had no effect on ettringite except for those acids which present effective calcium chelators such as citric, tartaric, and gluconic acid. They delay both nucleation and crystal growth. In a recent study, we have investigated the impact of polycarboxylate ethers possessing different anionicity on the nucleation and crystal growth of synthetic ettringite precipitated from aqueous solutions of $Ca(OH)_2$ and $Al_2(SO_4)_3$.[7] It was found that PCEs generally lead to a reduced crystal size, with the effect depending on their specific anionic charge amount, while the aspect ratio of the crystals did not change significantly. This result suggested that the polymers adsorb not only on the side faces of the hexagonal ettringite prisms but also on the top and bottom faces and thus inhibited the crystal growth in all directions. Comparative studies performed on parabolic flights under microgravity conditions showed a weaker effect of the different polymers on ettringite crystallization which was attributed to the absence of convection.

As mentioned previously, the hydration of portland cement constitutes a complex process. For this reason, studies on the crystallization of pure synthetic ettringite are not necessarily representative for the interaction of PCE with ettringite in cementitious systems where pH and ion concentrations are different. In a simplified system, consisting of C_3A, calcium sulfate and calcite, Dalas et al found, that in the presence of a methacrylate ester-based PCE, less ettringite is formed after 120 minutes of hydration compared with the system without PCE.[8] This effect was even more pronounced at increasing PCE dosages. Furthermore, after 5 minutes of hydration the surface area of ettringite was considerably higher for the samples prepared at increased PCE dosages and decreased over the following 2 hours. This suggests a strong interaction between ettringite and superplasticizers already in the first seconds of hydration. Other studies on short-term hydration of portland cement have shown that an abundant amount of ettringite is precipitated within the first 10 seconds of cement hydration.[9,10] All those experiments were performed at a low PCE dosage of 0.05% by weight of cement (bwoc) using CEM I 42.5 R and CEM I 42.5 N samples possessing low C_3A contents. It was observed that the presence of PCEs leads to larger crystals exhibiting a higher aspect ratio, especially under terrestrial conditions.

The aim of this study was to investigate the effect of PCE dosage on the nucleation and crystallization of ettringite, particularly in the first seconds of cement hydration. For this purpose, 2 chemically different PCE superplasticizers were dosed in different amounts to cement and the effect on ettringite crystal growth during the first 10 seconds of hydration was assessed. A highly reactive commercial portland cement (CEM I 52.5 N) exhibiting a high C_3A content was used as base which allows to differentiate the effects of the PCEs on the short-term hydration. Furthermore, all experiments were conducted under terrestrial and microgravity conditions and the results were compared. Due to the absence of convection and the limitation of crystal growth by ion transport, the microgravity experiments can be understood to reveal the nucleation step in the formation of ettringite, while the terrestrial experiments represent both the nucleation and crystal growth of ettringite.

2 | EXPERIMENTAL SECTION

2.1 | Materials

2.1.1 | Cement samples

The cement sample used in this study was an ordinary portland cement CEM I 52.5 N (Milke brand, from Geseke plant) provided by HeidelbergCement AG (Germany). The phase compositions as determined via Q-XRD using *Rietveld* refinement is presented in Table 1. Average particle size (d_{50} value, determined by Laser granulometer Cilas 1064, Marseille, France) of cement sample was 12 ± 0.2 µm. The density (Helium pycnometry) was 3.14 g/cm^3.

TABLE 1 Phase composition of the commercial portland cement sample commercial portland cement (CEM) I 52.5 N, as determined by quantitative XRD analysis using *Rietveld* refinement

Phases	CEM I 52.5 N
C_3S, m	54.32
C_2S, m	26.54
C_3A, c	3.26
C_3A, o	4.24
C_4AF, o	2.44
Free lime, *Franke*	0.10
Periclase	0.03
Anhydrite	2.63
Hemihydrate[a]	1.20
Dihydrate[a]	0.03
Calcite	3.59
Quartz	1.16
Arcanite	0.46
Sum	100.00

[a]Determined via thermogravimetry.

2.1.2 | Chemicals

Deionized water obtained from Millipore Synergy UV (Merck KGaA, Darmstadt, Germany) was used as mixing water. Reagent grade acetone (>99.9%, Merck KGaA, Darmstadt, Germany) was applied to quench the hydration reaction.

As superplasticizers, 2 different polycarboxylate ethers were used. One polymer was a MPEG-based polycarboxylate consisting of ω-methoxypoly(ethylene glycol) methacrylate ester with 45 EO units and methacrylic acid at a molar ratio of 1:6. It is henceforth denoted as MPEG-45PC6. The second one, denoted as IPEG-52PC8, was based on isoprenyloxy poly(ethylene glycol) macromonomer possessing a side-chain length of 52 ethylene oxide (EO) units, and acrylic acid reacted at a molar ratio of 1:8. The superplasticizer samples used in this study were synthesized via aqueous free radical copolymerization as described elsewhere.[11] The chemical structure of the 2 polymers and their characteristic properties are displayed in Figure 1 and Table 2, respectively.

2.2 | Experimental methods

2.2.1 | 10 seconds cement hydration

The experimental setup for conducting the hydration experiment consists of 3 syringes (BD Discardit II 20 mL, Becton Dickinson, Franklin Lakes, New Jersey, USA) connected via a three-way valve. One syringe serves as the reaction container. It was loaded with 5 g of cement. The next syringe was filled with 6 mL mixing water holding the PCE (1 mL dead volume) and the third syringe contained 10 mL acetone to stop the hydration. Thus, the water-to-cement ratio in the reaction container was 1.0. This syringe was equipped with a cellulose filter (MN520, thickness 1.5 mm, Macherey-Nagel, Düren, Germany) to hold back the cement particles when after 10 seconds of reaction time the hydrated cement was separated from the pore solution. All experiments were carried out 3 times to confirm the results.

2.2.2 | Microgravity experiments

Additional experiments were conducted under microgravity conditions on a parabolic flight campaign in 2016 initiated by Deutsches Zentrum für Luft- und Raumfahrt (DLR, German Aerospace Center) onboard an Airbus A 300 aircraft from Novespace (Paris, France). Details of the flight conditions have been described before.[7,9,10] On such flights, microgravity periods of ~22 seconds are realized which allow to perform exactly the same 10 seconds cement hydration experiment as described in Section 2.2.1 using the same equipment as there.

2.3 | Analysis of samples

2.3.1 | SEM imaging

In order to analyze the morphology of ettringite formed on the cement surface and to determine its crystal size SEM imaging was performed. The micrographs were collected on a FEI XL 30 FEG environmental scanning electron microscope at an accelerating voltage of 4 kV at a working distance of 7.5 mm and a tilt angle of 20°. Samples were prepared by applying a conductive carbon paint on the sample stub to fix the cement particles. From each sample, 30 representative images from different areas were collected at a magnification of 40 000×. The lengths and diameters of the ettringite crystals formed were then measured and the mean sizes and standard deviation were calculated.

2.3.2 | X-ray diffraction

XRD patterns were collected in the range of 5-70° 2θ on a Bruker AXS D8 Advance instrument (Bruker, Karlsruhe, Germany) with a *Bragg-Brentano* geometry and Cu Kα source (30 kV, 35 mA). The quantification of the amount of ettringite formed was conducted analogous to a method described in the literature for clay minerals.[12] For this purpose, the characteristic reflection for ettringite at ~9.2° 2θ was analyzed with a polynom of second order and smoothed using a 15-point *Savitzky-Golay* filter. Followed by an impulse analysis of the data obtained, the average peak intensity of 3 independent measurements was reported as final value for the amount of ettringite.

3 | RESULTS AND DISCUSSION

3.1 | Cement hydrated in the absence of PCE

According to SEM analysis the neat cement sample hydrated for 10 seconds revealed already numerous ettringite crystals with sizes in the nanometer range (see Figures 2 and 3). The nanocrystals exhibit the characteristic hexagonal-prismatic morphology of ettringite and are evenly spread across the cement surface. The average length of the crystals is ~450 nm while the average diameter was found at ~180 nm, yielding an aspect ratio of approximately 2.8. Under μ *g* conditions, a general decrease in the crystal dimensions (length and diameter) was observed. This effect was explained before by the absence of convection which limits the ion transport to the crystal faces to diffusion and thus slows down crystal

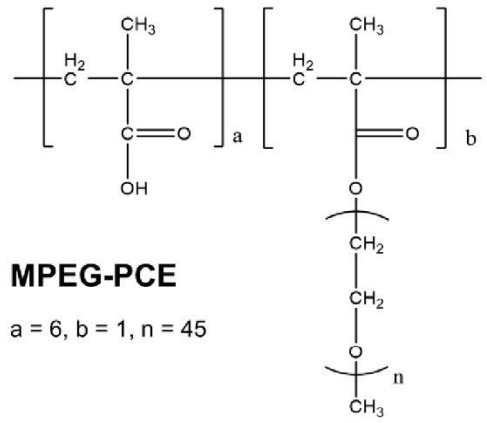

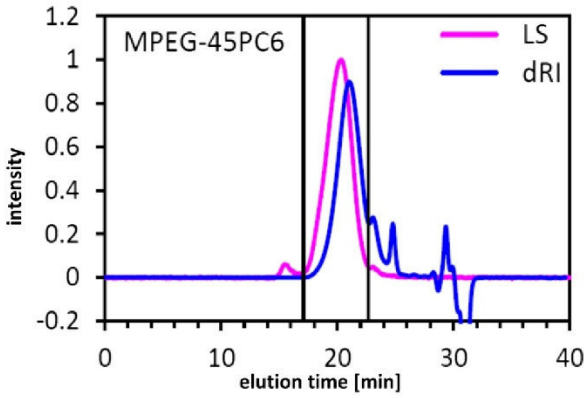

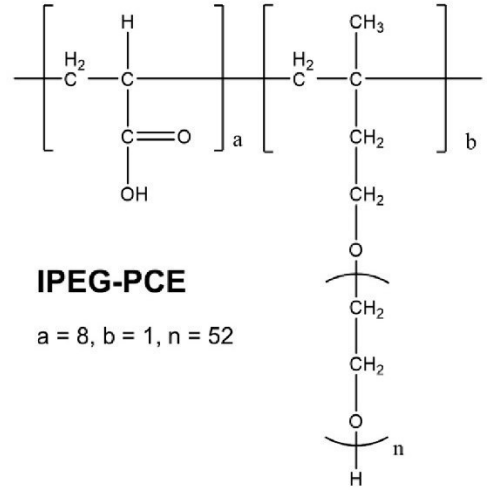

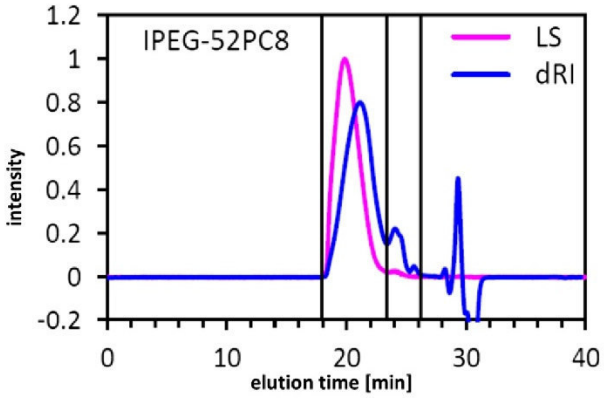

FIGURE 1 Chemical structures and gel permeation chromatograms of the PCE samples. PCE, polycarboxylate

TABLE 2 Characteristic properties of the polycarboxylate (PCE) samples

PCE sample	Yield (%)	M_W (g mol^{-1})	M_n (g mol-$^{-1}$)	PDI	Specific anionic charge amount @ pH 12.5 (μeq g^{-1})
MPEG-45PC6	90	28.500	16.000	1.8	3.600
IPEG-52PC8	87	24.000	12.000	2.0	3.200

growth.[13,14] While the crystals formed under μ *g* are generally smaller, their amount is ~20% higher as quantified via XRD. This effect has already been described in previous studies.[9,10] Under μ *g* conditions, the movement of ions occurs only via diffusion which leads to a higher oversaturation at the interface cement-pore solution. This local higher oversaturation causes the formation of more nuclei which then can grow only to smaller sizes. Besides ettringite, no other cement hydrates were found both in SEM and XRD analysis (Figure 4).

3.2 | Cement hydrated in the presence of MPEG PCE

Upon addition of only 0.05% bwoc of the methacrylate ester-based PCE superplasticizer MPEG-45PC6, the crystal size of ettringite changes. The crystals now are longer and slightly smaller in diameter compared with the crystals formed in the absence of the admixture (Figure 3). The change in aspect ratio (ratio between crystal length and diameter) becomes even more pronounced at increasing

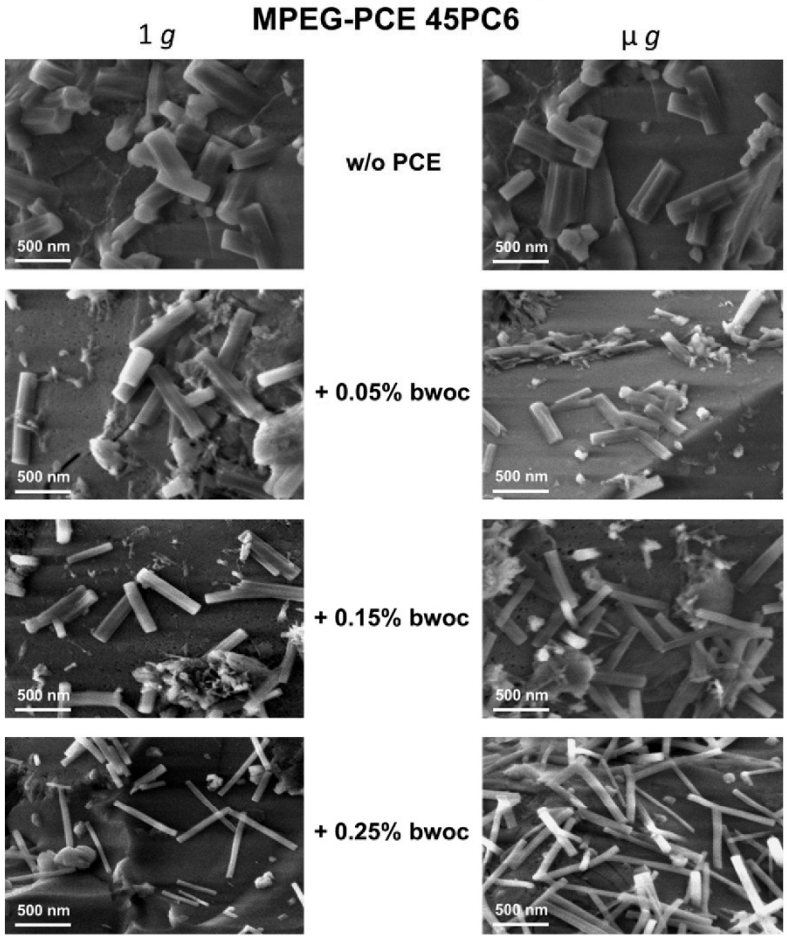

FIGURE 2 SEM images of CEM I 52.5 N sample hydrated for 10 seconds in the presence of increasing dosages of PCE sample MPEG-45PC6 under terrestrial and microgravity conditions. CEM, commercial portland cement; PCE, polycarboxylate

polymer dosages. There, the average crystal lengths increase continuously with dosage while the diameters decrease steadily leading to aspect ratios from 2.8 for neat cement to 3.4, 4.7, and 6.9 at PCE dosages of 0.05%, 0.15%, and 0.25%, respectively (Table 3). These results suggest that crystal growth along the a- and b-axes is hindered, whereas growth along the *c*-axis of the ettringite crystal can proceed unabashed in the presence of polymer. For example, the ettringite crystals formed at 0.25% PCE dosage constitute long and thin needles, whereas the samples without polymer or at a low dosage of 0.05% bwoc present rather stocky crystals (Figure 2). This general trend was observed under terrestric as well as under microgravity conditions.

The relative amounts of ettringite crystals formed under terrestrial and microgravity conditions at different dosages of the methacrylate ester-based PCE are comparable to the amount found in the short-term hydration of the neat cement paste. Moreover, XRD analysis did not reveal any other cement hydrate phase besides ettringite in the presence of MPEG-PCE sample 45PC6. These findings suggest, that the presence of this methacrylate ester-based PCE does not have an influence on crystal nucleation in the short-term hydration but on the ettringite crystal growth. However, studies by Dalas et al have shown that MPEG-based PCEs with a high anionic backbone can impede the formation of ettringite not in the first minutes but at longer hydration times.[8]

Under μ *g*, the crystals obtained are generally smaller in length and diameter (see Figures 2 and 3) than for the neat cement and under terrestrial conditions, and the aspect ratios increase in a similar way than under 1 *g*, given the accuracy of the measurements (Table 3). This result instigates that under microgravity, the effect of the PCE on the crystal growth and size of ettringite remains the same, the only difference being that under μ *g*, crystal growth is limited as has been explained before (Figure 3).

3.3 | Cement hydrated in the presence of IPEG-PCE

SEM images of the hydrated cement admixed with the isoprenolether-based polycarboxylate sample IPEG-52PC8

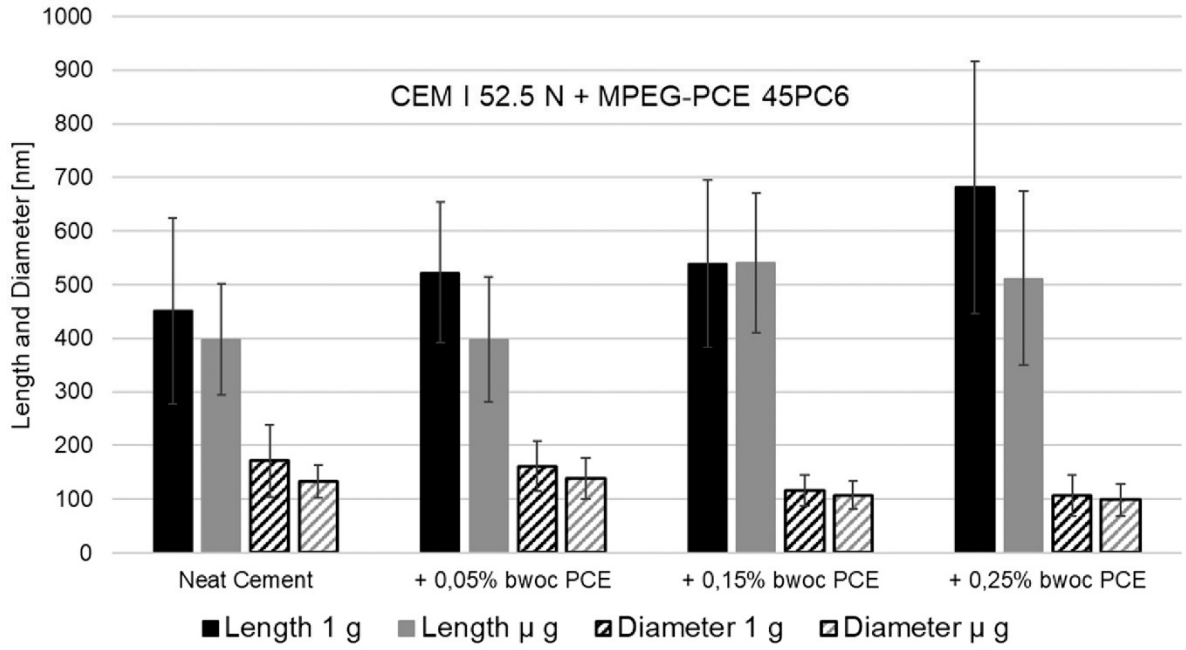

FIGURE 3 Average length and diameter of ettringite crystals obtained from CEM I 52.5 N admixed with different dosages of PCE sample MPEG-45PC6 hydrated under 1 *g* and µ *g* conditions, respectively. CEM, commercial portland cement; PCE, polycarboxylate

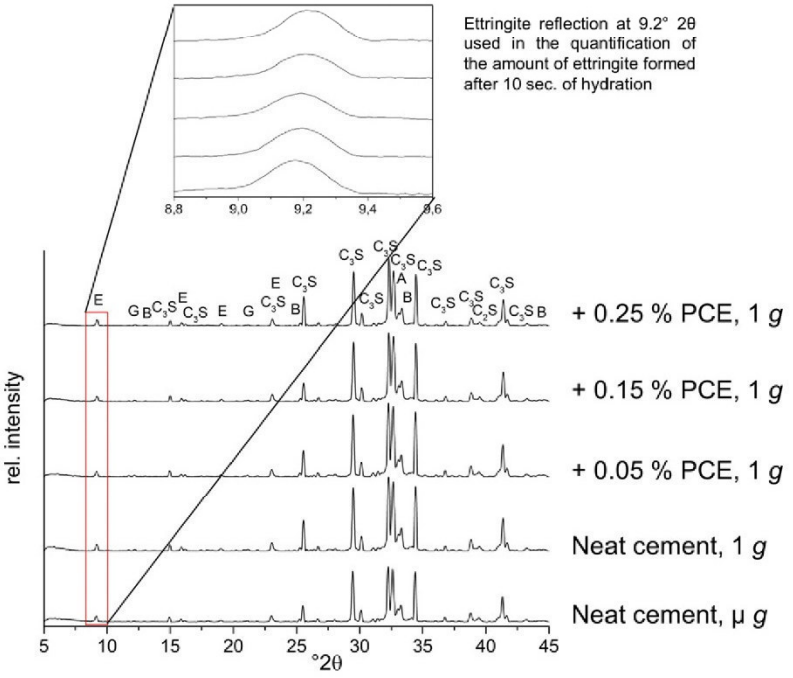

FIGURE 4 XRD patterns of the CEM I 52.5 N sample admixed with different dosages of PCE sample MPEG-45PC6 and hydrated for 10 seconds (w/c = 1.0). CEM, commercial portland cement; PCE, polycarboxylate

again revealed an increase in crystal length and a decrease in diameter for the ettringite crystals (Figures 5 and 6). At the same time, the diameters of the crystals did not decrease as much as for the MPEG-PCE, thus resulting in similar aspect ratios for both PCEs (Tables 3 and 4). However, the increase in crystal length was significantly larger than from the methacrylate-based PCE 45PC6. In microgravity environment, this effect was less pronounced. In

TABLE 3 Average aspect ratios of ettringite crystals grown under 1 *g* and μ *g* conditions on commercial portland cement (CEM) I 52.5 N sample admixed with different dosages of methacrylate ester-based PCE 45PC6

Condition	Neat Cement	+ 0.05% bwoc PCE	+ 0.15% bwoc PCE	+ 0.25% bwoc PCE
1 *g*	2.8 ± 1.0	3.4 ± 0.9	4.7 ± 1.1	6.9 ± 2.5
μ *g*	3.1 ± 0.7	2.9 ± 0.6	5.2 ± 1.3	5.5 ± 2.0

PCE, polycarboxylate.

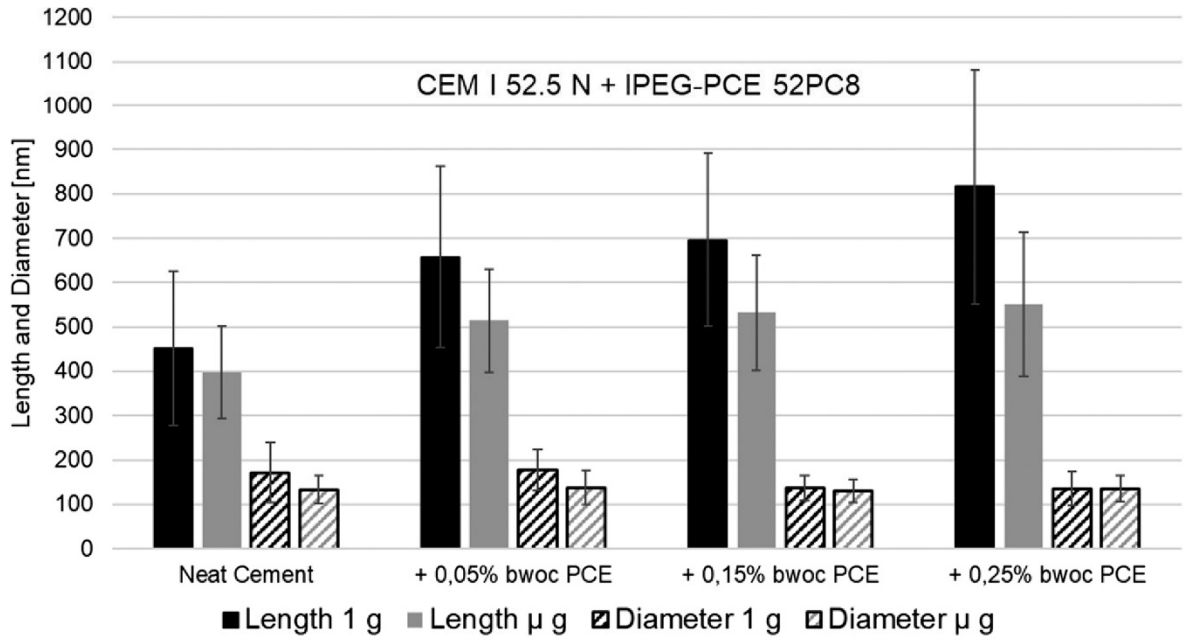

FIGURE 5 Average length and diameter of ettringite crystals obtained from CEM I 52.5 N admixed with different dosages of IPEG-PCE sample 52PC8, hydrated under 1 *g* and μ *g* conditions, respectively. CEM, commercial portland cement; PCE, polycarboxylate

the latter case, the grown ettringite crystals were thus overall smaller at every PCE dosage compared with the crystals grown under 1 *g* conditions. Again, the smaller crystal size under μ *g* conditions can be explained by the limited ion transport in the absence of convection slowing down crystal growth and increasing supersaturation at the surface of the cement grains (see Section 3.1).

The inhibited crystal growth along the *a*- and *b*-axes and the enhanced growth along the c-axis suggest that the polymer preferentially adsorbs on the lateral faces of the ettringite crystal rather than on the top and bottom faces. Thus, crystal growth occurs preferably along the c-axis, as the adsorbed PCE hinders ion transport from the bulk solution to the lateral faces of the ettringite crystal.

XRD analysis revealed similar amounts of ettringite formed in the presence of different dosages of the IPEG-PCE sample under terrestrial gravity. However, in the absence of gravity, less ettringite crystals (up to ~42%) were formed with increasing dosage of PCE.

Under microgravity, the effect of this PCE on the crystal sizes (length and diameter) and consequently on the aspect ratio is nearby independent of the dosage of the PCE, which differs from the behavior of the MPEG-PCE sample. Apparently, already a small dosage of the IPEG-PCE is sufficient to instigate its effect on the nucleation and growth of ettringite while the MPEG-PCE requires higher dosage to gradually modulate the morphology of ettringite. A potential explanation for this difference is that the IPEG-PCE occupies the surface of ettringite more densely even at low dosage, as a consequence of its more rigid backbone. The higher amount of non-adsorbed IPEG-PCE polymers are then available in the pore solution to complex calcium ions and thus inhibit ettringite nucleation.

3.4 | Comparison of the effects of two chemically different PCEs

As has been shown before, the MPEG-based PCE generally produces shorter, but slimmer ettringite crystals than the

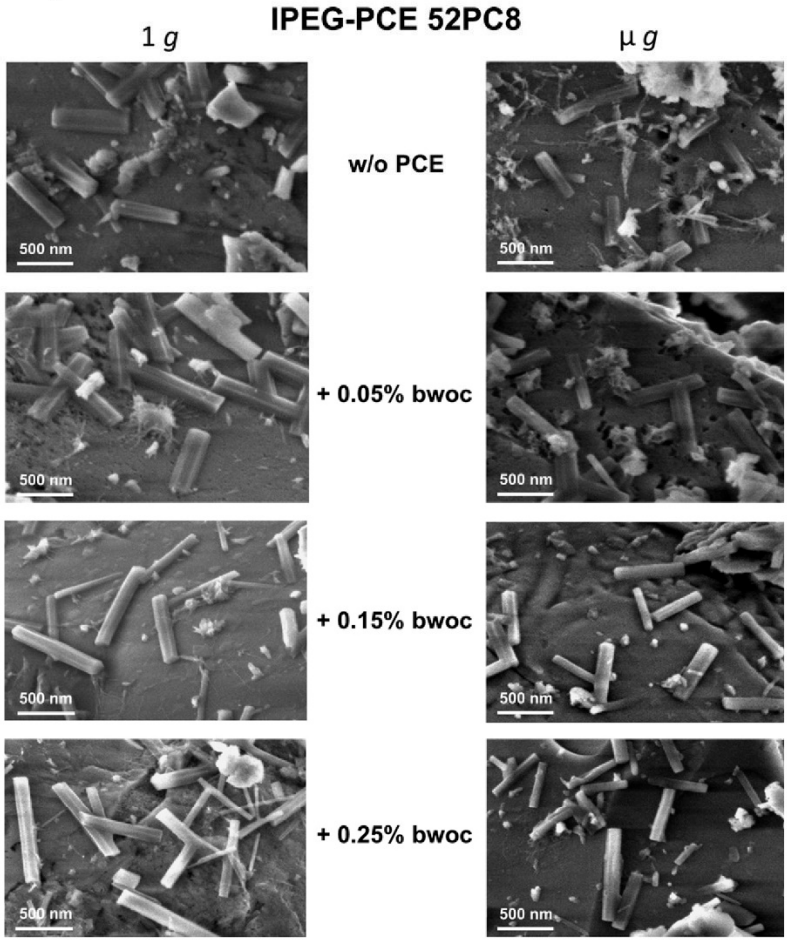

FIGURE 6 SEM images of CEM I 52.5 N sample hydrated for 10 seconds in the presence of increasing dosages of IPEG-PCE 52PC8 under terrestrial and microgravity conditions. CEM, commercial portland cement; PCE, polycarboxylate

TABLE 4 Average aspect ratios of ettringite crystals grown under 1 *g* and μ *g* conditions on commercial portland cement (CEM) I 52.5 N sample admixed with different dosages of IPEG-PCE 52PC8

Condition	Neat cement	+ 0.05% bwoc PCE	+ 0.15% bwoc PCE	+ 0.25% bwoc PCE
1 *g*	2.8 ± 1.0	3.8 ± 1.0	5.4 ± 1.7	6.4 ± 2.3
μ *g*	3.1 ± 0.7	3.9 ± 1.3	4.2 ± 1.1	4.4 ± 1.5

PCE, polycarboxylate.

IPEG-based PCE. The latter kind of PCE results in particularly elongated crystals, while the diameter of the crystals remain almost the same as in the absence of PCE. Apparently, the 2 PCEs exhibit different affinities to cement. Previous studies on the adsorption behavior of these PCE samples with this cement have shown that the IPEG-PCE sample 52PC8 reaches the maximum adsorbed amount of ~1 mg/g cement already at a dosage of ~0.3% bwoc, while the MPEG-PCE sample 45PC6 reaches a saturation point at ~2.5 mg/g cement when ~0.5% bwoc are dosed to cement.[15] In the study by Lange et al, where a mixing time of 4 minutes was applied, the adsorption ratios for the IPEG-PCE sample at dosages of 0.5, 0.15, and 0.25% bwoc were found to be 80%, 52%, and 36%, while for the MPEG-PCE 100%, 93%, and 70% of adsorbed superplasticizer were found. As ettringite constitutes the primary phase for the adsorption of anionic polymers on cement, it suggests that a higher amount of the MPEG-PCE is adsorbed on ettringite compared with the IPEG-PCE. The crystal surface therefore becomes more densely covered with molecules of the MPEG-PCE, and ion diffusion from the bulk solution to the crystal surface is more impeded than in the case of the IPEG-PCE. Crystal growth is therefore stronger inhibited than in the presence of the IPEG-

PCE which adsorbs in lower amount and still allows ion diffusion to the crystal surface. This results in longer ettringite crystals exhibiting a larger diameter compared with crystals grown in the presence of the strongly adsorbing MPEG-PCE. The amount of nonadsorbed PCE molecules is therefore higher for the IPEG-PCE sample leading to calcium depletion in the pore solution due to complexation of Ca^{2+} ions by the PCE molecules and thus to delayed formation of cement hydrates. This might be a possible explanation of the lower amounts of ettringite found in the presence of the IPEG-PCE sample compared with the MPEG-PCE.

4 | CONCLUSION

The impact of 2 chemically different PCE superplasticizers on ettringite crystallization was studied by hydrating a commercial CEM I 52.5 N sample for 10 seconds at 4 different PCE dosages (0%, 0.05%, 0.15%, and 0.25% bwoc). It was found that after 10 seconds of hydration only, a significant amount of ettringite is formed, owed to fast dissolution of C_3A and calcium sulfates. Moreover, ettringite crystals formed under microgravity conditions are generally smaller compared with those obtained under terrestrial conditions, as the crystal growth of ettringite is limited by ion diffusion (no convection) in the absence of gravity. XRD analysis showed that the MPEG-PCE sample had no influence on the formed amounts of ettringite while the presence of the IPEG-PCE sample lead to a significant decrease in the amount of ettringite crystals under microgravity conditions.

The presence of PCE leads to longer, yet slimmer ettringite crystals than in the neat cement paste. This effect becomes even more pronounced at increasing PCE dosages. Generally, at higher PCE dosages the crystals attain a more needle-like morphology compared with the stocky crystals observed from the neat cement paste. This change in morphology is expressed by the ascending aspect ratios of the ettringite crystals formed at higher PCE dosages.

Furthermore, it was found that chemically different PCE superplasticizers can differently impact the crystal growth of ettringite. Polycarboxylates exhibiting a high affinity to the surface of the cement, i.e. a higher adsorption ability on ettringite, cover the crystal surfaces more densely, especially along the lateral faces, and thus inhibit crystal growth in this direction stronger.

ACKNOWLEDGMENT

The authors are most grateful to *Deutsches Zentrum für Luft- und Raumfahrt* (DLR) for sponsoring the parabolic flight campaign in 2016 which allowed us to perform these experiments. In this respect, the support received from Dr. Ulrike Friedrich and Dr. Rainer Forke is especially acknowledged. Furthermore, our thanks go to Frederic Gai from Novespace, Bordeaux whose advice on the experimental design with respect to feasibility on the aircraft was of great importance.

ORCID

Johann Plank https://orcid.org/0000-0002-4129-4784

REFERENCES

1. Zingg A, Holzer L, Kaech A, et al. The microstructure of dispersed and non-dispersed fresh cement pastes – new insight by cryo-microscopy. *Cem Concr Res*. 2008;38:522-529.
2. Jansen D, Neubauer J, Goetz-Neunhoeffer F, et al. Change in reaction kinetics of a Portland cement caused by a superplasticizer – calculation of heat flow curves from XRD data. *Cem Concr Res*. 2012;42:327-332.
3. Kreppelt F, Weibel M, Zampini D, et al. Influence of solution chemistry on the hydration of polished clinker surfaces – a study of different types of polycarboxylic acid-based admixtures. *Cem Concr Res*. 2002;32:187-198.
4. Yoshioka K, E-i Tazawa, Kawai K, et al. Adsorption characteristics of superplasticizers on cement component minerals. *Cem Concr Res*. 2002;32:1507-1513.
5. Plank J, Chatziagorastou P, Hirsch C. New model describing distribution of adsorbed superplasticizer on the surface of hydrating cement grain. *J Build Mater*. 2007;10:7-13.
6. Cody AM, Lee H, Cody RD, et al. The effects of chemical environment on the nucleation, growth, and stability of ettringite $[Ca_3Al(OH)_6]_2(SO_4)_3{\cdot}26H_2O$. *Cem Concr Res*. 2004;34:869-881.
7. Meier MR, Plank J. Crystal growth of $[Ca_3Al(OH)_6{\cdot}12H_2O]_2{\cdot}(SO_4)_3{\cdot}26H_2O$ (ettringite) under microgravity: on the impact of anionicity of polycarboxylate comb polymers. *J Cryst Growth*. 2016;446:92-102.
8. Dalas F, Pourchet S, Rinaldi D, et al. Modification of the rate of formation and surface area of ettringite by polycarboxylate ether superplasticizers during early C_3A-$CaSO_4$ hydration. *Cem Concr Res*. 2015;69:105-113.
9. Lei L, Meier MR, Rinkenburger A, Zheng B, Fu L, Plank J. Early hydration of portland cement admixed with polycarboxylates studied under terrestric and microgravity conditions. *J Adv Concr Technol*. 2016;14:102-107.
10. Meier MR, Sarigaphuti M, Sainamthip P, et al. Early hydration of Portland cement studied under microgravity conditions. *Constr Build Mater*. 2015;93:877-883.
11. Lange A, Hirata T, Plank J. Influence of the HLB value of polycarboxylate superplasticizers on the flow behavior of mortar and concrete. *Cem Concr Res*. 2014;60:45-50.
12. Bhaskar R, Li J, Xu L. A comparative study of particle size dependency of IR and XRD methods for quartz analysis. *Am Ind Hyg Assoc J*. 1994;55:605-609.
13. Chernov AA. Crystallization in solutions: effects of micogravity conditions. In: Ratke L, Walter H, Feuerbacher B, eds. *Materials and Fluids Under low Gravity: Proceedings of the IXth European*

Symposium on Gravity-Dependent Phenomena in Physical Sciences. Vol. 464. Heidelberg, Germany: Springer Verlag; 1996: 137-154.

14. Li C, Tsukamoto K, Satoh H. The reduction and recovery of step velocity in crystal growth induced by convection variation under various gravities. *J Cryst Growth*. 2005;277:560-565.
15. Lange A. Studien zur Zementkompatibilität von Polycarboxylat-Fließmitteln sowie zum Einfluss ihres HLB-Wertes auf das rheologische Verhalten von Mörtel (Study on cement compatibility of polycarboxylate superplasticizers and the influence of their HLB-value on the rheological behavior of mortars). Dissertation, Lehrstuhl für Bauchemie, Technische Universität München. 2015.

How to cite this article: Schönlein M, Plank J. Influence of PCE kind and dosage on ettringite crystallization performed under terrestrial and microgravity conditions. *J Am Ceram Soc*. 2018;00:1–10. https://doi.org/10.1111/jace.15513

5.3.4. Impact of a Polyphosphate comb polymer on ettringite crystallization

The following results have not been published and are therefore presented in detail here. A new kind of superplasticizers for cement are polyphosphate comb polymers. Their structure is similar to that of polycarboxylate ethers. However, instead of carboxylic groups which possess only one anionic charge per functional group, phosphate groups exhibiting a divalent anionic charge are implemented as anchor groups to attach onto positively charged cement and hydrate surfaces. The higher anionic charge allows higher adsorption compared to common polycarboxylates. The aim of the following study was to investigate the impact of this new class of additives on ettringite crystal growth in comparison to a conventional MPEG-type PCE. A commercial CEM I 52.5 N cement sample was hydrated for 10 s in the presence of 0.05 % bwoc of such polyphosphate comb polymer under terrestrial and microgravity conditions. For comparison, a MPEG-PCE sample having a similar side chain of 45 EO units and a molar ratio of methacrylic acid to ω-methoxy poly(ethylene glycol) methacrylate ester of 6:1 was chosen. This PCE was added in dosages of 0.05 %, 0.15 % and 0.25 % bwoc to CEM I 52.5 N.

SEM imaging shows extraordinary long, thin and needle-like ettringite crystals for the hydration in the presence of the polyphosphate comb polymer 45PC0P3 already at a low dosage of 0.05 % bwoc (see **Figure 58**). The reference experiments with the corresponding MPEG-PCE sample show slightly less stocky crystals compared to those obtained from the neat cement paste. Furthermore, it can be observed that at increased dosages of 0.15 % and 0.25 %, the morphology of the ettringite crystals changes significantly. Here, the diameter of the ettringite crystals decreases while the crystal length increases.[167]

Determination of the average ettringite crystal size at the different MPEG-PCE dosages shows clearly a strong decrease in crystal diameter and an increase of the crystal lengths with increasing PCE dosage (see **Figure 59**). Comparing the values found for the ettringite crystals formed in the presence of the polyphosphate comb polymer to those of the MPEG-PCE it can be derived that a dosage between 0.15 % and 0.25 % bwoc of the MPEG-PCE sample is necessary to obtain ettringite crystals of similar size than those formed with 0.05 % bwoc of the polyphosphate comb polymer.

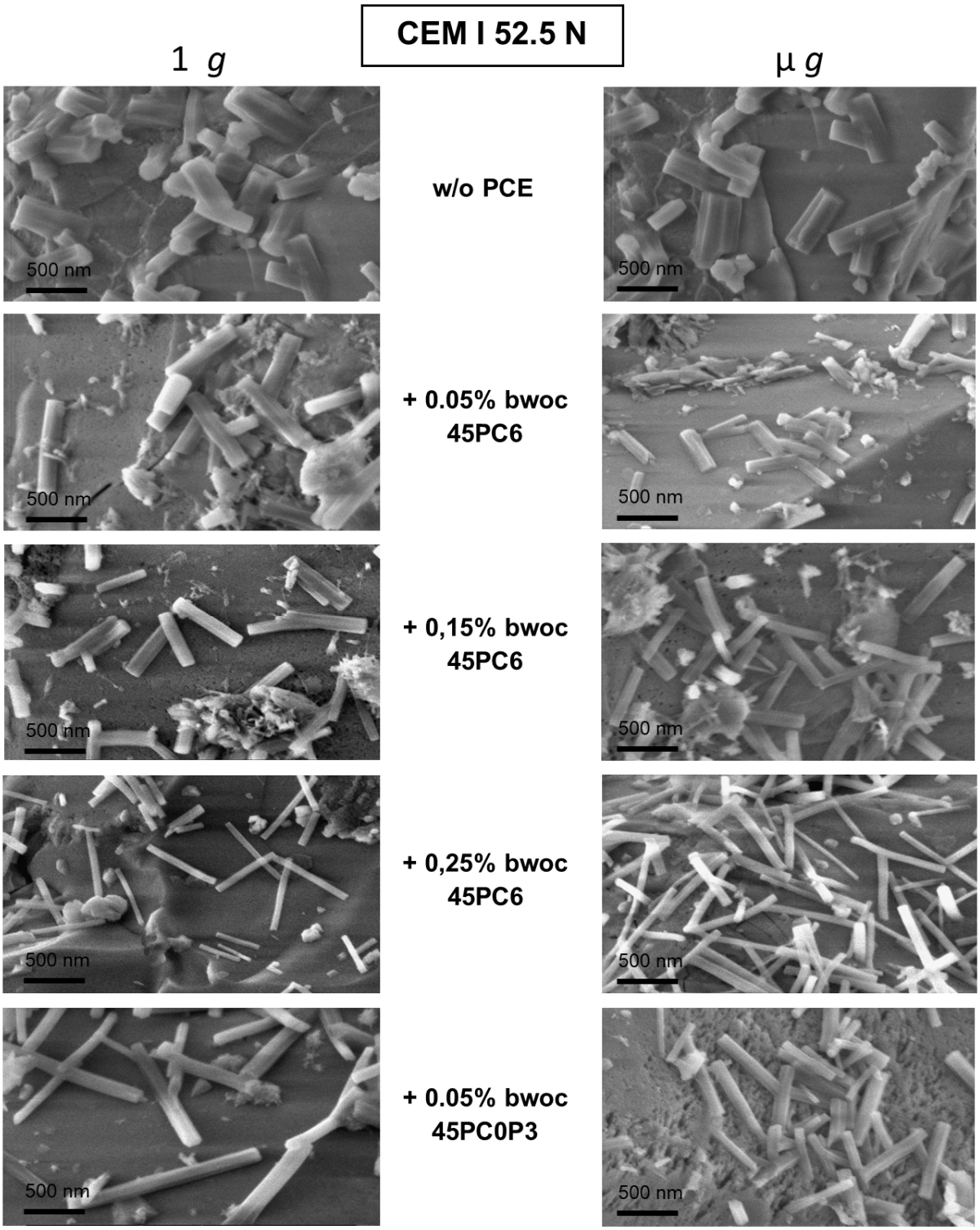

Figure 58: SEM images of CEM I 52.5 N sample hydrated for 10 s in the presence of 0.05 %, 0.15 % and 0.25 % bwoc of MPEG-PCE sample 45PC6 and of 0.05 % bwoc of the Phosphate polymer sample 45PC0P3 under terrestrial (left) and microgravity (right) conditions. All images were collected at 40 k magnification.

As can be observed, the presence of superplasticizers causes a change in morphology of ettringite. Assuming that the crystal size is correlating with the adsorption ability of the polymers, one can conclude that the Phosphate polymer adsorbs stronger than the MPEG-PCE, although it has less anionic groups in the backbone. This suggests that the divalent charge of the PO_3^{2-} groups compensate the lower amount of functional groups in the backbone and have an even higher affinity to the positively charged AF_t surfaces than carboxylic groups.

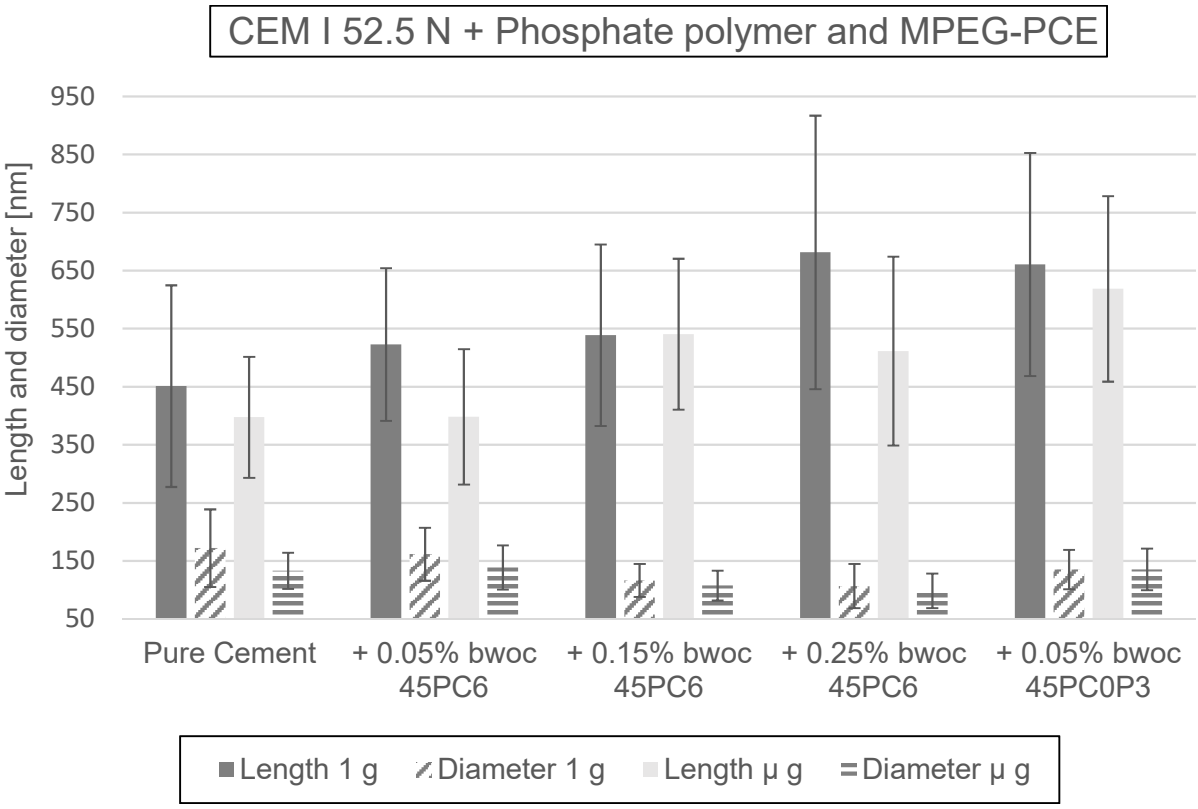

Figure 59: Average length and diameter of ettringite crystals obtained from CEM I 52.5 N admixed with 0.05 %, 0.15 % and 0.25 % bwoc of MPEG-PCE sample 45PC6 and with 0.05 % bwoc of the Phosphate polymer sample 45PC0P3 under terrestrial and microgravity conditions.

Table 12: Average aspect ratios of ettringite crystals grown under 1 *g* and μ *g* conditions on CEM I 52.5 N admixed with different dosages of MPEG-PCE sample 45PC6 and 0.05% bwoc of the Phosphate polymer sample 45PC0P3.

Condition	Neat Cement	+ 0.05 % bwoc MPEG-PCE 45PC6	+ 0.15 % bwoc MPEG-PCE 45PC6	+ 0.25 % bwoc MPEG-PCE 45PC6	+ 0.05 % bwoc Phosphate polymer 45PC0P3
1 *g*	2.8 ± 1.0	3.4 ± 0.9	4.7 ± 1.1	6.9 ± 2.5	5.0 ± 1.4
μ *g*	3.1 ± 0.7	2.9 ± 0.6	5.2 ± 1.3	5.5 ± 2.0	4.8 ± 1.5

5.3.5. Impact of polycondensates on ettringite crystallization

This chapter describes results which were not published so far. Besides polycarboxylate ethers there is another class of mature and popular superplasticizers for cement: the polycondensates. These consist of linear polymers possessing a high anionic charge density. Very common representatives of the class of polycondensates are melamin-formaldehyde-sulfite (MFS), β-naphthalene sulfonate formaldehyde (BNS) and acetone-formaldehyde sulfite (AFS) polymers. Due to their linear structure and their high anionic charge, their dispersing mechanism is based solely on electrostatic repulsion. In previous studies it has been shown that these polymers can alter the morphology of ettringite crystals.[20, 168] While these studies have focused on the adsorbed amount of polymer on synthetic ettringite over very long reaction times of 2h, the aim of this study was to investigate the impact of the polycondensates on ettringite nucleation and crystal growth in the first seconds of cement hydration. Two commercial OPC samples, namely CEM I 52.5 N and CEM I 42.5 R, were admixed with 0.05 % bwoc of MFS, BNS and AFS, respectively, and hydrated for 10 s under terrestrial and microgravity conditions. The applied water-cement-ratio is 1.0.

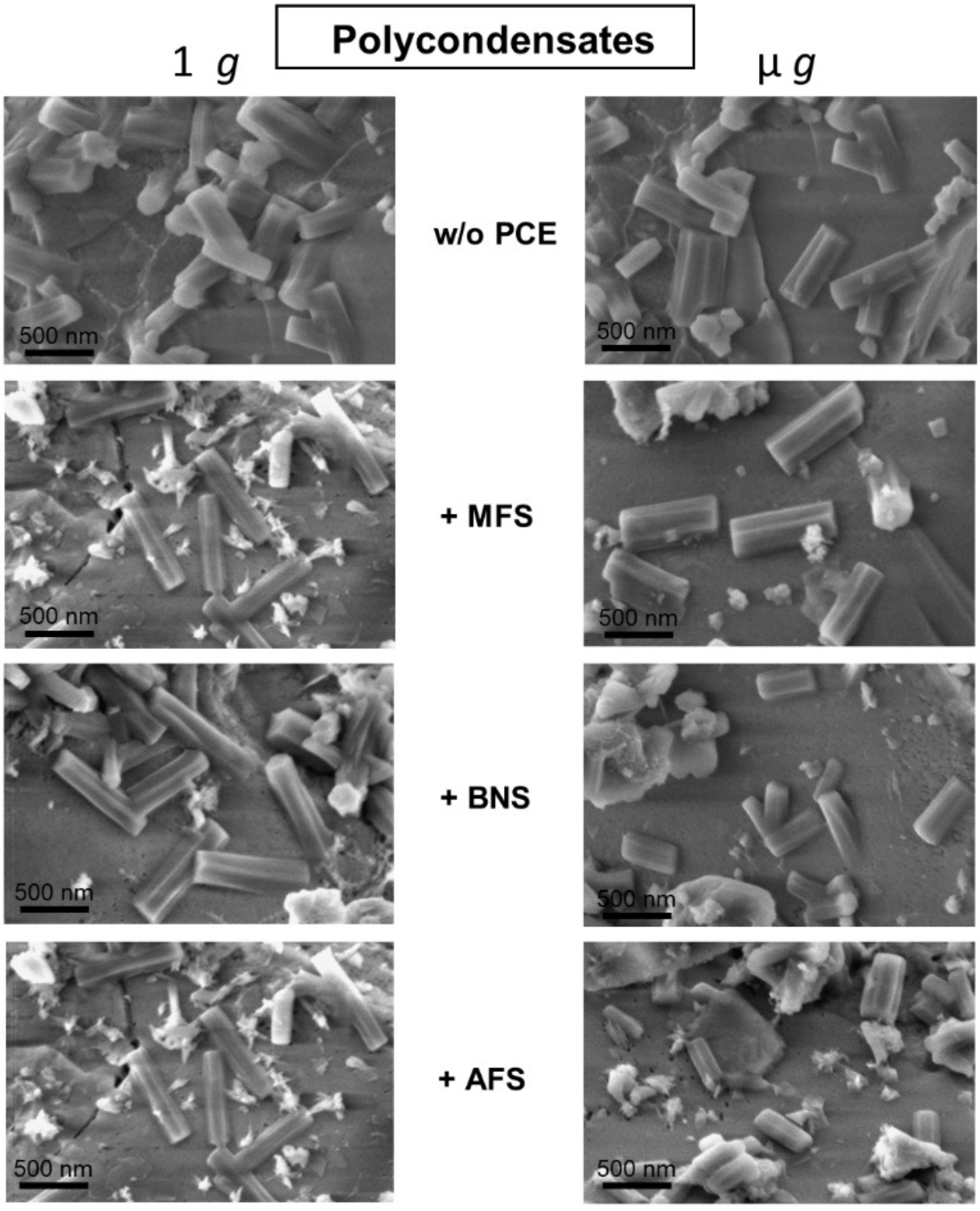

Figure 60: SEM images of CEM I 52.5 N sample hydrated for 10 s in the presence of 0.05 % bwoc of polycondensate samples MFS, BNS and AFS, possessing increasing anionic charge under terrestrial (left) and microgravity (right) conditions. All images were collected at 40 k magnification.

The ettringite crystals formed in the absence of the polycondensate admixtures are rather short and stocky for the cement sample CEM I 52.5 N (see **Figure 60**). In the presence of 0.05 % bwoc of the MFS polycondensate, the ettringite crystals obtained under terrestrial gravity appear longer than those in the neat cement paste. In microgravity, however, the crystals appear rather stocky and are comparable to those without admixture. Ettringite crystals grown in the presence of all polycondensate samples (MFS, BNS and AFS) show similar morphology for terrestrial and microgravity conditions as was observed by electron microscopy.

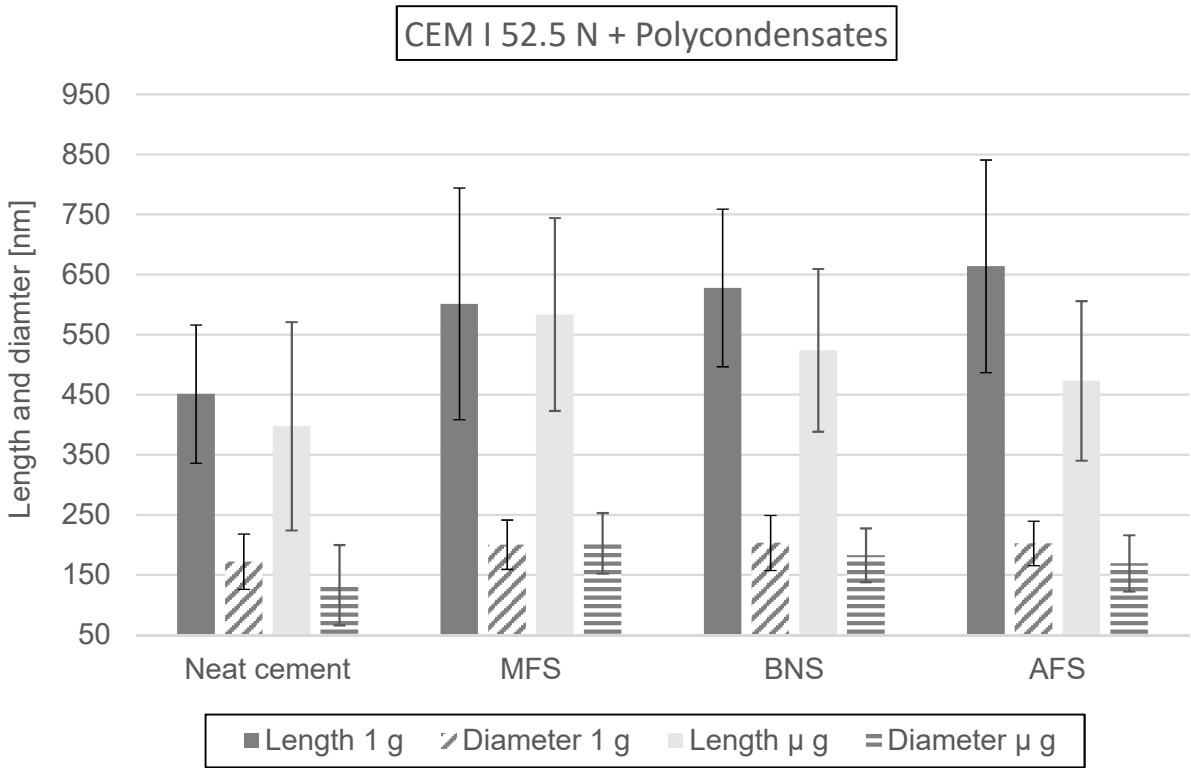

Figure 61: Average length and diameter of ettringite crystals obtained from CEM I 52.5 N admixed with 0.05 % bwoc of polycondensate samples MFS, BNS and AFS possessing increasing anionic charge, grown under terrestrial and microgravity conditions.

These observations were confirmed by the evaluation of the crystal sizes (see **Figure 61** and **Table 13**). While under microgravity conditions the aspect ratio of the crystals stays almost constant and is independent of the presence and type of polycondensate, under normal gravity an increase in the ratio of length to diameter was found with increasing anionic charge density of the polycondensate from MFS (1,985 µeq/g) to BNS (2,531 µeq/g) to AFS (4,062 µeq/g).

Table 13: Average aspect ratios of ettringite crystals grown under 1 *g* and µ *g* conditions on CEM I 52.5 N admixed with 0.05% bwoc of polycondensate superplasticizers MFS, BNS and AFS possessing increasing anionic charge.

Condition	Neat Cement	+ MFS	+ BNS	+ AFS
1 *g*	2.8 ± 1.0	3.1 ± 0.9	3.2 ± 0.9	3.4 ± 0.9
µ *g*	3.1 ± 0.7	3.0 ± 0.7	2.9 ± 0.7	2.9 ± 0.8

Ettringite crystals obtained from hydration of the cement sample CEM I 42.5 R which yields already larger ettringite crystals without additives than CEM I 52.5 N, under terrestrial gravity conditions show a change in morphology in the presence of MFS and BNS which possess low anionic charge (see **Figure 62**). There, the AF_t crystals were found to be longer compared to those from neat cement paste.

Furthermore, especially under microgravity conditions ettringite crystal growth in direction of the *a* and *b* axis was more pronounced in the presence of these polycondensates. Generally, crystal length and diameter decreased with increasing anionic charge of the polymers. This effect is most pronounced in the sample admixed with AFS (see **Figure 63**).

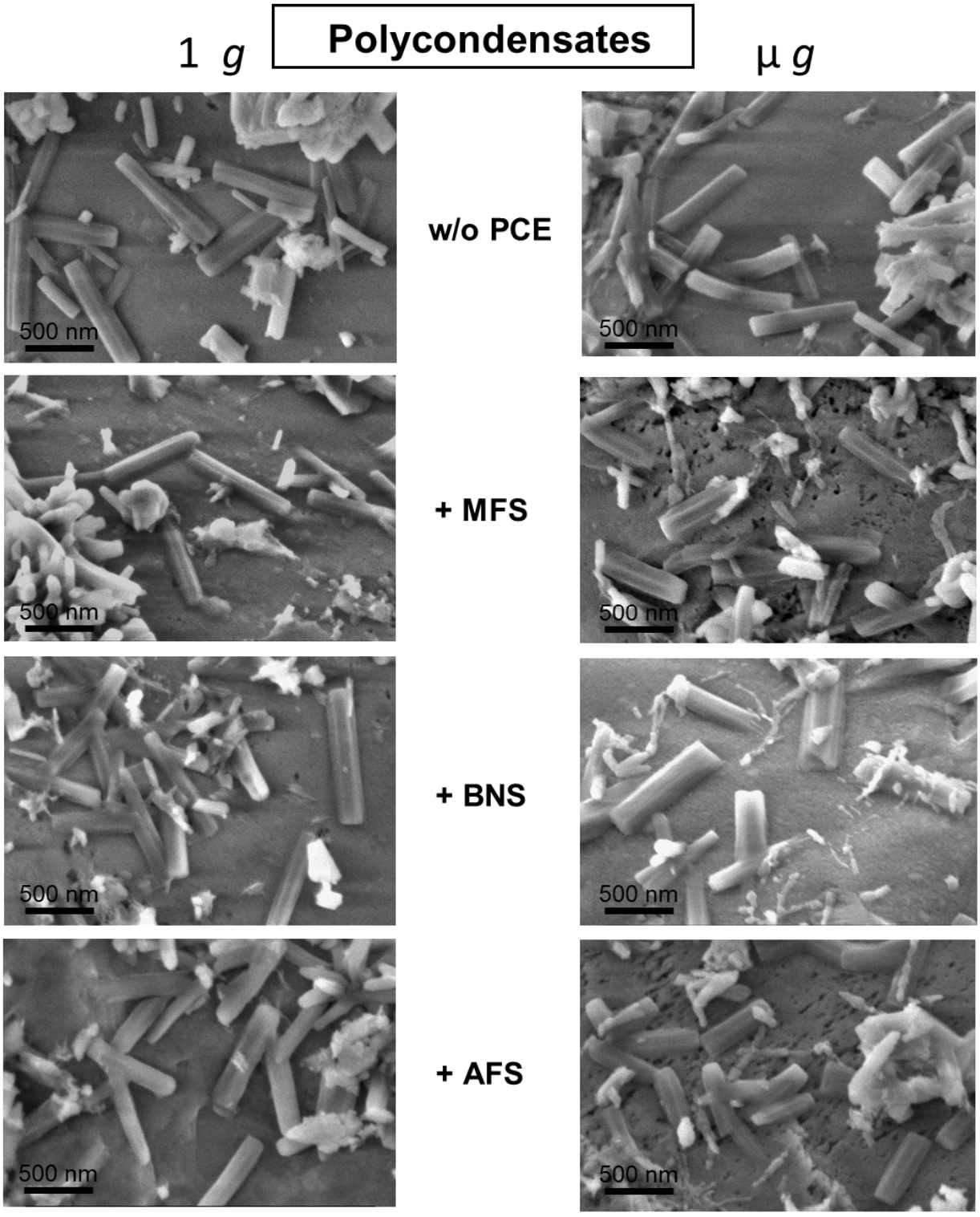

Figure 62: SEM images of CEM I 42.5 R sample hydrated for 10 s in presence of 0.05 % bwoc polycondensate samples MFS, BNS and AFS possessing increasing anionic charge under terrestrial (left) and microgravity (right) conditions. All images were collected at 40 k magnification.

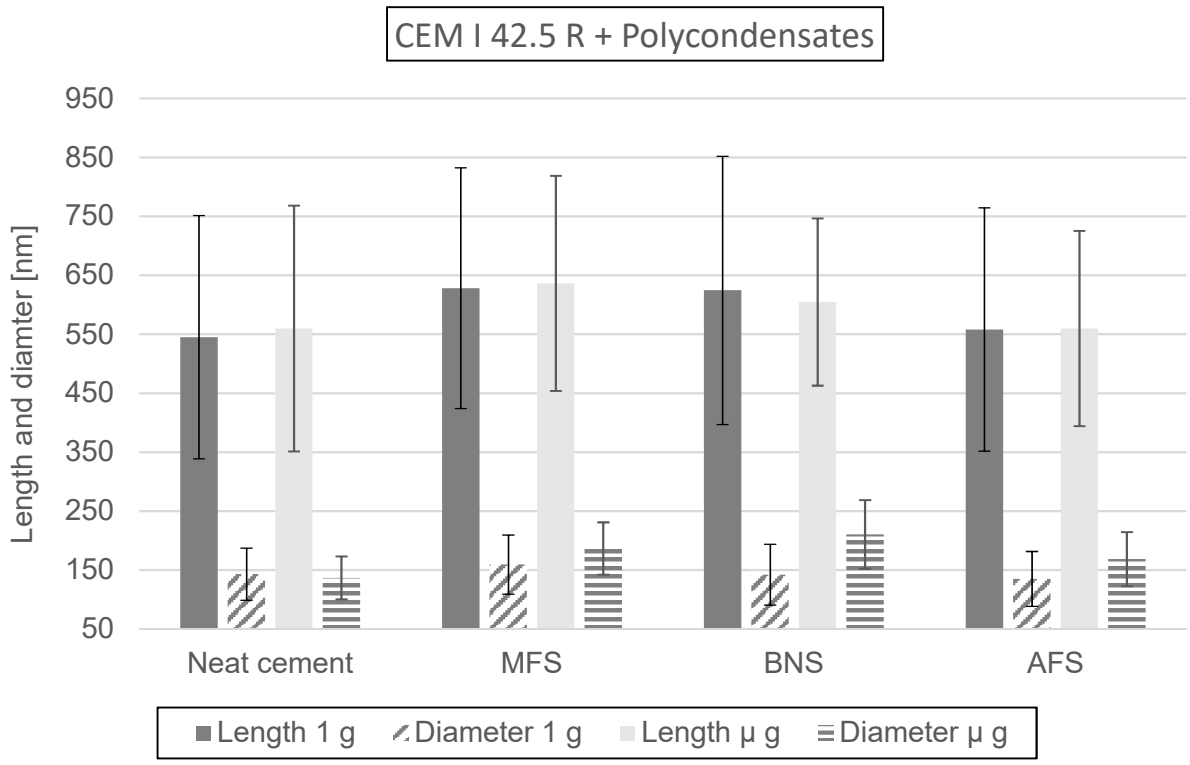

Figure 63: Average length and diameter of ettringite crystals obtained from CEM I 42.5 R admixed with 0.05 % bwoc of polycondensate samples MFS, BNS and AFS possessing increasing anionic charge, grown under terrestrial and microgravity conditions.

The calculated aspect ratios of the ettringite crystals formed in the experiments with polycondensates show that in the absence of convection, rather stocky crystals are formed as can be seen from the lower aspect ratios, while with convection, no clear trend is observable (see **Table 14**).

Table 14: Average aspect ratios of ettringite crystals grown under 1 *g* and µ *g* conditions on CEM I 42.5 R admixed with 0.05% bwoc of polycondensate superplasticizers MFS, BNS and AFS possessing increasing anionic charge.

Condition	Neat Cement	+ MFS	+ BNS	+ AFS
1 *g*	3.9 ± 1.4	4.1 ± 1.3	4.8 ± 1.8	4.4 ± 1.5
µ *g*	4.1 ± 1.3	3.5 ± 1.0	3.0 ± 0.8	3.5 ± 1.0

Comparing these results to the trends observed for PCE superplasticizers, for polycondensates there is no clear trend relating to the adsorption ability of the polymers on the lateral faces of the hexagonal prisms. This suggests that the linear structure of polycondensates allows comparable adsorption of the polymers on all ettringite crystal surfaces allowing also crystal growth along the a and b axis, while in the presence of PCEs mainly crystal growth along the c axis was observed.

5.4. Short-term hydration of pure clinker phases under terrestrial and microgravity conditions

The following results have not been published so far. The above investigations on nucleation and crystal growth of ettringite have shown that the cement composition, especially the C_3A and C_4AF content and sulfate carriers, play a significant role for the very early hydration of cement. It is known that early C_3A hydration has a strong influence on the rheology of Portland cement pastes and thus on that of concrete. Sulfate carriers like gypsum are used to control the setting of concrete. Without sulfates in the mortar mix, C_3A hydration leads to the formation of AF_m phases exhibiting a platelet structure which can easily grow together and lead to stiffening of the paste. By introducing a surplus of SO_4^{2-} ions into the mixture, long ettringite needles are formed instead of AF_m phases. These long needles do not interlock as strong as the AF_m platelets and thus the stiffening of the paste is delayed. There is still a lot of dispute about the reactivity of C_3A and C_4AF in combination with calcium sulfates.[28, 169]

Within this chapter, the very early hydration of the two aluminate phases C_3A and C_4AF will be investigated in the presence and absence of convection. To control the setting, usually a mixture of gypsum ($CaSO_4 \cdot 2H_2O$) and hemihydrate ($CaSO_4 \cdot ½H_2O$) or anhydrite ($CaSO_4$) is used, as the latter ones have higher solubility than gypsum and provide more free SO_4^{2-} ions for the ettringite formation. Due to the short reaction time of 10 s during parabolic flights, hemihydrate was chosen next to gypsum for this experiment as it has the highest solubility of the calcium sulfates. Additionally, synthetic cement pore solution was used as mixing water to simulate actual conditions in cement. A mixture of 5 wt.-% gypsum and 15 wt.-% hemihydrate and 80 wt.-% of cubic C_3A or C_4AF was used.

Furthermore, the formation of AF_m phases, namely of Hydroxide-LDH and monosulfate, was studied. In the presence of sulfates like gypsum, hemihydrate or anhydrite, ettringite is formed instantaneously within the first seconds. The pure C_3A and C_4AF were hydrated in different media, namely saturated $Ca(OH)_2$ solution, saturated $CaSO_4 \cdot ½ H_2O$ solution and synthetic cement pore solution, respectively, under terrestrial and microgravity conditions. For all experiments a water/solid ratio of 1.0 was applied.

5.4.1. Hydration of C_3A in the presence of sulfate carriers in synthetic cement pore solution

In order to investigate ettringite crystal growth from cubic C_3A in the presence of gypsum and hemihydrate, the solid powder mixture comprising 80 wt.-% C_3A_C, 15 wt.-% $CaSO_4 \cdot ½H_2O$ and 5 wt.-% $CaSO_4 \cdot 2H_2O$ was hydrated for 10 s in synthetic cement pore solution under terrestrial and microgravity conditions.

The XRD pattern revealed significant ettringite formation for both 1 *g* and µ *g* condition, as can be seen at the distinct reflection at 9.2° 2θ (see **Figure 64**). It can also be seen that the reflections of both sulfate carriers, gypsum and hemihydrate, decreased significantly during the 10 s of hydration. While the reflections of hemihydrate disappeared almost completely in both hydrated samples, the reflection of gypsum at 11.7° 2θ exhibited significantly less intensity in the sample hydrated under terrestrial conditions, compared to the one hydrated in µ *g*. These results clearly show the higher solubility of hemihydrate compared to gypsum.

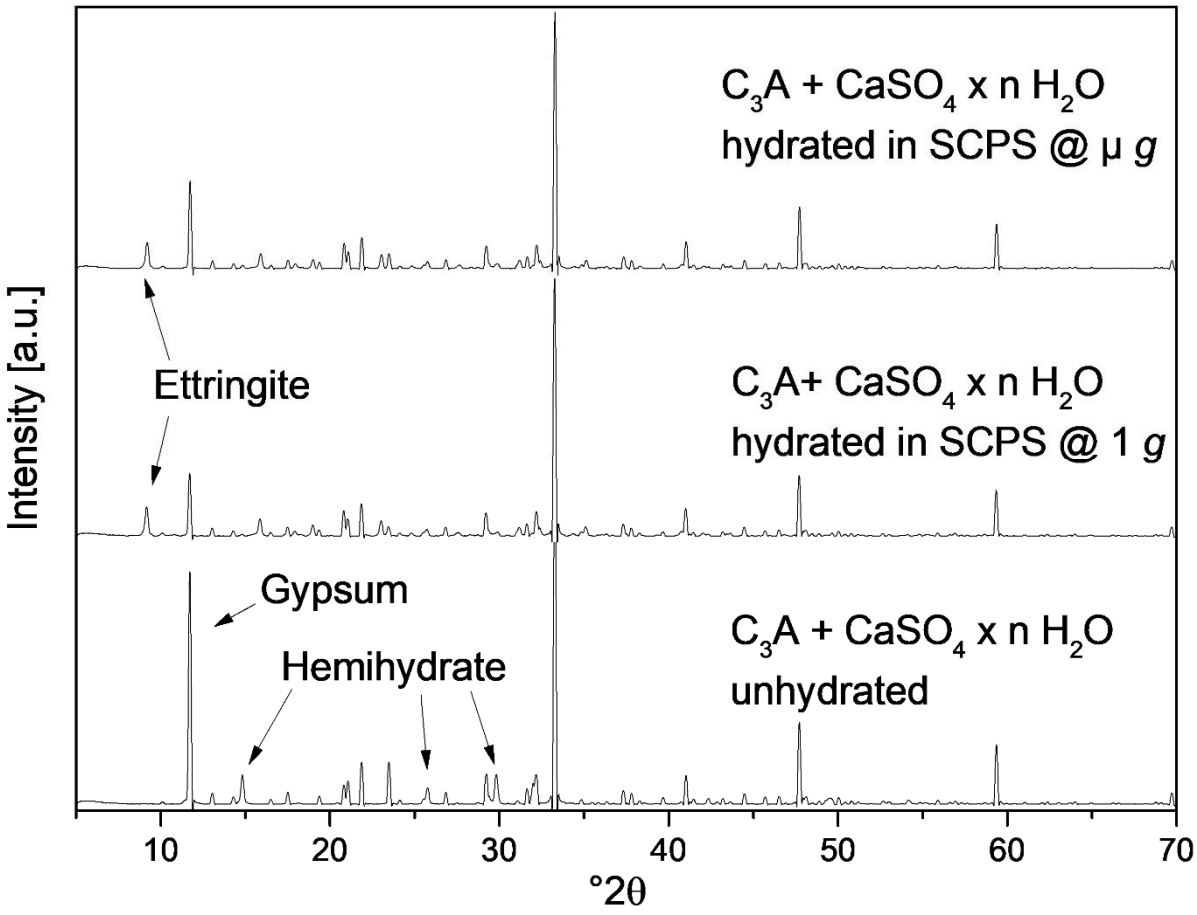

Figure 64: XRD pattern of a blend composed of 80 wt.% of neat C_3A_C, 15 wt.-% $CaSO_4$ hemihydrate and 5 wt.-% gypsum (C_3A + $CaSO_4$ x n H_2O), hydrated in synthetic cement pore solution for 10 s under terrestrial (1 *g*) and microgravity (µ *g*) conditions.

Furthermore, the formation of ettringite in both hydrated samples was tracked by electron microscopy. There, an abundancy of hexagonal, long ettringite crystals was found for both gravity conditions. The amount of crystals was significantly higher compared to the Portland cement samples previously investigated (see **chapter 5.3.**). In between the AF_t crystals, some rather large, but thin platelets were found which most likely are the corresponding AF_m phase incorporating sulfate.

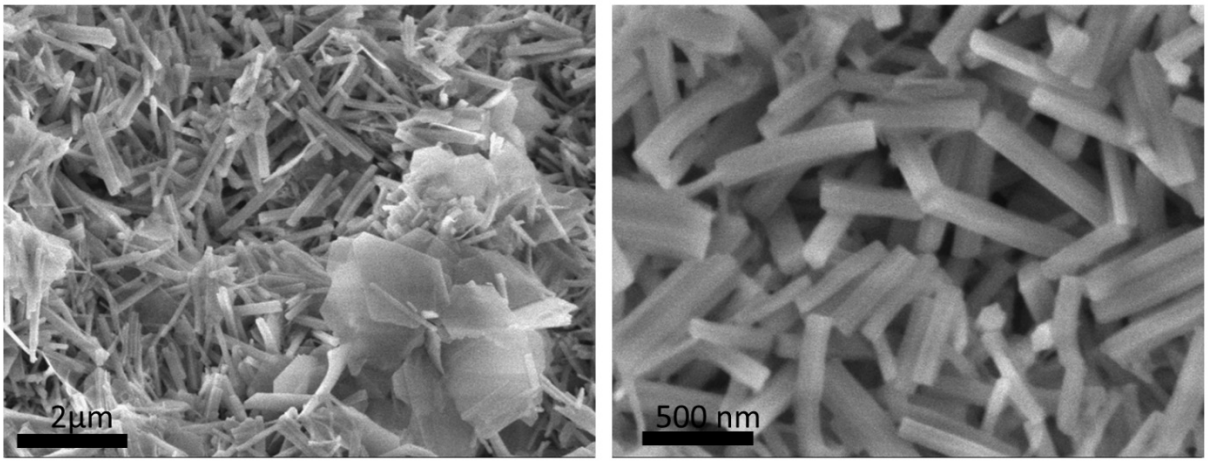

Figure 65: SEM images of a blend composed of 80 wt.% of neat C_3A_C, 15 wt.-% $CaSO_4$ hemihydrate and 5 wt.-% gypsum, hydrated in synthetic cement pore solution for 10 s under microgravity. Magnification: 10 k (left) and 40 k (right).

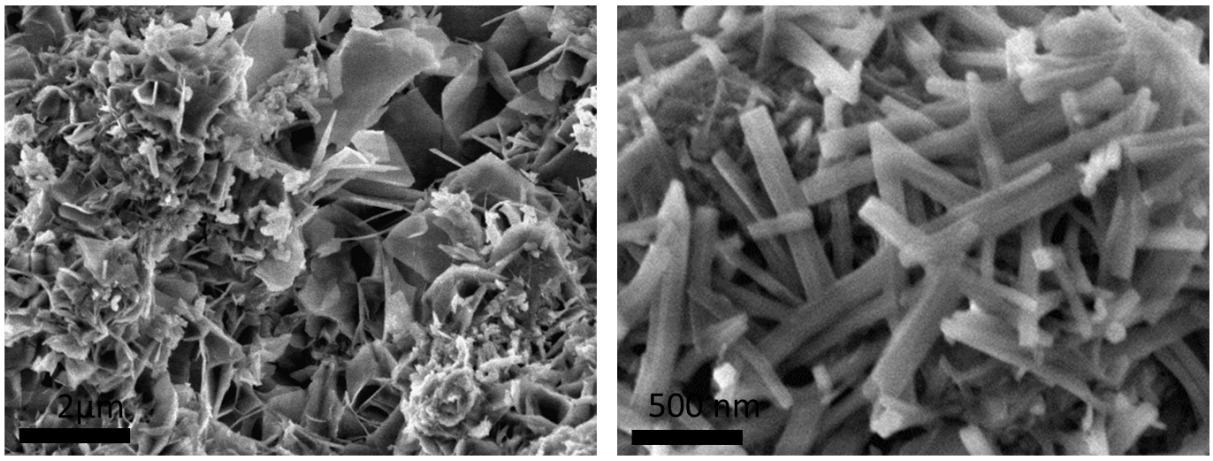

Figure 66: SEM images of a blend composed of 80 wt.% of neat C_3A_C, 15 wt.-% $CaSO_4$ hemihydrate and 5 wt.-% gypsum, hydrated in synthetic cement pore solution for 10 s under terrestrial gravity. Magnification: 10 k (left) and 40 k (right).

The ettringite crystals of both hydrated samples were measured in size to evaluate the impact of the absence of convection. The results are displayed in **Table 15**. The obtained ettringite crystals showed comparable lengths and diameters under both gravity conditions. Consequently, the calculated aspect ratios of the ettringite crystals from both experiments are similar, too.

Table 15: Lengths and diameters of ettringite crystals obtained from hydration of a blend composed of 80 wt.% of neat C_3A_C, 15 wt.-% $CaSO_4$ hemihydrate and 5 wt.-% gypsum in synthetic cement pore solution for 10 s at a w/s ratio = 1.0 under terrestrial and microgravity.

	1 *g*	**μ *g***
Length [nm]	880.1 ± 282.7	829.7 ± 325.4
Diameter [nm]	163.5 ± 50.9	163.4 ± 55.4
Aspect ratio [L/D]	5.7 ± 2.0	5.4 ± 2.1

These results indicate that the nucleation and crystal growth of ettringite crystals during hydration in SCPS are not dominated by dissolution and mass transport processes. Apparently, the alkaline pH and the variety of ions supplied by the SCPS speeds up dissolution and precipitation of hydrate phases and decreases the effect of ion concentration gradients induced by the absence of convection. Another potential mechanism might be a fast precipitation of a low-permeable $Al(OH)_3$ gel on the C_3A surface after initial dissolution, preventing further crystal growth under both gravity conditions.

5.4.2. Hydration of C_4AF in the presence of sulfate carriers in synthetic cement pore solution

Besides C_3A, another aluminate-based clinker phase is present in Portland cement, namely brownmillerite (C_4AF). This phase contains a higher amount of calcium than C_3A and a ferrite phase, $Ca_2Fe_2O_5$ with which $Ca_2Al_2O_5$ forms a solid solution. During crystallization, Fe^{3+} ions can take the positions of Al^{3+} ions in the ettringite or monosulfate crystal structures. In the following, brownmillerite was admixed with sulfate carriers similar to the experimental setup with cubic C_3A, i.e. with 5 wt.-% gypsum and 15 wt.-% hemihydrate by weight of the total mix. The mixture was hydrated for 10 s under terrestrial and microgravity conditions in synthetic cement pore solution.

The results of the XRD analysis of both hydrated samples are displayed in **Figure 67**. Formation of ettringite is proven by the presence of the reflection at 9.2° 2θ after hydration. Similar to the hydration of C_3A, the hemihydrate reflections are almost gone after hydration. Reflections of gypsum (e.g. 11.7° 2θ) show again a stronger decline in intensity in the experiment under 1 *g* compared to µ *g*.

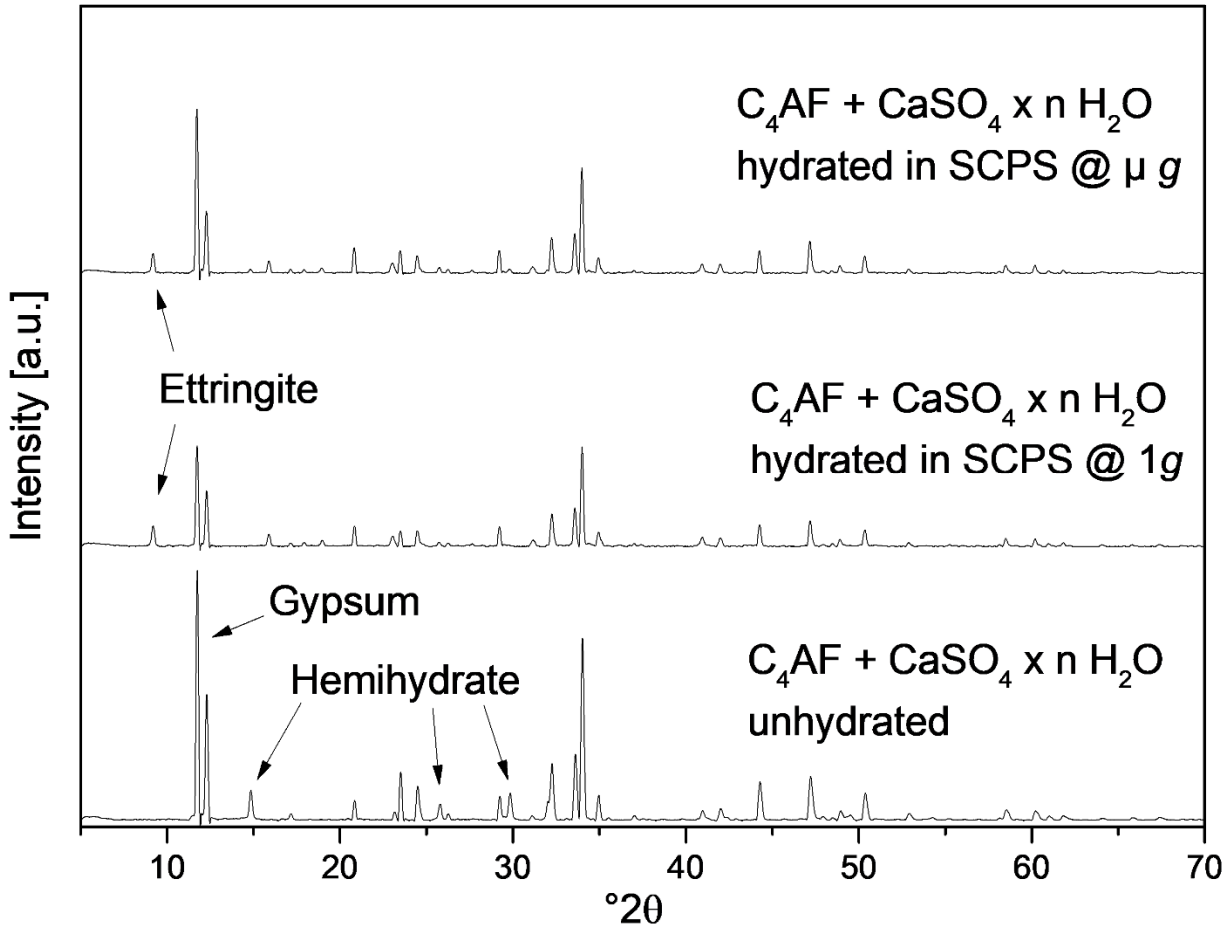

Figure 67: XRD pattern of a blend composed of 80 wt.% of neat C_4AF, 15 wt.-% $CaSO_4$ hemihydrate and 5 wt.-% gypsum (C_4AF+$), hydrated in synthetic cement pore solution for 10 s under terrestrial (1 *g*) and microgravity (µ *g*) conditions.

Electron microscopy revealed abundant formation of ettringite crystals on the clinker surface, as was observed before for C_3A (see **Figure 68**). The obtained crystals exhibited the typical hexagonal needle-like shape. In contrast, the amount of monosulfate formed was less and the size of the AF_m phases significantly smaller. They appeared only as small thin foils growing topotactical on the C_4AF surface in a few areas.

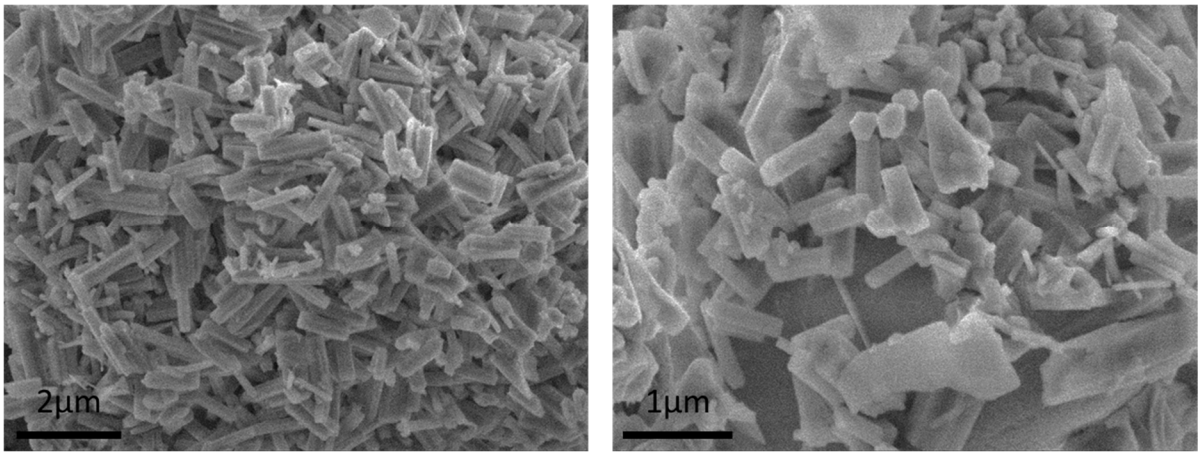

Figure 68: SEM images of a blend composed of 80 wt.% of neat C_4AF, 15 wt.-% $CaSO_4$ hemihydrate and 5 wt.-% gypsum, hydrated in synthetic cement pore solution for 10 s under microgravity conditions. Magnification: 10 k (left) and 20 k (right).

The ettringite crystals found in the sample hydrated under terrestrial gravity appeared longer and less stocky than the crystals formed under microgravity. This observation was confirmed by the size measurements (see **Table 16**). Crystals formed at 1 *g* exhibited an average length of ~ 1.2 µm, compared to ~ 0.9 µm for hydration under µ *g*. Larger diameters were as well found for the terrestrial sample. Overall, the aspect ratios of the ettringite crystals formed under 1 *g* is 4.7, compared to 4.1 for the crystals obtained from hydration under µ *g*.

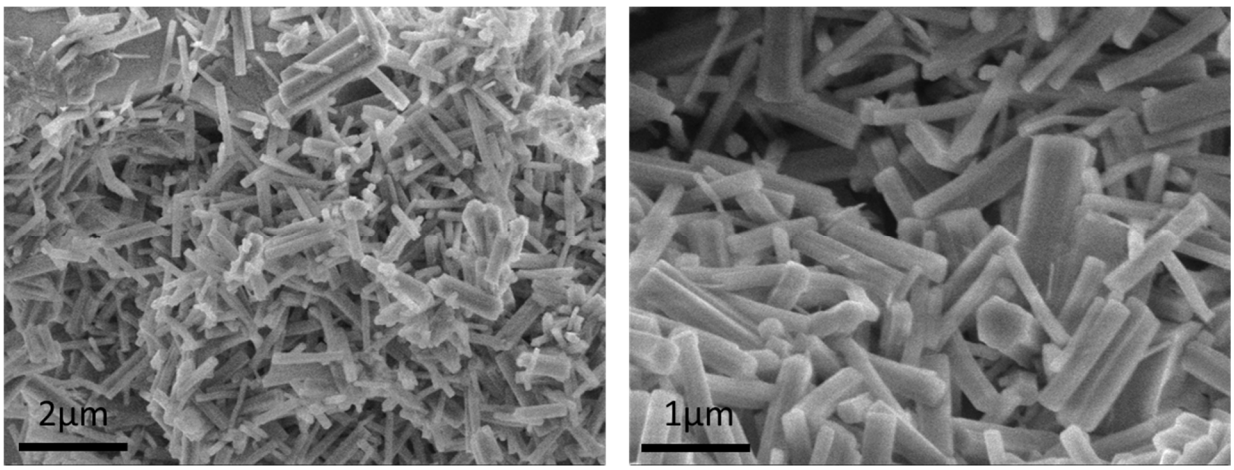

Figure 69: SEM-images of a blend composed of 80 wt.% of neat C_4AF, 15 wt.-% $CaSO_4$ hemihydrate and 5 wt.-% gypsum, hydrated in synthetic cement pore solution for 10 s under terrestrial gravity conditions. Magnification: 10 k (left) and 20 k (right).

Table 16: Lengths and diameters of ettringite crystals obtained from hydration of a blend composed of 80 wt.% of neat C_4AF, 15 wt.-% $CaSO_4$ hemihydrate and 5 wt.-% gypsum in synthetic cement pore solution for 10 s at a w/s ratio = 1.0 under terrestrial and microgravity.

	1 *g*	**μ *g***
Length [nm]	1209.6 ± 376.1	900.8 ± 245.1
Diameter [nm]	288.6 ± 131.6	243.8 ± 117.0
Aspect ratio [L/D]	4.7 ± 1.9	4.1 ± 1.4

Formation of ettringite crystals from hydration of C_4AF admixed with sulfates in synthetic cement pore solution was significantly enhanced under terrestrial conditions, as the obtained crystals were bigger in size. Furthermore, the crystals are longer and thicker than the ettringite crystals formed under similar conditions from C_3A. Thus, their appearance is rather stocky compared to the long needles found after hydration of C_3A. Ettringite crystals obtained from C_3A and C_4AF under microgravity are quite comparable in size. While with C_3A the difference between the gravity conditions is negligible, the larger sizes of ettringite crystals formed during hydration of C_4AF in the presence of convection suggest that – surprisingly - the reactivity of C_4AF is slightly higher than that of C_3A which might be attributed to a slower formation of amorphous $Fe(OH)_3$ gel or a higher permeability of the latter compared to the $Al(OH)_3$ gel formed from C_3A. Thus, the effect of increased mass transport under terrestrial conditions supporting the dissolution of C_4AF and subsequent ettringite crystal growth is more pronounced.

5.4.3. Hydration of cubic C_3A in the presence of $Ca(OH)_2$

So far, the main hydration product of the aluminate phases in the previous experiments was the AF_t phase ettringite. To get insight into the crystallization of AF_m phases, e.g. C_4AH_x and monosulfate, hydration of C_3A_C in a saturated calcium hydroxide solution was chosen to obtain exclusively the AFm phase C_4AH_x ($[Ca_2Al(OH)_6](OH) \cdot x\ H_2O$) as main product. The impact of the absence of convection and thus limited mass transport of dissolved ions from the clinker

surface to the bulk solution in the hydration under microgravity conditions on the amount of crystals and their morphology was investigated by electron microscopy and x-ray diffraction. As a reference, the same experiment was performed under normal gravity.

For both experiments, the XRD pattern revealed very intense C_3A_C reflections due to the short reaction time. Besides that, there is a characteristic reflection for the OH-LDH at 10.1° 2θ with a corresponding basal spacing of d = 0.79 nm which was reported by others as well.[11, 170]

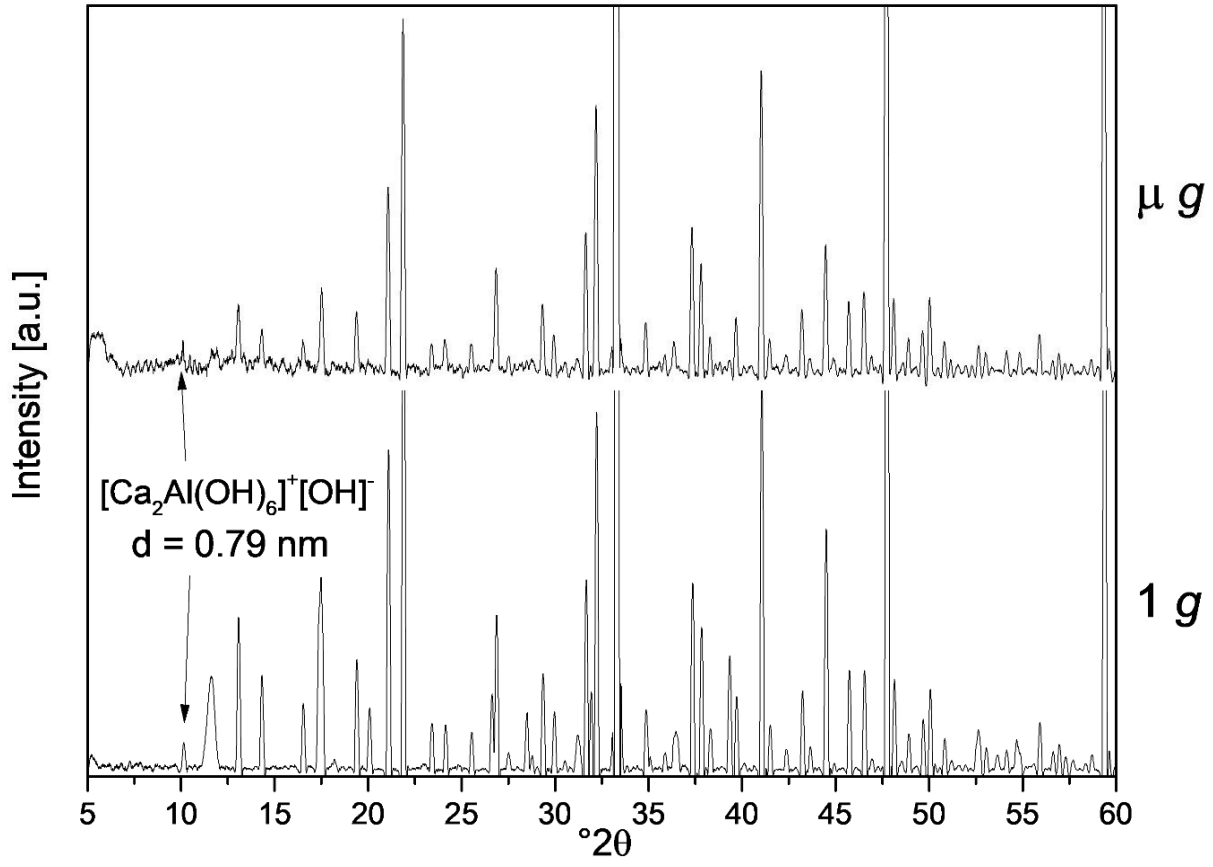

Figure 70: XRD patterns of cubic C_3A hydrated in a saturated $Ca(OH)_2$ solution for 10 s under terrestrial (1 *g*) and microgravity (μ *g*) conditions.

Hydration under microgravity conditions resulted in the characteristic foil-like morphology of AF_m phases, as was observed by SEM imaging (see **Figure 71**). The foils are growing topotactical on the clinker surface, covering it very densely.

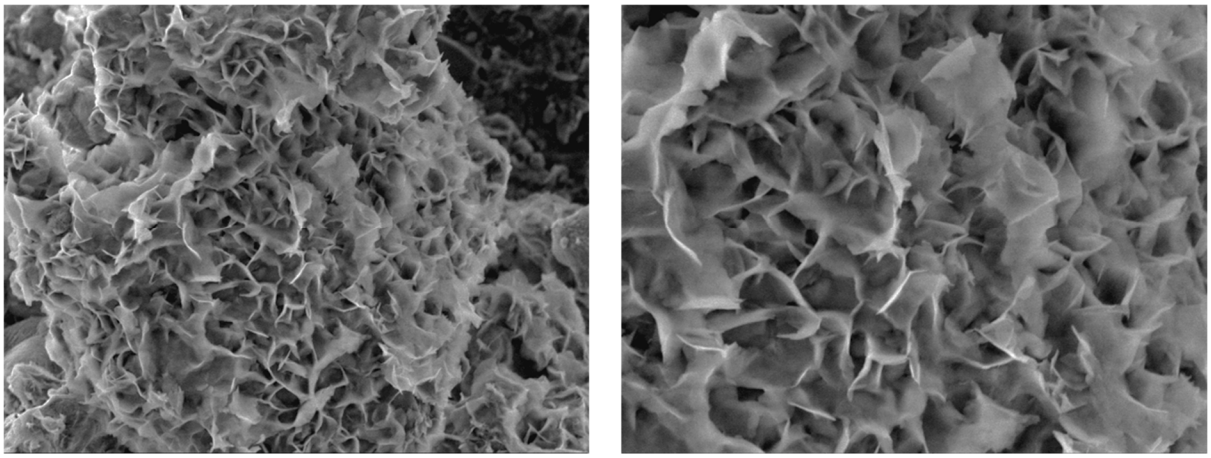

Figure 71: SEM images of cubic C_3A hydrated in a saturated $Ca(OH)_2$ solution for 10 s under microgravity. Magnifications: 5 k (left) and 10 k (right).

Under microgravity conditions, the C_3A surface was completely covered by copious amounts of thin foils of AF_m phases. Whereas under 1 *g*, rather widely spread hydration products were observed, and parts of the C_3A surface were still visible.

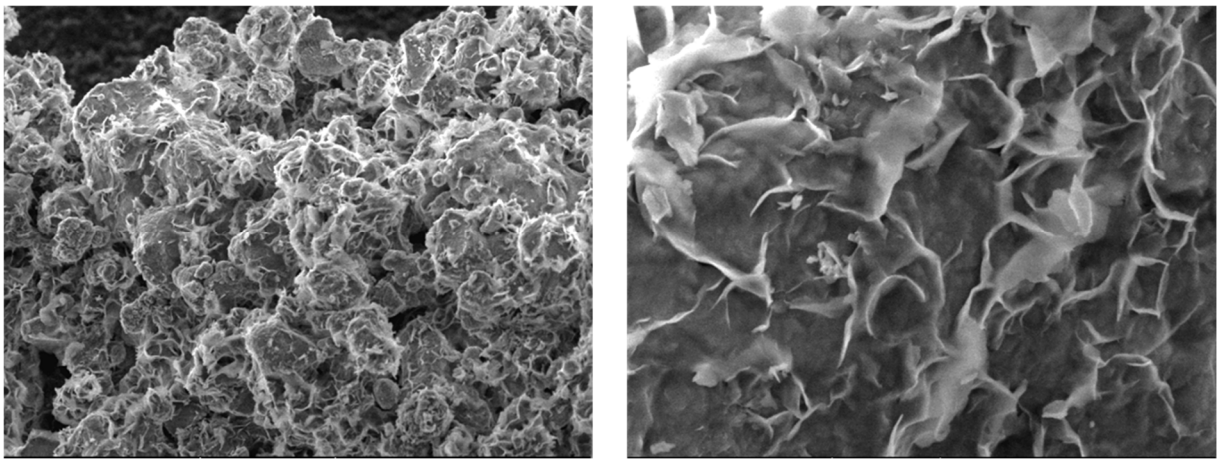

Figure 72: SEM images of cubic C_3A hydrated in a saturated $Ca(OH)_2$ solution for 10 s under terrestrial gravity. Magnifications: 2.5 k (left) and 10 k (right).

The more abundant formation of C_4AH_x phases under microgravity can be explained by the absence of convection leading to a high supersaturation in the boundary zone between the C_3A surface and bulk solution and thus to the formation of more critical nuclei resulting in a higher amount of crystals, compared to terrestrial conditions where mass transport by

convection leads to low supersaturation in the boundary zone and hence less nuclei possessing the critical size for crystal growth are formed.[8, 58, 60]

5.4.4. Hydration of cubic C_3A in the presence of $CaSO_4$ Hemihydrate

Monosulfate generally forms during cement hydration when SO_4^{2-} ions in the pore solution are depleting (c < 2.85 mg/L) which occurs mainly due to abundant ettringite formation during the first hours. Then ettringite converts via a through-solution process into the thermodynamically favoured AF_m phase monosulfate or, at low SO_4^{2-} concentrations, monosulfate may be formed directly from hydration of C_3A. To investigate the crystal growth of monosulfate, hydration of cubic C_3A in a saturated $CaSO_4$ hemihydrate solution was chosen, with a molar ratio of Al/SO_4^{2-} = 2:1. Again, hydration was performed under microgravity and terrestrial conditions in order to determine the influence of convection on the crystallization.

The collected XRD patterns of both hydration experiments show reflections for the cubic C_3A phase which are similar like in the hydration with calcium hydroxide solution (see **Figure 73**), due to the short reaction time. But the (003) reflection of the LDH at 9.3° 2θ suggests that there SO_4^{2-} is intercalated as anion. The corresponding value for the interlayer distance is 0.9 nm which is in good agreement with previous studies on monosulfates.[170]

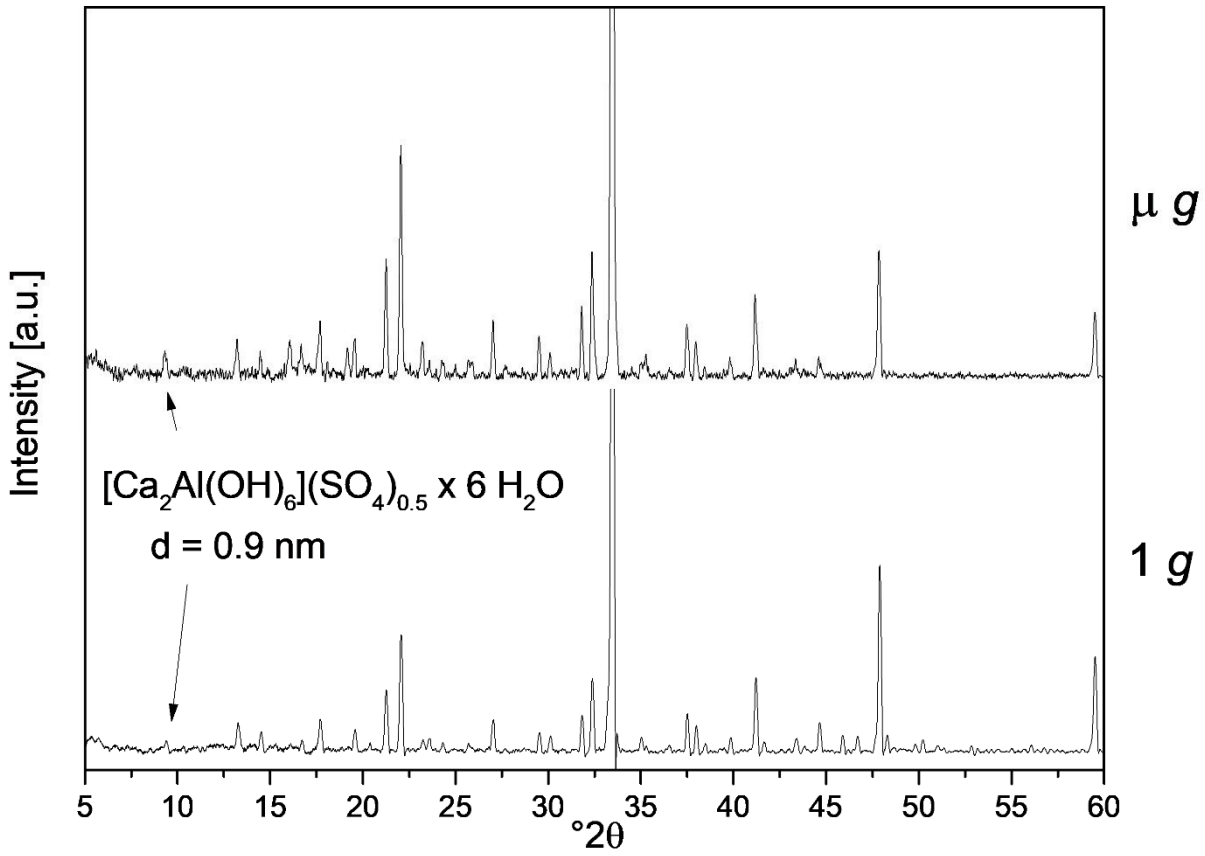

Figure 73: XRD patterns of cubic C_3A hydrated in a saturated $CaSO_4$ hemihydrate solution for 10 s under terrestrial (1 *g*) and microgravity (μ *g*) conditions.

The monosulfate obtained exhibited a similar plate-like morphology as for the Hydroxy-AF_m phase Ca_2Al-OH-LDH (see **Figure 74** and **75**). The C_3A surfaces are again densely covered by thin LDH platelets which in the absence of convection grow topotactical from the surface.

In a few areas, thin hexagonal rods were found by SEM imaging which is most likely ettringite that was formed due to a local surplus of sulfate ions. Due to the low amount formed, there is no reflection visible in the XRD pattern.

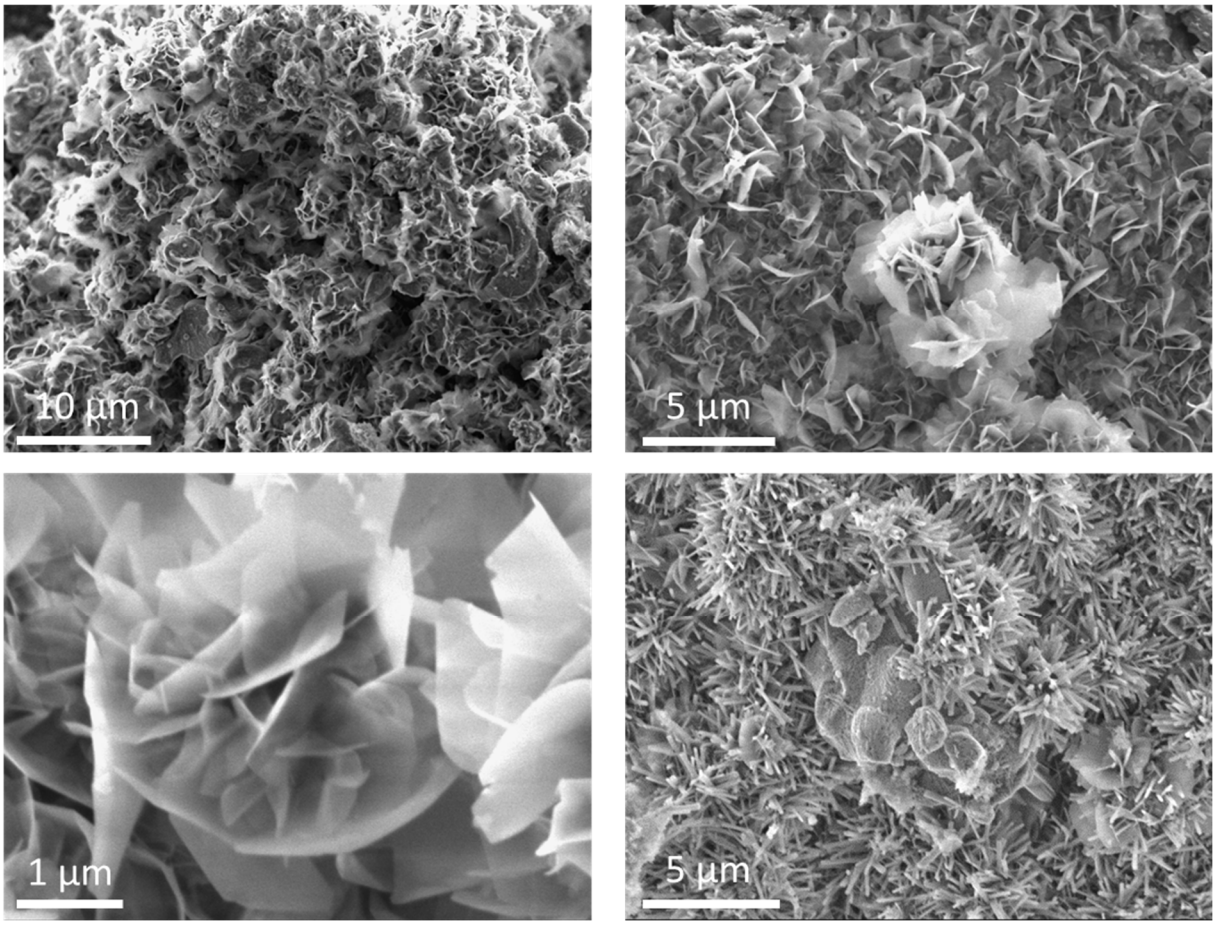

Figure 74: SEM images of cubic C_3A hydrated in a saturated $CaSO_4$ hemihydrate solution for 10 s under microgravity. Magnifications: 2.5 k (top left), 5 k (top right and bottom right) and 20 k (bottom left).

Under terrestrial gravity, a similar morphology was found for monosulfate than in microgravity, but the foils appear generally smaller in size and again less abundant than in the absence of convection. This is in good agreement with the results above obtained for C_4AH_x (see **chapter 5.4.3.**). When hydrated in saturated hemihydrate solution, many unreacted C_3A sites were detected, too. Like for the microgravity experiment, ettringite was observed here as by-product of the hydration in few areas of the sample as well.

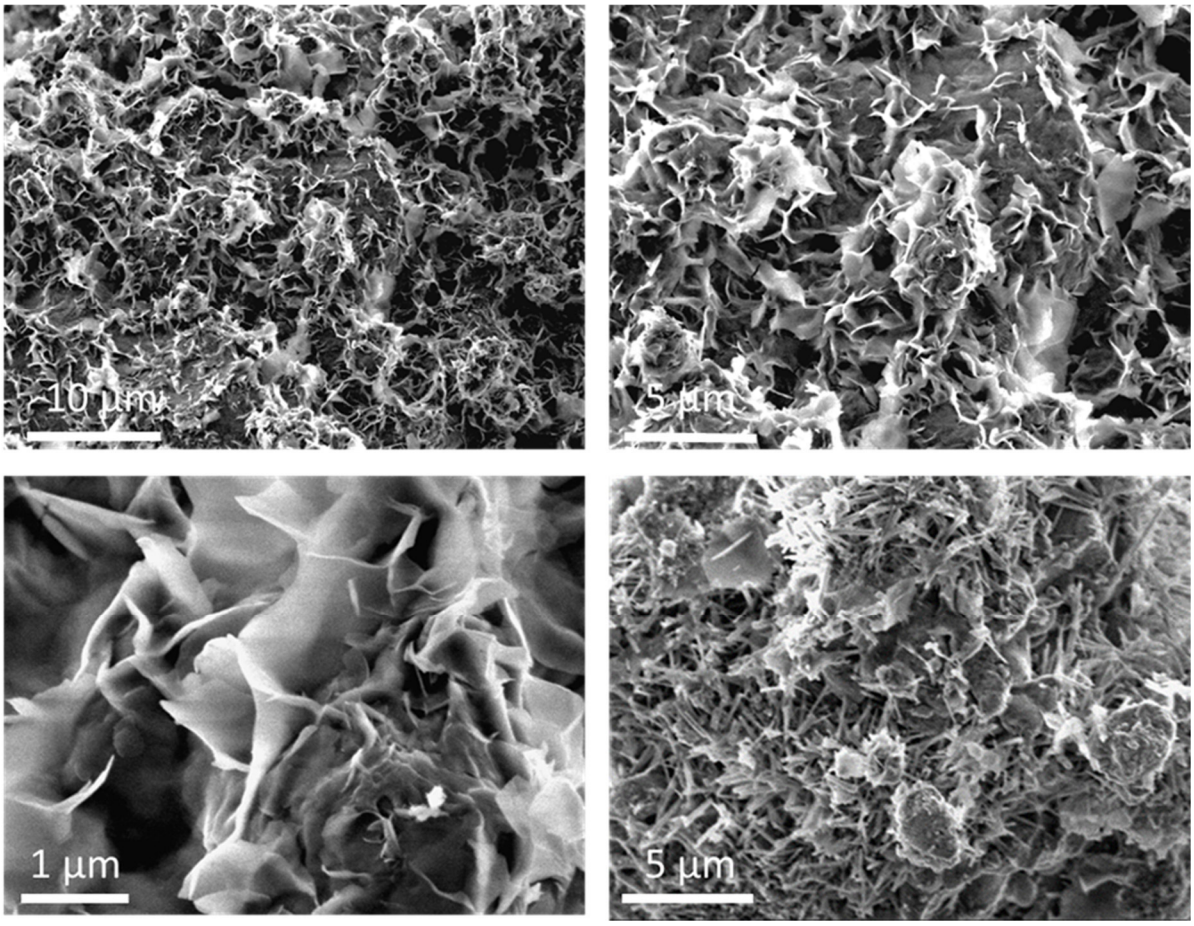

Figure 75: SEM images of cubic C_3A clinker hydrated in a saturated $CaSO_4$ hemihydrate solution for 10 s under terrestrial gravity. Magnifications: 2.5 k (top left), 5 k (top right and bottom right) and 20 k (bottom left).

5.5. C-S-H crystallization under terrestrial and microgravity conditions

Calcium silicate hydrate, formed by the reaction of C_3S with water, is the main hydration product in Portland cement. Due to its amorphous, poorly crystalline structure its nucleation and composition today is still the subject of many investigations. Depending on the reaction conditions, e.g. initial Ca/Si ratio or pH, it can exhibit different morphologies such as small globules, fibrils or foils.[171-172] Owed to its slow dissolution compared to aluminate phases, the main C_3S hydration begins after approximately 6 hours.[173]

In order to investigate the nucleation and early crystallization processes within the ~ 25 s microgravity period on parabolic flights, synthetic C-S-H preparation via flash precipitation from aqueous solutions of $Ca(NO_3)_2$ and Na_2SiO_3 was chosen. Moreover, it is well known that the presence of polycarboxylate ethers can delay C-S-H formation.[81] Recently, C-S-H nanoparticles, prepared by co-precipitation of $Ca(NO_3)_2$ and Na_2SiO_3 solutions in the presence of superplasticizers have also received much attention as seeding material for Portland cement hydration with regard to their application as accelerators for the early strength development of concretes.[129-130] Therefore, different types of PCEs were added to the $Ca(NO_3)_2$ solution to analyse their influence on nucleation and crystallization of C-S-H.

5.5.1. Influence of pH on C-S-H crystallization

Recently, it was found that the morphology of synthetic C-S-H nanoparticles is strongly depending on the pH of the bulk solution during nucleation and crystallization at constant Ca/Si ratios.[129] The critical value for the pH which exerts the biggest change in morphology, namely from globular particles to C-S-H nanofoils was found to be 10.9. Below this pH value, globular and agglomerated C-S-H particles where formed whereas at higher pH values a foil-like morphology was always observed after 24 hours reaction time. Aim of this study was to analyse the influence of microgravity on the nucleation and early crystallization of C-S-H precipitated from aqueous solutions of $Ca(NO_3)_2$ and Na_2SiO_3 with a molar ratio of Ca/Si = 1 in the absence and presence of different types of PCE superplasticizers. For comparison, the same experimental procedure was carried out under terrestrial gravity conditions. The obtained C-S-H nanoparticles were characterized by transmission electron microscopy and dynamic light scattering.

Precipitation of C-S-H from aqueous solutions of $Ca(NO_3)_2$ and Na_2SiO_3 and a reaction time of 10 s resulted immediately in a white suspension. As evidenced by TEM, small nanoparticles of C-S-H were obtained for both gravity conditions (see **Figure 76**). Different morphologies were obtained at different pH conditions during synthesis. While precipitation at pH 10.5 clearly yielded exclusively globular nanoparticles, at pH 11.6 C-S-H globules as well as nanofoils were detected. Further studies (see **chapter 5.6**) have revealed that also at pH 11.6 and 10 s of

reaction time, initially formed C-S-H exhibits exclusively a globular morphology which transforms over time into nanofoils. Due to the nanosize of the formed precipitate it was not possible to extract the reaction product completely as the filter got plugged by the nanoparticles. Thus, after acetone addition to stop the reaction process it is possible that at pH 11.6 a part of the globular C-S-H nanoparticles continued to react into thin nanofoils until the samples were dried in the laboratories at the ground. In contrast, C-S-H formed at pH 10.5 did not transform into foils and was stable until TEM analysis. Particle size measurements via DLS were not possible, as the C-S-H particles sedimented within the measurement sequence, possibly due to agglomeration.

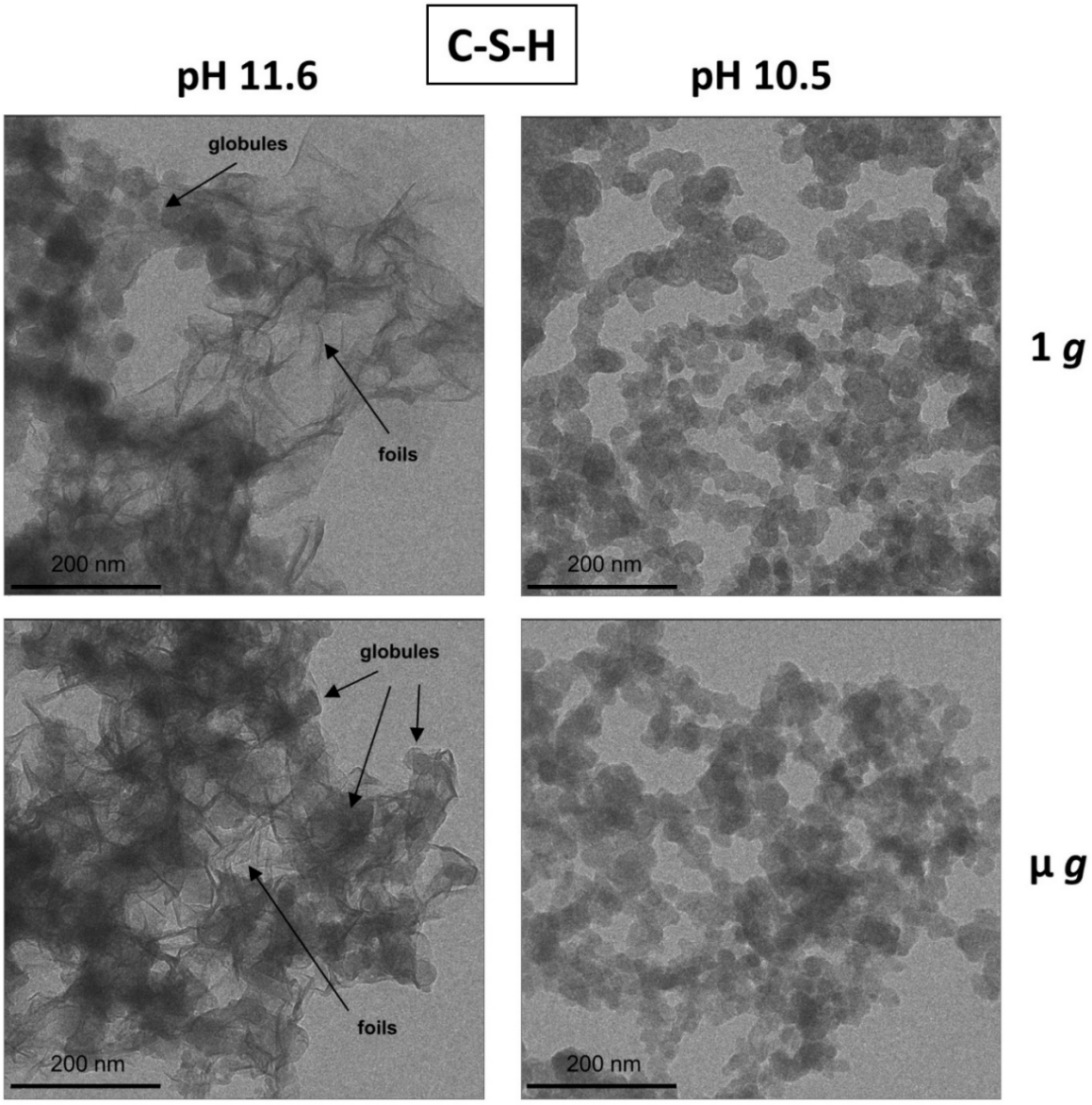

Figure 76: Synthetic C-S-H precipitated from aqueous solutions of $Ca(NO_3)_2$ and Na_2SiO_3 at a molar ratio of Ca/Si = 1 over for 10 s at pH = 11.6 (left) and pH = 10.5 (right) under terrestrial (top) and microgravity (bottom) conditions. Magnification: 30 k.

In further experiments, the influence of different types of PCEs on the C-S-H formation was investigated. The PCE was added to the $Ca(NO_3)_2$ solution. APEG-34 was chosen as representative sample for APEG-PCEs, IPEG-50PC6 for IPEG-PCEs and MPEG-114PC6 and MPEG-45PC10 were chosen as MPEG-PCE samples.

Again, C-S-H nanoparticles formed in the presence of these different types of PCEs. With all polymers they exhibited a globular morphology independent of pH value and the presence or absence of convection. On the surface, the C-S-H globules were completely coated with a polymer film, as can be seen on TEM images (see **Figure 77**). Furthermore, in the presence of PCEs, no C-S-H nanofoils were detected at a pH of 11.6. This suggests that the globular morphology is stabilized by the polymer film. This is in good agreement with results from the follow-up study (see **chapter 5.7**).

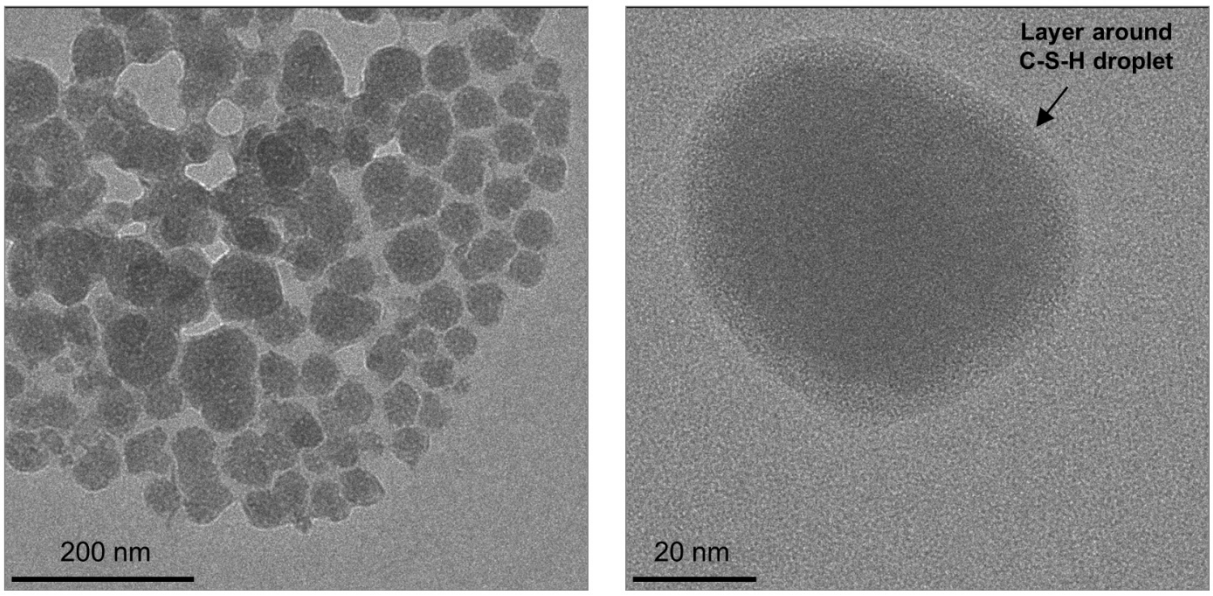

Figure 77: TEM images of C-S-H formed in the presence of MPEG-114PC6 at pH = 11.6 under microgravity. Magnifications: 30 k and 200 k.

TEM imaging revealed that the globules, i.e. the primary particles, formed in the presence of the APEG-PCE sample show a rather aspherical shape, while those formed with other types of PCEs exhibit mostly spherical globules (see **Figure 78** and **79**). Further is to note that the globules formed in the presence of the IPEG-PCE sample present quite monodisperse primary particles, compared to the very polydisperse globules crystallized in the presence of MPEG- and APEG-PCEs.

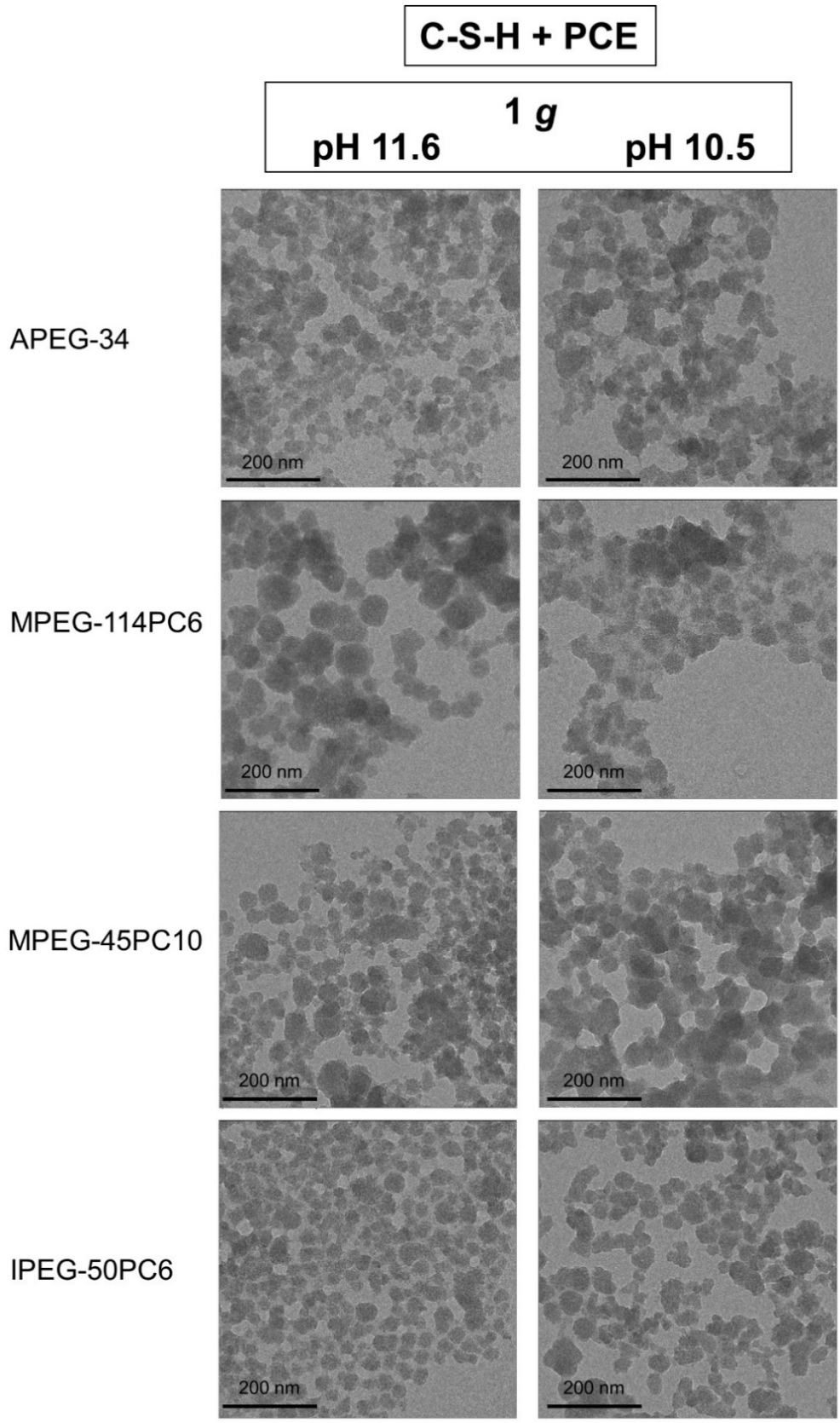

Figure 78: Synthetic C-S-H precipitated from aqueous solutions of $Ca(NO_3)_2$ and Na_2SiO_3 with a molar ratio of Ca/Si = 1 after 10 s at pH = 11.6 and pH = 10.5 under terrestrial gravity. Magnification: 30 k.

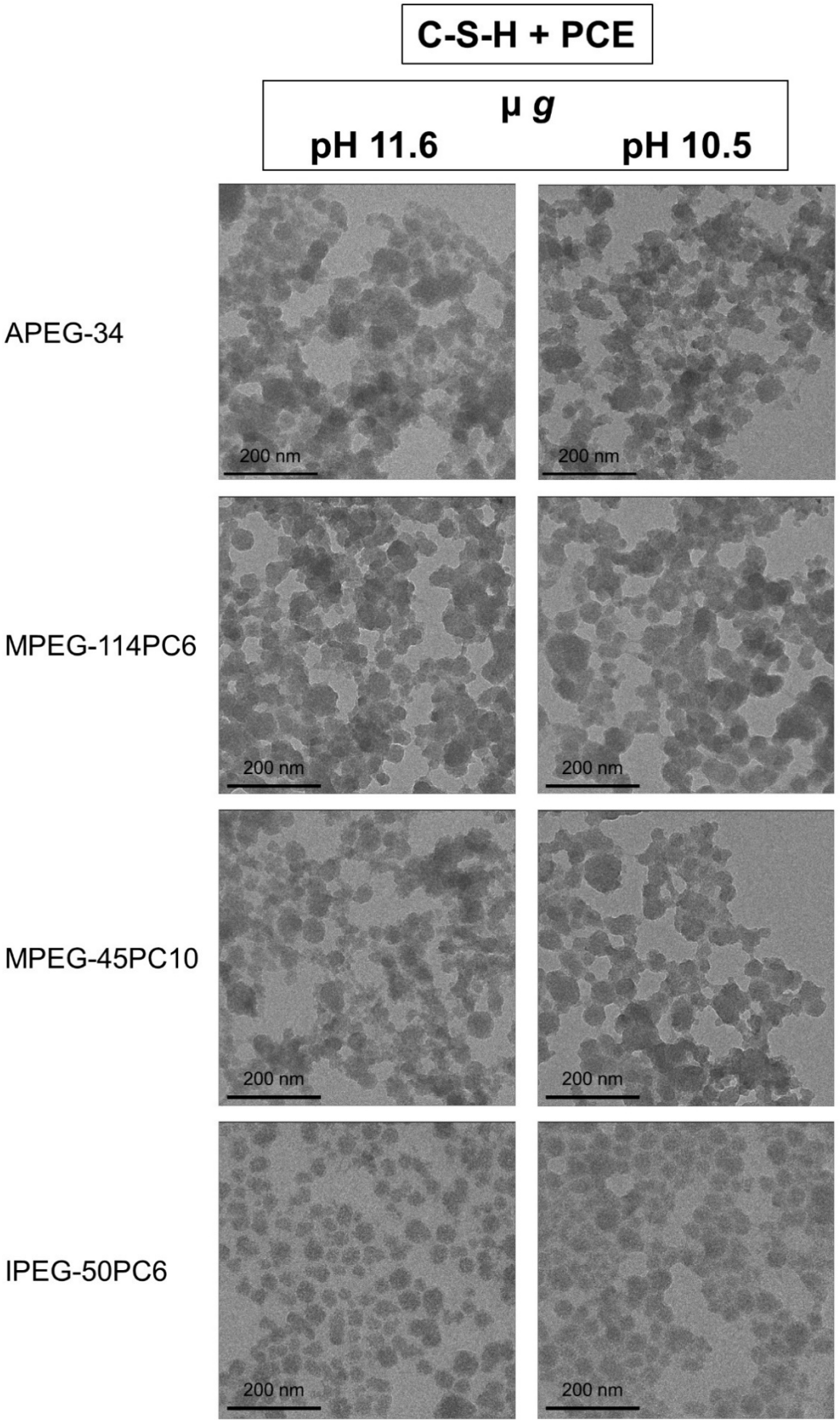

Figure 79: Synthetic C-S-H precipitated from aqueous solutions of $Ca(NO_3)_2$ and Na_2SiO_3 with a molar ratio of Ca/Si = 1 after 10 s at pH = 11.6 and pH = 10.5 under microgravity. Magnification: 30 k.

The particle sizes of the recovered C-S-H precipitates were further characterized via DLS. **Figures 80** and **81** show the different particle size distributions of the C-S-H-PCE nanocomposites at pH = 11.6 and pH = 10.5 prepared by flash precipitation under microgravity conditions. The results for the DLS measurements from the 1 *g* experiments can be found in the appendix.

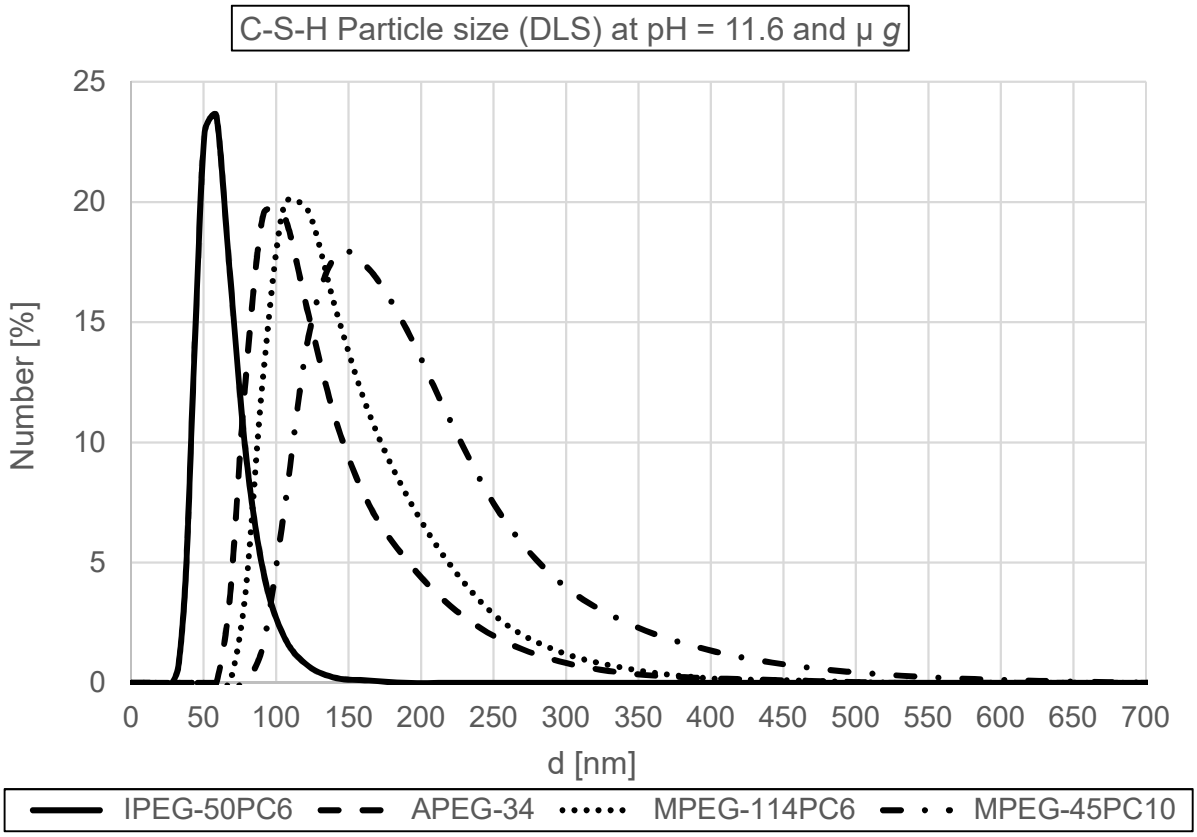

Figure 80: Particle size distributions of C-S-H precipitated at pH = 11.6 in the presence of different PCE superplasticizers, determined by dynamic light scattering in isopropanol.

As can be seen in **Figure 80**, C-S-H formed in the presence of IPEG-50PC6 has the smallest average particle size at pH = 11.6 and pH = 10.5. The particle size distribution is quite narrow, too, in contrast to the other samples which confirms the observation made on TEM images of rather monodisperse particles. The mean particle sizes by number are 60 nm at pH = 11.6 and 63 nm at pH = 10.5. Comparison of these values with the sizes of the C-S-H nanoparticles from TEM imaging reveals that not only primary particles, but mostly small agglomerates of primary particles were detected by DLS. The particle size distributions for C-S-H globules formed in the presence of the APEG- and MPEG-PCEs clearly show that only agglomerates of primary particles were detected, as there were no particles present in the

range of the size of the primary particles found in TEM analysis (< 50 nm). For example, C-S-H precipitated with MPEG-45PC10 at pH = 11.6 under μ *g* consists of the largest particles ranging from approximately 80 nm up to 670 nm, as evidenced by DLS. But TEM images reveal an abundance of C-S-H nanoparticles with a diameter in the range of ~ 30 nm (see **Figure 78**). The DLS measurements can thus be interpreted as an indicator for the degree of agglomeration of the C-S-H particles which basically correlates with the stabilizing ability of the PCEs for the primary particles.

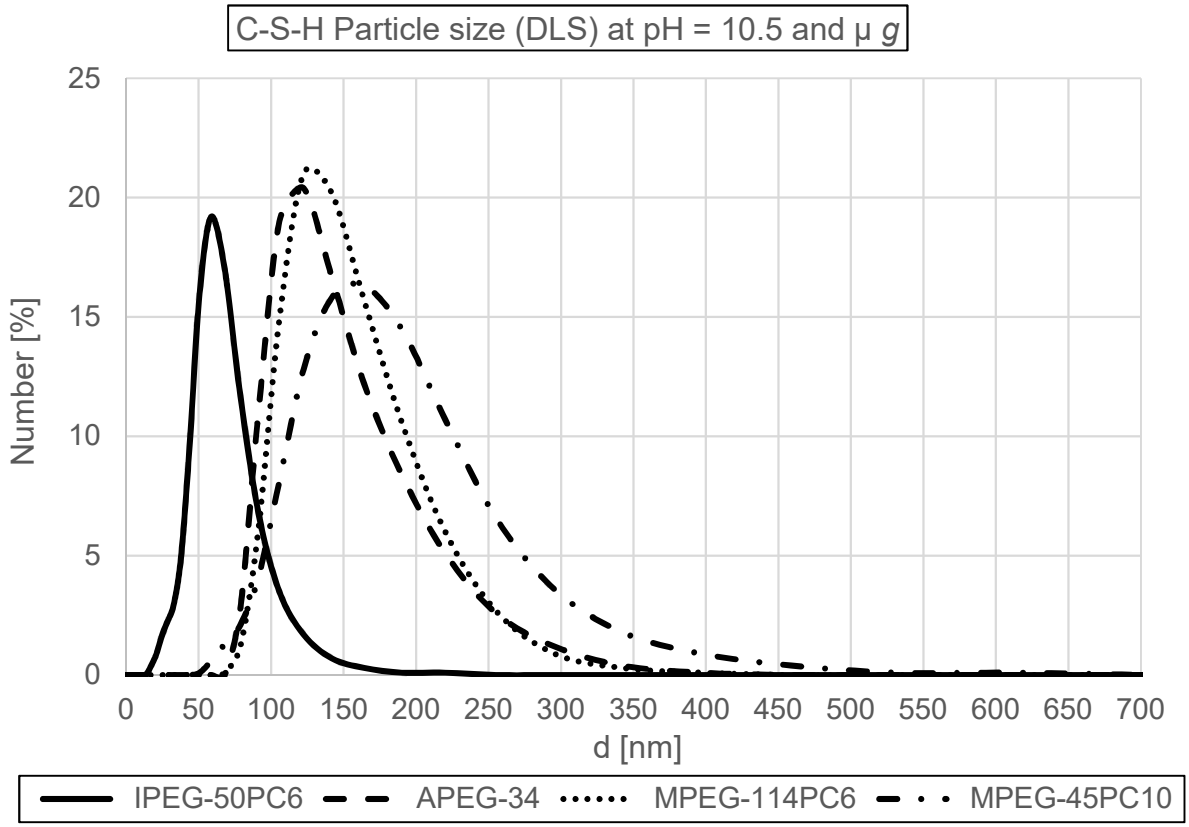

Figure 81: Particle size distributions of C-S-H precipitated at pH = 10.5 in the presence of different PCE superplasticizers determined by dynamic light scattering in isopropanol.

C-S-H precipitation in the presence of convection yielded similar particle size distributions as found for microgravity conditions for the different kinds of PCE, except for the IPEG-PCE sample. There, an increased amount of agglomerates was found for both pH ranges which resulted in a broader particle size distribution, as evidenced by DLS measurements (see **Appendix**, **Figures A7** and **A8**). Despite these findings, the degree of agglomeration for the

C-S-H-PCE nanocomposites obtained across all reaction parameters (pH = 11.6 & 10.5, 1 *g*, µ *g*) increases as follows:

IPEG-50PC6 < APEG-34 < MPEG-114PC6 < MPEG-45PC10

This series suggests that the molecular structure of the PCEs plays a decisive role in the stabilization of synthetically prepared C-S-H nanoparticles. Due to the limited number of experiments on the parabolic flight campaigns, a more profound investigation which requires a higher sample amount for microgravity conditions was not possible. Within a follow-up study (see **chapter 5.5.2.**) the influence of the molecular structure of these types of polycarboxylates on the C-S-H formation under terrestrial gravity conditions was investigated in more detail.

5.5.2. Influence of different types of PCEs on C-S-H crystallization

The previous studies on the influence of pH on the C-S-H formation in the presence of different types of PCEs (see **chapter 5.5.1.**) indicate that the agglomeration of primary particles of C-S-H obtained by flash precipitation is dependent on the molecular structure of polycarboxylate superplasticizers. To get more insight into this subject and to verify these observations made by transmission electron microscopy and dynamic light scattering, C-S-H-PCE composites prepared by flash precipitation at pH = 11.6 under terrestrial gravity were further characterized by x-ray diffraction, energy-dispersive x-ray spectroscopy, thermogravimetric analysis, infrared-spectroscopy and ^{29}Si MAS NMR spectroscopy. Furthermore, another IPEG-PCE sample, namely IPEG93PC6.5 possessing a longer side chain of 93 EO units, was included in this study. Pure C-S-H, synthesized in the absence of PCEs, was prepared as reference.

5.5.2.1. TEM imaging

Flash precipitation was employed to synthesize C-S-H nanoparticles in the absence and presence of different types of polycarboxylate ethers. The morphology of the samples was

investigated by transmission electron microscopy. As discussed previously in **chapter 5.5.1**., C-S-H formed by flash precipitation at pH = 11.6 exhibits a globular morphology after 10 s of reaction in the absence and presence of polymers. The primary particles of the pure C-S-H are rarely spherical as they tend to agglomerate already within 10 s.

Representative TEM images of C-S-H precipitated in the presence of PCE after 10 seconds are shown in **Figure 82**. In contrast to pure C-S-H, a thin layer is surrounding the C-S-H nanoparticles. Thus, mostly spherical primary particles were found for C-S-H precipitated in the presence of PCEs. Due to the different contrast of the layer to the particles and the copper grid the surrounding layer is most likely PCE. The C-S-H-PCE composites formed agglomerates as well, with the polymer layer preventing direct contact between C-S-H from different globules.

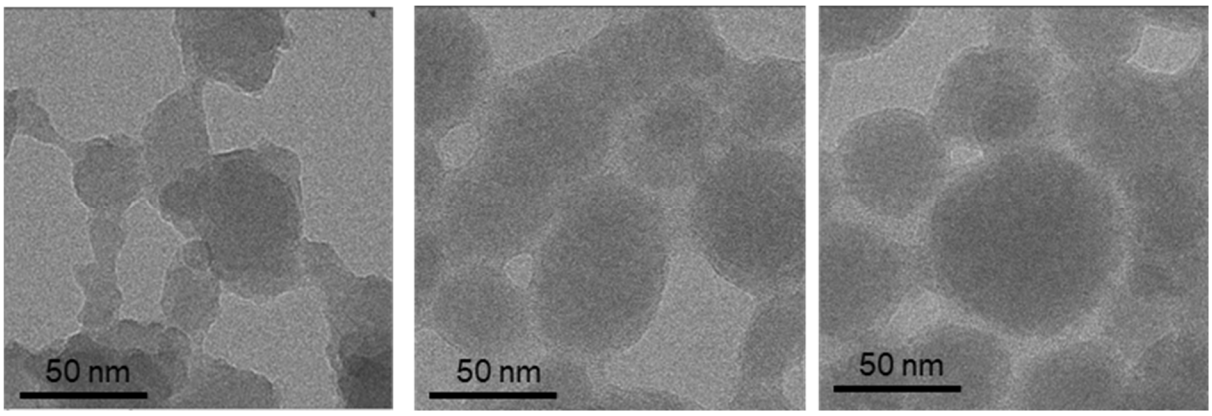

Figure 82: TEM images of C-S-H obtained by flash precipitation in the absence of PCE (left), in the presence of IPEG-50PC6 (middle) and IPEG-93PC6.5 (right). All images were collected at a magnification of 120k.

5.5.2.2. Dynamic light scattering

In order to determine the influence of the different PCEs on the formation of globules and the stability of the primary particles, the particle sizes were measured by dynamic light scattering to determine the degree of agglomeration. Pure C-S-H particles could not be measured, as the obtained agglomerates were already so big in size that they sedimented during the measurement. In contrast, the C-S-H-polymer nanocomposites were finely dispersed in

isopropanol like a sol with particles sizes in the range of 25 – 550 nm (see **Figure 83**). As one can see from the TEM images (see **Appendix**, **Figure A9**), particle sizes above approximately 60 nm represent primary agglomerates of the globules.

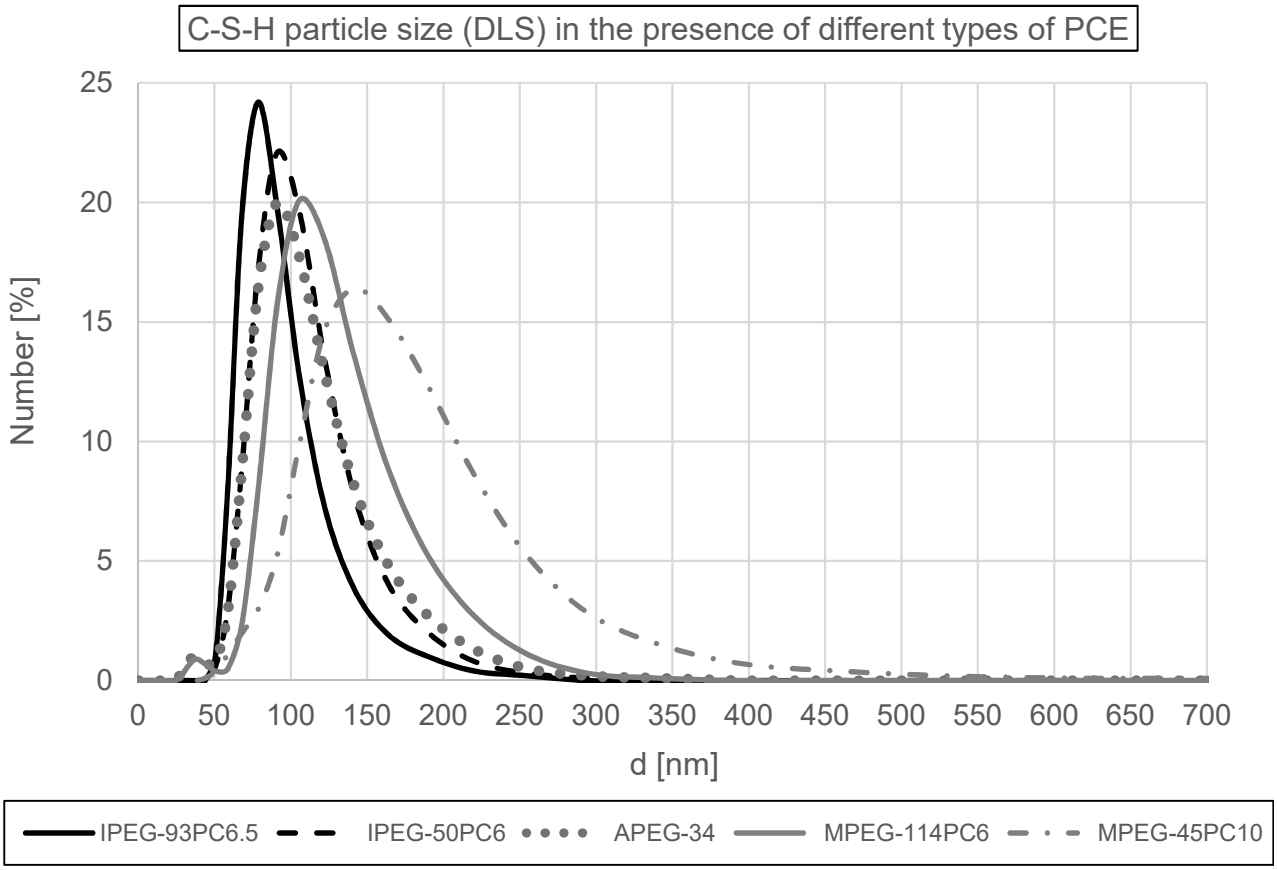

Figure 83: Particle size distributions of C-S-H precipitated in the presence of different PCE superplasticizers as determined by dynamic light scattering in isopropanol.

The highest degree of agglomeration was found for the MPEG-PCEs, followed by APEG- and IPEG-PCEs. This can be explained by a model for PCE conformation in ion solutions developed by *Shu* et al. (see **Figure 17**).[105] They found that PCEs that contain a high number of methyl groups in their backbone have a lower ability to complex cations, e.g. here Ca^{2+} ions, due to steric hindrance and a hydrophobic environment. Thus, MPEG-based PCEs have a more rigid backbone in ion solutions which leads to more exposed carboxylic groups and a lower adsorbed layer thickness. In contrast, PCEs without or only a low amount of methyl groups, like APEG- or IPEG-PCEs, have a more condensed backbone conformation due to Ca^{2+} complexation, resulting in a higher adsorbed layer thickness. The increased steric hindrance compared to MPEG-PCEs, inhibits agglomeration of C-S-H particles stronger.

5.5.2.3. Powder X-ray Diffraction

For further characterization of the differences between the prepared C-S-H-PCE nanocomposites, X-ray diffraction (XRD) was performed. The collected XRD patterns are consistent with the reflections of 1.4 nm tobermorite (JCPDS 29-0331), except for the reflection of the basal spacing which mostly disappeared (see **Figure 84**). Only in the case of C-S-H-MPEG-114PC6, a broad reflection occurred with a d-spacing of 2.5 nm which suggests partial intercalation of the PCE into the C-S-H layers. Furthermore, it can be observed that the structural order of pure C-S-H is higher than that of the C-S-H-PCE composite materials, while amongst them there is a decrease in crystallinity from MPEG-114PC6 > MPEG-45PC10 > IPEG-93PC6.5 > IPEG-50PC6 > APEG-34. The XRD pattern of the C-S-H-APEG-34 composite suggests a completely amorphous structure. As described before, PCEs containing only few or no methyl groups in their backbone can easier complex free Ca^{2+} ions and thus hinder C-S-H formation by calcium sequestration from the bulk solution. Thus, the observed lower crystallinity of C-S-H-PCE composites obtained with APEG- and IPEG-PCEs compared to MPEG-PCEs can be explained.

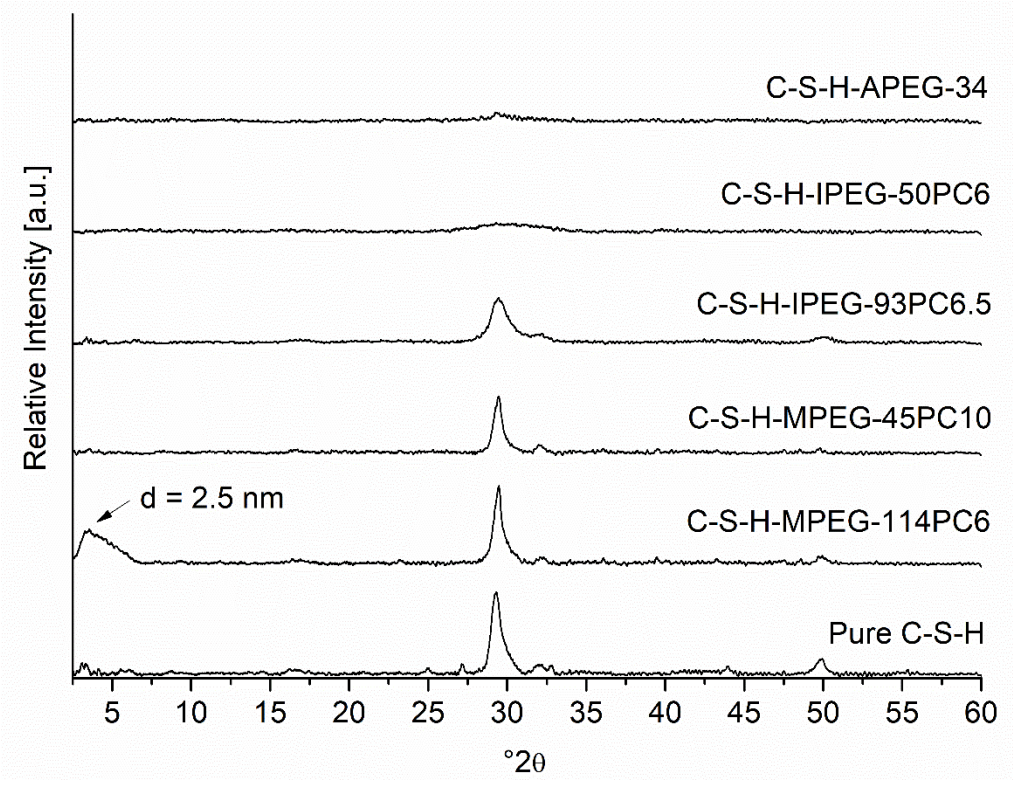

Figure 84: XRD patterns of the C-S-H samples prepared via flash precipitation in the presence of different PCEs and at pH = 11.6, ordered by increasing crystallinity from top to bottom.

5.5.2.4. Energy Dispersive X-ray Spectroscopy

C-S-H-PCE composites were precipitated with an initial Ca/Si molar ratio of 1.0. As was shown by x-ray powder diffraction, the presence of different types of PCEs influences the crystallinity of the precipitated C-S-H nanoparticles. The complexation of Ca^{2+} ions by PCEs might play a decisive role during nucleation. **Figure 85** shows the results of the energy dispersive X-ray spectroscopy (EDX) with regard to the Ca/Si molar ratio found in the obtained C-S-H-PCE composites.

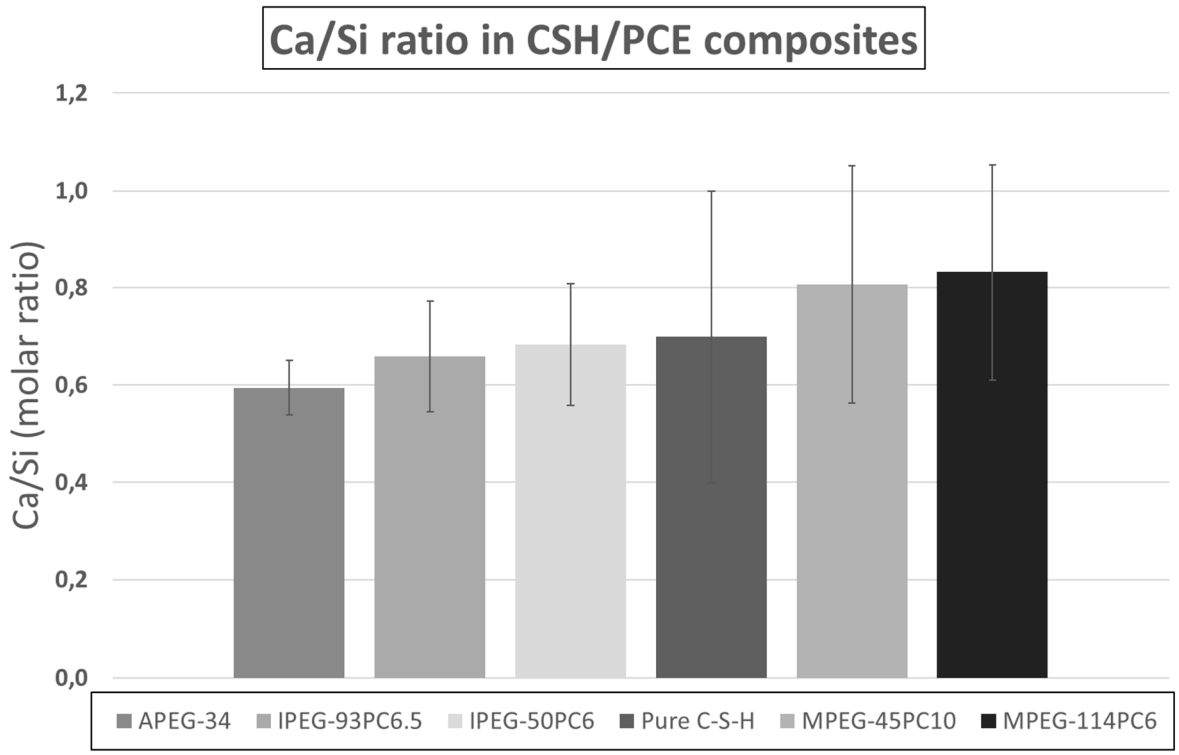

Figure 85: Actual Ca/Si molar ratios of C-S-H samples precipitated in the presence of different PCEs, as determined by EDX spectroscopy.

Pure C-S-H particles exhibited a Ca/Si molar ratio of 0.7 which is significantly lower than the feeding value of 1.0. Globular particles precipitated in the presence of MPEG-PCEs exhibited the highest Ca/Si molar ratios, e.g. 0.83 for C-S-H-MPEG-114PC6 and 0.81 for C-S-H-MPEG-45PC10. For the C-S-H-IPEG-PCE composites, the Ca/Si molar ratios were 0.68 for IPEG-50PC6 and 0.66 for IPEG-93PC6.5. The lowest Ca/Si molar ratio was found for the composite containing APEG-34, namely 0.59. This suggests that the sample consists of a significant amount of amorphous silica gel which is in good agreement with the low degree of crystallinity of its XRD pattern (see **Figure 84**). Regarding the standard deviation of the mean values for

Ca/Si obtained by the EDX analysis, it can be observed that the Ca/Si ratio in the compounds is varying more without polymer and with MPEG-PCEs, compared to IPEG- and the APEG-PCEs. It can be concluded that in all C-S-H samples the average actual Ca/Si molar ratios are lower than the feeding value of 1.0 and that there is a strong correlation between the crystallinity and the Ca/Si ratio of the compounds.

5.5.2.5. Thermogravimetric Analysis

The above results have shown that the actual Ca/Si molar ratio is lower than the initial value of 1.0, and that calcium incorporation into the C-S-H is influenced by the type of PCE. The initial polymer dosage was 40 wt.-% of $Ca(NO_3)_2$ for all samples. Due their diverse molecular architecture, they exhibit different affinities for the C-S-H phases. Polymers that have a high negative charge, for example, will adsorb in a higher amount on the calcium oxide sheets. Others which possess a high affinity for calcium complexation will rather stay in solution and adsorb only in a minor amount.

All samples were analyzed in the temperature range from 30 – 800°C under air with a heating rate of 10°C/min. The ion currents for H_2O (m/z = 18) and CO_2 (m/z = 44) were collected to observe the release of water and the decomposition of polymers. The obtained graphs of the TG-MS analysis are shown in the appendix (see **Figures A10 – A14**). Mass losses of the samples are displayed in **Table 17**.

The final mass of all samples after heating to 800°C lies between 53 – 68 wt.-%. In all composites, a CO_2 signal could be detected resulting from adsorbed polymer. Polymer decomposition takes place in all composites in the range of 200 – 500 °C which is accompanied by a further release of water. Interestingly, for pure C-S-H, only one peak for H_2O release up to 200°C was found having its maximum at 132°C. This strongly suggests that the layer surrounding the C-S-H globules observed in TEM analysis is polymer. However, the PCE layer might also prevent the evaporation of water from the interlayer space of the C-S-H globules until it decomposes. Due to these overlapping mass signals of CO_2 and H_2O from PCE

decomposition and H_2O from the release of interlayer water molecules, a quantitative evaluation of the amount of adsorbed polymer unfortunately was not possible.

Nevertheless, comparison of the ion currents of the CO_2 signals suggests a higher adsorbed amount of polymer for both MPEG-PCEs and IPEG-50PC6 followed by APEG-34 and IPEG-93PC6.5.

Table 17: Mass losses (wt.-%) from C-S-H and C-S-H-PCE composites, as determined by thermogravimetric analysis.

Sample	25-200°C	200-400°C	400-600°C	600-800°C	Final Mass
C-S-H	34.49	3.55	2.39	3.21	56.36
C-S-H-APEG-34	14.12	12.07	2.71	2.84	68.26
C-S-H-MPEG-45PC10	24.75	12.53	5.08	4.76	52.88
C-S-H-MPEG-114PC6	7.26	18.18	7.40	5.14	62.02
C-S-H-IPEG-50PC6	13.59	14.32	3.79	3.20	65.10
C-S-H-IPEG-93PC6.5	15.52	8.56	5.58	2.25	68.09

5.5.2.6. Infrared Spectroscopy

To investigate the impact of the different PCEs on a molecular level, Fourier-transformed infrared (IR) spectroscopy was performed. IR spectroscopy is a useful tool to analyze the degree of silicate polymerization and other local structures of solids. The characteristic bands of silicates are in the range of 400 – 500 cm^{-1}, corresponding to a deformation of SiO_4 tetrahedra.[174] Bands at approximately 660 cm^{-1} can be attributed to Si-O-Si bending vibrations and in the range of 800 – 1200 cm^{-1} result from the symmetric and asymmetric stretching vibrations of Si-O bonds.[51]

The IR spectra of the prepared samples are shown in **Figure 86**. Very intense peaks were observed for the Si-O-Si stretching vibrations (~ 950 cm^{-1}) for the pure C-S-H and the MPEG-

composites, indicating a high degree of polymerization. Samples containing IPEG-PCEs or APEG-PCE show only a broad peak with low intensity, corresponding to a lower degree of polymerization. The small peak in the spectra of the C-S-H-MPEG-114PC6 composite at approximately 1210 cm^{-1} which appears due to Si-O stretching vibrations in Q^3 sites suggests a minor amount of crosslinked silicate chains for this sample. Besides that, the band at ~ 875 cm^{-1} shows slight carbonation for all samples. Incorporation of CO_2 is hard to prevent when the samples are exposed to air, e.g. during the drying process.

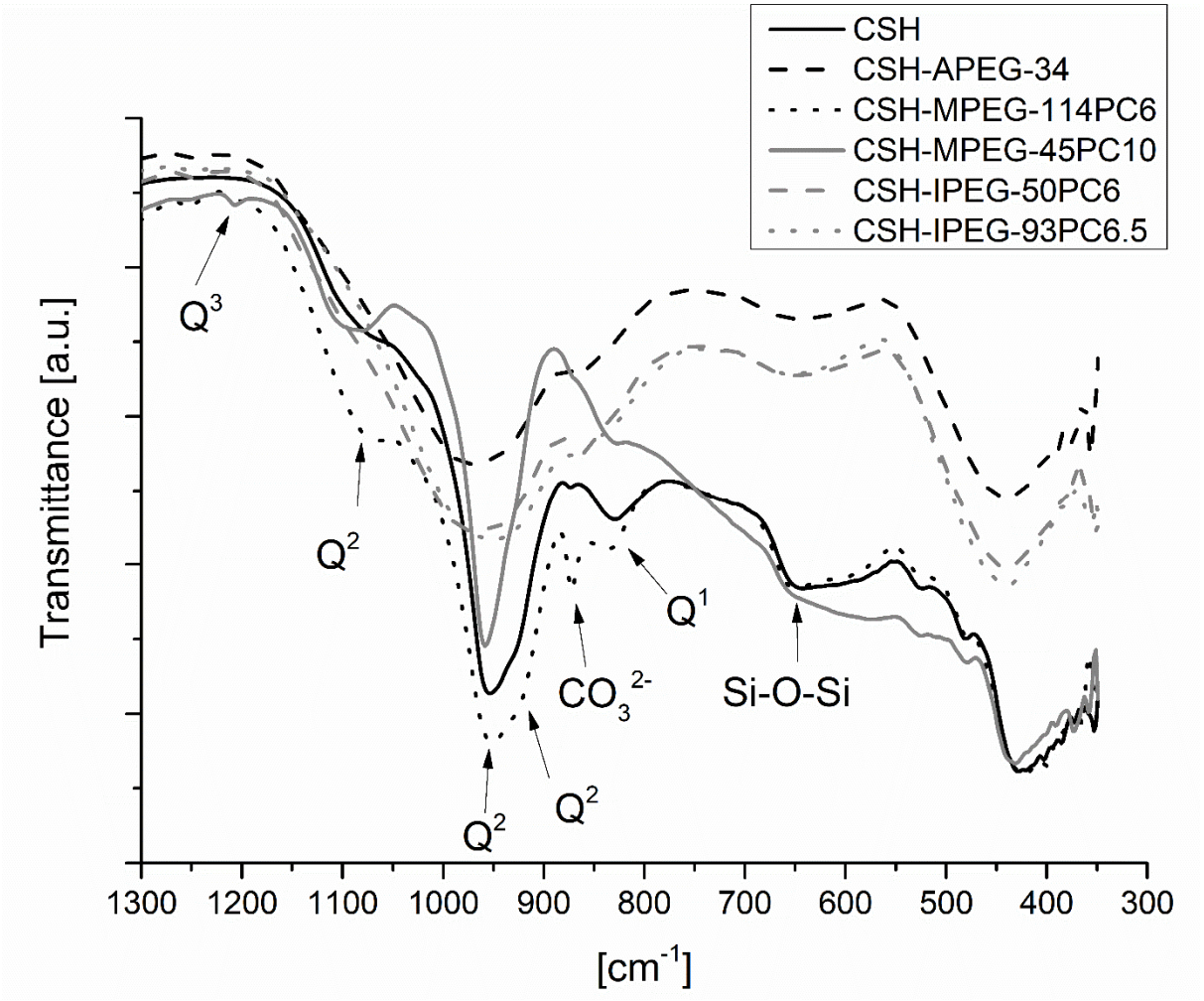

Figure 86: FTIR spectra for pure C-S-H and C-S-H-PCE composites.

5.5.2.7. ^{29}Si MAS NMR Spectroscopy

While IR spectroscopy gives more of a qualitative indication of the degree of polymerization of silicate chains, more detailed information, especially on the vicinity of the studied atoms, can be obtained from solid-state NMR spectroscopy. Therefore, the objective of the ^{29}Si MAS NMR study was to get a more clear view of the nature of the interactions between C-S-H and the various types of PCE on a molecular level. The relative number of end-chain (Q^1) and in-chain (Q^2) tetrahedra can be derived by deconvolution. In previous studies, another peak in between the Q^1 (~ -79 ppm) and the Q^2 (~ -85 ppm) signal was found around -83 ppm. This peak can be assigned to the linking tetrahedron in the *dreierketten* arrangement and is denoted as Q^{2l}.[45] Signals in the range from -90 to -100 ppm are attributed to Q^3 units associated with crosslinking in highly polymerized silicate chains.[175] In the case of crosslinking Q^3 tetrahedra, the chemical environment of the neighboring Q^2 unit changes and shifts to more negative values around -87.5 ppm. Such peaks were denoted as Q^{2v} by *Klur* et al..[45] From the ratio of Q^{2tot}/Q^1 signals, the degree of polymerization (DP) can be precisely calculated and thus the mean chain length (MCL) as number of connected tetrahedra (which is 2(DP+1)) can be easily determined when no Q^3 signals are present. By using geometrical relations, the length of the edge of a SiO_4 tetrahedron can be estimated to be about 2.6 Å if the Si-O bond length is ~ 1.6 Å. Multiplying the length of the edge of a tetrahedron with the value for MCL, the silicate chain length can be estimated.[51] In case the Q^2/Q^{2l} ratio is 2, the *dreierketten* arrangement of silicate tetrahedra can be applied and the according mean silicate chain length derived.

For all compounds, typical spectra for the so-called C-S-H type I with a Ca/Si ratio < 1.0 were obtained. Only for C-S-H-APEG-34 it was not possible to distinguish the characteristic peaks which suggests a highly disordered structure consisting of amorphous silica gel and C-S-H. This is in agreement with the results from x-ray diffraction and the Ca/Si molar ratio as determined by EDX. In **Figure 87**, the spectra for all compounds are displayed. The data derived from deconvolution is shown in the appendix (peak positions and populations are given in **Table A1**).

Only the samples with the IPEG-PCEs show small shoulders on the right side of the Q^2 signal (at ~ 85 ppm) which can be attributed to Q^3 units. But they are only minor, with 3.2 % for C-S-

H-IPEG-50PC6 and 6.5 % for C-S-H-IPEG-93PC6.5, so the calculated values for the DP and MCL still represent a good approximation of these samples.

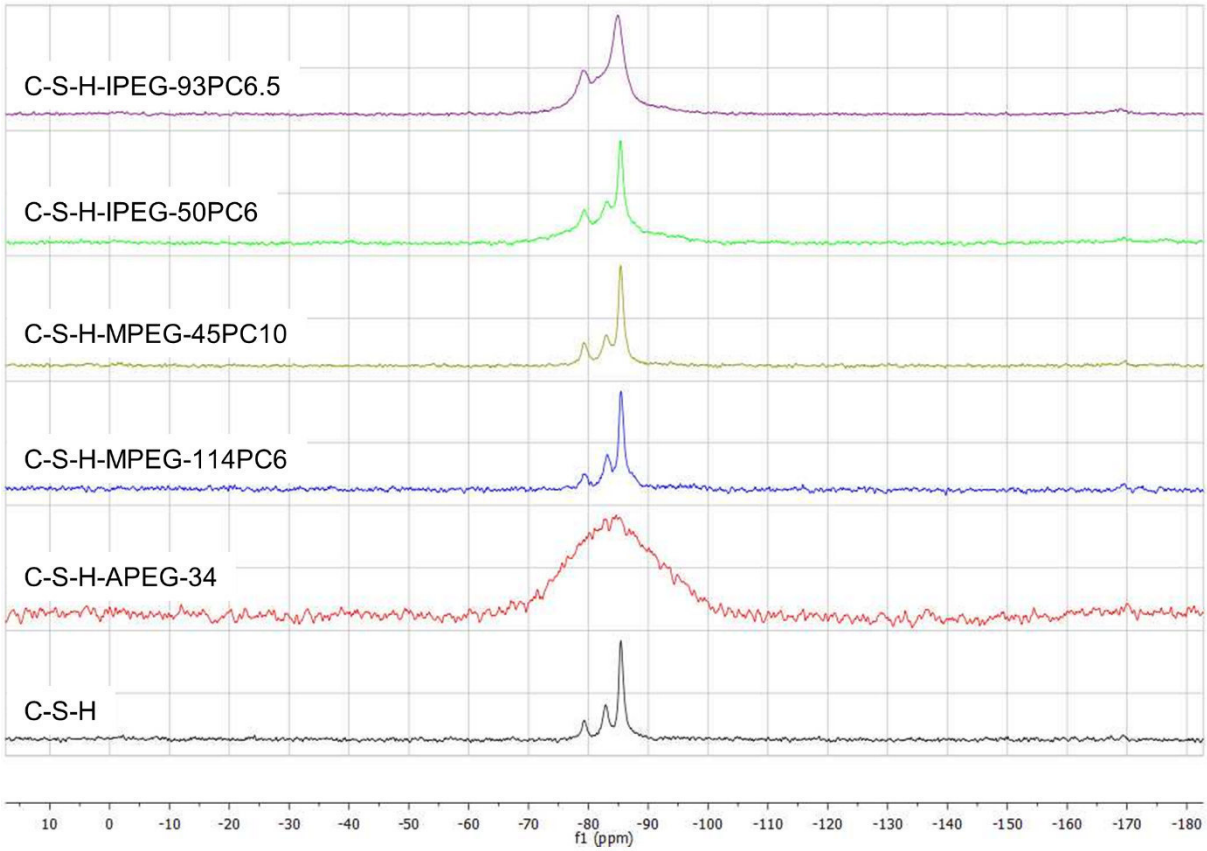

Figure 87: ^{29}Si MAS NMR spectra of C-S-H and C-S-H-PCE nanocomposites, acquired at a MAS frequency of 5 kHz.

The precipitation of pure C-S-H without any additive leads to a degree of polymerization of 5.2 and a mean chain length of 12.5 tetrahedra (see **Table 18**). Comparing the DP of all the samples, one can see that both IPEG-PCEs lead to a very low degree of polymerization in the C-S-H structure, resulting in mean silicate chain lengths of 15.6 to 18.9 tetrahedra. Whereas, MPEG-PCEs, lead to silicate chains of at least twice the length.

Generally, the values for the DP and MCL obtained from C-S-H phases prepared by flash precipitation from combined solutions of $Ca(NO_3)$ and Na_2SiO_3 are comparable to those obtained by other synthetic preparation methods but are much higher than those found for C-S-H phases synthesized via pozzolanic reaction or hydration of C_3S in the literature.[51, 176-177]

This is not surprising though, as the C-S-H formation in the latter cases is strongly limited by the dissolution of the clinker phase.

Table 18: Degree of polymerization (DP) and mean silicate chain length (MCL) of the C-S-H samples precipitated with and without PCEs.

C-S-H Sample	DP (Q^{2tot}/Q^1)	MCL	Estimated chain length (Å)	Q^2/Q^1	Q^2/Q^{2l}	Q^3/Q^{2v}
C-S-H	5.2	12.5	42.5	3.5	2.0	-
C-S-H-APEG-34	-	-	-	-	-	-
C-S-H-MPEG-114PC6	9.3	20.5	53.3	5.4	2.0	-
C-S-H-MPEG-45PC10	5.0	12.0	31.1	3.4	2.2	-
C-S-H-IPEG-50PC6	2.6	7.3	18.9	1.6	2.0	0.5
C-S-H-IPEG-93PC6.5	2.0	6.0	15.6	1.1	2.1	0.5

Furthermore, previous studies have revealed an increase in the degree of polymerization with decreasing Ca/Si ratio in pure C-S-H due to replacement of protons in the interlayer by Ca^{2+} ions, leading to distortions of the silicate chains.[175, 178-180] In this study, an increase in the degree of polymerization and hence in the mean silicate chain length with increasing Ca/Si ratio was observed. In contrast to other studies, here the variation of the Ca/Si ratio is induced by the type of PCE present.

The relationship between the Ca/Si ratio and the DP can be seen clearly by plotting the population of Q^i signals versus the Ca/Si ratio (see **Figure 88**). With increasing calcium content, the Q^1 peaks decrease, while the Q^2 peaks rise. The Q^3 signals, present in the composites with IPEG-PCEs, also decrease as well with increasing Ca/Si ratio. This can be attributed to the incorporation of labile calcium ions in the interlayer space, offsetting an excessive positive charge and initiating a loss of protons at the bridging tetrahedra.[178] The resulting increase of the interlayer space between the linear silicate chains makes crosslinking harder in samples with Ca/Si molar ratio ≥ 0.70.

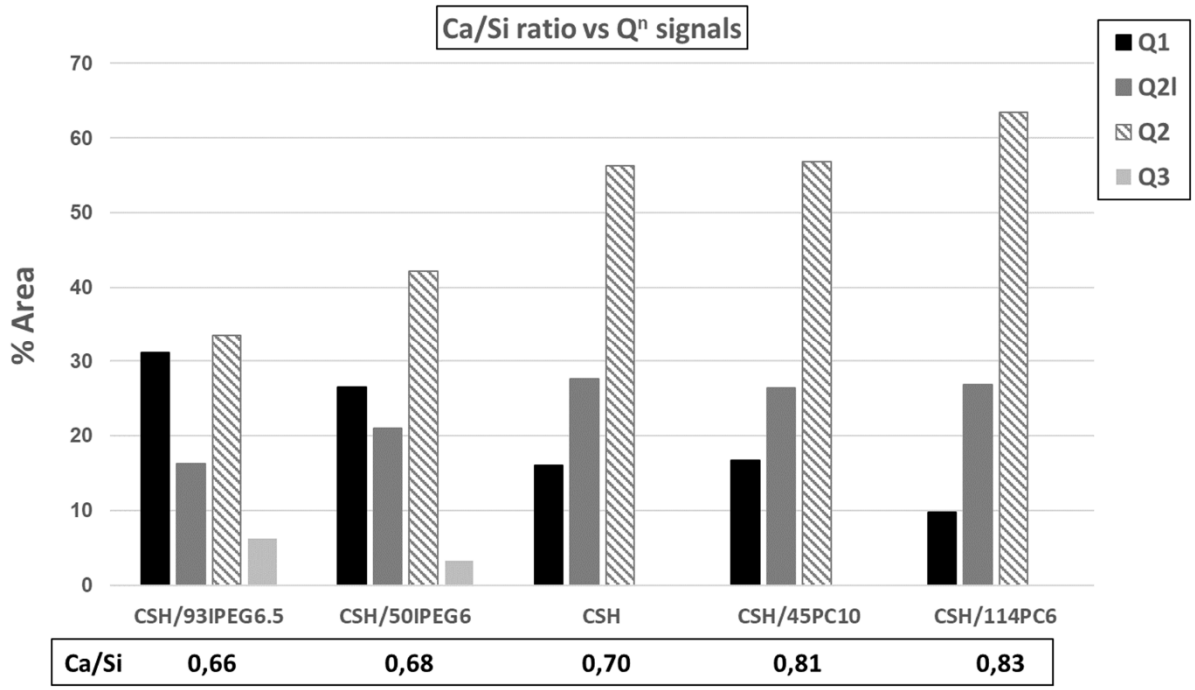

Figure 88: Ca/Si molar ratio in precipitated C-S-H samples vs. populated area [%] of Q^i units, as obtained by ^{29}Si MAS NMR spectroscopy.

5.5.2.8. Proposed mechanism for C-S-H-PCE interactions

As discussed above, the Ca^{2+} ion affinity and the number of methyl groups from monomers like methacrylic acid in the backbone of the polymers can significantly affect the nanostructure of precipitated C-S-H. While MPEG-based PCEs can only complex a minor amount of Ca^{2+}, they lead to composite materials with higher Ca/Si ratios than IPEG- and APEG-PCEs. IPEG- and APEG-PCEs lack the steric hindrance of methyl groups in the acid of the backbone and can thus complex Ca^{2+} in a higher amount. Especially APEG-34 which is based on maleic anhydride and has two neighboring carboxylic groups, has a high affinity to complex cations. This leads to less free calcium available for the formation of CaO sheets. In the tobermorite crystal structure, CaO sheets represent the anchoring site for silica tetrahedra. After binding to the calcium layer of the CaO sheets, silicate polymerization takes place on the surface. The sequestration of Ca^{2+} from the solution equilibrium by polymers leads to the formation of shorter CaO sheets and limits thus the polymerization of the silicates, as is the case for IPEG- and APEG-PCEs. Therefore, shorter mean silicate chain lengths develop for the C-S-H phases

precipitated in the presence of APEG- and IPEG-PCEs compared to MPEG-PCEs, as is shown in **Figure 89**.

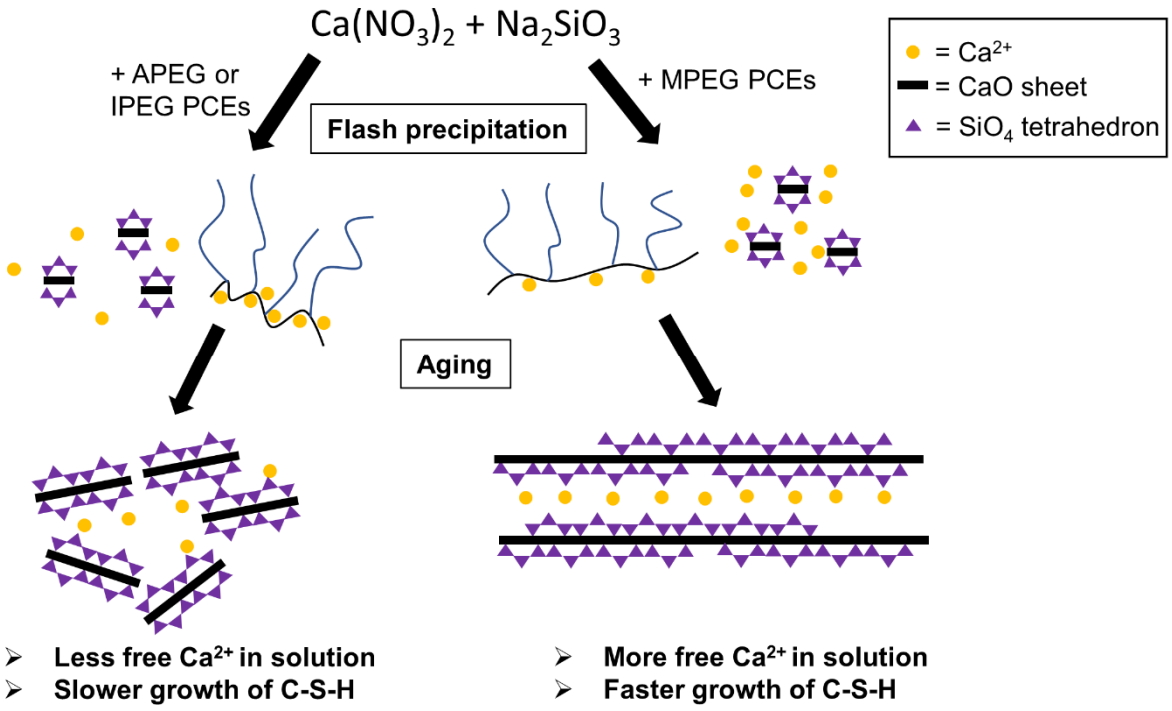

Figure 89: Schematic illustration of the proposed mechanism for the C-S-H formation in the presence of different PCE polymers.

While C-S-H has been prepared in this study by flash precipitation from aqueous solutions of $Ca(NO_3)_2$ and Na_2SiO_3, its formation during cement hydration is a more complex process, with many other ions present. However, experiments carried out meanwhile by another Ph.D. student in our group revealed that also in cement pore solution, C-S-H initially precipitates as globules which later transform into nanofoils as will be shown later (see **chapter 5.6.**), suggesting that also in actual cement C-S-H formation proceeds in a similar manner like in the experiments described in this thesis.[181] Nonetheless, the slower growth of C-S-H sheets in the presence of PCEs with a high affinity for Ca^{2+} complexation might help to explain the retarding effect reported for some PCEs during OPC hydration.

5.6. Nucleation and crystal growth of C-S-H in the absence and presence of polycarboxylate superplasticizers

The results presented in the following were published as publication #2 and #3.

The previous results have clearly shown that the pH value and the presence of PCE have a strong impact on the elemental composition, structure and morphology of calcium silicate hydrates. In the following chapter, the nucleation and early crystal growth of C-S-H was investigated. Flash precipitation of C-S-H at pH = 11.6 from aqueous solutions of $Ca(NO_3)_2$ and Na_2SiO_3 with an initial Ca/Si ratio of 1.0 led to two distinct morphologies, namely globules and foils, as evidenced by TEM (see **chapter 5.5.1.**), while C-S-H precipitated at pH = 10.5 exhibited solely a globular morphology. These results suggested a change in morphology of synthetic C-S-H prepared at pH = 11.6 based on concentration gradients in the solution. Furthermore, it was shown that the type of PCE exerts significant changes in the molecular structure of the C-S-H.

To obtain more insight into the nucleation and early crystal growth of C-S-H, synthetic C-S-H was prepared by flash precipitation at pH = 11.6 and aged for several hours during which period its morphological development was monitored via TEM. The precipitation was carried out in the presence of two different MPEG-type PCEs possessing low (MPEG-45PC2) and high (MPEG-45PC10) anionic charge, respectively. The heat flow of the reactions was monitored via calorimetry and the morphology of C-S-H was investigated by TEM over time. The nanoparticles obtained were analysed by XRD, ^{29}Si MAS NMR and TGA immediately after mixing and again after 24 hours by ^{29}Si MAS NMR and dynamic light scattering.

All C-S-H nanoparticles obtained in the absence and presence of PCE exhibited a globular morphology in the first minutes after mixing. In agreement with our previous studies (see **chapter 5.5.1.**), a polymer layer surrounding the C-S-H globules was found for the C-S-H precipitates when PCE was present. Heat flow calorimetry revealed that the formation of globules is an endothermic process, i.e. the globular morphology is thermodynamically unfavoured under the chosen conditions. Subsequently, within ~ 45 minutes the C-S-H

globules transformed gradually into thin nanoscale foils (see **Figure 90**) which was accompanied by a heat release, indicating an exothermic process.

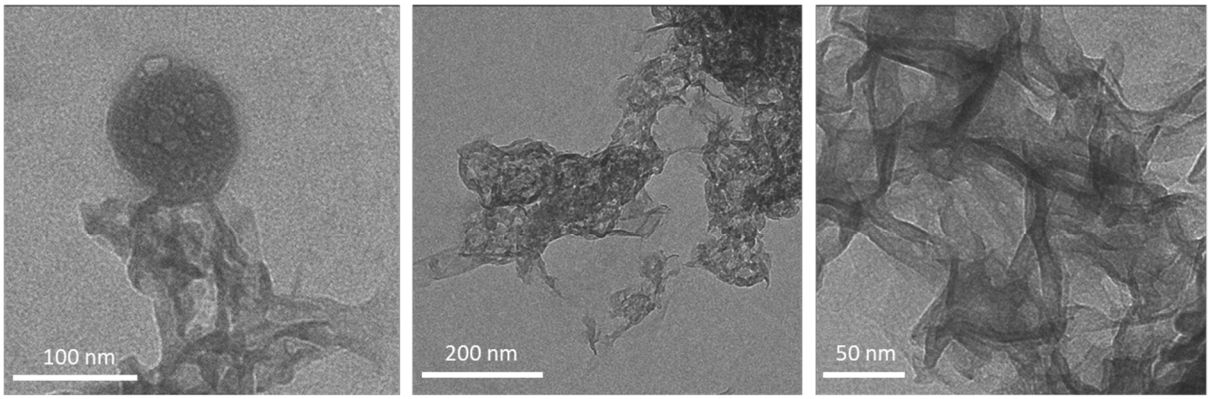

Figure 90: TEM images of C-S-H precipitated from $Ca(NO_3)_2$ and Na_2SiO_3 solutions, after 15 minutes, 45 minutes and 60 minutes of reaction time. Magnifications: 60k, 30k and 80k.

In the presence of PCEs, a similar crystallization process was observed, but there, the transformation from globules to foils was significantly delayed and started only after 1 – 2 hours of crystallization, compared to pure C-S-H (there, conversion started already after ~ 15 minutes). Interestingly, the transformation proceeded faster in the presence of the PCEs possessing low anionic charge which can be attributed to their lower adsorption capacity.

According to these findings, the adsorbed PCE layer stabilizes the C-S-H globules and might impede water diffusion to the C-S-H core. Thus, the conversion from globules to foils is impeded by the polymers. ^{29}Si MAS NMR measurements showed also differences in the molecular structure of the globules and foils. While globules consist of C-S-H with branched Si-O chains as evidenced by the presence of an additional Q^3 signal, the spectrum of the foils revealed only signals for Q^1 and Q^2 Si species which represent linear silicate chains. The foils obtained in the presence of low anionic PCEs were much larger than those obtained from highly anionic PCEs which retard the transformation. These results are presented in detail in the publication #2 and #3 which follow.

The crystallization of pure synthetic C-S-H via the metastable globular precursor exhibiting a completely different morphology than the final nanofoils represents a non-classical crystallization pathway. While the conditions are somewhat different from those present during cement hydration, these findings suggest that a non-classical nucleation via a metastable precursor should be considered as well for the hydration of calcium silicates in cement.

Publication #2

A TEM study on the very early crystallization of C-S-H in the presence of polycarboxylate superplasticizers: Transformation from initial C-S-H globules to nanofoils

M. Schönlein, J. Plank

Cement and Concrete Research
Volume 106, April 2018, Pages 33 - 39

Cement and Concrete Research 106 (2018) 33–39

Contents lists available at ScienceDirect

Cement and Concrete Research

journal homepage: www.elsevier.com/locate/cemconres

A TEM study on the very early crystallization of C-S-H in the presence of polycarboxylate superplasticizers: Transformation from initial C-S-H globules to nanofoils

Markus Schönlein, Johann Plank*

Technische Universität München, Chair for Construction Chemistry, Lichtenbergstr. 4, 85747 Garching, Germany

ARTICLE INFO

Keywords:
A: Calcium-silicate-hydrate
B: Microstructure
B: TEM
Nucleation
Crystallization

ABSTRACT

Polycarboxylate superplasticizers (PCEs) present common admixtures to adjust the rheology of concrete. Previous studies revealed that they can also influence the crystallization of cement hydrates, such as e.g. ettringite. In this study, we investigated the impact of methacrylate ester-based PCEs on the nucleation and crystal growth of C-S-H precipitated from aqueous solutions of $Ca(NO_3)_2$ and Na_2SiO_3. TEM imaging revealed that in the absence of PCEs following a non-classical nucleation mechanism C-S-H initially precipitates as metastable, globular nanoparticles (droplets, d ~ 20–60 nm) which within less than one hour convert to the characteristic nanofoils of early C-S-H. In the presence of PCEs, the initial globuli exhibit a core-shell morphology, presumably with PCE as shell. The shell was found to delay the conversion to nanofoils for several hours by stabilizing the metastable globules. The PCE polymer exhibiting higher anionicity delayed the conversion to nanofoils more than the PCE possessing fewer carboxylate groups.

1. Introduction

Calcium silicate hydrate (C-S-H) not only presents a promising precursor in biomedical applications such as drug delivery and bone tissue engineering, foremost it constitutes the main hydration product of ordinary Portland cement [1–4]. There, C-S-H is formed from the hydration of tricalcium silicate (C_3S) and dicalcium silicate (C_2S). Its structural properties are still the subject of many investigations, due to its semi-crystalline character. Generally, C-S-H exhibits a disordered layered structure consisting of linear silicate chains arranged in so-called "dreierketten", analogous to that of tobermorite (Ca/Si = 0.8–1.5) or jennite (Ca/Si = 1.5–2.0) [5]. A very thorough insight into the complex structure of cementitious C-S-H at the atomic and three-dimensional level was presented recently by Bowen et al. [6]. Their study revealed that bridging interlayer calcium ions constitute the defining structural characteristic of single-phase C-S-H.

As the demands for concrete concerning strength, durability and workability rise steadily, almost every formulation nowadays contains one or several organic admixtures. Among the most important admixtures are superplasticizers. Their most effective representatives include polycarboxylate ethers (PCEs) which possess a *comb*-like structure with carboxylate anchor groups at the backbone and polyethylene oxide side chains. It has been found that specific PCE polymers can exert a noticeable retarding effect on the hydration of the calcium silicates [7–9]. A study even suggests that these admixtures can induce changes to the nanostructure of C-S-H which negatively impacts the mechanical properties of concrete [10]. On the other hand, nanocomposites prepared via precipitation of C-S-H in PCE solution present excellent seeding materials for the nucleation of C-S-H, and thus can produce remarkably high early strengths. Their accelerating effect was found to rely on the formation of nanoscale C-S-H foils with lengths preferably < 100 nm [11,12]. In view of these discrepancies, it is of greatest interest to understand the interactions between C-S-H and PCE on a molecular level.

So far, few reports on the interaction of polymers with calcium silicate hydrates have been published. The effect of polyethylene glycols on C-S-H was studied by Alizadeh et al. using ^{29}Si MAS NMR spectroscopy [13]. They found that the presence of organic additives increases the degree of polymerization for the silicate chains (Q^2/Q^1 ratio). In another study the interaction between different methacrylate ester (MPEG)-based PCEs and C-S-H prepared from tricalcium silicate (C_3S) which was hydrated for 40 days was investigated. On one hand, the PCEs delayed the hydration of C_3S, i.e. more unreacted silicate (Q^0) was found when PCE was present, while on the other hand the C-S-H formed in the presence of this PCE possessed a higher degree of polymerization (DP) compared to the one obtained in water only. Furthermore, DP was

* Corresponding author.
E-mail address: sekretariat@bauchemie.ch.tum.de (J. Plank).

https://doi.org/10.1016/j.cemconres.2018.01.017
Received 26 June 2017; Received in revised form 16 January 2018; Accepted 19 January 2018

higher for PCEs exhibiting high anionic charge density and reactivity of C_3S was lower in the presence of PCEs with short and few side chains [14]. These studies reveal that polycarboxylates can significantly impact the composition and structure of C-S-H.

Generally, the nucleation and crystallization of inorganic minerals is described by two divergent theories. The first concept ("nucleation theory") is based on the initial formation of critical nuclei (their volume energy being higher than their surface energy) through random collision and aggregation of ions. Nuclei exhibiting a smaller radius than the critical radius will dissolve again while those possessing a larger radius will grow [15–17]. The second concept ("non-classical nucleation theory") which is more recent suggests the formation of so-called "precritical clusters" and "pseudo phases". These precursors evolve into "postcritical clusters" through aggregation facilitated by diffusion and convection [18]. A characteristic of the non-classical nucleation concept is that the morphology of the precritical clusters differs significantly from that of the final bulk crystal. For example, droplets and amorphous nanoparticles have been reported as precursors for polyhedral bulk crystals [19]. The presence of organic additives can increase induction times, stabilize the amorphous precursors, lead to the formation of mesocrystals or modify the crystal size and shape [20,21]. Probably the most thoroughly investigated case of crystal growth via amorphous precursor clusters is silica [22,23]. Furthermore, also for calcium carbonate a non-classical crystallization mechanism has been observed [24–26].

In our study, we investigated the very early nucleation of C-S-H (0–5 h) precipitated from $Ca(NO_3)_2$ and Na_2SiO_3 solutions at a Ca/Si ratio of 1.0 in the presence of different PCE superplasticizers by capturing the very first precursors via transmission electron microscopy (TEM). Furthermore, characterization of the precipitates by XRD, EDX, TG-MS, ^{29}Si MAS NMR spectroscopy and isothermal heat flow calorimetry was performed with the goal to better understand the nucleation mechanism and early growth of C-S-H.

2. Materials and methods

2.1. Precipitation of C-S-H

C-S-H was obtained by combining aqueous solutions of Ca $(NO_3)_2{\cdot}4H_2O$ (p.a., AppliChem GmbH, Darmstadt, Germany) and $Na_2SiO_3{\cdot}5H_2O$ (Alfa Aesar, Karlsruhe, Germany). First, Solution A was prepared by dissolving 0.316 g $Na_2SiO_3{\cdot}5H_2O$ (1.5 mmol) and 0.14 g of PCE polymer in 10 mL DI water. Second, Solution B was obtained by dissolving 0.35 g $Ca(NO_3)_2{\cdot}4H_2O$ (1.5 mmol) in 5 mL of deionized (DI) water. The reaction was carried out using three syringes connected via a three-way valve: The reaction container, syringe #1, was loaded with Solution A, while syringe #2 was charged with Solution B and syringe #3 held 10 mL of acetone (> 99.9% Merck KGaA, Darmstadt/Germany) to stop the crystallization process. To separate the mother liquor from the precipitated C-S-H, syringe #1 was equipped with a disc filter holding a glass fiber membrane (pore size: 0.4–0.45 µm, GD/X GMF, GE 173 Healthcare, Little Chalfont, UK). In synthesis, within 1–2 s Solution B in syringe #2 was injected into syringe #1 holding Solution A, kept there for 5 min, 45 min, 2 h, 3 h, 3.5 h and 4 h, respectively and was then filtrated into syringe #2. Then acetone was injected from syringe #3 into the reaction container (syringe #1) to stop crystallization. The precipitated C-S-H was collected from syringe #1, centrifuged (10 min., 8500 rpm), washed thrice with acetone and suspended in acetone under nitrogen atmosphere prior to analysis.

2.2. Polycarboxylate ether samples

PCE samples were self-synthesized via aqueous free radical copolymerization as described elsewhere [27]. Two methacrylate ester (MPEG)-based PCEs (denominated as MPEG-45PC2 and MPEG-45PC10) exhibiting side chains made of 45 ethylene oxide (EO) units and molar ratios between methacrylic acid and the methacrylate ester macromonomer of 2:1 (MPEG-45PC2) and 10:1 (MPEG-45PC10), respectively were utilized.

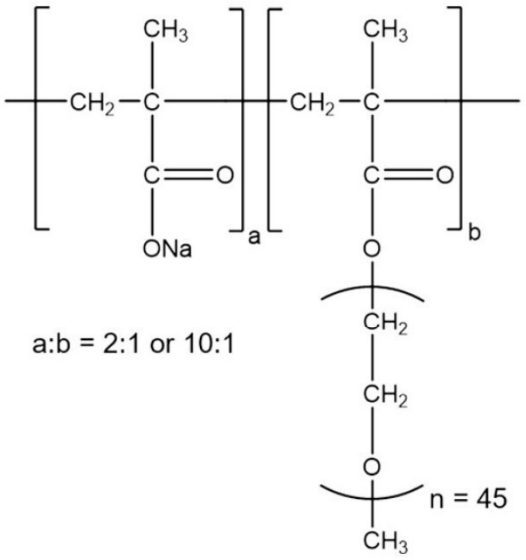

Fig. 1. Molecular structure of the synthesized MPEG-ester based PCE samples.

The molecular structure of the synthesized PCEs is displayed in Fig. 1 and their molecular properties are listed in Table 1.

2.3. Transmission electron microscopy

TEM micrographs were collected on a JEM 2011 microscope (JEOL, Eching, Germany) equipped with a LaB_6 cathode. Acetone suspensions of the C-S-H samples as prepared were placed on a carbon-coated copper grid and analyzed.

2.4. Heat flow calorimetry

Calorimetric studies were performed on a TAM-Air isothermal heat conduction calorimeter equipped with an admix-ampoule set from Thermometric, Järfälla, Sweden. In a typical experiment, 4 mL of the $Na_2SiO_3{\cdot}9H_2O$/PCE solution (denoted above as Solution A) were placed in a tubular glass ampoule (reaction container) while the syringe of the admix-ampoule was loaded with 2 mL of the $Ca(NO_3)_2$ solution (Solution B). The reaction container was placed inside the calorimeter and equilibrated until the baseline was stable. Solution B was then injected within 1–2 s to solution A in the reaction container and mixed for 30 s. The heat flow resulting from crystallization was monitored at a constant temperature of 20 °C.

2.5. Powder X-ray diffraction

Sample composition and degree of crystallinity of the C-S-H phases were analyzed using powder X-ray diffraction. XRD patterns were collected in the range of 0.5–60° 2θ using an AXS D8 Advance instrument (Bruker, Karlsruhe, Germany) with a Bragg-Brentano geometry and a Cu Kα source (30 kV, 35 mA).

2.6. ^{29}Si MAS NMR spectroscopy

Solid-state MAS NMR measurements were conducted on a Bruker Advance 300 MHz instrument that was operated at a frequency of 59.63 MHz. Samples were packed into a 7 mm Zirconia rotor at a

Table 1
Molecular properties of the synthesized polycarboxylate samples.

Superplasticizer sample	Conversion of macromonomer [%]	M_w [g mol^{-1}]	M_n [g mol^{-1}]	PDI (M_W/M_n)	Specific anionic charge amount @ pH 12.5 [μeq g^{-1}]
45PC2	89	30.500	18.000	1.7	1.500
45PC10	90	18.900	10.600	1.8	5.000

spinning frequency of 5 kHz. All spectra were obtained at a pulse width of 6 μs and a repetition time of D 1–45 s. Tetrakis(trimethylsilyl)silane was used as external standard.

2.7. Energy dispersive X-ray spectroscopy

Elemental analysis (Ca/Si ratio) was performed on a FEI XL 30 FEG environmental scanning electron microscope equipped with an EDX detector. For statistics, 50 random spots of each sample were analyzed and the average value for the Ca/Si molar ratio as calculated was taken.

2.8. Thermogravimetric analysis

TGA was conducted using a NETZSCH STA409PC Luxx instrument equipped with a mass spectrometer for weight loss investigation. Samples were heated up to 800 °C under air at a heating rate of 10 °C/min.

3. Results and discussion

3.1. Nucleation of C-S-H

Flash precipitation was employed to capture the precursor particles of C-S-H and their subsequent growth. There, $Ca(NO_3)_2$ and Na_2SiO_3 solutions were combined within 2 s and nucleation was allowed to occur over five minutes after which C-S-H particles exhibiting a tobermorite-like structure as confirmed by XRD (see Fig. 2a) were detected. EDX analysis revealed a Ca/Si ratio of 0.70 for the precipitated C-S-H phases which is lower than that in the initial feeding solutions (Ca/Si = 1.0). Thermogravimetric analysis produced a mass loss of ~35 wt.-% up to 200 °C which is attributed to the release of adsorbed water (see Fig. 2c). Further mass loss can be assigned to continuous release of small amounts of interlayer water. ^{29}Si MAS NMR spectroscopy suggests a composition which is characteristic for so-called type I C-S-H formed at Ca/Si ratios < 1.0 [28,29] (see Fig. 2b). Most interestingly, TEM imaging reveals polydisperse C-S-H particles exhibiting a globular morphology after the first minutes of reaction, with diameters generally ranging between 20 and 60 nm and the most prevalent sizes being 40–50 nm (see Fig. 2d). A close-up image of an individual C-S-H globule exhibiting the shape of a droplet suggesting that the precursor is formed according to a non-classical nucleation mechanism is presented in Fig. 3.

3.2. Conversion of C-S-H globules to nanofoils

Next, the time-dependent behavior of the globular C-S-H precursors was tracked via TEM imaging. Most interestingly, it was observed that after a few minutes only (~15 min), nanofoils outgrow from the surface of the globules (see Fig. 4). With time, the nanofoils become more abundant and larger at the expense of the globules which continuously shrink and dissolve. After ~60 min, the globular precursor particles have disappeared entirely while a dense network of C-S-H nanofoils (length ~150 nm, thickness ~5 nm) is observed. These results suggest that under those conditions, at first a thermodynamically unstable precursor is formed which then transforms into the well-known, stable C-S-H nanofoils following a non-classical nucleation mechanism.

The conversion of the globular precursors to nanofoils was also

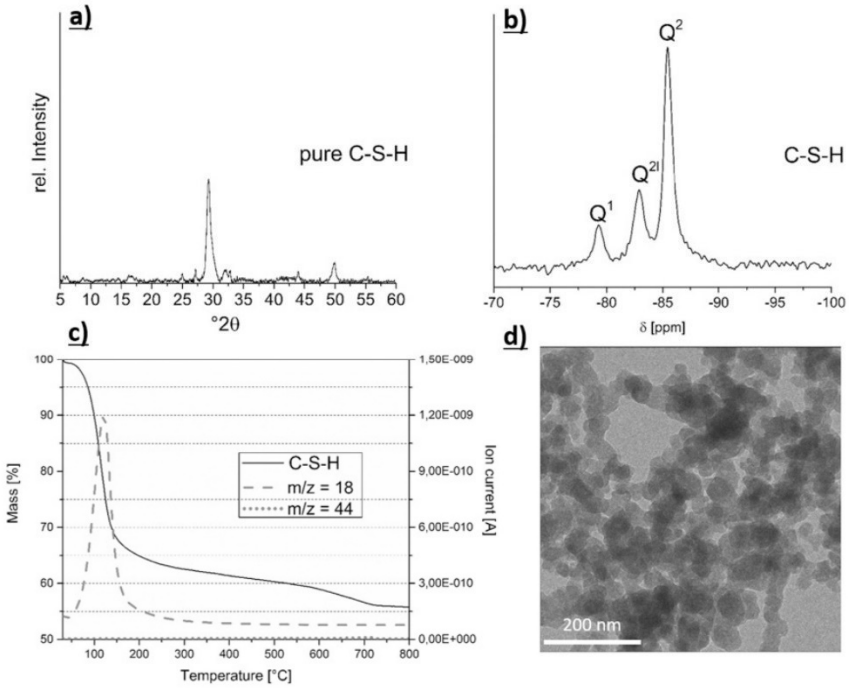

Fig. 2. a) XRD pattern, b) ^{29}Si MAS NMR spectrum, c) TG-MS curves and d) TEM image (magnification: 30 k) of C-S-H precipitated from Ca$(NO_3)_2$ and Na_2SiO_3 solutions after five minutes of ageing.

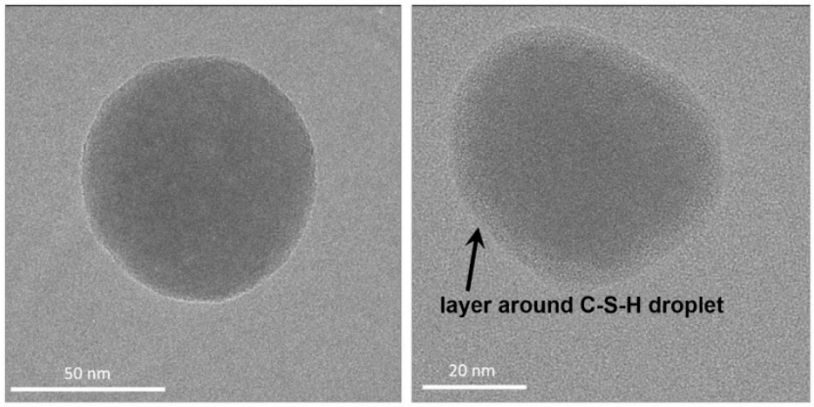

Fig. 3. TEM images of a C-S-H droplet formed in the absence (left) and presence of MPEG-PCE sample 45PC10 (right); magnifications: 150 k, 200 k.

monitored over the first 2 h by heat flow calorimetry. When the Ca $(NO_3)_2$ solution is injected into the Na_2SiO_3 solution ($t = 0$ h), at first an endothermic process occurs which is followed by a significant heat release during the subsequent hour (see Fig. 5). This curve suggests that at first in an endothermic process a metastable precursor (= globules) is formed which then accompanied by an exothermic reaction gradually transforms into the thermodynamically more favored foil-like modification of C-S-H.

3.3. Nucleation of C-S-H in the presence of PCEs

The unusual occurrence of a metastable C-S-H precursor and its conversion to nanofoils made one wonder whether PCEs would impact this process. To investigate, two different MPEG-PCE superplasticizers were dissolved in the Na_2SiO_3 solution prior to addition of the calcium nitrate solution, and the nucleation of C-S-H in the presence of these polymers was studied. To elucidate the effect of anionicity of the polymers on the C-S-H crystallization, PCE sample 45PC2 exhibiting a low anionic charge density and PCE sample 45PC10 with high anionic charge density were chosen.

The XRD patterns of the C-S-H precipitated in the presence of the polymers exhibited similar reflections as for pure C-S-H (see Fig. 6a). Furthermore, no reflections in the low 2θ region which signify the intercalation of organic molecules into C-S-H can be observed [30]. This fact suggests that the polymers are not incorporated into the layered C-S-H structure, but – if any interaction has occurred – they might be adsorbed on the C-S-H surface. EDX analysis revealed a Ca/Si ratio of 0.80 for C-S-H from 45PC10 and of 0.82 for 45PC2. Those values are higher than the value obtained for pure C-S-H which was 0.70. ^{29}Si MAS NMR spectra show the peaks characteristic for end-chain (Q^1), bridging (Q^{2l}) and in-chain (Q^2) silica tetrahedra, similar to those of C-S-H formed in the absence of PCE [28] (see Fig. 6b). Presence of the PCE

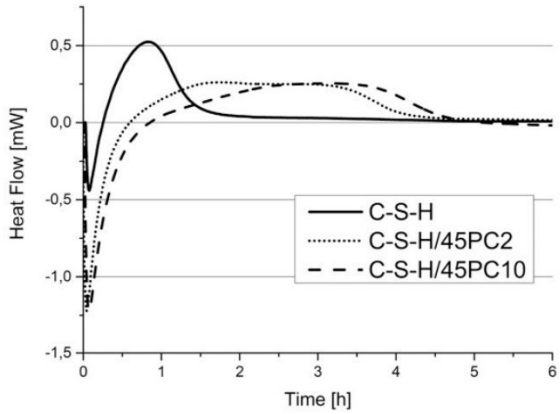

Fig. 5. Heat flow occurring during the synthesis and crystallization of pure C-S-H precipitated from $Ca(NO_3)_2$ and Na_2SiO_3 solutions, and of C-S-H precipitated in the presence of two different PCEs.

polymers in the precipitates was confirmed by TG-MS analysis (see Fig. 6c). There, for both precipitates the decomposition of the polymers was evidenced by a CO_2 signal occurring in the range of 250–450 °C. The release of CO_2 was accompanied by a second release of water which was not observed for the pure C-S-H. This additional water release can be assigned to interlayer water which the polymer may have prevented from evaporation at lower temperatures.

TEM imaging again revealed a globular morphology for the C-S-H precipitate similar to that of pure C-S-H, however, the particles were less agglomerated (see Fig. 6d). Most interestingly, a thin shell (thickness ~3–5 nm) surrounding the C-S-H globules can be observed. A

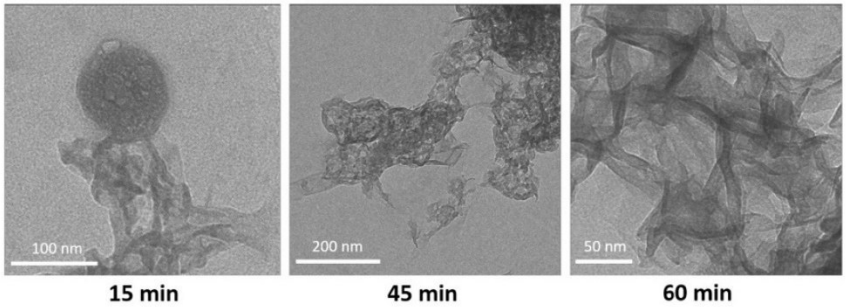

Fig. 4. TEM images of C-S-H precipitated from Ca $(NO_3)_2$ and Na_2SiO_3 solutions after 15 min, 45 min and 60 min of crystallization. Magnifications: 60 k, 30 k and 80 k.

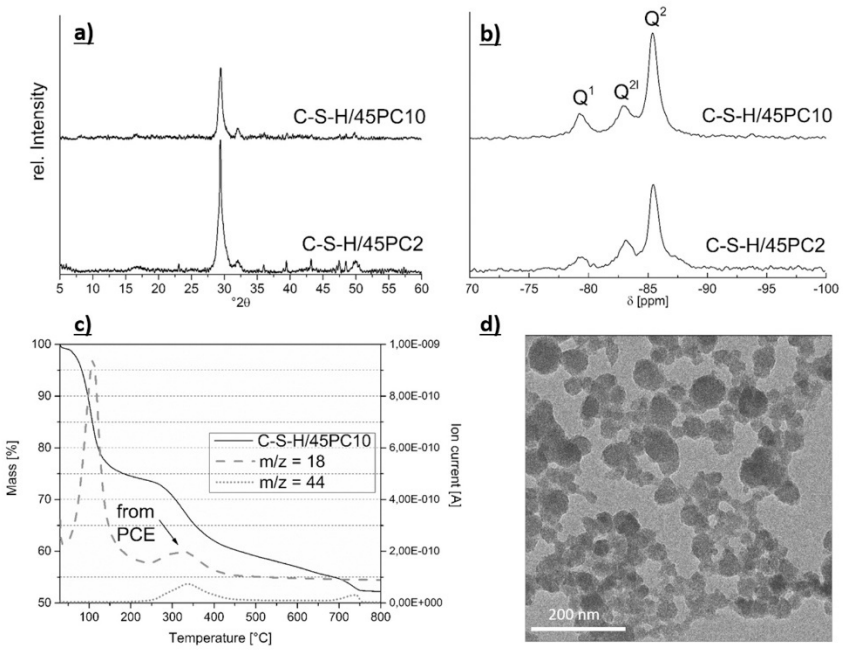

Fig. 6. a) XRD pattern, b) ^{29}Si MAS NMR spectrum, c) TG-MS spectrum and d) TEM image (magnification: 30 k) of C-S-H/45PC10 precipitate; all samples analyzed after 5 min of ageing.

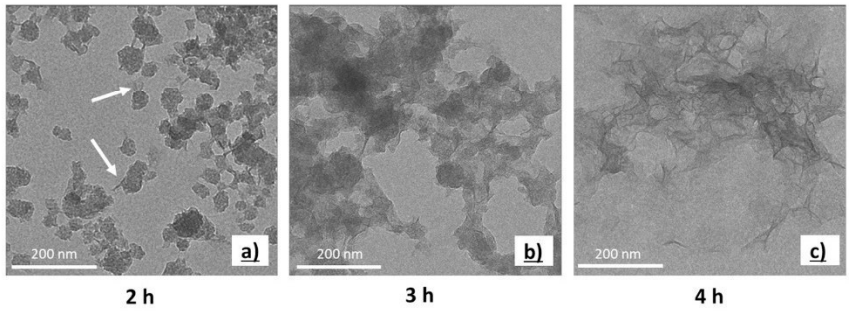

Fig. 7. TEM images of C-S-H precipitated from $Ca(NO_3)_2$ and Na_2SiO_3/45PC10 solutions after 2 h, 3 h and 4 h of crystallization. Magnification: 30 k.

plausible explanation for the shell is that the PCE polymer has coated the precursor droplet which presents the first nucleus of C-S-H. For direct comparison, high resolution TEM images of a C-S-H droplet precipitated in the absence of PCE and another one formed in the presence of MPEG-PCE 45PC10 exhibiting a shell are displayed in Fig. 3.

Analysis of the heat evolution during C-S-H formation in the presence of the PCEs again showed an endothermic process to occur immediately after the $Ca(NO_3)_2$ and the Na_2SiO_3/PCE solutions were combined (see Fig. 5). However, here this endothermic peak is almost thrice as high than for the precipitation of C-S-H in the absence of PCE. On the other hand, the following exothermic reaction is less intense, but much more prolonged (~5 h) when the PCEs are present. These observations again suggest that the PCE polymers significantly impact the transformation of the globules to nanofoils. Additionally, the effect appears to depend on the anionicity of the PCE polymers: PCE sample 45PC2 possessing a lower anionic charge produces an earlier exothermic peak compared to the polymer 45PC10.

3.4. Transformation from globules to nanofoils

Next, conversion of the C-S-H globuli formed in the presence of the PCEs into nanofoils was monitored via TEM imaging.

As has been shown before, in the presence of PCEs the C-S-H precursor particles are less agglomerated and exhibit a layer (shell) which is of lower density than the core. Visibly, the solution obtained immediately after combining the $Ca(NO_3)_2/Na_2SiO_3$ + PCE solutions stays longer clear than in the case of pure C-S-H before it turns opaque as a result of particle growth. This observation already suggests that when PCE polymers are present, the conversion from the globules to nanofoils is delayed. TEM imaging confirmed this assumption. The layer surrounding the C-S-H particles seems to hinder the transformation of the metastable globules to the thermodynamically more favored foil morphology as the C-S-H particles cannot dissolve as easy in order to recrystallize. Only after 1–2 h of crystallization and thus much later than for pure C-S-H (there, ~15 min. were recorded, see Fig. 5), the globular particles finally start to burst and release the first nanofoils (Fig. 7 exemplifies this process for MPEG-PCE sample 45PC10). The transformation is complete after ~4 h, compared to only ~60 min for pure C-S-H (see Fig. 4).

A similar time-dependent behavior was found for MPEG-45PC2, however there the transformation was completed faster after ~3.5 h. The transformation times observed via TEM imaging are in good agreement with the time-dependent heat release curves recorded in Fig. 5.

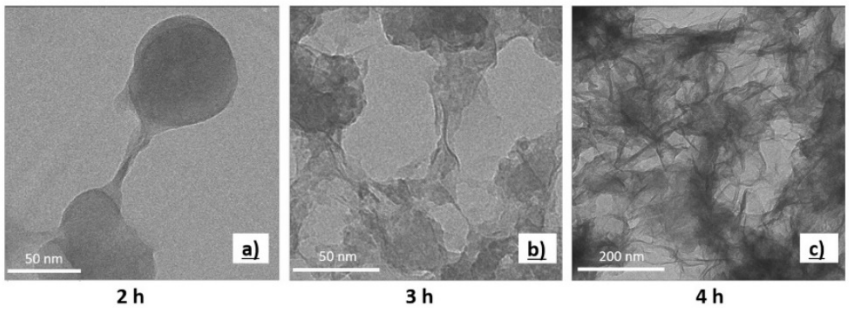

Fig. 8. TEM images of C-S-H precipitated from $Ca(NO_3)_2$ and Na_2SiO_3/45PC2 solutions after a) 2 h, b) 3 h and c) 4 h of crystallization. Magnifications: a) 100 k, b) 80 k and c) 30 k.

To elucidate the critical steps in the conversion in more detail, TEM images of much higher magnifications were captured. For both PCEs, after ~2 h beginning transformation was evidenced by the appearance of first thin and needle-like C-S-H crystallites which grow from the inner core and penetrate the shell (see Figs. 8a and 9a, respectively). As a result of such outgrowing foils, the particles now intergrow and agglomerate more (see Figs. 8b, c and 9b, c respectively). Once the C-S-H crystallites have reached a critical size, the shell bursts completely, the transformation into foils proceeds swiftly now and completes fast.

As has been shown by heat flow calorimetry (see Fig. 5), the transformation from globules to nanofoils proceeds slightly faster in the presence of MPEG-PCE sample 45PC2 compared to sample 45PC10. This is supported by the TEM images presented in Fig. 8 and Fig. 9, respectively. For PCE polymer 45PC2 which exhibits a high grafting ratio and therefore forms a less dense polymer layer the formation of thin C-S-H foils growing from the inner core of the globules into the outer shell is more progressed after 2 h of reaction compared to that of 45PC10 (see Figs. 8a and 9a). After 3 h, for the sample from 45PC2 more disrupted shells and intergrown foils of C-S-H are observed than from 45PC10 (see Figs. 8b, c and 9b, c). In the presence of the more anionic PCE 45PC10, C-S-H foils occur later, presumably due to the stronger adsorption capacity of this polymer which shields the globules more effectively, thus delays the disruption of the shells and hinders the transformation from globules to nanofoils. This behavior is supported by earlier studies which demonstrated that PCE polymers with lower anionic charge density adsorb less strongly on C-S-H particles and possess a lower ability to complex free Ca^{2+} ions [31,32].

4. Conclusion

The very early nucleation and crystallization of C-S-H precipitated from $Ca(NO_3)_2$ and Na_2SiO_3 solutions in the presence and absence of polycarboxylate superplasticizers was studied. It was found that under the conditions chosen here, at first a thermodynamically unstable precursor exhibiting a globular morphology is formed which gradually converts to the well-known nanofoils of C-S-H. Thus, C-S-H is formed according to a non-classical nucleation mechanism which involves precursors with completely different morphology than the final crystalline product. Isothermal heat flow calorimetry revealed that the formation of the globules represents an endothermic process which is followed by an exothermic step whereby the globules transform to foil-like C-S-H. During this period of heat release, gradual dissolution of the droplets followed by crystallization of C-S-H in the form of nanoscale foils was observed.

This general pattern is the same for pristine C-S-H and C-S-H formed in the presence of PCEs. However, the presence of PCEs strongly influences the kinetics of the conversion from globular to nanofoil-like C-S-H. In the presence of PCEs, this conversion is much delayed, because a layer forms around the globular C-S-H particles leading to a core-shell morphology. Thermogravimetric analysis suggests that the shell may consist of PCE polymers. Such a layer of adsorbed polymer can hinder the supply of water molecules to the core and as such reduce the dissolution and recrystallization of the core particles. Also, PCEs possessing low anionic charge density (e.g. PCE polymer 45PC2) delay the transformation of the globules into foils less than PCEs possessing high anionicity such as polymer 45PC10. Interestingly, those PCEs exhibiting high negative charge are known to retard the early strength development of concrete noticeably. The trend observed for the conversion kinetics of globules to foils can be explained by the lower adsorption capacity of weakly charged PCE polymers, resulting in decreased stabilization of the C-S-H globules. Currently, further research is ongoing which aims to elucidate more details relating to the structure, composition and function of the layer around the globules.

Our study provides evidence that under the synthesis conditions selected here C-S-H first precipitates in the form of droplets. This mechanism corresponds to a non-classical nucleation mechanism. Subsequently, these precursor particles convert to the thermodynamically more stable nanofoils. PCEs control the kinetics of this conversion, presumably by forming a polymer layer around the initial C-S-H droplets. This effect might explain the retarding effect of some PCEs on early strength development of concrete.

Of course, it can be debated whether in actual cement C-S-H is formed in the same way as described here, as conditions differ from those in our experiment. It might however be possible that in cement C-

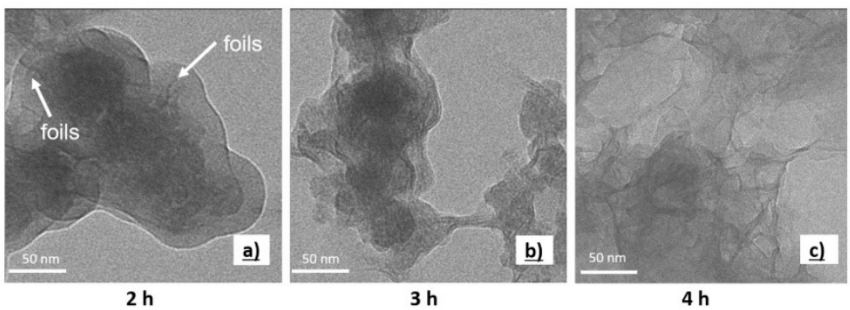

Fig. 9. TEM images of C-S-H precipitated from $Ca(NO_3)_2$ and Na_2SiO_3/45PC10 solutions after a) 2 h, b) 3 h and c) 4 h of crystallization. Magnification: 80 k.

S-H is actually formed according to different nucleation mechanisms, depending on the time-dependent specific environments existing in cement pore solution (pH, type of ions, ion concentrations etc.). At least, our study suggests that a non-classical nucleation mechanism involving metastable precursors should be considered for the hydration of the silicates in cements as well.

Acknowledgment

Markus Schönlein wishes to thank Dr. Marianne Hanzlik, Dr. Oksana Storcheva and Vipasri Kanchanason (TU München) for taking the TEM images and Dr. Oksana Storcheva for the ^{29}Si MAS NMR measurements.

References

[1] W. Xue, A. Bandyopadhyay, S. Bose, Mesoporous calcium silicate for controlled release of bovine serum albumin protein, Acta Biomater. 5 (2009) 1686–1696.
[2] S. Xu, K. Lin, Z. Wang, J. Chang, L. Wang, J. Lu, C. Ning, Reconstruction of calvarial defect of rabbits using porous calcium silicate bioactive ceramics, Biomaterials 29 (2008) 2588–2596.
[3] K.L. Scrivener, A. Nonat, Hydration of cementitious materials, present and future, Cem. Concr. Res. 41 (2011) 651–665.
[4] L. Nicoleau, E. Schreiner, A. Nonat, Ion-specific effects influencing the dissolution of tricalcium silicate, Cem. Concr. Res. 59 (2014) 118–138.
[5] F.P. Glasser, E.E. Lachowski, D.E. Macphee, Compositional model for calcium silicate hydrate (C-S-H) gels, their Solubilities, and free energies of formation, J. Am. Ceram. Soc. 70 (1987) 481–485.
[6] A. Kumar, B.J. Walder, A.K. Mohamed, A. Hofstetter, B. Srinivasan, A.J. Rossini, K. Scrivener, L. Emsley, P. Bowen, The atomic-level structure of cementitious calcium silicate hydrate, J. Phys. Chem. C 121 (2007) 17188–17196.
[7] F. Winnefeld, S. Becker, J. Pakusch, T. Götz, Effects of the molecular architecture of comb-shaped superplasticizers on their performance in cementitious systems, Cem. Concr. Compos. 29 (2007) 251–262.
[8] F. Ridi, E. Fratini, P. Luciani, F. Winnefeld, P. Baglioni, Tricalcium silicate hydration reaction in the presence of comb-shaped superplasticizers: boundary nucleation and growth model applied to polymer-modified pastes, J. Phys. Chem. C 116 (2012) 10887–10895.
[9] D. Jansen, J. Neubauer, F. Goetz-Neunhoeffer, R. Haerzschel, W.D. Hergeth, Change in reaction kinetics of a Portland cement caused by a superplasticizer - calculation of heat flow curves from XRD data, Cem. Concr. Res. 42 (2012) 327–332.
[10] H. Manzano, J.S. Dolado, A. Ayuela, Elastic properties of the main species present in Portland cement pastes, Acta Mater. 57 (2009) 1666–1674.
[11] L. Nicoleau, T. Gadt, L. Chitu, G. Maier, O. Paris, Oriented aggregation of calcium silicate hydrate platelets by the use of comb-like copolymers, Soft Matter 9 (2013) 4864–4874.
[12] V. Kanchanason, J. Plank, Effectiveness of C-S-H – PCE nanocomposites possessing globular and foil-like morphology on early strength development of Portland cement, 2nd International Conference on the Chemistry of Construction Materials (ICCCM), GDCh-Monographie, 2016, pp. 85–88.
[13] J.J. Beaudoin, L. Raki, R. Alizadeh, A 29Si MAS NMR study of modified C–S–H nanostructures, Cem. Concr. Compos. 31 (2009) 585–590.
[14] E. Cappelletto, S. Borsacchi, M. Geppi, F. Ridi, E. Fratini, P. Baglioni, Comb-shaped polymers as nanostructure modifiers of calcium silicate hydrate: A29Si solid-state NMR investigation, J. Phys. Chem. C 117 (2013) 22947–22953.
[15] J. Gibbs, Equilibrium of heterogeneous substances, trans connect, Acad. Sci. 3 (1876) 108–248.
[16] J. Zeldovich, On the theory of new phase formation: cavitation, Acta Physicochim URSR, 18 1943, pp. 1–22.
[17] J. Frenkel, A general theory of heterophase fluctuations and pretransition phenoma, J. Phys. Chem. 7 (1939) 538–547.
[18] P.G. Vekilov, Nucleation, Cryst. Growth Des. 10 (2010) 5007–5019.
[19] J.J. De Yoreo, P.U.P.A. Gilbert, N.A.J.M. Sommerdijk, R.L. Penn, S. Whitelam, D. Joester, H. Zhang, J.D. Rimer, A. Navrotsky, J.F. Banfield, A.F. Wallace, F.M. Michel, F.C. Meldrum, H. Cölfen, P.M. Dove, Crystallization by particle attachment in synthetic, biogenic, and geologic environments, Science 349 (2015).
[20] D. Gebauer, H. Cölfen, A. Verch, M. Antonietti, The multiple roles of additives in $CaCO_3$ crystallization: a quantitative case study, Adv. Mater. 21 (2009) 435–439.
[21] T. Kato, Polymer/calcium carbonate layered thin-film composites, Adv. Mater. 12 (2000) 1543–1546.
[22] D.J. Belton, O. Deschaume, C.C. Perry, An overview of the fundamentals of the chemistry of silica with relevance to biosilicification and technological advances, FEBS J. 279 (2012) 1710–1720.
[23] D. Gebauer, M. Kellermeier, J.D. Gale, L. Bergstrom, H. Cölfen, Pre-nucleation clusters as solute precursors in crystallisation, Chem. Soc. Rev. 43 (2014) 2348–2371.
[24] J. Rieger, Precursor structures during crystallization of $CaCO_3$ and control by polyelectrolytes, PMSE Prepr. 96 (2007) 125–126.
[25] M. Faatz, F. Gröhn, G. Wegner, Amorphous calcium carbonate: synthesis and potential intermediate in biomineralization, Adv. Mater. 16 (2004) 996–1000.
[26] A.-W. Xu, Y. Ma, H. Cölfen, Biomimetic mineralization, J. Mater. Chem. 17 (2007) 415–449.
[27] J. Plank, K. Pöllmann, N. Zouaoui, P.R. Andres, C. Schaefer, Synthesis and performance of methacrylic ester based polycarboxylate superplasticizers possessing hydroxy terminated poly(ethylene glycol) side chains, Cem. Concr. Res. 38 (2008) 1210–1216.
[28] I. Klur, B. Pollet, J. Virlet, A. Nonat, C-S-H Structure Evolution with Calcium Content by Multinuclear NMR, in: P. Colombet, H. Zanni, A.-R. Grimmer, P. Sozzani (Eds.), Nuclear Magnetic Resonance Spectroscopy of Cement-Based Materials, Springer, Berlin, Heidelberg, 1998, pp. 119–141.
[29] E. Tajuelo Rodriguez, I.G. Richardson, L. Black, E. Boehm-Courjault, A. Nonat, J. Skibsted, Composition, silicate anion structure and morphology of calcium silicate hydrates (C-S-H) synthesised by silica-lime reaction and by controlled hydration of tricalcium silicate (C3S), Adv. Appl. Ceram. 114 (2015) 362–371.
[30] H. Matsuyama, J.F. Young, Synthesis of calcium silicate hydrate/polymer complexes: part I. Anionic and nonionic polymers, J. Mater. Res. 14 (1999) 3379–3388.
[31] J. Plank, B. Sachsenhauser, Experimental determination of the effective anionic charge density of polycarboxylate superplasticizers in cement pore solution, Cem. Concr. Res. 39 (2009) 1–5.
[32] F. Dalas, A. Nonat, S. Pourchet, M. Mosquet, D. Rinaldi, S. Sabio, Tailoring the anionic function and the side chains of comb-like superplasticizers to improve their adsorption, Cem. Concr. Res. 67 (2015) 21–30.

Publication #3

Study on the early crystallization of calcium silicate hydrate (C-S-H) in the presence of polycarboxylate superplasticizers

J. Plank, M. Schönlein, V. Kanchanason

Journal of Organometallic Chemistry
Volume 869, 15. August 2018, Pages 227 - 232

Journal of Organometallic Chemistry xxx (2018) 1–6

Contents lists available at ScienceDirect

Journal of Organometallic Chemistry

journal homepage: www.elsevier.com/locate/jorganchem

Study on the early crystallization of calcium silicate hydrate (C-S-H) in the presence of polycarboxylate superplasticizers

J. Plank [a, *], M. Schönlein [a], V. Kanchanason [a, b]

[a] Technische Universität München, 85747, Garching, Lichtenbergstraße 4, Germany
[b] Siam Research and Innovation Company, 51 Moo 8, Tub Kwang, Kaeng Khoi, Saraburi, 18260, Thailand

ARTICLE INFO

Article history:
Received 2 January 2018
Received in revised form
2 February 2018
Accepted 2 February 2018
Available online xxx

This article is dedicated to Prof. Wolfgang A. Herrmann on occasion of his 70th birthday.

Keywords:
C-S-H
Polycarboxylate
Non-classical nucleation
Globules
Nanofoils

ABSTRACT

Calcium silicate hydrate (C-S-H) presents the strength-providing phase in hardened cement and concrete. Its nucleation and very early overall growth are not yet fully understood. Here, the impact of methacrylate ester-based PCEs (a common type of dispersant used to fluidize concrete) on the nucleation and crystallization of C-S-H precipitated from aqueous solutions of $Ca(NO_3)_2$ and Na_2SiO_3 was investigated. It was found that in the absence of PCEs, most unexpectedly globular nanoparticles of C-S-H with a diameter of ~20–60 nm are favored. Thereafter, within less than 1 h the globuli convert to the well-known nanofoils of C-S-H. According to these observations, the very early C-S-H is formed following a non-classical nucleation mechanism. In the presence of PCEs, the initial globules show a core-shell morphology, presumably with PCE polymers as shell which delays the conversion to the nanofoils for several hours. The PCE polymers exhibiting higher anionicity delayed the transformation to nanofoils more than the PCEs possessing lower anionic charge.

1. Introduction

Calcium silicate hydrate (C-S-H) presents the main hydration product of ordinary Portland cement. There, C-S-H is generated from the hydration of tricalcium silicate (C_3S) and dicalcium silicate (C_2S) [1,2]. Its structural properties are still the subject of many investigations, due to its semi-crystalline character. Generally, C-S-H exhibits a disordered layered structure consisting of linear silicate chains arranged in so-called "dreierketten", analogous to that of tobermorite (Ca/Si = 0.8–1.5) or jennite (Ca/Si = 1.5–2.0) [3,4].

The nucleation and crystallization of inorganic minerals is described by two theories. The first concept (nucleation theory) is based on the initial formation of critical nuclei. Nuclei exhibiting a larger radius than the critical radius will grow while the smaller ones will re-dissolve [5–7]. The second concept is designated as non-classical nucleation theory. A characteristic of the non-classical nucleation concept is that the morphology of the precritical clusters differs significantly from that of the final bulk crystal [8–11]. Another characteristic of this nucleation mechanism is occurrence of an amorphous intermediate (e.g. droplets, amorphous nanoparticles) which then converts to the crystals exhibiting the morphology of the final product.

Polycarboxylate (PCE) superplasticizers, also known as high range water reducers, are used to fluidize (disperse) cement with the goal to improve the workability of concrete and mortar. They reduce the viscosity of concrete via an electrosteric dispersing effect. PCEs possess a comb-like structure with carboxylate anchor groups at the backbone and polyethylene glycol lateral chains. It has been found that calcium silicate hydrate precipitated from $Ca(NO_3)_2/Na_2SiO_3$ in an aqueous PCE solution forms a nanocomposite ("C-S-H-PCE") which presents an excellent seeding material which can greatly accelerate cement hydration [12–14]. Moreover, it has been reported that the C-S-H nanofoils contained in the C-S-H-PCE nanocomposite provided a particularly strong seeding effect owed to their particularly small size (lengths 20–60 nm) [15]. This effect is particularly important when so-called "low CO_2" cements (cements consisting of a blend of Portland cement clinker and a pozzolanic material such as fly ash, ground granulated blast furnace slag, calcined clay etc.) are used, because such cements generally exhibit poor early strength development. In spite of their huge industrial importance, the initial nucleation and early crystallization of C-S-H in the presence

* Corresponding author.
E-mail address: sekretariat@bauchemie.ch.tum.de (J. Plank).

https://doi.org/10.1016/j.jorganchem.2018.02.005
0022-328X/

of PCEs is still not well understood.

Here, we investigated the very early nucleation and crystallization of C-S-H (0–4 h) precipitated from $Ca(NO_3)_2$ and Na_2SiO_3 solutions at a Ca/Si ratio of 1.0 in the presence of different PCE superplasticizers by capturing the very first precursors via transmission electron microscopy (TEM). Additionally, they were characterized via ^{29}Si MAS NMR spectroscopy and particle size measurement.

2. Experimental

2.1. Raw materials

The starting materials used in the synthesis of C-S-H were $Ca(NO_3)_2 \cdot 4H_2O$ (p.a., AppliChem GmbH, Darmstadt, Germany) and $Na_2SiO_3 \cdot 5H_2O$ (Alfa Aesar, Karlsruhe, Germany).

Two methacrylate ester (MPEG)-based PCEs were synthesized according to literature descriptions [16], yielding aqueous solutions with solids content of ~40 wt %. They contained side chain made of 45 ethylene oxide (EO) units and the molar ratios of methacrylic acid (MAA) to the methacrylate ester macromonomer were 2:1 (MPEG-45PC2) and 10:1 (MPEG-45PC10). The molecular structure of the synthesized PCEs is displayed in Fig. 1 and their molecular properties are listed in Table 1.

2.2. Synthesis of C-S-H seeds

For the synthesis of the C-S-H seeds, a molar ratio for Ca: Si of 1: 1 was selected which is below that of C-S-H formed in cement hydration (there it is ~1.6–1.8). The lower ratio was chosen based on previous experiments which demonstrated a superior seeding and accelerating effect for C-S-H of this molar ratio.

In the preparation, at first a solution A was prepared by dissolving 0.316 g $Na_2SiO_3 \cdot 5H_2O$ (1.5 mmol) in 10 mL DI water. Second, Solution B was obtained by dissolving 0.35 g $Ca(NO_3)_2 \cdot 4H_2O$ (1.5 mmol) in 5 mL of deionized (DI) water. The reaction was carried out using three syringes connected via a three way valve: The reaction container, syringe #1, was loaded with Solution A, while syringe #2 was charged with Solution B and syringe #3 held 10 mL of acetone. To separate the mother liquor from the precipitated C-S-H, syringe #1 was equipped with a disc filter holding a glass fiber membrane (pore size: 0.4–0.45 μm, GD/X GMF, GE 173 Healthcare, Little Chalfont, UK). In synthesis, within 1–2 s Solution B in syringe #2 was injected into syringe #1 holding Solution A, kept there for 5 min, 15 min, 45 min, 2 h, 3 h, and 4 h, respectively and was then filtrated into syringe #2. Then acetone was injected from syringe #3 into the reaction container (syringe #1) to stop any further hydration and crystallization. The precipitated C-S-H was collected from syringe #1, centrifuged (10 min, 8500 rpm), washed thrice with acetone and stored in acetone under nitrogen atmosphere prior to analysis.

When C-S-H was precipitated in PCE solution to obtain the C-S-H-PCE nanocomposite, then 0.14 g of PCE polymer (as solid) were dissolved in the 10 mL DI water of solution A and Na_2SiO_3 was dissolved there.

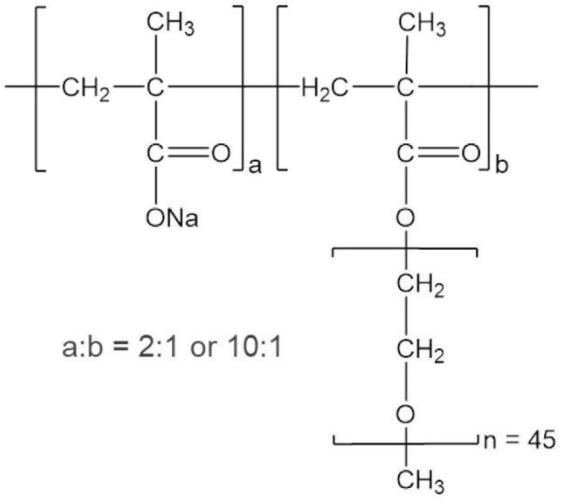

Fig. 1. Molecular structure of the synthesized MPEG PCE samples.

2.3. TEM imaging

TEM micrographs were collected on a JEM 2011 microscope (JEOL, Eching, Germany) equipped with a LaB_6 cathode. Acetone suspensions of the C-S-H samples as prepared were placed on a carbon-coated copper grid and analyzed.

2.4. Particle size measurements

Particle size of the C-S-H or C-S-H-PCE nanocomposites was measured via dynamic light scattering (DLS) using a Zetasizer Nano ZS apparatus (Malvern Instruments, Workestershire, UK). The samples were suspended in DI water at a concentration of 0.1 g/L. An ultrasonic bath was used to disperse the particles for 15 min prior to measurement.

2.5. ^{29}Si MAS NMR spectroscopy

The silicate present in the synthesized C-S-H and C-S-H – PCE nanocomposites was identified by ^{29}Si MAS NMR spectroscopy using a Bruker Avance 300 MHz instrument operating at a resonance frequency of 59.595 MHz. The powder samples were filled into a 7 mm zirconia rotor and spun at 5 KHz. All spectra were recorded with a relaxation delay of 45 s, and tetrakis(trimethylsilyl) silane was used as external standard.

3. Results and discussion

3.1. Initial nucleation of C-S-H

The initial nucleation and crystallization of C-S-H precipitated from aqueous solutions of $Ca(NO_3)_2$ and Na_2SiO_3 in the absence and presence of PCEs was first monitored via TEM measurements. After 5 min of reaction, the images reveal polydisperse C-S-H and C-S-H-PCE nanoparticles exhibiting globular morphology, with diameters of ~20–60 nm (Fig. 2). The particles of C-S-H precipitated in the presence of a PCE polymer (e.g. 45PC10) were always less agglomerated.

The occurrence of globular C-S-H particles as initial nucleation product was much surprising, because hitherto only foil- or later needle-like morphologies have been reported for C-S-H [17].

Furthermore, high resolution TEM images of individual C-S-H and C-S-H-PCE globules clearly confirm the shape of a droplet (Fig. 3). Most interestingly, a thin shell (thickness ~ 3–5 nm) surrounding the droplet was observed for the C-S-H precipitated in the presence of MPEG-PCE 45PC10 (Fig. 3).

The results suggest that for C-S-H, following a non-classical nucleation mechanism at first a spherical particle is formed which at a later time converts to the known foils and needles of C-

Please cite this article in press as: J. Plank, et al., Journal of Organometallic Chemistry (2018), https://doi.org/10.1016/j.jorganchem.2018.02.005

Table 1
Molecular properties of the synthesized polycarboxylate (PCE) samples.

Polymer Sample	M_w (g/mol)	M_n (g/mol)	PDI (M_w/M_n)	Specific anionic charge amount at pH 12.5 (μeq/g)
45PC2	30,500	18,000	1.7	1500
45PC10	18,900	10,600	1.8	5000

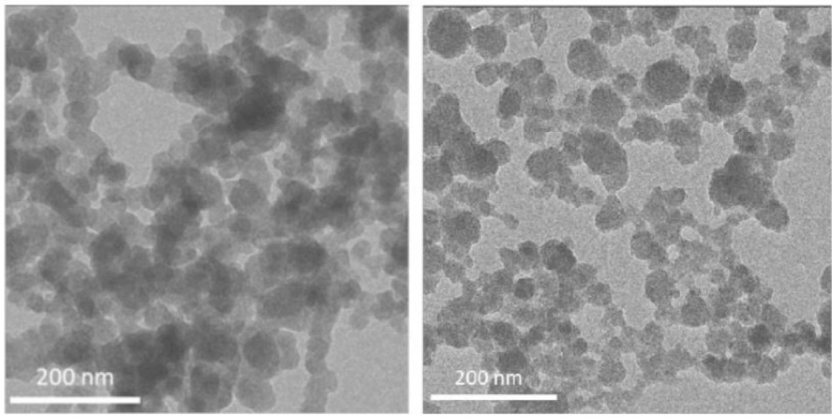

Fig. 2. TEM images of C-S-H (left) and C-S-H-PCE (PCE = 45PC10) (right) precipitates after 5 min of ageing.

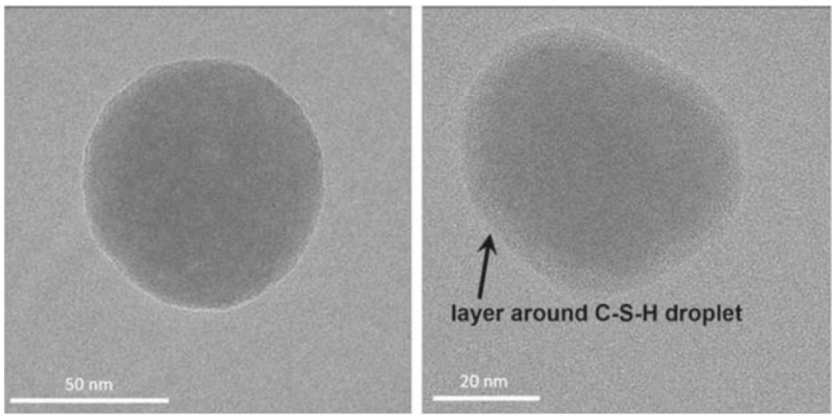

Fig. 3. High resolution TEM images of a C-S-H droplet formed in the absence (left) and presence (right) of MPEG-PCE sample 45PC10.

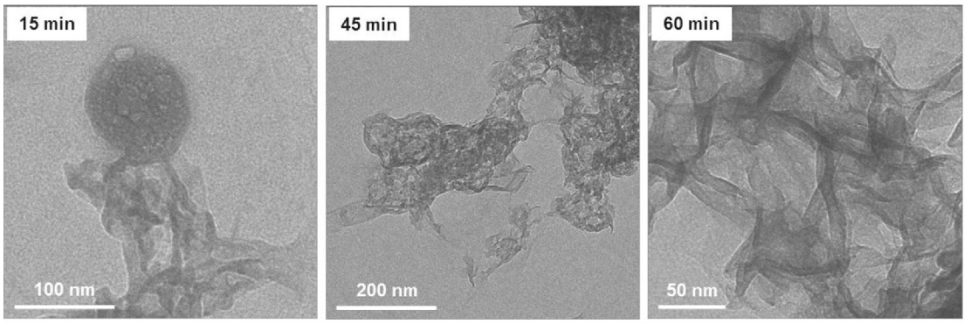

Fig. 4. TEM images of C-S-H particles 15, 45 and 60 min after precipitation.

Please cite this article in press as: J. Plank, et al., Journal of Organometallic Chemistry (2018), https://doi.org/10.1016/j.jorganchem.2018.02.005

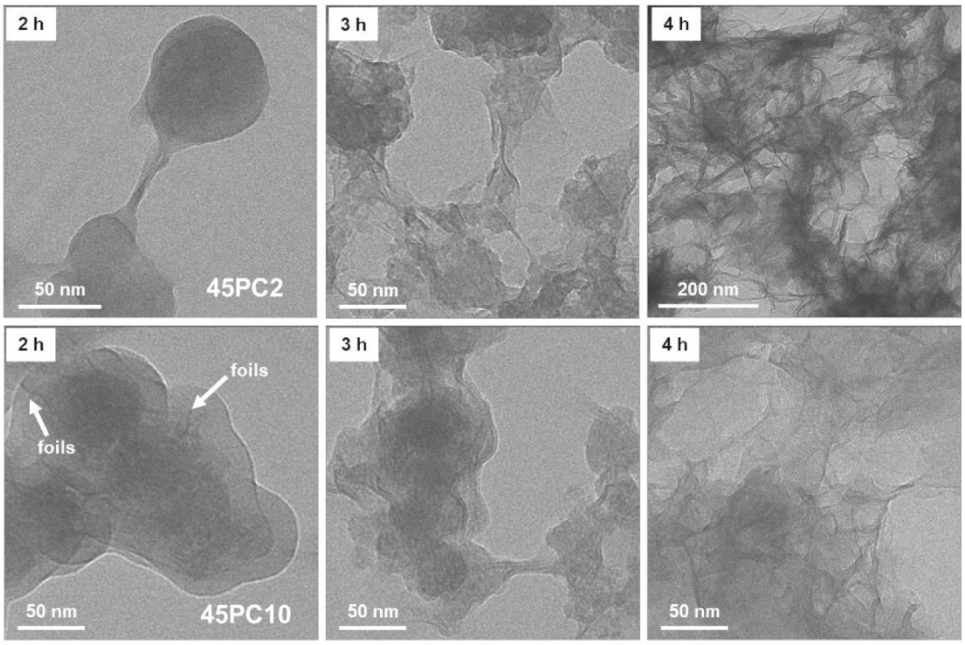

Fig. 5. TEM images of C-S-H precipitated in the presence of PCE polymer 45PC2 (top) and 45PC10 (bottom) after 2, 3 and 4 h of crystallization.

S-H. Moreover, a layer of organic PCE polymer coats the precursor droplet when C-S-H is precipitated in the PCE solution. Thus, in the presence of the PCE comb polymer at first a core-shell particle results.

3.2. Conversion of C-S-H globules to nanofoils

The shelf life of the globular C-S-H and C-S-H-PCE precursors was monitored over time via TEM imaging.

For the globules of pure C-S-H, it was observed that after 15 min only nanofoils outgrow from its surface (Fig. 4). After that, the globules continuously dissolve and recrystallize into the well-known nanofoils which then become more abundant and larger. At 60 min, the globular precursor particles have completely disappeared while a dense network of C-S-H nanofoils with lengths of ~150 nm and thicknesses of ~5 nm is observed.

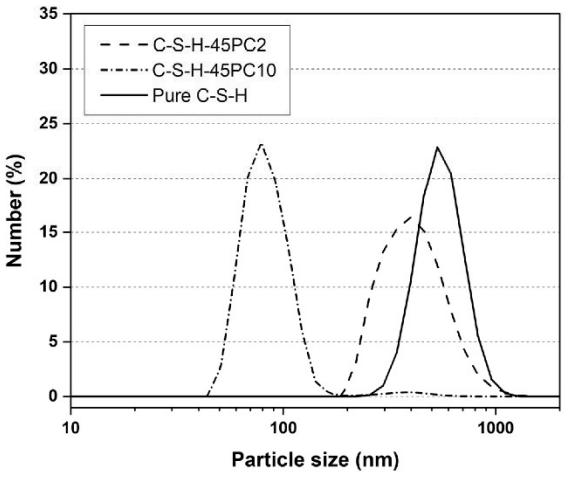

Fig. 6. Particle size distribution (by number) of C-S-H precipitated in the absence and presence of the PCE polymers 45PC2 and 45PC10, respectively, measured after 24 h.

Next, the morphological change of C-S-H synthesized in the presence of PCE polymers was investigated. Two different MPEG-PCE superplasticizers including a polymer a possessing low anionic charge density (45PC2) and one of high anionic charge density (45PC10) were selected for the experiment.

Interestingly, TEM imaging of the obtained C-S-H-PCE precipitates reveals a delayed transformation from the globules to the nanofoils. The conversion started only after 2 h versus after 15 min for the pure C-S-H (Fig. 5). Apparently, the PCE polymer layer surrounding the C-S-H particles obstructs the dissolution of the C-S-H globules and their recrystallization to the thermodynamically more favored foil morphology. For both PCEs, beginning conversion was evidenced after ~2 h by the appearance of first needle-like C-S-H crystallites which grow from the inner core and penetrate the shell. The C-S-H crystallites continue to grow until they reach a critical size, then the shell bursts completely and transformation into foils progresses rapidly.

Additionally, it was observed that PCE polymer 45PC2 which is characterized by a high side chain density and low anionic charge forms a less thick polymer layer around the C-S-H globules, compared to the layer from polymer 45PC10 which exhibits a high anionic charge density. Therefore, for 45PC2 the thin C-S-H foils start to grow earlier (after ~ 2 h) from the inner core to the outer shell of the globules than for 45PC10 (after ~ 3 h). For the nanocomposite from 45PC2, more disrupted C-S-H shells and intergrowing of numerous C-S-H nanofoils into a dense network are observed already after 3 h.

In the presence of the more anionic PCE polymer 45PC10, the C-S-H nanofoils occur later, presumably due to the stronger adsorption ability of this PCE and the resulting more dense polymer layer

Please cite this article in press as: J. Plank, et al., Journal of Organometallic Chemistry (2018), https://doi.org/10.1016/j.jorganchem.2018.02.005

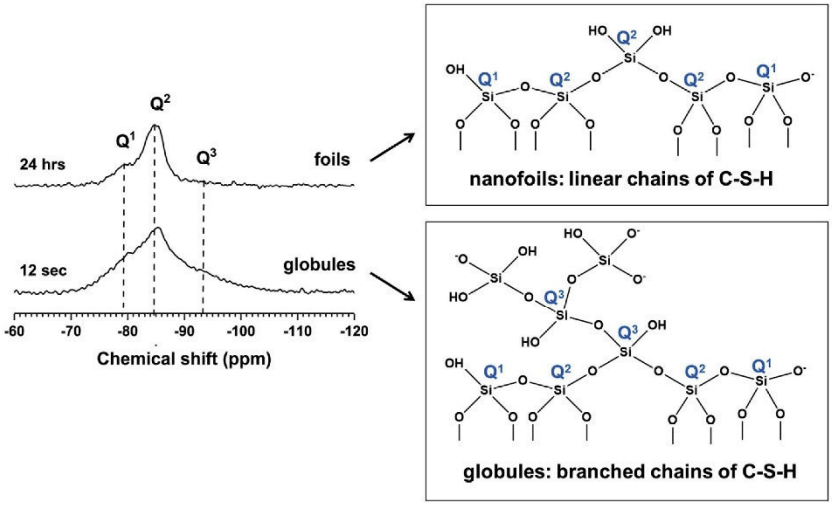

Fig. 7. ^{29}Si MAS NMR spectra of pure C-S-H precipitates obtained at various ageing times (left) and illustration of structural model of linear and branched silicate chains present in the globular C-S-H particles and the C-S-H foils, respectively.

on the C-S-H particles. This PCE shields the C-S-H globules more efficiently, it therefore delays the disruption of the shell and hinders the transformation from globules to nanofoils more effectively than the less anionic PCE polymer 45PC2.

3.3. Particle size measurements

The particle size distribution of pure C-S-H and C-S-H-PCE composites obtained after 24 h is presented in Fig. 6. It was observed that the PCE polymer significantly affects the particle size of the synthesized C-S-H which decreases with increased anionic charge density of the PCE polymer. In the presence of highly anionic PCE polymer 45PC10, an average particle size of ~80 nm was detected. For the PCE possessing low charge density (45PC2), a much larger particle size of ~400 nm was observed which was only slightly less than that of pure C-S-H (~550 nm). This implies that PCEs of higher anionic charge density modulate the particle size of C-S-H to a much smaller value which is most advantageous for the seeding effect in cement.

3.4. ^{29}Si MAS NMR spectroscopy

The ^{29}Si MAS NMR spectra of pure C-S-H obtained from the precipitation are presented in Fig. 7. Immediately after nucleation (12 s), the spectrum showed a broad peak covering the entire range for Q^1, Q^2 and Q^3 Si species, thus suggesting coexistence of silica units positioned as terminal, chain member and branching site. However, after ageing (24 h), the branching units have disappeared signifying that only linear silicate chains are present in the nanofoils [18]. This result corroborates that the C-S-H globules obtained at very early ageing showed branched silicate chains while the C-S-H nanofoils resulting from the transformation of the globules exhibited only linear silicate chains of C-S-H.

4. Conclusions

The very early nucleation and crystallization of C-S-H precipitated from aqueous $Ca(NO_3)_2$ and Na_2SiO_3 solutions in the presence and absence of polycarboxylate superplasticizers was studied.

Unexpectedly, it was found that initially a metastable, amorphous precursor exhibiting a globular morphology is formed which then converts to the well-known nanofoils of C-S-H. As such, the nucleation of C-S-H presents one of the rare examples of a non-classical nucleation mechanism.

^{29}Si MAS NMR spectroscopy revealed that in the globular precursor particles, branched chains of C-S-H are present while in the C-S-H foils which occur after the transformation, only linear, non-branched chains of C-S-H occur.

Precipitation of C-S-H in the presence of PCEs strongly delays the conversion from globular to nanofoil-like C-S-H because of a shell which is formed around the globules and consists of adsorbed PCE polymer. PCEs possessing high anionic charge density (e.g. 45PC10) delay the transformation of the globules to foils more than PCEs possessing low anionicity such as polymer 45PC2. Moreover, the slower transformation of globular C-S-H-PCE to nanofoils as compared to pure C-S-H produces significantly smaller nanofoils, as was evidenced by particle size measurements. Such smaller nanofoils are superior seeding materials which can strongly accelerate cement hydration.

Acknowledgements

The authors would like to thank Prof. S. Weinkauf and her team from the center of Electron Microscopy at TUM's Chemistry department for capturing the TEM images. V. Kanchanason wishes to thank SCG Cement-Building Materials for financial support of her study at TU München.

References

[1] H.F.W. Taylor, Cement Chemistry, second ed., Thomas Telford Publishing, London, 1997.
[2] I.G. Richardson, The calcium silicate hydrates, Cement Concr. Res. 38 (2008) 137–158.
[3] J.J. Beaudoin, L. Raki, R. Alizadeh, A ^{29}Si MAS NMR study of modified C-S-H nanostructures, Cement Concr. Compos. 31 (2009) 585–590.
[4] F.P. Glasser, E.E. Lachowski, D.E. Macphee, Compositional model for calcium silicate hydrate (C-S-H) gels, their solubilities, and free energies of formation, J. Am. Ceram. Soc. 70 (1987) 481–485.
[5] J. Gibbs, Equilibrium of heterogeneous substances, Trans. Conn. Acad. Sci. 3 (1876) 108–248.

Please cite this article in press as: J. Plank, et al., Journal of Organometallic Chemistry (2018), https://doi.org/10.1016/j.jorganchem.2018.02.005

[6] J. Zeldovich, On the theory of new phase formation: cavitation, Acta Physicochim URSR 18 (1943) 1–22.
[7] J. Frenkel, A general theory of heterophase fluctuations and pretransition phenoma, J. Phys. Chem. 7 (1939) 538–547.
[8] J.J. De Yoreo, P.U.P.A. Gilbert, N.A.J.M. Sommerdijk, R.L. Penn, S. Whitelam, D. Joester, H. Zhang, J.D. Rimer, A. Navrotsky, J.F. Banfield, A.F. Wallace, F.M. Michel, F.C. Meldrum, H. Cölfen, P.M. Dove, Crystallization by particle attachment in synthetic, biogenic, and geologic environments, Science 349 (2015).
[9] J. Rieger, Precursor structures during crystallization of $CaCO_3$ and control by polyelectrolytes, PMSE Prepr. 96 (2007) 125–126.
[10] H. Cölfen, M. Antonietti, Mesocrystals and Nonclassical Crystallization, first ed., John Wiley & Sons Ltd, Chichester, 2008.
[11] A.-W. Xu, Y. Ma, H. Cölfen, Biomimetic mineralization, J. Mater. Chem. 17 (2007) 415–449.
[12] L. Nicoleau, The acceleration of cement hydration by seeding: influence of the cement mineralogy, ZKG Int. 1 (2013) 40–49.
[13] L. Nicoleau, Accelerated growth of calcium silicate hydrates: experiments and simulations, Cement Concr. Res. 41 (2011) 1339–1348.
[14] V. Kanchanason, J. Plank, C-S-H–PCE nanocomposites for enhancement of early strength of Portland cement, 14th ICCC, Beijing, China, in: C. Shi, Y. Yao (Eds.), Proceedings CD, Section 4: Admixtures, 2015.
[15] V. Kanchanason, J. Plank, C-S-H–PCE nanocomposites for enhancement of early strength of cement, in: 19th Ibausil, Bauhaus-universität Weimar, Tagungsband 1, Weimar, Germany, 2015, pp. 759–766.
[16] J. Plank, K. Pöllmann, N. Zouaoui, P.R. Andres, C. Schaefer, Synthesis and performance of methacrylic ester based polycarboxylate superplasticizers possessing hydroxy terminated poly(ethylene glycol) side chains, Cement Concr. Res. 38 (2008) 1210–1216.
[17] P.C. Hewlett, Lea's Chemistry of Cement and Concrete, fourth ed., Butterworth-Heinemann Publishing, Oxford, 2003.
[18] E. Cappelletto, S. Borsacchi, M. Geppi, F. Ridi, E. Fratini, P. Baglioni, Comb-shaped polymers as nanostructure modifiers of calcium silicate hydrate: a ^{29}Si solid-state NMR investigation, J. Phys. Chem. C 117 (2013) 22947–22953.

Please cite this article in press as: J. Plank, et al., Journal of Organometallic Chemistry (2018), https://doi.org/10.1016/j.jorganchem.2018.02.005

6. Summary and Outlook

In the first part of this work, the interaction of two different retarding admixtures which are commonly applied in oil well cementing with the most reactive clinker phase present in Portland cement, C_3A, was investigated. A synthesis method was developed which allows successful intercalation of both retarders into the hydrocalumite structure of Ca_2Al-OH-LDH, yielding an inorganic-organic host-guest compound (Ca_2Al-retarder-LDH). The interlayer distance increased upon intercalation of the co-polymers from 0.8 nm to 1.45 nm for AA/AMPS co-polymer and to 1.68 nm for the IA/AMPS co-polymer, respectively. TG-MS measurements revealed that the intercalated co-polymers possess increased heat resistance. Furthermore, the obtained Ca_2Al-retarder-LDHs were subjected to an anion exchange with SO_4^{2-}. There up to ~ 80 % of the highly anionic AA/AMPS co-polymer was released from the LDH structure at a sulfate concentration of 200 % anion exchange capacity, while only ~ 20 % of the IA/AMPS co-polymer which possesses low anionic charge, were exchanged. This suggests that the IA/AMPS co-polymer possesses a higher affinity to the positively charged LDH structure compared to the AA/AMPS co-polymer and is not easily released once it is intercalated. These findings were confirmed by heat-flow calorimetry of a commercial API Class G oil well cement admixed with the individual co-polymers and the Ca_2Al-retarder-LDHs, respectively. While cement admixed with Ca_2Al-AA/AMPS-LDH showed almost a similar retardation as admixed with the pure co-polymer, the cement admixed with Ca_2Al-IA/AMPS-LDH did not show any retardation.

The findings above indicate that the stability of the Ca_2Al-retarder-LDHs is not exclusively depending on the high anionic charge of the co-polymers, but also on their molecular structure and weight. The IA/AMPS co-polymer possesses a higher molecular weight and more sulfonate anchor groups and therefore showed less tendency to be released from the interlayer than the AA/AMPS co-polymer with more carboxylate groups and a lower molecular weight. This study has shown that during cement hydration retarding admixtures can intercalate into layered AF_m phases, and the obtained inorganic-organic host-guest compounds possess different stabilities towards sulfate. Especially cements rich in C_3A and low in sulfate content can exhibit a loss in the desired retarding effect of the admixtures, owed to intercalation.

In the second part, the potential of Ca_2Al-formate-LDHs as hardening accelerators for mortars was evaluated. A pre-requisite for the application of this type of LDH as admixture, is the development of a synthesis method that can be easily up-scaled, like e.g. co-precipitation. The successful preparation of Ca_2Al-formate-LDH by combining aqueous solutions of $Ca(HCOO)_2$ and $Al(HCOO)_3$ was confirmed by XRD and SEM analysis. The basal spacings of the Ca_2Al-formate-LDHs prepared by rehydration and co-precipitation were comparable and both LDHs exhibited the typical exfoliated morphology, as evidenced by SEM.

A significant accelerating effect of the synthesized Ca_2Al-formate-LDH on the compressive and flexural strengths of mortars containing the admixture within the first 24 h of hydration was only observed for the coarse CEM I 32.5 R. The mortars prepared with the two other OPC samples did not show increased strength values after 16 h and 24 h. The mechanism of acceleration was studied further by heat flow calorimetry and in-situ XRD measurements. During the first 24 h, a higher decrease in the intensity of the reflections of the clinker phases could be observed when the cement was admixed with Ca_2Al-formate-LDH. In contrast, the amount of heat released during the first 24 h was not higher compared to the neat cement, as evidenced by calorimetry. Furthermore, it was found that an increased heat release occurred during the period of sulfate depletion (at 20 – 48 hours). The latter finding suggests that the hydrocalumite-type Ca_2Al-formate-LDH might act as a heterogeneous nucleation seed in the through-solution conversion process and thus accelerates the transformation of ettringite to monosulfate. While the focus of this study was to provide an applicable, facile synthesis method and to assess the potential of the prepared Ca_2Al-formate-LDH as an accelerating admixture in general, there are some open topics that need to be clarified in future research to allow a final statement:

- The obtained results indicate that not only the amount of aluminate phase, but also their modification, i.e. orthorhombic or cubic C_3A, present in the cement might be decisive for the accelerating effect of the Ca_2Al-formate-LDH.
- It is of interest for future investigations to test the compressive and flexural strengths of mortars not only after 24 h, but also e.g. after 7 days and to further investigate the microstructure of mortars within this time frame to confirm an accelerating effect from nucleation seeding during the transformation from ettringite to monosulfate.

- Studies on the accelerating effect of C-S-H nanoseeds have shown that the chemical structure and size of the particles is of great importance for the accelerating effect and there are many reaction parameters which they depend upon.[35, 129] There is still room for optimization of the Ca_2Al-formate-LDH e.g. via pH value adjustment during reaction, Ca/Al ratio, stabilization by polyelectrolytes like PCEs. Such modifications might allow to obtain a monodisperse particle size distribution in the nanometer range.

In the next chapter, ettringite crystallization during the first 10 s of hydration of two commercial Portland cement samples was studied under terrestrial and microgravity conditions, i.e. in the presence and absence of convection. The experiments under microgravity conditions were conducted on parabolic flights. Hydration of the neat cement samples confirmed findings of previous studies where generally smaller, but more abundant ettringite crystals were formed under microgravity conditions.[159] This is attributed to the slower mass transport of growth units to the crystal surface in the absence of convection. Moreover, the ettringite crystallization is strongly depending on the composition of the cement, especially on the amount and type of aluminate phase and the amount of gypsum present.

The scope of this study was to get more insight into the interactions between superplasticizers and their main anchoring phase, i.e. ettringite, during the first seconds of cement hydration. The findings of the impact of superplasticizers on ettringite crystal growth can be summarized as follows:

- The presence of superplasticizers generally leads to slimmer, but longer crystals compared to the rather stocky ettringite crystals found in the neat cement paste.
- An influence of the side chain length of MPEG-PCEs possessing comparable anionic charge density in the backbone, but varying numbers of ethylene oxide units in the side chain increasing from 6 up to 114 on the morphology of ettringite crystals could not be observed within 10 s of hydration.
- With increasing anionic charge density of MPEG-PCEs possessing similar side chains, the aspect ratio of the ettringite crystals formed increased more strongly, i.e. the ettringite crystals possessed smaller diameters and were longer when they were formed in the presence of highly anionic PCEs, such as the MPEG-sample 45PC10.

- With PCE dosage increasing from 0.05 % bwoc to 0.15 % bwoc and 0.25 % bwoc, the ettringite crystals exhibited a rather needle-like morphology due to decreasing diameters, but longer crystals.
- Polyphosphate comb-polymers can adsorb more strongly on ettringite than polycarboxylate ethers and alter its morphology already at a low dosage of 0.05 % bwoc.
- In the presence of polycondensate superplasticizers, increased ettringite crystal lengths and diameters were found. The aspect ratio increases with the anionic charge density of the polymers.

The effects described above were generally found to be more pronounced under terrestrial gravity than under microgravity. This is owed to the slower dissolution of the clinkers and the slower mass transport of ions away from the boundary zone into the bulk solution as well as slower diffusion of polymers in the absence of convection. Furthermore, a dosage of 0.05 % bwoc might be too low to impact ettringite growth more strongly under microgravity. Here, not all crystals were inhibited in their growth by adsorbed polymers which influences the average crystal sizes measured, and this might cloud the effect of the polymers on the ettringite crystal growth in the overall statistics.

The resulting higher aspect ratios of ettringite crystals found in the presence of PCEs suggest that fast adsorption of the polymers on the lateral faces of the ettringite crystals occurs and thus crystal growth is inhibited along the *a* and *b* axis, while growth along the *c* axis proceeds rather unrestricted. The increased crystal diameters and lengths found in the presence of polycondensates, on the other hand, indicate that dissolution of the aluminates is pronounced in their presence, and a rather random adsorption on lateral faces or top and bottom faces on the ettringite crystals occurs.

The results obtained generally show that the nucleation and crystallization of ettringite is influenced by superplasticizers during the first seconds of hydration. The impact of different admixtures varies within the first 10 s of hydration, depending on their properties such as anionic charge, type of anchor group, molecular structure, but also on the dosage applied. However, investigation of the impact of the side chain length of MPEG-PCEs did not lead to

significantly different ettringite crystal sizes, especially under microgravity, despite that it is well established that the combination of electrostatic and steric effect of dispersants is the most effective. This leads to three hypotheses for future investigations:

1) For high molecular PCEs possessing very long side chains, a hydration time of 10 s is too short to adsorb on the ettringite crystal surfaces to inhibit crystal growth in specific directions, especially under microgravity conditions where mass transport is the limiting factor.
2) The chosen dosage of 0.05 % bwoc for the PCEs is too low and therefore only few ettringite crystals are interacting with the PCEs while the majority grows regularly and thus the impact of PCEs statistically is not clearly visible.
3) The anionic charge of the superplasticizers, i.e. the ratio of methacrylic acid to macromonomer, is the determining force for adsorption on ettringite crystals and thus for the inhibition of ettringite crystal growth on the faces where polymers are adsorbed on the crystal surface.

Within the fourth part of this work, hydration of blends composed of 80 wt.% of neat C_3A_C or C_4AF, 15 wt.-% $CaSO_4$ hemihydrate and 5 wt.-% gypsum in synthetic cement pore solution under terrestrial and microgravity conditions was studied. The experiments conducted under terrestrial gravity conditions showed that…

- hydration of the $C_3A/CaSO_4 \cdot n\ H_2O$ blend leads to precipitation of an abundance of ettringite crystals exhibiting a rather stocky morphology and formation of some large hexagonal platelets of monosulfate.
- hydration of the $C_4AF/CaSO_4 \cdot n\ H_2O$ blend leads to ettringite crystals that are longer, but also thicker than in the case of C_3A_C. Additionally, only a small amount of monosulfate constituting of thin foils growing topotactical on the clinker was observed.

On the other hand, the hydration experiments performed under microgravity conditions showed that…

- hydration of the $C_3A/CaSO_4 \cdot n\ H_2O$ blend leads to ettringite crystals of similar size than those obtained in the presence of convection.
- hydration of the $C_4AF/CaSO_4 \cdot n\ H_2O$ blend leads to smaller ettringite crystals which are comparable in size to those obtained from the $C_3A/CaSO_4 \cdot n\ H_2O$ blend hydration.

It is known that the fast dissolution of the aluminate phases in the presence of sulfates leads to immediate precipitation of nanosized ettringite crystals and an alumina or ferrite gel possessing a low permeability, upon which the dissolution rate decreases strongly, and the dormant period of cement hydration starts. The comparable size of ettringite crystals formed in the $C_3A/CaSO_4$ system in the absence and presence of convection is probably due to this fast precipitation of low-permeable hydrates which hinders further crystal growth. Consequently, the bigger size of ettringite crystals formed in the presence of convection in the $C_4AF/CaSO_4$ system leads to the conclusion that mass transport is the rate determining step of ettringite crystal growth. The enhanced crystal growth might thus be attributed to a higher permeability of the hydrate phases precipitated on the aluminate surface, especially of the $Fe(OH)_3$ gel, or a lower precipitation rate which allows longer dissolution than in the case of C_3A.

Furthermore, the formation of the AF_m phases monosulfate and calcium aluminate hydrate was studied under terrestrial and microgravity conditions. Here, hydration of C_3A_C was conducted for 10 s with aqueous solutions containing $Ca(OH)_2$ or $CaSO_4$, respectively. Formation of the AF_m phases was successfully proven by XRD analysis. SEM imaging revealed that in the absence of convection, the clinker surface was covered in both cases very densely with thin foils of the calcium aluminate hydrates. In contrast, the experiments under terrestrial gravity conditions showed less, but thicker AF_m foils growing topotactical on the clinker surface. This is in accordance with previous experiments within this work where upon addition of water dissolution of the clinker phases starts, and consequently the boundary zone will be highly supersaturated very fast, while the bulk solution will possess a lower supersaturation, due to the limited mass transport away from the clinker surface. Consequently, it is likely that an

equilibrium between the solid clinker and the dissolved ions is reached and dissolution stops until nucleation and crystal growth starts. Because of the high supersaturation in the clinker-near zone, formation of an abundance of small nuclei in this boundary zone will occur, while nucleation in the bulk solution will be rather limited.

In the last part of this work, the crystallization of synthetic C-S-H prepared from flash precipitation of aqueous solutions of $Ca(NO_3)_2$ and Na_2SiO_3 was studied. The first series of experiments revealed that the primary particles of synthetic C-S-H prepared at pH values of 11.6 and 10.5 exhibit a globular morphology, precipitated under terrestrial as well as under microgravity conditions. In the neat C-S-H, the primary particles agglomerated to larger particles which sedimented. Precipitation of C-S-H in the presence of various types of PCEs also leads to C-S-H with a globular morphology, but the agglomerates were much smaller which was already indicated by the opacity of the obtained dispersion. The primary C-S-H particles were surrounded by a PCE polymer layer which stabilized the particles. Particle size distributions of the obtained C-S-H-PCE composites revealed that the size of the agglomerates is further dependent on the type of PCE present and is the same for all other reaction parameters (pH = 11.6 & 10.5, absence and presence of convection). The size of the agglomerates increased in the following order:

IPEG-50PC6 < APEG-34 < MPEG-114PC6 < MPEG-45PC10

A more detailed study on the impact of different types of PCEs on the structure and composition of synthetic C-S-H revealed that the type of PCE alters the crystallinity, the Ca/Si ratio and the molecular structure of C-S-H. A mechanism for the interaction of the PCE with C-S-H during crystallization was proposed. PCEs that lack of methyl groups in the acid present in their backbone, such as APEG- and IPEG-based PCEs have a higher ability to sequestrate Ca^{2+} ions from the solution, and thus inhibit the crystal growth of C-S-H and lead to lower Ca/Si ratios. Consequently, the formed C-S-H exhibits shorter silicate chains and the C-S-H sheets are more distorted which results in lower crystallinity.

In a further series of experiments, the crystallization of C-S-H in the absence and presence of two MPEG-PCE samples possessing different anionic charge was investigated. Freshly

precipitated C-S-H exhibited globular morphology, as described above. The obtained globules then transformed slowly into the characteristic foil-like morphology of C-S-H. Thus, it could be shown for the first time that C-S-H crystallization under the reaction parameters chosen follows a non-classical nucleation pathway, involving formation of a metastable precursor which must not exhibit the final crystal morphology. Heat flow calorimetry revealed that the formation of the metastable globular precursors is an endothermic process, confirming that the globular morphology is thermodynamically unfavoured. Subsequently, the globular droplets gradually dissolve and recrystallize into the well-known C-S-H nanofoils which is accompanied by an exothermic heat flow. On a molecular level, it was found that C-S-H in globular particles possesses more branched silicate chains, while the C-S-H nanofoils obtained exhibited rather long, unbranched silicate chains. Meanwhile, our earlier findings of this two-step nucleation process via amorphous spherical precursors with subsequent transformation into foils was also published by *Krautwurst* et al..[182]

In the presence of PCEs, however, the globular morphology of C-S-H is stabilized over a longer period of time by a polymer shell surrounding the C-S-H droplets. During aging, small nanofoils start to form within the droplets until the shell bursts and then recrystallization into the thermodynamically favoured foil modification proceeds rapidly. It was found that PCEs possessing a low anionic charge have a lower ability to stabilize the metastable globules than PCEs of a high anionic charge.

The findings within this work have shown that certain admixtures strongly interact with early cement hydrates already during the first seconds of hydration. Especially the formation of ettringite which represents the main anchoring site for superplasticizers, but also that of C-S-H which is the main constituent in Portland cement and responsible for its strength, was altered in the presence of PCEs. Despite of the different reaction conditions present in concretes (pH, ion concentration, various admixtures) this study has demonstrated that interactions such as intercalation, adsorption and encapsulation between early cement hydrates and admixtures present in concrete formulations, but also the possibility of non-classical crystallization pathways should be considered in future research and application.

7. Zusammenfassung

Im ersten Teil dieser Thesis wurde die Wechselwirkung zweier chemisch unterschiedlich aufgebauter Verzögerer, welche häufige Anwendung in der Tiefbohrzementierung finden, mit der reaktivsten Klinkerphase im Portlandzementsystem, dem C_3A, untersucht. Es konnte die erfolgreiche Interkalation beider Verzögerer während der Hydratation von C_3A in die Zwischenschichten der Doppelschichthydroxidstruktur von C_4AH_x gezeigt werden und somit die Bildung einer organisch-anorganischen Gast-Wirt-Struktur. Der Zwischenschichtabstand erhöhte sich durch die Interkalation der Co-Polymere von 0,8 nm auf 1,45 nm für das AA/AMPS Co-Polymer bzw. auf 1,68 nm für das IA/AMPS Co-Polymer. TG-MS Messungen zeigten, dass die interkalierten Co-Polymere höhere Temperaturstabilität besitzen. Darüber hinaus wurden die erhaltenen Ca_2Al-Verzögerer-LDHs einem Anionenaustausch mit SO_4^{2-} unterzogen, bei dem ca. 80% des hoch anionischen AA/AMPS Co-Polymers freigesetzt wurden bei einer Sulfatkonzentration entsprechend 200% der Anionenaustauschkapazität. Im Vergleich dazu wurden lediglich ca. 20% des IA/AMPS Co-Polymers, welches eine niedrigere anionische Ladungsdichte aufweist, ausgetauscht. Diese Ergebnisse zeigen, dass das IA/AMPS Co-Polymer, im Gegensatz zum AA/AMPS Co-Polymer, eine sehr starke Anziehungskraft gegenüber der positiv geladenen LDH-Struktur aufweist und nur sehr schwer wieder aus den Zwischenschichten herausdiffundiert sobald es einmal interkaliert ist. Dies konnte anhand von Wärmeflussmessungen während der Hydratation eines kommerziellen API Class G Tiefbohrzements, der einmal mit den reinen Co-Polymeren sowie den Ca_2Al-Verzögerer-LDHs versetzt wurde, bestätigt werden. Während die Hydratation des Zements im Falle eines Zusatzes des Ca_2Al-AA/AMPS-LDHs eine nahezu vergleichbare Verzögerung aufwies wie bei Zusatz des entsprechenden Co-Polymers selbst, konnte bei Zugabe de Ca_2Al-IA/AMPS-LDHs keine Verzögerung der Hydratation festgestellt werden.

Darüber hinaus legen die oben genannten Ergebnisse nahe, dass die Stabilität der Ca_2Al-Verzögerer-LDHs nicht ausschließlich von der anionischen Ladungsdichte des Co-Polymers abhängt, sondern auch von deren Molekülstruktur und Molekulargewicht. Das hochmolekulare IA/AMPS Co-Polymer, welches außerdem mehr Sulfatankergruppen besitzt, neigt deutlich weniger dazu aus den Zwischenschichten des LDHs freigesetzt zu werden als das AA/AMPS Co-Polymer, welches niedermolekularer ist und mehr Carboxylatgruppen besitzt.

Zusammenfassend hat diese Studie gezeigt, dass Verzögerer während der Zementhydratation in die schichtartigen AF_m-Phasen interkalieren können und die erhaltenen organisch-anorganischen Gast-Wirt-Strukturen unterschiedliche Stabilitäten aufweisen. Besonders während der Hydratation von C_3A-reichen Zementen mit niedrigem Sulfatträgergehalt kann es folglich durch Interkalation zu einem Verlust des gewünschten verzögernden Effekts dieser Zusatzmittel kommen.

Im zweiten Teil wurde das Potenzial von Ca_2Al-Formiat-LDHs als Erhärtungsbeschleuniger für Mörtel bewertet. Eine Voraussetzung für die Anwendung dieses Typs von LDH als Zementzusatzmittel ist die Entwicklung einer Synthesemethode, die leicht zur Produktion im industriellen Maßstab aufskaliert werden kann, wie z.B. die Synthese durch Co-Präzipitation. Die erfolgreiche Herstellung des Ca_2Al-Formiat-LDHs mittels Co-Präzipitation aus wässrigen Lösungen von $Ca(HCOO)_2$ und $Al(HCOO)_3$ konnte mittels XRD und SEM-Analyse bestätigt werden. Die Zwischenschichtabstände der Ca_2Al-Formiat-LDHs, welche durch Rehydratation und Co-Präzipitation hergestellt wurden, waren sehr gut vergleichbar und beide LDHs besaßen die typische folienartige Morphologie, wie mittels Rasterelektronenmikroskopie bestätigt werden konnte.

Ein signifikanter beschleunigender Effekt der synthetisierten Ca_2Al-Formiat-LDHs auf die Druck- und Biegezugfestigkeit von Mörteln innerhalb der ersten 24 Stunden der Hydratation konnte nur für den groben CEM I 32,5 R mit einem hohen Anteil an Aluminatphasen (18%) beobachtet werden. Die Mörtel, die mit den anderen beiden OPC-Proben hergestellt wurden, zeigten keine gesteigerte Festigkeit nach 16 und 24 Stunden. Der Mechanismus der Beschleunigung wurde mittels Wärmeflusskalorimetrie und in situ XRD-Messungen untersucht. Innerhalb der ersten 24 Stunden konnte eine deutlichere Abnahme der Intensität der Beugungsreflexe der Zementklinkerphasen in den Diffraktogrammen beobachtet werden, wenn dem Zement Ca_2Al-Formiat-LDH zugesetzt war. Im Gegensatz dazu konnte in der Kalorimetrie keine höhere Wärmefreisetzung innerhalb der ersten 24 Stunden beobachtet werden im Vergleich zur reinen Zementprobe. Darüber hinaus wurde eine erhöhte Wärmeentwicklung im Stadium der Sulfatverarmung (zwischen 20 – 48 Stunden) in Gegenwart des Ca_2Al-Formiat-LDHs beobachtet. Letzteres deutet darauf hin, dass das zum Hydrocalumit strukturverwandte Ca_2Al-formate-LDH hier als heterogener Nukleationskeim für den

Umkristallisationsprozess dient und damit die Umwandlung von Ettringit zu Monosulfat beschleunigt. Der Fokus dieser Studie war, eine simple, aufskalierbare Synthesemethode zu entwickeln sowie das Potenzial des damit hergestellten Ca_2Al-Formiat-LDH als Erhärtungsbeschleuniger allgemein zu bewerten. Um eine finale Bewertung des Potenzials geben zu können, müssen noch einige offene Fragen geklärt werden:

- Die hier erhaltenen Ergebnisse deuten darauf hin, dass nicht nur die Menge an Aluminatphase, sondern auch die Modifikation, d.h. orthorhombisches oder kubisches C_3A, im Zement eine entscheidende Rolle beim Zusatz von Ca_2Al-Formiat-LDH als Beschleuniger spielt.
- In zukünftigen Untersuchungen sollte nicht nur die Frühfestigkeit nach 24 Stunden, sondern auch die Festigkeit zu späteren Zeitpunkten, bspw. nach 7 Tagen, geprüft, sowie die Mikrostruktur der Mörtel in diesem Zeitraum untersucht werden, um einen beschleunigenden Effekt als Nukleationskeim für die Umwandlung von Ettringit zu Monosulfat zu bestätigen.
- Studien zum beschleunigenden Effekt von C-S-H Nanokeimen haben mittlerweile gezeigt, dass die Molekularstruktur und Partikelgröße von großer Bedeutung für die Wirkung der Additive sind und dass diese von sehr vielen Reaktionsparametern abhängig sind.[35, 129] Hier gibt es noch viele Stellschrauben für die Optimierung der Ca_2Al-Formiat-LDHs, z.B. mittels Variation des pH-Wertes während der Fällung, Variation des Ca/Al-Verhältnisses und somit der Oberflächenladung der Schichten oder die Stabilisierung der Partikel mittels Polyelektrolyten wie PCEs, um eine monodisperse Partikelgrößenverteilung im Nanometerbereich zu erhalten.

Im nächsten Kapitel dieser Arbeit wurde die Kristallisation von Ettringit in den ersten zehn Sekunden der Hydratation zweier kommerzieller Portlandzementproben unter irdischer und Mikrogravitation, d.h. in Gegenwart und Abwesenheit von Konvektion, untersucht. Die Experimente unter Mikrogravitation wurden auf Parabelflügen durchgeführt. Bei der Hydratation der reinen Zementproben konnten die Ergebnisse früherer Studien bestätigt werden, wo unter Mikrogravitation generell mehr, dafür aber kleinere Ettringitkristalle gebildet wurden.[159] Diese Beobachtungen können dem langsameren Stofftransport der Wachstumsbausteine zur Kristalloberfläche in Abwesenheit von Konvektion zugeordnet

werden. Außerdem konnte bestätigt werden, dass die Ettringitkristallisation sehr von der Zusammensetzung des Zements, insbesondere vom Anteil und der Modifikation der Aluminatphasen und der Gipsmenge, abhängig ist.

Ziel dieser Studie war es, mehr Klarheit bezüglich der Wechselwirkungen zwischen Fließmitteln und deren bevorzugter Adsorptionsstelle, dem Ettringit, während der ersten Sekunden der Zementhydratation zu bekommen. Die Erkenntnisse der Auswirkungen von Fließmitteln auf das Kristallwachstum von Ettringit können wie folgt zusammengefasst werden:

- In Gegenwart von Fließmitteln werden generell dünnere aber längere Kristalle gebildet, im Vergleich zu den eher untersetzten Ettringitkristallen, welche in der reinen Zementpaste gefunden wurden.
- Ein Einfluss der Seitenkettenlänge von MPEG-basierten PCEs, welche eine vergleichbare anionische Ladungsdichte im Polymerrückgrat aufwiesen, aber eine unterschiedliche Anzahl an Ethylenoxideinheiten (6 – 114) in der Seitenkette, auf die Morphologie von Ettringitkristallen konnte innerhalb der ersten zehn Sekunden der Hydratation nicht beobachtet werden.
- Mit zunehmender anionischer Ladungsdichte von MPEG-PCEs mit vergleichbaren Seitenkettenlängen konnte eine starke Erhöhung des Aspektverhältnisses beobachtet werden, insbesondere in Gegenwart stark anionischer PCEs wie der MPEG-PCE-Probe 45PC10. Die erhaltenen Ettringitkristalle besaßen geringere Durchmesser, aber nahmen in ihrer Länge zu.
- Mit Erhöhung der PCE-Dosierung von 0,05 Gew.-% bezogen auf den Zement auf 0,15 Gew.-% und 0,25 Gew.-% wurden Ettringitkristalle mit einer nahezu nadelförmigen Morphologie aufgrund von stark abnehmenden Durchmessern und zunehmenden Kristalllängen, gefunden.
- Polyphosphat-Kammpolymere weisen eine deutlich höhere Affinität zur Ettringitoberfläche auf als Polycarboxylatether und beeinflussen die Kristallmorphologie bereits signifikant bei einer niedrigen Dosierung von 0,05 Gew.-% bezogen auf den Zement.

- In Gegenwart von Polykondensat-Fließmitteln wurden höhere Werte für die Längen und Durchmesser der Ettringitkristalle gefunden. Das Aspektverhältnis nimmt mit zunehmender anionischer Ladungsdichte der Polymere zu.

Die oben genannten Effekte waren bei den Experimenten unter Erdgravitation generell stärker ausgeprägt als unter Mikrogravitation. Dies ist der langsameren Auflösungsgeschwindigkeit der Phasen und dem verringerten Stofftransport der Ionen aus der Grenzzone in die Bulklösung sowie der limitierten Diffusion der Polymere in Abwesenheit der Konvektion zuzuschreiben. Darüber hinaus deuten die Ergebnisse darauf hin, dass eine PCE-Dosierung von 0,05 Gew.-% bezogen auf den Zement möglicherweise zu niedrig ist, speziell für die erhöhte Anzahl an Kristallen, welche unter Mikrogravitation gebildet wurden. Dadurch werden weniger Kristalle in ihrem Wachstum von adsorbierten Polymeren beeinflusst, was sich wiederum in den gemessenen durchschnittlichen Kristallgrößen ausdrückt und folglich den Effekt der Polymere auf das Ettringitkristallwachstum in der Statistik verschleiert.

Die beobachteten erhöhten Aspektverhältnisse der Ettringitkristalle, welche in Gegenwart von Fließmitteln gebildet wurden, deutet darauf hin, dass eine schnelle Adsorption der Polymere auf den Seitenflächen der Ettringitkristalle stattfindet, welche das Wachstum in Richtung der *a*- und *b*-Achsen behindert, wohingegen das Wachstum entlang der *c*-Achse uneingeschränkt voranschreiten kann. Die erhöhten Kristalldurchmesser und -längen, welche in Gegenwart von Polykondensaten beobachtet wurden, legen die Vermutung nahe, dass die Auflösung von C_3A durch die Anwesenheit der Polymere unterstützt wird und eine eher zufällige Adsorption der Polymere auf den seitlichen Kristallflächen sowie auf den Endflächen oben und unten des Ettringits stattfindet.

Die erhaltenen Ergebnisse zeigen letztendlich, dass Nukleation und Kristallwachstum von Ettringit innerhalb der ersten Sekunden der Hydratation bereits von Fließmitteln beeinflusst werden. Die Auswirkung der unterschiedlichen Zusatzmittel variiert innerhalb der ersten zehn Sekunden in Abhängigkeit von deren Eigenschaften wie anionische Ladungsdichte, Art der Ankergruppe, Molekülstruktur aber auch der Dosierung. Es konnte jedoch kein signifikanter Effekt der Seitenkettenlänge von MPEG-PCEs auf die Ettringitkristallgröße gefunden werden,

insbesondere unter Mikrogravitation. Dies führt zu drei Hypothesen für zukünftige Untersuchungen:

- Die Hydratationszeit von zehn Sekunden ist zu kurz, insbesondere unter Mikrogravitationsbedingungen, wo Stofftransport der limitierende Schritt ist, damit hochmolekulare PCEs mit langen Seitenketten auf den Oberflächen der Ettringitkristalle adsorbieren und das Kristallwachstum in spezifische Richtungen inhibieren können.
- Die gewählte Dosierung von 0,05 Gew.-% für hochmolekulare PCEs ist zu gering, weshalb nur ein Bruchteil der Ettringitkristalle mit den PCEs wechselwirkt, während die Mehrheit der Kristalle uneingeschränkt wachsen kann und somit der Einfluss der PCEs statistisch nicht sichtbar wird.
- Die anionische Ladungsdichte der MPEG-PCE Fließmittel, d.h. das Verhältnis von Methacrylsäure zu Makromonomer, ist die entscheidende Größe für die Adsorption auf Ettringitkristallen und somit für die Behinderung des Kristallwachstums in jene Richtungen, wo die Polymere adsorbieren.

Im Rahmen des vierten Teils dieser Arbeit wurde die Hydratation von Mischungen bestehend aus 80 Gew.-% reinem C_3A_C bzw. C_4AF, 15 Gew.-% $CaSO_4$ Halbhydrat und 5 Gew.-% Gips in synthetischer Zementporenlösung unter Erd- und Mikrogravitation untersucht. Die Experimente unter Erdgravitation zeigten, dass…

- die Hydratation von $C_3A/CaSO_4 \cdot n\ H_2O$-Gemischen zur Ausfällung einer großen Menge an Ettringitkristallen führt, welche eine eher untersetzte Morphologie aufwiesen. Außerdem konnte die Bildung einer geringen Menge Monosulfat beobachtet werden, das aus großen hexagonalen Plättchen bestand.
- die Hydratation von $C_4AF/CaSO_4 \cdot n\ H_2O$-Gemischen zur Bildung von Ettringitkristallen führt, die länger aber auch dicker waren als im Falle des C_3A_C. Zusätzlich wurde ebenfalls ein sehr geringer Anteil an Monosulfat gebildet, welches aus sehr dünnen Folien bestand, die topotaktisch auf dem C_3A aufwuchsen.

Auf der anderen Seite zeigten die Versuche unter Mikrogravitation, dass…

- die Hydratation von $C_3A/CaSO_4 \cdot n\ H_2O$-Gemischen zu Ettringitkristallen von vergleichbarer Größe wie in Gegenwart von Konvektion führt.
- die Hydratation von $C_4AF/CaSO_4 \cdot n\ H_2O$-Gemischen zu generell kleineren Ettringitkristallen führt, welche bezüglich Größe vergleichbar mit denen sind, die während der Hydratation von $C_3A/CaSO_4 \cdot n\ H_2O$-Gemischen gebildet wurden.

Es ist bekannt, dass die schnelle Auflösung von Aluminatphasen in Gegenwart von Sulfaten zu einer sofortigen Ausfällung von nanokristallinem Ettringit führt sowie zur Bildung von Aluminat- bzw. Eisenhydroxidgelen, welche eine geringe Durchlässigkeit besitzen. Dadurch wird die Auflösungsgeschwindigkeit stark reduziert und die dormante Periode der Zementhydratation beginnt. Die vergleichbaren Größen der gebildeten Ettringitkristalle im $C_3A/CaSO_4 \cdot n\ H_2O$ System in Ab- und Anwesenheit von Konvektion ist voraussichtlich auf diese sehr schnelle Ausfällung von Hydratphasen mit geringer Permeabilität zurückzuführen, welche ein weiteres Wachstum behindern. Folglich sind die beobachteten erhöhten Kristallgrößen in Gegenwart der Konvektion im $C_4AF/CaSO_4 \cdot n\ H_2O$-System auf den Stofftransport als geschwindigkeits-bestimmenden Schritt für das Ettringitkristallwachstum zurückzuführen. Das erhöhte Kristallwachstum könnte somit auf einer höheren Durchlässigkeit der ausgefällten Hydratphasen, insbesondere des $Fe(OH)_3$-Gels, auf der C_4AF-Oberfläche beruhen oder einer langsameren Ausfällungsrate der Hydratphase, welche eine längere Auflösungszeit zur Folge hätte als im Falle des C_3A.

In weiteren Experimenten wurde die Bildung der AF_m-Phasen Calciumaluminathydrat und Monsosulfat unter Erd- und Mikrogravitation untersucht. Hierzu wurde kubisches C_3A für zehn Sekunden in wässrigen Lösungen von $Ca(OH)_2$ bzw. $CaSO_4$-Hemihydrat hydratisiert. Die Bildung der oben genannten AF_m-Phasen konnte mittels XRD Analyse bestätigt werden. Durch Rasterelektronenmikroskopie konnte weiter gezeigt werden, dass die C_3A-Oberfläche in Abwesenheit von Konvektion im Falle beider Synthesen sehr dicht mit dünnen Folien der Calciumaluminathydrate bewachsen war. Im Gegensatz dazu wurden bei den Experimenten unter Erdgravitation weniger aber deutlich dickere AF_m-Folien gefunden, welche topotaktisch auf der Oberfläche aufwuchsen. Das ist in guter Übereinstimmung mit vorangehenden

Experimenten, bei denen generell mit der Wasserzugabe die Auflösung der Phasen beginnt und sich als Konsequenz sehr schnell eine hohe Übersättigung in der Grenzschicht zwischen Zementphase und Bulklösung einstellt, während die Bulklösung selbst, aufgrund des geringen Stofftransports vom C_3A weg, eine geringe Übersättigung aufweist. Daraus folgend ist es naheliegend, dass sich ein Lösungsgleichgewicht zwischen der festen Phase und den gelösten Ionen einstellt und die Auflösung stoppt, bis Nukleation und Kristallwachstum starten. Aufgrund der hohen Übersättigung in der C_3A-nahen Region kommt es zur Bildung von sehr vielen kleinen Kristallisationskeimen in dieser Grenzschicht, wohingegen Keimbildung in der weniger übersättigten Bulklösung limitiert ist.

Im letzten Abschnitt dieser Arbeit wurde die Kristallisation von synthetischem C-S-H, welches durch Ausfällung aus wässrigen $Ca(NO_3)_2$- und Na_2SiO_3-Lösungen hergestellt wurde, untersucht. Die erste Serie von Experimenten zeigte, dass die Primärpartikel von bei pH-Werten von 10,5 bzw. 11,6 ausgefälltem C-S-H eine globulare Morphologie aufweisen, sowohl unter Erd- als auch unter Mikrogravitation. Reines ausgefälltes C-S-H agglomerierte zu großen Partikeln, die schnell sedimentierten. Ausfällung in Gegenwart von unterschiedlichen Arten von PCEs hingegen führte ebenfalls zu einer globularen Morphologie, aber die gebildeten Agglomerate waren deutlich kleiner, was sich bereits durch die Opazität der erhaltenen Dispersion bemerkbar machte. Die C-S-H Primärpartikel waren umgeben von einer Polymerschicht, welche die Partikel stabilisierte. Die bestimmten Partikelgrößenverteilungen der C-S-H-PCE Komposite zeigten, dass die Größe der Agglomerate augenscheinlich in erster Linie von der Art des zugegebenen PCEs abhängig ist und darüber hinaus gleich über alle anderen Reaktionsparameter ist (pH 11,6 & 10,5, An- und Abwesenheit von Konvektion). Die Größe der Agglomerate nimmt gemäß folgender Reihe zu:

IPEG-50PC6 < APEG-34 < MPEG-114PC6 < MPEG-45PC10

Eine detaillierte Untersuchung zum Einfluss der unterschiedlichen PCE-Typen auf die Struktur und Zusammensetzung des synthetischen C-S-H zeigte, dass je nach Art des PCEs Kristallinität, Ca/Si-Verhältnis und die molekulare Struktur von C-S-H beeinflusst werden können. Ein Mechanismus zur Wechselwirkung von PCEs mit C-S-H während der Kristallisation wurde vorgeschlagen. Folglich haben PCEs, die in ihrem Rückgrat keine oder

nur wenige Methylgruppen haben, wie bspw. APEG- oder IPEG-basierte PCEs, eine höhere Fähigkeit Ca^{2+}-Ionen aus der Lösung zu komplexieren und somit zu entfernen, wodurch das Kristallwachstum von C-S-H behindert wird und es zu niedrigeren Ca/Si-Verhältnissen kommt. Daraus ergeben sich auch kürzere Silikatkettenlängen und die C-S-H-Schichten ordnen sich verzerrter an, was sich in geringerer Kristallinität auszeichnet.

In weiteren Untersuchungen wurde die Kristallisation von C-S-H in Gegenwart und Abwesenheit von zwei MPEG-PCE-Proben mit unterschiedlicher anionischer Ladungsdichte beobachtet. Frisch ausgefälltes C-S-H zeigte eine globulare Morphologie, wie bereits oben beschrieben. Die erhaltenen Globuli wandelten sich langsam in die charakteristische Folien-Morphologie des C-S-H um. Somit konnte erstmals gezeigt werden, dass C-S-H unter den gegebenen Reaktionsbedingungen einem nicht-klassischen Nukleationspfad folgt, welcher die Bildung eines metastabilen Precursors, der nicht zwingend die finale Kristallstruktur besitzen muss, einschließt. Wärmeflusskalorimetriemessungen bestätigten, dass die Bildung des metastabilen globularen Precursors ein endothermer Prozess ist und dass die globulare Morphologie thermodynamisch ungünstig ist. Darauffolgend lösen sich die globularen Tröpfchen schrittweise auf und bilden mittels Umkristallisation die bekannten C-S-H-Nanofolien. Dieser Vorgang wird von einem exothermen Wärmefluss begleitet. Auf molekularer Ebene konnte gezeigt werden, dass C-S-H mit globularer Morphologie mehr verzweigte Silikatketten aufweist, während die erhaltenen C-S-H-Folien eher aus langen unverzweigten Silikatketten bestanden. Mittlerweile wurde dieser von uns zuerst entdeckte, zweistufige Nukleationspozess von C-S-H über die Bildung eines amorphen sphärischen Precursors mit anschließender Umwandlung in Folien ebenfalls von *Krautwurst* et al. nachgewiesen.[182]

In Gegenwart von PCEs konnte beobachtet werden, dass die globulare Morphologie von C-S-H über einen längeren Zeitraum durch die Bildung einer die Tröpfchen umgebenden Polymerhülle stabilisiert wird. Während der Alterung bildeten sich im Kern der Globuli langsam kleine Nanofolien aus, bis diese schlussendlich die Polymerhülle durchbrechen. Die nachfolgende Umkristallisation in die thermodynamisch bevorzugte Folien-Morphologie schreitet schließlich schnell voran. PCEs, die eine geringe anionische Ladungsdichte besitzen,

können die metastabilen Globuli weniger gut stabilisieren als PCEs mit einer hohen anionischen Ladungsdichte.

Im Rahmen dieser Arbeit konnte gezeigt werden, dass bestimmte Zusatzmittel bereits in den ersten Sekunden der Hydratation starke Wechselwirkungen mit den frühen Zementhydratphasen eingehen. Insbesondere die Bildung von Ettringit, welcher die Hauptadsorptionsfläche für Fließmittel zur Verfügung stellt, aber auch die Bildung von C-S-H, welches maßgeblich für die Festigkeit in Portlandzement ist, wurden durch die Gegenwart von PCEs beeinflusst. Trotz der unterschiedlichen Reaktionsbedingungen in Betonen (pH, Ionenkonzentrationen, verschiedene Zusatzmittel) konnte in dieser Studie gezeigt werden, dass Wechselwirkungen wie z.B. Interkalation, Adsorption oder Verkapselung zwischen frühen Hydratphasen und Zusatzmitteln in Betonformulierungen, aber auch die Möglichkeit nicht-klassischer Kristallisationsvorgänge in zukünftiger Forschung und Anwendung berücksichtigt werden sollten.

8. References

1. https://www.statista.com/statistics/219343/cement-production-worldwide/ (accessed 26.05.2018).
2. https://de.wikipedia.org/wiki/Marina_Bay_Sands (accessed 06.12.2018).
3. Li, Z., Fresh Concrete. In *Advanced Concrete Technology*, Wiley: Hoboken, NJ, USA, **2011**.
4. Black, L.; Garbev, K.; Stemmermann, P.; Hallam, K. R.; Allen, G. C., Characterisation of crystalline C-S-H phases by X-ray photoelectron spectroscopy. *Cement and Concrete Research* **2003**, *33* (6), 899-911.
5. De Yoreo, J. J.; Gilbert, P. U. P. A.; Sommerdijk, N. A. J. M.; Penn, R. L.; Whitelam, S.; Joester, D.; Zhang, H.; Rimer, J. D.; Navrotsky, A.; Banfield, J. F.; Wallace, A. F.; Michel, F. M.; Meldrum, F. C.; Cölfen, H.; Dove, P. M., Crystallization by particle attachment in synthetic, biogenic, and geologic environments. *Science* **2015**, *349* (6247).
6. DeLucas, L. J.; Moore, K. M.; Long, M. M.; Rouleau, R.; Bray, T.; Crysel, W.; Weise, L., Protein crystal growth in space, past and future. *Journal of Crystal Growth* **2002**, *237-239*, 1646-1650.
7. McPherson, A., Virus and protein crystal growth on earth and in microgravity. *Journal of Physics D: Applied Physics* **1993**, *26* (8B), B104.
8. Meier, M. R.; Sarigaphuti, M.; Sainamthip, P.; Plank, J., Early hydration of Portland cement studied under microgravity conditions. *Construction and Building Materials* **2015**, *93*, 877-883.
9. Meier, M. R.; Plank, J., Crystal growth of $[Ca_3Al(OH)_6 \cdot 12H_2O]_2 \cdot (SO_4)_3 \cdot 2H_2O$ (ettringite) under microgravity: On the impact of anionicity of polycarboxylate comb polymers. *Journal of Crystal Growth* **2016**, *446*, 92-102.
10. Habbaba, A.; Dai, Z.; Plank, J., Formation of organo-mineral phases at early addition of superplasticizers: The role of alkali sulfates and C3A content. *Cement and Concrete Research* **2014**, *59*, 112-117.
11. Plank, J.; von Hoessle, F., Formation of an Inorganic-Organic Host-Guest Material by Intercalation of Acetone Formaldehyde Sulfite Polycondensate into a Hydrocalumite Structure. *Zeitschrift für anorganische und allgemeine Chemie* **2010**, *636* (8), 1533-1537.

12. von Hoessle, F.; Plank, J.; Leroux, F., Intercalation of sulfonated melamine formaldehyde polycondensates into a hydrocalumite LDH structure. *Journal of Physics and Chemistry of Solids* **2015**, *80*, 112-117.
13. Aggoun, S.; Cheikh-Zouaoui, M.; Chikh, N.; Duval, R., Effect of some admixtures on the setting time and strength evolution of cement pastes at early ages. *Construction and Building Materials* **2008**, *22* (2), 106-110.
14. Heikal, M., Effect of calcium formate as an accelerator on the physicochemical and mechanical properties of pozzolanic cement pastes. *Cement and Concrete Research* **2004**, *34* (6), 1051-1056.
15. Bentz, D. P.; Zunino, F.; Lootens, D., Chemical vs. Physical Acceleration of Cement Hydration. *Concrete international : design & construction* **2016**, *38* (11), 37-44.
16. Nicoleau, L.; Gädt, T.; Chitu, L.; Maier, G.; Paris, O., Oriented aggregation of calcium silicate hydrate platelets by the use of comb-like copolymers. *Soft Matter* **2013**, *9* (19), 4864-4874.
17. Gordijo, C. R.; Leopoldo Constantino, V. R.; de Oliveira Silva, D., Evidences for decarbonation and exfoliation of layered double hydroxide in N,N-dimethylformamide–ethanol solvent mixture. *Journal of Solid State Chemistry* **2007**, *180* (7), 1967-1976.
18. Iyi, N.; Ebina, Y.; Sasaki, T., Water-Swellable MgAl−LDH (Layered Double Hydroxide) Hybrids: Synthesis, Characterization, and Film Preparation. *Langmuir* **2008**, *24* (10), 5591-5598.
19. Manohara, G. V.; Kunz, D. A.; Kamath, P. V.; Milius, W.; Breu, J., Homogeneous Precipitation by Formamide Hydrolysis: Synthesis, Reversible Hydration, and Aqueous Exfoliation of the Layered Double Hydroxide (LDH) of Ni and Al. *Langmuir* **2010**, *26* (19), 15586-15591.
20. Plank, J.; Hirsch, C., Superplasticizer Adsorption on Synthetic Ettringite. *Special Publication* **2003**, *217*.
21. Zou, N.; Plank, J., Intercalation of Sulfanilic Acid-Phenol-Formaldehyde Polycondensate into Hydrocalumite Type Layered Double -Hydroxide. *Zeitschrift für anorganische und allgemeine Chemie* **2012**, *638* (14), 2292-2296.
22. Locher, F. W., *Zement: Grundlagen der Herstellung und Verwendung*. Verlag Bau und Technik: Düsseldorf, Germany, **2000**.

23. Odler, I., 6 - Hydration, Setting and Hardening of Portland Cement. In *Lea's Chemistry of Cement and Concrete (Fourth Edition)*, Hewlett, P. C., Ed., Butterworth-Heinemann: Oxford, UK, **1998**; pp 241-297.
24. Stark, J.; Wicht, B., *Zement und Kalk: Der Baustoff als Werkstoff*. Birkhäuser Verlag: Basel, Switzerland, **2000**.
25. Plank, J.; Stephan, D.; Hirsch, C., Bauchemie. In *Chemische Technik - Prozesse und Produkte, Band 7: Industrieprodukte*, Küchler, W., Ed. Wiley-VCH: Weinheim, Germany, **2004**; Vol. Band 7.
26. Pommersheim, J.; Chang, J., Kinetics of hydration of tricalcium aluminate in the presence of gypsum. *Cement and Concrete Research* **1988**, *18* (6), 911-922.
27. Collepardi, M.; Baldini, G.; Pauri, M.; Corradi, M., Retardation of Tricalcium Aluminate Hydration by Calcium Sulfate. *Journal of the American Ceramic Society* **1979**, *62* (1-2), 33-35.
28. Brown, P.; Barret, P.; Double, D. D.; Frohnsdorff, G.; Johansen, V.; Parrot, L. J.; Pommersheim, J. M.; Regourd, M.; Scrivener, K.; Taylor, H. F. W.; Young, J. F., The hydration of tricalcium aluminate and tetracalcium aluminoferrite in the presence of calcium sulfate. *Materials and Structures* **1986**, *19* (2), 137-147.
29. Taylor, H. F. W., *Cement Chemistry*. Thomas Telford: London, UK, **1997**.
30. Xue, W.; Bandyopadhyay, A.; Bose, S., Mesoporous calcium silicate for controlled release of bovine serum albumin protein. *Acta Biomaterialia* **2009**, *5* (5), 1686-1696.
31. Jain, S. K.; Awasthi, A. M.; Jain, N. K.; Agrawal, G. P., Calcium silicate based microspheres of repaglinide for gastroretentive floating drug delivery: Preparation and in vitro characterization. *Journal of Controlled Release* **2005**, *107* (2), 300-309.
32. Rodríguez-Lorenzo, L. M.; García-Carrodeguas, R.; Rodríguez, M. A.; De Aza, S.; Jiménez, J.; López-Bravo, A.; Fernandez, M.; Román, J. S., Synthesis, characterization, bioactivity and biocompatibility of nanostructured materials based on the wollastonite-poly(ethylmethacrylate-co-vinylpyrrolidone) system. *Journal of Biomedical Materials Research Part A* **2009**, *88A* (1), 53-64.
33. Xu, S.; Lin, K.; Wang, Z.; Chang, J.; Wang, L.; Lu, J.; Ning, C., Reconstruction of calvarial defect of rabbits using porous calcium silicate bioactive ceramics. *Biomaterials* **2008**, *29* (17), 2588-2596.

34. Lothenbach, B.; Nonat, A., Calcium silicate hydrates: Solid and liquid phase composition. *Cement and Concrete Research* **2015**, *78*, 57-70.
35. John, E.; Matschei, T.; Stephan, D., Nucleation seeding with calcium silicate hydrate – A review. *Cement and Concrete Research* **2018**, *113*, 74-85.
36. Garrault-Gauffinet, S.; Nonat, A., Experimental investigation of calcium silicate hydrate (C-S-H) nucleation. *Journal of Crystal Growth* **1999**, *200* (3), 565-574.
37. Garrault, S.; Finot, E.; Lesniewska, E.; Nonat, A., Study of C-S-H growth on C_3S surface during its early hydration. *Materials and Structures* **2005**, *38* (4), 435-442.
38. Gauffinet, S.; Finot, É.; Lesniewska, E.; Nonat, A., Observation directe de la croissance d'hydrosilicate de calcium sur des surfaces d'alité et de silice par microscopie à force atomique. *Comptes Rendus de l'Académie des Sciences - Series IIA - Earth and Planetary Science* **1998**, *327* (4), 231-236.
39. Glasser, F. P.; Lachowski, E. E.; Macphee, D. E., Compositional Model for Calcium Silicate Hydrate (C-S-H) Gels, Their Solubilities, and Free Energies of Formation. *Journal of the American Ceramic Society* **1987**, *70* (7), 481-485.
40. Lecoq, X. Etude de l'hydratation a concentration controlee du silicate tricalcique Ca_3SiO_5 et des caracteristiques de ses produits de reaction. *Thesé de doctorat*, Université de Bourgogne, Dijon, **1993**.
41. Grutzeck, M.; Benesi, A.; Fanning, B., Silicon-29 Magic Angle Spinning Nuclear Magnetic Resonance Study of Calcium Silicate Hydrates. *Journal of the American Ceramic Society* **1989**, *72* (4), 665-668.
42. Stade, H.; Wieker, W., Zum Aufbau schlecht geordneter Calciumhydrogensilicate. I. Bildung und Eigenschaften einer schlecht geordneten Calciumhydrogendisilicatphase. *Zeitschrift für anorganische und allgemeine Chemie* **1980**, *466* (1), 55-70.
43. Myers, R. J.; Bernal, S. A.; San Nicolas, R.; Provis, J. L., Generalized Structural Description of Calcium–Sodium Aluminosilicate Hydrate Gels: The Cross-Linked Substituted Tobermorite Model. *Langmuir* **2013**, *29* (17), 5294-5306.
44. Damidot, D.; Nonat, A.; Barret, P.; Bertrandie, D.; Zanni, H.; Rassem, R., C_3S hydration in diluted and stirred suspensions: (III) NMR study of C-S-H precipitated during the two kinetic steps. *Advances in Cement Research* **1995**, *7* (25), 1-8.
45. Klur, I.; Pollet, B.; Virlet, J.; Nonat, A., C-S-H Structure Evolution with Calcium Content by Multinuclear NMR. In *Nuclear Magnetic Resonance Spectroscopy of Cement-Based*

Materials, Colombet, P.; Zanni, H.; Grimmer, A.-R.; Sozzani, P., Eds., Springer Berlin Heidelberg: Berlin, Heidelberg, Germany, **1998**; pp 119-141.

46. Okada, Y.; Ishida, H.; Mitsuda, T., ^{29}Si NMR Spectroscopy of Silicate Anions in Hydrothermally Formed C-S-H. *Journal of the American Ceramic Society* **1994**, *77* (3), 765-768.
47. Manzano, H.; Dolado, J. S.; Ayuela, A., Elastic properties of the main species present in Portland cement pastes. *Acta Materialia* **2009**, *57* (5), 1666-1674.
48. Matsuyama, H.; Young, J. F., Synthesis of calcium silicate hydrate/polymer complexes: Part I. Anionic and nonionic polymers. *Journal of Materials Research* **1999**, *14* (08), 3379-3388.
49. Beaudoin, J. J.; Raki, L.; Alizadeh, R., A ^{29}Si MAS NMR study of modified C–S–H nanostructures. *Cement and Concrete Composites* **2009**, *31* (8), 585-590.
50. Popova, A.; Geoffroy, G.; Renou-Gonnord, M.-F.; Faucon, P.; Gartner, E., Interactions between Polymeric Dispersants and Calcium Silicate Hydrates. *Journal of the American Ceramic Society* **2000**, *83* (10), 2556-2560.
51. Cappelletto, E.; Borsacchi, S.; Geppi, M.; Ridi, F.; Fratini, E.; Baglioni, P., Comb-Shaped Polymers as Nanostructure Modifiers of Calcium Silicate Hydrate: A ^{29}Si Solid-State NMR Investigation. *The Journal of Physical Chemistry C* **2013**, *117* (44), 22947-22953.
52. Rives, V.; Angeles Ulibarri, M. a., Layered double hydroxides (LDH) intercalated with metal coordination compounds and oxometalates. *Coordination Chemistry Reviews* **1999**, *181* (1), 61-120.
53. Li, F.; Duan, X., Applications of Layered Double Hydroxides. In *Layered Double Hydroxides*, Duan, X.; Evans, D. G., Eds., Springer Berlin Heidelberg: Berlin, Heidelberg, Germany, **2006**; pp 193-223.
54. Evans, D. G.; Slade, R. C. T., Structural Aspects of Layered Double Hydroxides. In *Layered Double Hydroxides*, Duan, X.; Evans, D. G., Eds. Springer Berlin Heidelberg: Berlin, Heidelberg, Germany, **2006**; pp 1-87.
55. Goh, K.-H.; Lim, T.-T.; Dong, Z., Application of layered double hydroxides for removal of oxyanions: A review. *Water Research* **2008**, *42* (6), 1343-1368.
56. Lerf, A., Different modes and consequences of electron transfer in intercalation compounds. *Journal of Physics and Chemistry of Solids* **2004**, *65* (2), 553-563.

57. O´Hare, D., In *Inorganic Materials*, Bruce, D. W.; O'Hare, D., Eds., J. Wiley: England, **1992**; p 166.
58. He, J.; Wei, M.; Li, B.; Kang, Y.; Evans, D. G.; Duan, X., Preparation of Layered Double Hydroxides. In *Layered Double Hydroxides*, Duan, X.; Evans, D. G., Eds., Springer Berlin Heidelberg: Berlin, Heidelberg, Germany, **2006**; pp 89-119.
59. P. Newman, S.; Jones, W., Synthesis, characterization and applications of layered double hydroxides containing organic guests. *New Journal of Chemistry* **1998**, *22* (2), 105-115.
60. Cavani, F.; Trifirò, F.; Vaccari, A., Hydrotalcite-type anionic clays: Preparation, properties and applications. *Catalysis Today* **1991**, *11* (2), 173-301.
61. Plank, J.; Zou, N.; Zhao, Z.; Dekany, I., Preparation and Properties of a Graphene Oxide Intercalation Compound Utilizing Hydrocalumite Layered Double Hydroxide as Host Structure. *Zeitschrift für anorganische und allgemeine Chemie* **2014**, *640* (7), 1413-1419.
62. Yu, B.; Bian, H.; Plank, J., Self-assembly and characterization of Ca–Al–LDH nanohybrids containing casein proteins as guest anions. *Journal of Physics and Chemistry of Solids* **2010**, *71* (4), 468-472.
63. Israëli, Y.; Taviot-Guého, C.; Besse, J.-P.; Morel, J.-P.; Morel-Desrosiers, N., Thermodynamics of anion exchange on a chloride-intercalated zinc–aluminum layered double hydroxide: a microcalorimetric study. *Journal of the Chemical Society, Dalton Transactions* **2000**, (5), 791-796.
64. Morel-Desrosiers, N.; Pisson, J.; Israëli, Y.; Taviot-Guého, C.; Besse, J.-P.; Morel, J.-P., Intercalation of dicarboxylate anions into a Zn–Al–Cl layered double hydroxide: microcalorimetric determination of the enthalpies of anion exchange. *Journal of Materials Chemistry* **2003**, *13* (10), 2582-2585.
65. Carlino, S., The intercalation of carboxylic acids into layered double hydroxides: a critical evaluation and review of the different methods. *Solid State Ionics* **1997**, *98* (1), 73-84.
66. Kim, T.-H.; Heo, Il; Paek, S.-M.; Park, C.-B.; Choi, A.-J.; Lee, S.-H.; Choy, J.-H.; Oh, J.-M., Layered Metal Hydroxides Containing Calcium and Their Structural Analysis. *Bulletin of the Korean Chemical Society* **2012**, *33* (6), 1845-1850.
67. Khan, A. I.; O'Hare, D., Intercalation chemistry of layered double hydroxides: recent developments and applications. *Journal of Materials Chemistry* **2002**, *12* (11), 3191-3198.

68. Uchikawa, H.; Sawaki, D.; Hanehara, S., Influence of kind and added timing of organic admixture on the composition, structure and property of fresh cement paste. *Cement and Concrete Research* **1995**, *25* (2), 353-364.
69. Aitcin, P.-C.; Jolicoeur, C.; MacGregor, J. G., Superplasticizers: How they work and why they occasionally don't. *Concrete international* **1994**, *16* (5), 45-52.
70. Sakai E.; Yamada. K.; Ohta A. , Molecular Structure and Dispersion-Adsorption Mechanisms of Comb-Type Superplasticizers Used in Japan. *Journal of Advanced Concrete Technology* **2003**, *1* (1), 16-25.
71. Plank, J.; Dai, Z.; Andres, P. R., Preparation and characterization of new Ca–Al–polycarboxylate layered double hydroxides. *Materials Letters* **2006**, *60* (29), 3614-3617.
72. Plank, J.; Keller, H.; Andres, P. R.; Dai, Z., Novel organo-mineral phases obtained by intercalation of maleic anhydride–allyl ether copolymers into layered calcium aluminum hydrates. *Inorganica Chimica Acta* **2006**, *359* (15), 4901-4908.
73. Raki, L.; Beaudoin, J. J.; Mitchell, L., Layered double hydroxide-like materials: nanocomposites for use in concrete. *Cement and Concrete Research* **2004**, *34* (9), 1717-1724.
74. Moore, A.; Taylor, H. F. W., Crystal Structure of Ettringite. *Nature* **1968**, *218*, 1048.
75. Mantellato, S.; Palacios, M.; Flatt, R. J., Impact of sample preparation on the specific surface area of synthetic ettringite. *Cement and Concrete Research* **2016**, *86*, 20-28.
76. Goetz-Neunhoeffer, F.; Neubauer, J., Refined ettringite ($Ca_6Al_2(SO_4)_3(OH)_{12}{\cdot}26H_2O$) structure for quantitative X-ray diffraction analysis. *Powder Diffraction* **2012**, *21* (1), 4-11.
77. Goetz-Neunhoeffer, F.; Neubauer, J.; Schwesig, P., Mineralogical characteristics of ettringites synthesized from solutions and suspensions. *Cement and Concrete Research* **2006**, *36* (1), 65-70.
78. Kreppelt, F.; Weibel, M.; Zampini, D.; Romer, M.; Influence of solution chemistry on the hydration of polished clinker surfaces - A study of different types of polycarboxylic acid-based admixtures. *Cement and Concrete Research* **2002**, *32* (2), 187-198.
79. Yoshioka, K.; Tazawa, E.-i.; Kawai, K.; Enohata, T., Adsorption characteristics of superplasticizers on cement component minerals. *Cement and Concrete Research* **2002**, *32* (10), 1507-1513.

80. Lange, A.; Plank, J., Formation of Nano-Sized Ettringite Crystals Identified as Root Cause for Cement Incompatibility of PCE Superplasticizers. In *Nanotechnology in Construction: Proceedings of NICOM5*, Sobolev, K.; Shah, S. P., Eds. Springer International Publishing: Cham, Switzerland, **2015**, pp 55-63.
81. Jansen, D.; Neubauer, J.; Goetz-Neunhoeffer, F.; Haerzschel, R.; Hergeth, W. D., Change in reaction kinetics of a Portland cement caused by a superplasticizer - Calculation of heat flow curves from XRD data. *Cement and Concrete Research* **2012**, *42* (2), 327-332.
82. Zingg, A.; Holzer, L.; Kaech, A.; Winnefeld, F.; Pakusch, J.; Becker, S.; Gauckler, L., The microstructure of dispersed and non-dispersed fresh cement pastes - New insight by cryo-microscopy. *Cement and Concrete Research* **2008**, *38* (4), 522-529.
83. Cody, A. M.; Lee, H.; Cody, R. D.; Spry, P. G., The effects of chemical environment on the nucleation, growth, and stability of ettringite $[Ca_3Al(OH)_6]_2(SO_4)_3 \cdot 26H_2O$. *Cement and Concrete Research* **2004**, *34* (5), 869-881.
84. Dalas, F.; Pourchet, S.; Rinaldi, D.; Nonat, A.; Sabio, S.; Mosquet, M., Modification of the rate of formation and surface area of ettringite by polycarboxylate ether superplasticizers during early C_3A-$CaSO_4$ hydration. *Cement and Concrete Research* **2015**, *69*, 105-113.
85. Lei, L.; Meier, M. R.; Rinkenburger, A.; Zheng, B.; Fu, L.; Plank, J., Early Hydration of Portland Cement Admixed with Polycarboxylates Studied Under Terrestric and Microgravity Conditions. *Journal of Advanced Concrete Technology* **2016**, *14* (3), 102-107.
86. Malinin, A., Development of PCE in Russia. In *2nd International Symposium on PCE Technology*, Plank, J., Ed., TUM Center for Advanced PCE Studies: Munich, Germany, **2015**.
87. Plank, J.; Dugonjić-Bilić, F.; Lummer, N. R., Modification of the molar anionic charge density of acetone–formaldehyde–sulfite dispersant to improve adsorption behavior and effectiveness in the presence of CaAMPS®-co-NNDMA cement fluid loss polymer. *Journal of Applied Polymer Science* **2009**, *111* (4), 2018-2024.
88. Lange, A., Studien zur Zementkompatibilität von Polycarboxylat-Fließmitteln sowie zum Einfluss ihres HLB-Wertes auf das rheologische Verhalten von Mörtel. *Dissertation,* Lehrstuhl für Bauchemie, Technische Universität München, München **2015**.

89. Nagare, K. Storage and/or transportation method of polyalkylene glycol monomers. US7030282B2, **2006**.
90. Mosquet, M.; Chevalier, Y.; Brunel, S.; Guicquero, J. P.; Le Perchec, P., Polyoxyethylene di-phosphonates as efficient dispersing polymers for aqueous suspensions. *Journal of Applied Polymer Science* **1997**, *65* (12), 2545-2555.
91. Dalas, F.; Nonat, A.; Pourchet, S.; Mosquet, M.; Rinaldi, D.; Sabio, S., Tailoring the anionic function and the side chains of comb-like superplasticizers to improve their adsorption. *Cement and Concrete Research* **2015**, *67*, 21-30.
92. Wieland, P.; Kraus, A.; Albrecht, G.; Becher, K.; Grassl H., Polycondensation product base on aromatic or heteroaromatic compounds, method for the production thereof, and use thereof. WO2006042709A8, **2008**.
93. Stecher, J.; Plank, J.; In *Polyphosphate comb polymers – A novel kind of concrete superplasticizer exhibiting unique properties*, 2nd International Conference on Polycarboxylate Superplasticizers (PCE 2017), Garching, Germany, Plank, J.; Lei, L., Eds., Garching, Germany, 2017; pp 235-250.
94. Plank, J.; Hirsch, C., Impact of zeta potential of early cement hydration phases on superplasticizer adsorption. *Cement and Concrete Research* **2007**, *37* (4), 537-542.
95. Feigin, R. I.; Napper, D. H., Depletion stabilization and depletion flocculation. *Journal of Colloid and Interface Science* **1980**, *75* (2), 525-541.
96. Pourchet, S.; Liautaud, S.; Rinaldi, D.; Pochard, I., Effect of the repartition of the PEG side chains on the adsorption and dispersion behaviors of PCP in presence of sulfate. *Cement and Concrete Research* **2012**, *42* (2), 431-439.
97. Winnefeld, F.; Becker, S.; Pakusch, J.; Goetz, T., Effects of the molecular architecture of comb-shaped superplasticizers on their performance in cementitious systems. *Cement and Concrete Composites* **2007**, *29* (4), 251-262.
98. Zingg, A.; Winnefeld, F.; Holzer, L.; Pakusch, J.; Becker, S.; Gauckler, L., Adsorption of polyelectrolytes and its influence on the rheology, zeta potential, and microstructure of various cement and hydrate phases. *Journal of Colloid and Interface Science* **2008**, *323* (2), 301-312.
99. Ran, Q.; Somasundaran, P.; Miao, C.; Liu, J.; Wu, S.; Shen, J., Adsorption Mechanism of Comb Polymer Dispersants at the Cement/Water Interface. *Journal of Dispersion Science and Technology* **2010**, *31* (6), 790-798.

100. Nawa, T., Effect of Chemical Structure on Steric Stabilization of Polycarboxylate-based Superplasticizer. *Journal of Advanced Concrete Technology* **2006**, *4* (2), 225-232.
101. Yoshioka, K.; Sakai, E.; Daimon, M.; Kitahara, A., Role of Steric Hindrance in the Performance of Superplasticizers for Concrete. *Journal of the American Ceramic Society* **1997**, *80* (10), 2667-2671.
102. Uchikawa, H.; Hanehara, S.; Sawaki, D., The role of steric repulsive force in the dispersion of cement particles in fresh paste prepared with organic admixture. *Cement and Concrete Research* **1997**, *27* (1), 37-50.
103. Flatt, R. J.; Schober, I.; Raphael, E.; Plassard, C.; Lesniewska, E., Conformation of Adsorbed Comb Copolymer Dispersants. *Langmuir* **2009**, *25* (2), 845-855.
104. Giraudeau, C.; D'Espinose De Lacaillerie, J.-B.; Souguir, Z.; Nonat, A.; Flatt, R. J., Surface and Intercalation Chemistry of Polycarboxylate Copolymers in Cementitious Systems. *Journal of the American Ceramic Society* **2009**, *92* (11), 2471-2488.
105. Shu, X.; Ran, Q.; Liu, J.; Zhao, H.; Zhang, Q.; Wang, X.; Yang, Y.; Liu, J., Tailoring the solution conformation of polycarboxylate superplasticizer toward the improvement of dispersing performance in cement paste. *Construction and Building Materials* **2016**, *116*, 289-298.
106. Plank, J.; Sakai, E.; Miao, C. W.; Yu, C.; Hong, J. X., Chemical admixtures — Chemistry, applications and their impact on concrete microstructure and durability. *Cement and Concrete Research* **2015**, *78*, 81-99.
107. Edmeades, R. M.; Hewlett, P. C., 15 - Cement Admixtures. In *Lea's Chemistry of Cement and Concrete (Fourth Edition)*, Hewlett, P. C., Ed., Butterworth-Heinemann: Oxford, UK, **1998**; pp 841-905.
108. Ataie, F. F.; Juenger, M. C. G.; Taylor-Lange, S. C.; Riding, K. A., Comparison of the retarding mechanisms of zinc oxide and sucrose on cement hydration and interactions with supplementary cementitious materials. *Cement and Concrete Research* **2015,** *72*, 128-136.
109. Tiemeyer, C.; Plank, J., Working mechanism of a high temperature (200°C) synthetic cement retarder and its interaction with an AMPS®-based fluid loss polymer in oil well cement. *Journal of Applied Polymer Science* **2012,** *124* (6), 4772-4781.

110. Tan, H.; Zou, F.; Liu, M.; Ma, B.; Guo, Y.; Jian, S., Effect of the Adsorbing Behavior of Phosphate Retarders on Hydration of Cement Paste. *Journal of Materials in Civil Engineering* **2017**, *29* (9).
111. Coveney, P. V.; Humphries, W., Molecular modelling of the mechanism of action of phosphonate retarders on hydrating cements. *Journal of the Chemical Society, Faraday Transactions* **1996**, *92* (5), 831-841.
112. Double, D. D.; Hewlett, P. C.; Sing, K. S. W.; Raffle, J. F., New Developments in Understanding the Chemistry of Cement Hydration [and Discussion]. *Philosophical Transactions of the Royal Society of London. Series A, Mathematical and Physical Sciences* **1983**, *310* (1511), 53-66.
113. Ramachandran, V. S. F., R.; Beaudoin, J., *Concrete Science: A Treatise on Current Research*. Heyden and Son. Ltd.: Philadelphia, USA, **1982**.
114. Young, J. F., A review of the mechanisms of set-retardation in portland cement pastes containing organic admixtures. *Cement and Concrete Research* **1972**, *2* (4), 415-433.
115. Thomas, N. L.; Birchall, J. D., The retarding action of sugars on cement hydration. *Cement and Concrete Research* **1983**, *13* (6), 830-842.
116. Bishop, M.; Barron, A. R., Cement Hydration Inhibition with Sucrose, Tartaric Acid, and Lignosulfonate: Analytical and Spectroscopic Study. *Industrial & Engineering Chemistry Research* **2006**, *45* (21), 7042-7049.
117. Zhang, L.; Zhuang, J.; Liu, H.; Li, H. M.; Zhao, Z., Terpolymerization and performance of 2-acrylamide-2-methyl propane sulfonic acid / itaconic acid / N-vinyl-2-pyrrolidone. *Journal of Applied Polymer Science* **2010**, *117* (5), 2951-2957.
118. Myrdal, R., Accelerating admixtures for concrete; *Sintef Report*, Sintef: Trondheim, Norway, **2007**.
119. Ramachandran, V. S., 5 - Accelerators. In *Concrete Admixtures Handbook (Second Edition)*, Ramachandran, V. S., Ed. William Andrew Publishing: Park Ridge, NJ, USA, **1996**; pp 185-285.
120. Xu, S.; Chen, Z.; Zhang, B.; Yu, J.; Zhang, F.; Evans, D. G., Facile preparation of pure CaAl-layered double hydroxides and their application as a hardening accelerator in concrete. *Chemical Engineering Journal* **2009,** *155* (3), 881-885.

121. Wilding, C. R.; Walter, A.; Double, D. D., A classification of inorganic and organic admixtures by conduction calorimetry. *Cement and Concrete Research* **1984,** *14* (2), 185-194.
122. Dodson, V., Set Accelerating Admixtures. In *Concrete Admixtures*, Dodson, V., Ed., Springer, Boston, MA, USA, **1990**; pp 73-102.
123. Tenoutasse, N. In *The Hydration Mechanism of C_3A and C_3S in the Presence of Calcium Chloride and Calcium Sulphate*, Proceedings 5th International Symposium on the Chemistry of Cement, Tokyo, Japan, Cement Association of Japan: Tokyo, Japan, **1969**; pp 372-378.
124. Ramachandran, V. S. In *Investigation of the role of chemical admixture in concrete, a differential thermal approach*, 7th International Conference on Thermal Analysis, New York, Bernard, M., Ed., John Wiley and Sons: New York, USA, **1982**; pp 1296 – 1302.
125. Justnes, H.; Nygaard, E. C., Technical calcium nitrate as set accelerator for cement at low temperatures. *Cement and Concrete Research* **1995,** *25* (8), 1766-1774.
126. Kondo, R.; Daimon, M.; Sakai, E.; Ushiyama, H., Influence of inorganic salts on the hydration of tricalcium silicate. *Journal of Applied Chemistry and Biotechnology* **1977,** *27* (1), 191-197.
127. Thomas, J. J.; Jennings, H. M.; Chen, J. J., Influence of Nucleation Seeding on the Hydration Mechanisms of Tricalcium Silicate and Cement. *The Journal of Physical Chemistry C* **2009,** *113* (11), 4327-4334.
128. Liu, C.; Shen, W., Effect of crystal seeding on the hydration of calcium phosphate cement. *Journal of Materials Science: Materials in Medicine* **1997,** *8* (12), 803-807.
129. Kanchanason, V.; Plank, J., Role of pH on the structure, composition and morphology of C-S-H–PCE nanocomposites and their effect on early strength development of Portland cement. *Cement and Concrete Research* **2017,** *102*, 90-98.
130. Kanchanason, V.; Plank, J., Effectiveness of a calcium silicate hydrate – Polycarboxylate ether (C-S-H–PCE) nanocomposite on early strength development of fly ash cement. *Construction and Building Materials* **2018,** *169*, 20-27.
131. Hubler, M. H.; Thomas, J. J.; Jennings, H. M., Influence of nucleation seeding on the hydration kinetics and compressive strength of alkali activated slag paste. *Cement and Concrete Research* **2011,** *41* (8), 842-846.

132. Kanchanason, V. A Comprehensive Study on Calcium Silicate Hydrate – Polycarboxylate Superplasticizer (C-S-H – PCE) Nanocomposites as Accelerating Admixtures in Cement. *Dissertation*, Technische Universität München, München, **2018**.
133. Nicoleau, L. Gädt, T.; Grassl, H. Hardening accelerator composition, WO2014026938A1 **2012**.
134. Nicoleau, L.; Jetzlsperger, E.; Fridrich, D.; Vierle, M.; Lorenz, K.; Albrecht, G.; Schmitt, D.; Wohlhaupter, T.; Dorfner, R.; Leitner, H.; Bräu, M.; Hesse, C.; Montero Pancera, S.; Zürn, S.; Kutschera, M., Plasticizer-containing hardening accelerator composition, WO2010026155, **2009**.
135. Benz, K.-W.; Neumann, W., *Introduction to Crystal Growth and Characterization*. Wiley-VCH Verlag GmbH & Co. KGaA: Weinheim, Germany, **2014**.
136. Cubillas, P. A., M., Synthesis Mechanism: Crystal Growth and Nucleation. In *Zeolites and Catalysis: Synthesis, Reactions and Applications*, Čejka, J.; Corma, A.; Zones S., Eds., Wiley-VCH Verlag GmbH & Co. KGaA: Weinheim, Germany, **2010**; pp 1-55.
137. Kashchiev, D.; van Rosmalen, G. M., Review: Nucleation in solutions revisited. *Crystal Research and Technology* **2003**, *38* (7-8), 555-574.
138. Thomas, J. J., A New Approach to Modeling the Nucleation and Growth Kinetics of Tricalcium Silicate Hydration. *Journal of the American Ceramic Society* **2007**, *90* (10), 3282-3288.
139. Scherer, G. W.; Zhang, J.; Thomas, J. J., Nucleation and growth models for hydration of cement. *Cement and Concrete Research* **2012,** *42* (7), 982-993.
140. Volmer, M., Über gerichtetes Kristallwachstum. *Zeitschrift für Physik* **1922**, *9*, 193-196.
141. Kossel, W., Zur Energetik von Oberflächenvorgängen. *Annalen der Physik* **1934**, *413* (5), 457-480.
142. Stranski I. N., Zur Theorie des Kristallwachstums. *Zeitschrift für Physikalische Chemie* **1928**, *136U* (1), 259.
143. Giuffre, A. J.; Hamm, L. M.; Han, N.; De Yoreo, J. J.; Dove, P. M., Polysaccharide chemistry regulates kinetics of calcite nucleation through competition of interfacial energies. *Proceedings of the National Academy of Sciences* **2013**, *110* (23), 9261-9266.
144. Petsev, D. N.; Chen, K.; Gliko, O.; Vekilov, P. G., Diffusion-limited kinetics of the solution–solid phase transition of molecular substances. *Proceedings of the National Academy of Sciences* **2003**, *100* (3), 792-796.

145. Lowenstam, H. A.; Weiner, S., *On Biomineralization.* Oxford Univ. Press (New York and London): New York, USA, **1989**; Vol. 54, p 344-345.
146. Grotzinger, J. P.; James, N. P., Carbonate sedimentation and diagenesis in the evolving precambrian world. *SEPM Special Publication*, SEPM Society for Sedimentary Geology: Tulsa, OK, **2000**; Vol. 67, p 3-20.
147. Habraken, W. J.; Tao, J.; Brylka, L. J.; Friedrich, H.; Bertinetti, L.; Schenk, A. S.; Verch, A.; Dmitrovic, V.; Bomans, P. H. H.; Frederik, P. M.; Laven, J.; van der Schoot, P.; Aichmayer, B.; de With, G.; DeYoreo, J. J.; Sommerdijk, N. A., Ion-association complexes unite classical and non-classical theories for the biomimetic nucleation of calcium phosphate. *Nature Communications* **2013**, *4*, 1507.
148. Hassan, S. A., Morphology of ion clusters in aqueous electrolytes. *Physical Review E* **2008**, *77* (3), 031501.
149. Hughes, C. E.; Hamad, S.; Harris, K. D. M.; Catlow, C. R. A.; Griffiths, P. C., A multi-technique approach for probing the evolution of structural properties during crystallization of organic materials from solution. *Faraday Discussions* **2007**, *136* (0), 71-89.
150. Gebauer, D.; Völkel, A.; Cölfen, H., Stable Prenucleation Calcium Carbonate Clusters. *Science* **2008**, *322* (5909), 1819-1822.
151. Meldrum, F. C.; Sear, R. P., Now You See Them. *Science* **2008**, *322* (5909), 1802-1803.
152. Han, T. Y.-J.; Aizenberg, J., Calcium Carbonate Storage in Amorphous Form and Its Template-Induced Crystallization. *Chemistry of Materials* **2008**, *20* (3), 1064-1068.
153. Pouget, E. M.; Bomans, P. H. H.; Goos, J. A.; Frederik, P. M.; de With, G.; Sommerdijk, N. A., The Initial Stages of Template-Controlled $CaCO_3$ Formation Revealed by Cryo-TEM. *Science* **2009,** *323* (5920), 1455-1458.
154. Gal, A.; Habraken, W.; Gur, D.; Fratzl, P.; Weiner, S.; Addadi, L., Calcite Crystal Growth by a Solid-State Transformation of Stabilized Amorphous Calcium Carbonate Nanospheres in a Hydrogel. *Angewandte Chemie International Edition* **2013,** *52* (18), 4867-4870.
155. Lundager Madsen, H. E.; Christensson, F.; Chernov, A. A.; Polyak, L. E.; Suvorova, E. I., Crystallization of calcium phosphate in microgravity. *Advances in Space Research* **1995,** *16* (8), 65-68.

156. Chernov, A. A., Crystallization in solutions: Effects of micogravity conditions. In *Materials and Fluids Under Low Gravity: Proceedings of the IXth European Symposium on Gravity-Dependent Phenomena in Physical Sciences Held at Berlin, Germany, 2–5 May 1995*, Ratke, L.; Walter, H.; Feuerbacher, B., Eds., Springer Berlin Heidelberg: Berlin, Heidelberg, Germany, **1996**; pp 137-154.
157. Lundager Madsen, H. E.; Christensson, F.; Polyak, L. E.; Suvorova, E. I.; Kliya, M. O.; Chernov, A. A., Calcium phosphate crystallization under terrestrial and microgravity conditions. *J Cryst Growth* **1995**, *152* (3), 191-202.
158. Frates, R. A.; Nelson, D.; Friedrich, C.; Rubowitz, M.; Collins, C., Formation of Inorganic Precipitates in Microgravity on the STS40. *Proceedings of the Oklahoma Academy of Science* **1996**, *76*, 75-81.
159. Meier, M. R. Zementhydratation und Kristallisation von Ettringit unter Mikrogravitation in Gegenwart und Abwesenheit von Polycarboxylat-Fließmitteln. *Dissertation*, Lehrstuhl für Bauchemie, Technische Universität München, München, Germany, **2016**.
160. Wesselsky, A.; Jensen, O. M., Synthesis of pure Portland cement phases. *Cement and Concrete Research* **2009**, *39* (11), 973-980.
161. Lange, A.; Hirata, T.; Plank, J., Influence of the HLB value of polycarboxylate superplasticizers on the flow behavior of mortar and concrete. *Cement and Concrete Research* **2014**, *60*, 45-50.
162. Tiemeyer, C.; Lange, A.; Plank, J., Determination of the adsorbed layer thickness of functional anionic polymers utilizing chemically modified polystyrene nanoparticles. *Colloids and Surfaces A: Physicochemical and Engineering Aspects* **2014**, *456*, 139-145.
163. Habbaba, A.; Plank, J., Surface Chemistry of Ground Granulated Blast Furnace Slag in Cement Pore Solution and Its Impact on the Effectiveness of Polycarboxylate Superplasticizers. *Journal of the American Ceramic Society* **2012**, *95* (2), 768-775.
164. Mitchell, L. D.; Margeson, J. C., The effects of solvents on C–S–H as determined by thermal analysis. *Journal of Thermal Analysis and Calorimetry* **2006**, *86* (3), 591-594.
165. Collier, N. C.; Sharp, J. H.; Milestone, N. B.; Hill, J.; Godfrey, I. H., The influence of water removal techniques on the composition and microstructure of hardened cement pastes. *Cement and Concrete Research* **2008**, *38* (6), 737-744.

166. Mostafa Moujahid, E.; Besse, J.-P.; Leroux, F., Poly(styrene sulfonate) layered double hydroxide nanocomposites. Stability and subsequent structural transformation with changes in temperature. *Journal of Materials Chemistry* **2003**, *13* (2), 258-264.
167. Schönlein, M.; Plank, J., Influence of PCE kind and dosage on ettringite crystallization performed under terrestrial and microgravity conditions. *Journal of the American Ceramic Society* **2018**, *101* (8), 3575-3584.
168. Plank, J.; Chatziagorastou, P.; Hirsch, C., New model describing distribution of adsorbed superplasticizer on the surface of hydrating cement grain. *Jianzhu Cailiao Xuebao/Journal of Building Materials* **2007**, *10* (1), 7-13.
169. El-Alfi, S.; El-Awney, S.; Eldidamony, H., Hydration of C_4AF in the presence of artificial $CaSO_4$ and lime. *Indian Journal of Engineering and Materials Sciences* **2001**, *8*, 292-296.
170. Matschei, T.; Lothenbach, B.; Glasser, F. P., The AFm phase in Portland cement. *Cement and Concrete Research* **2007**, *37* (2), 118-130.
171. Richardson, I. G., The nature of C-S-H in hardened cements. *Cement and Concrete Research* **1999**, *29* (8), 1131-1147.
172. Richardson, I. G., Tobermorite/jennite- and tobermorite/calcium hydroxide-based models for the structure of C-S-H: Applicability to hardened pastes of tricalcium silicate, β-dicalcium silicate, Portland cement, and blends of Portland cement with blast-furnace slag, metakaolin, or silica fume. *Cement and Concrete Research* **2004**, *34* (9), 1733-1777.
173. *Zement-Taschenbuch*. Verein Deutscher Zementwerke: Düsseldorf, Germany, **2008**; Vol. 51.
174. Yu, P.; Kirkpatrick, R. J.; Poe, B.; McMillan, P. F.; Cong, X., Structure of Calcium Silicate Hydrate (C-S-H): Near-, Mid-, and Far-Infrared Spectroscopy. *Journal of the American Ceramic Society* **1999**, *82* (3), 742-748.
175. García-Lodeiro, I.; Fernández-Jiménez, A.; Sobrados, I.; Sanz, J.; Palomo, A., C–S–H Gels: Interpretation of ^{29}Si MAS-NMR Spectra. *Journal of the American Ceramic Society* **2012**, *95* (4), 1440-1446.
176. Tajuelo Rodriguez, E.; Richardson, I. G.; Black, L.; Boehm-Courjault, E.; Nonat, A.; Skibsted, J., Composition, silicate anion structure and morphology of calcium silicate

hydrates (C-S-H) synthesised by silica-lime reaction and by controlled hydration of tricalcium silicate (C_3S). *Advances in Applied Ceramics* **2015**, *114* (7), 362-371.

177. Grangeon, S.; Claret, F.; Roosz, C.; Sato, T.; Gaboreau, S.; Linard, Y., Structure of nanocrystalline calcium silicate hydrates: insights from X-ray diffraction, synchrotron X-ray absorption and nuclear magnetic resonance. *Journal of Applied Crystallography* **2016**, *49* (3), 771-783.
178. Faucon, P.; Delaye, J. M.; Virlet, J.; Jacquinot, J. F.; Adenot, F., Materials Research Society Symposium on Structure-Property Relationships in Hardened Cement Paste and Composites - Study of the structural properties of the C-S-H(I) by molecular dynamics simulation. *Cement and Concrete Research* **1997**, *27* (10), 1581-1590.
179. Faucon, P.; Charpentier, T.; Nonat, A.; Petit, J. C., Triple-Quantum Two-Dimensional ^{27}Al Magic Angle Nuclear Magnetic Resonance Study of the Aluminum Incorporation in Calcium Silicate Hydrates. *Journal of the American Chemical Society* **1998**, *120* (46), 12075-12082.
180. Faucon, P.; Petit, J. C.; Charpentier, T.; Jacquinot, J. F.; Adenot, F., Silicon Substitution for Aluminum in Calcium Silicate Hydrates. *Journal of the American Ceramic Society* **1999**, *82* (5), 1307-1312.
181. Plank, J. In *C-S-H Formation via Non-Classical Nucleation from an Amorphous Precursor and it's Transformation into C-S-H Foils*, 20. ibausil, Weimar, Germany, Weimar, Germany, **2018**.
182. Krautwurst, N.; Nicoleau, L.; Dietzsch, M.; Lieberwirth, I.; Labbez, C.; Fernandez-Martinez, A.; Van Driessche, A. E. S.; Barton, B.; Leukel, S.; Tremel, W., Two-Step Nucleation Process of Calcium Silicate Hydrate, the Nanobrick of Cement. *Chemistry of Materials* **2018**, *30* (9), 2895-2904.

9. Appendix

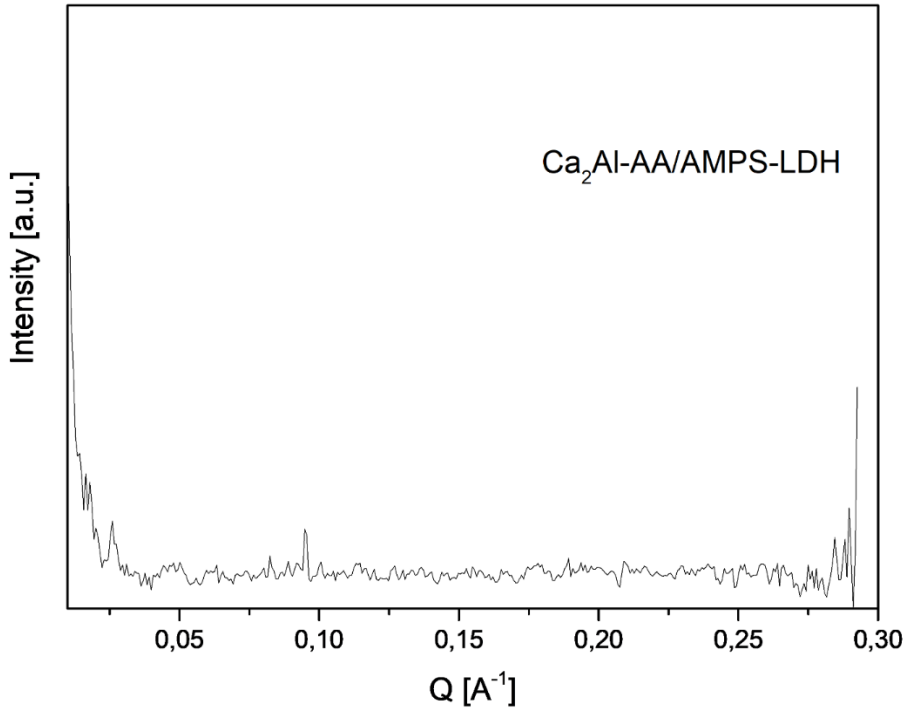

Figure A1: SAXS patterns of Ca_2Al-AA/AMPS-LDH obtained by rehydration of C_3A_C in the presence of the AA/AMPS co-polymer.

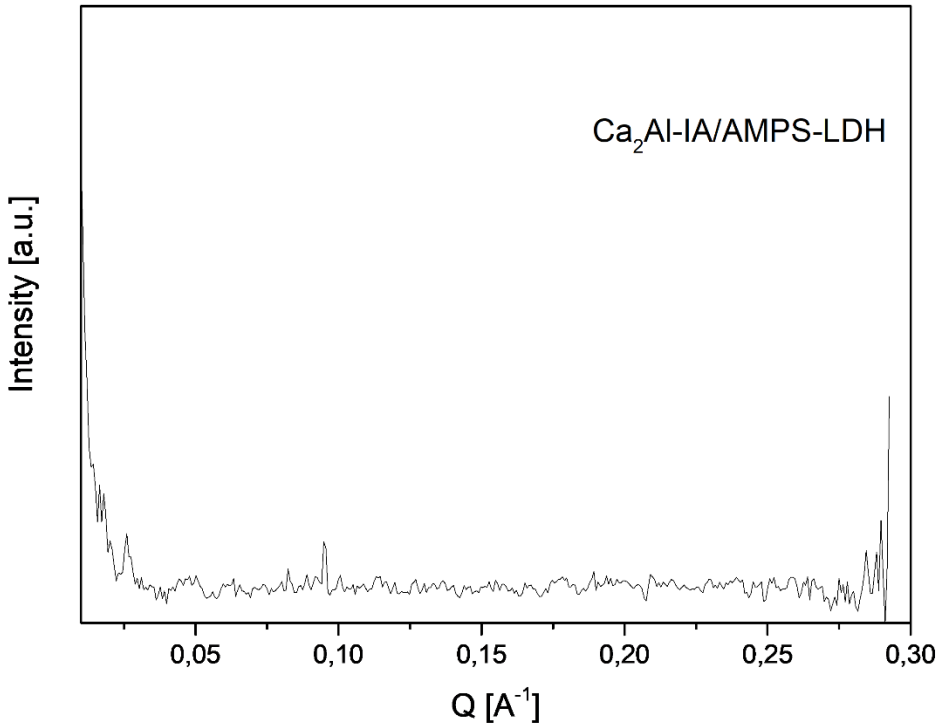

Figure A2: SAXS patterns of Ca_2Al-IA/AMPS-LDH obtained by rehydration of C_3A_C in the presence of the IA/AMPS co-polymer.

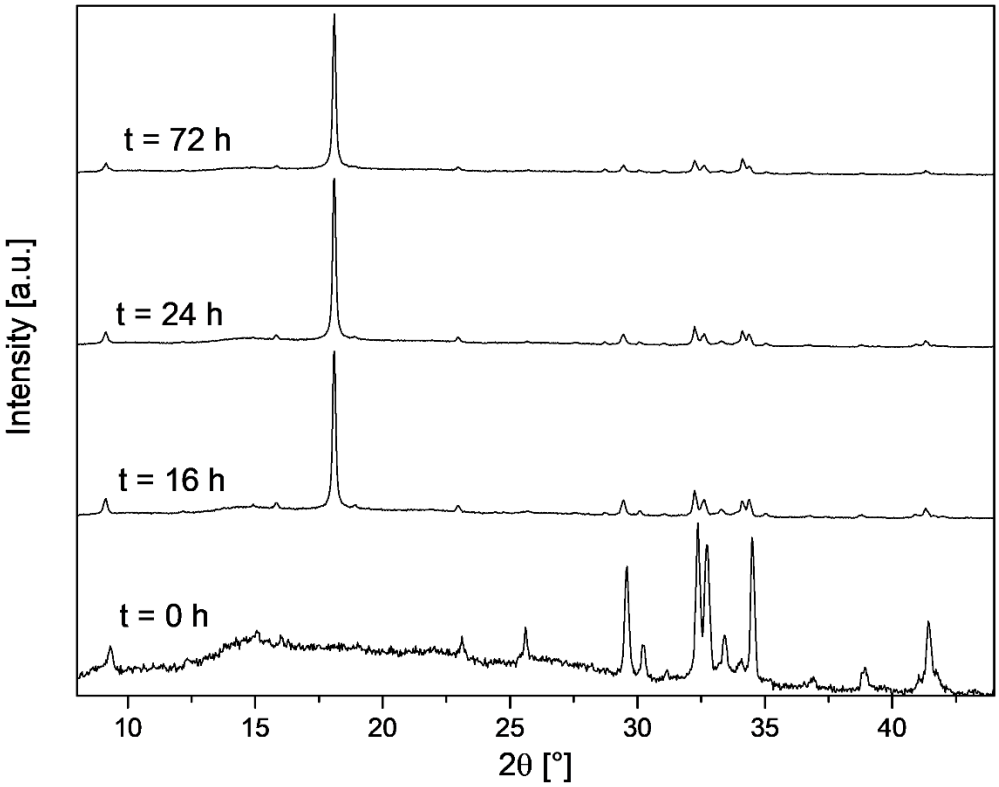

Figure A3: XRD patterns of CEM I 52.5 R at a w/c ratio = 0.5 after 0 minutes, 16, 24 and 72 hours.

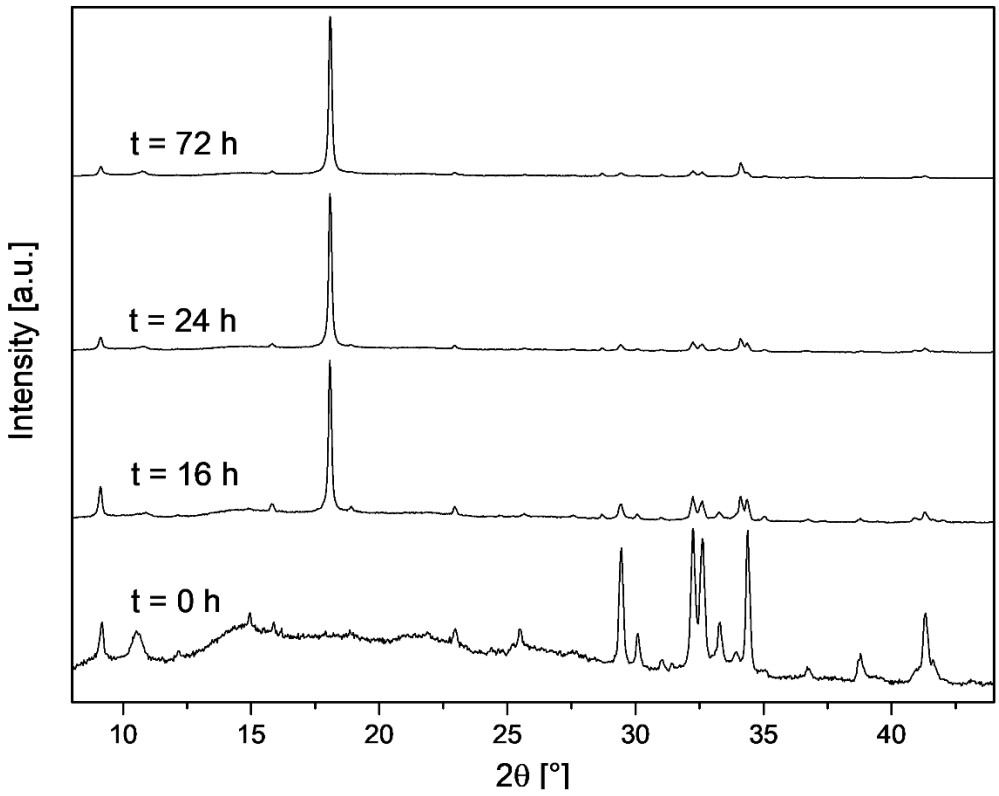

Figure A4: XRD patterns of CEM I 52.5 R with 2 % bwoc of Ca_2Al-formate-LDH at a w/c ratio = 0.5 after 0 minutes, 16, 24 and 72 hours.

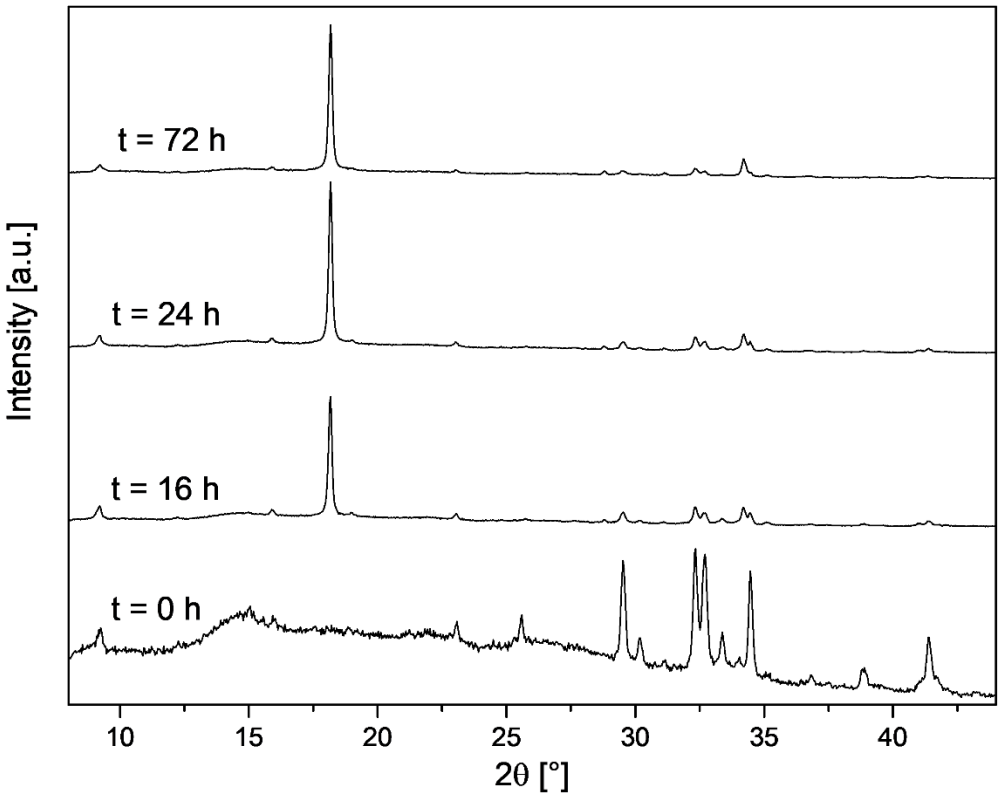

Figure A5: XRD patterns of CEM I 52.5 R with 2 % bwoc of Hydroxide-LDH at a w/c ratio = 0.5 after 0 minutes, 16, 24 and 72 hours.

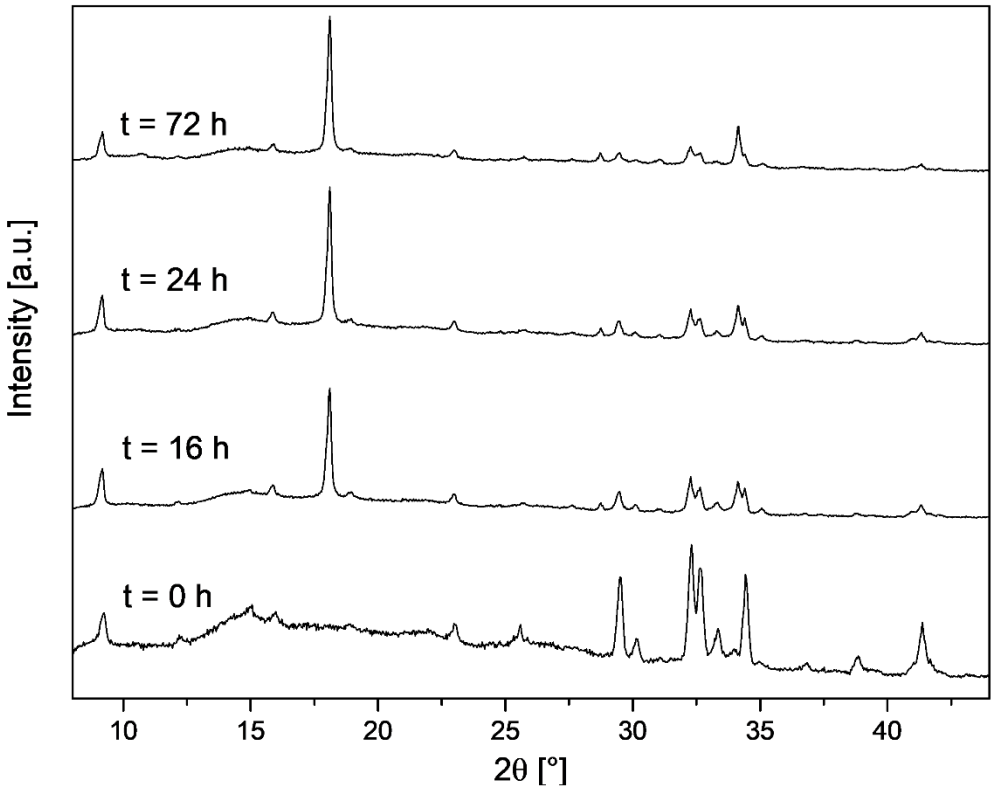

Figure A6: XRD patterns of CEM I 52.5 R with 0.7 % bwoc of $Ca(HCOO)_2$ (equal to the amount in 2 % bwoc of Ca_2Al-formate-LDH) at a w/c ratio = 0.5 after 0 minutes, 16, 24 and 72 hours.

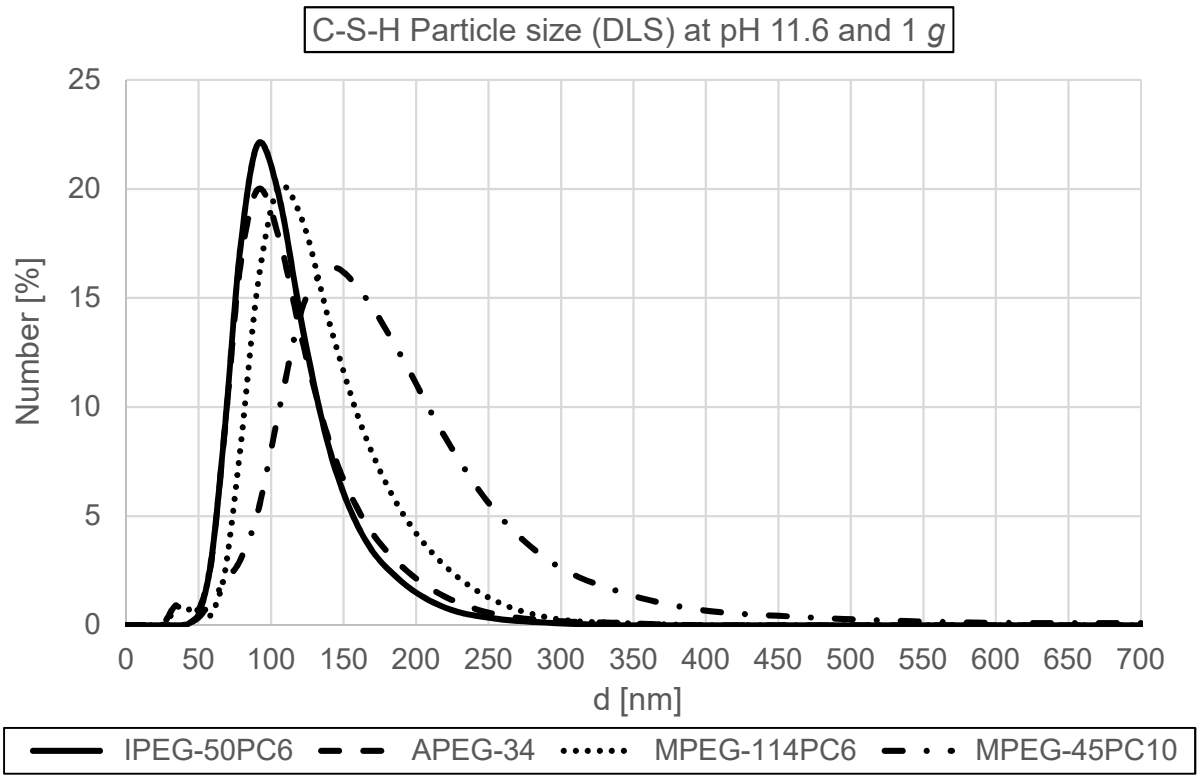

Figure A7: Particle size distributions of C-S-H precipitated at pH = 11.6 under terrestrial gravity in the presence of different PCE superplasticizers, determined by dynamic light scattering in isopropanol.

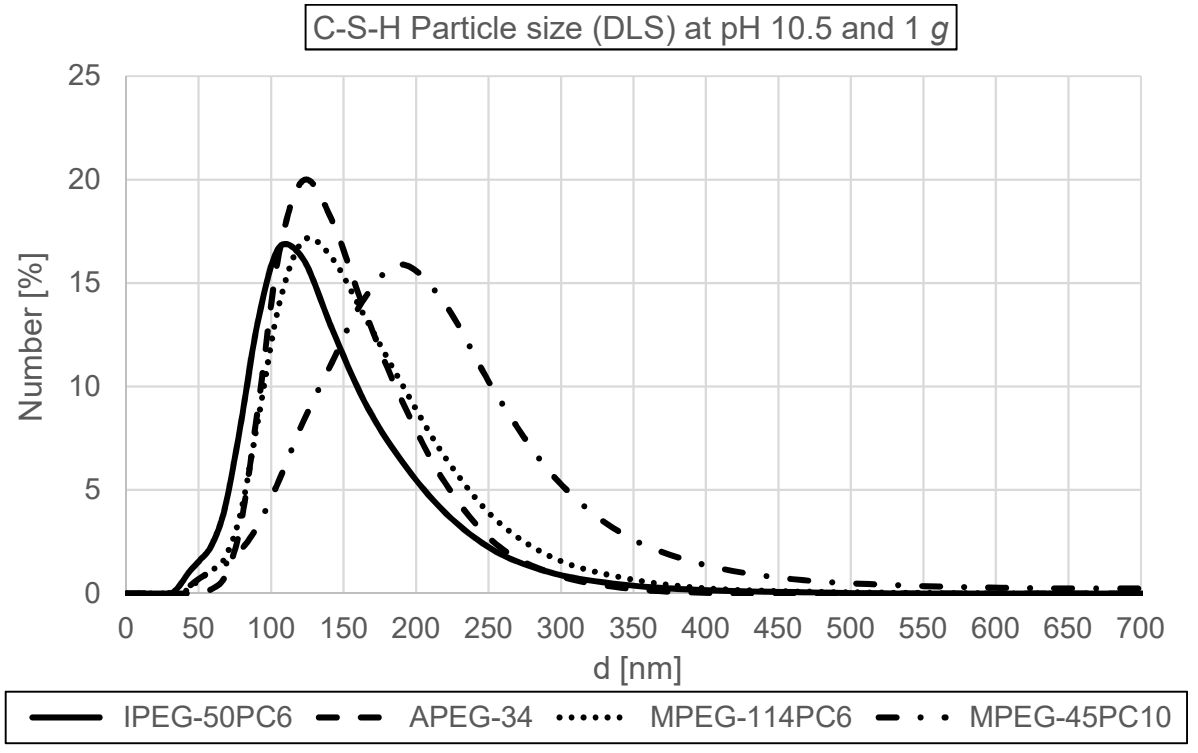

Figure A8: Particle size distributions of C-S-H precipitated at pH = 10.5 under terrestrial gravity in the presence of different PCE superplasticizers, determined by dynamic light scattering in isopropanol.

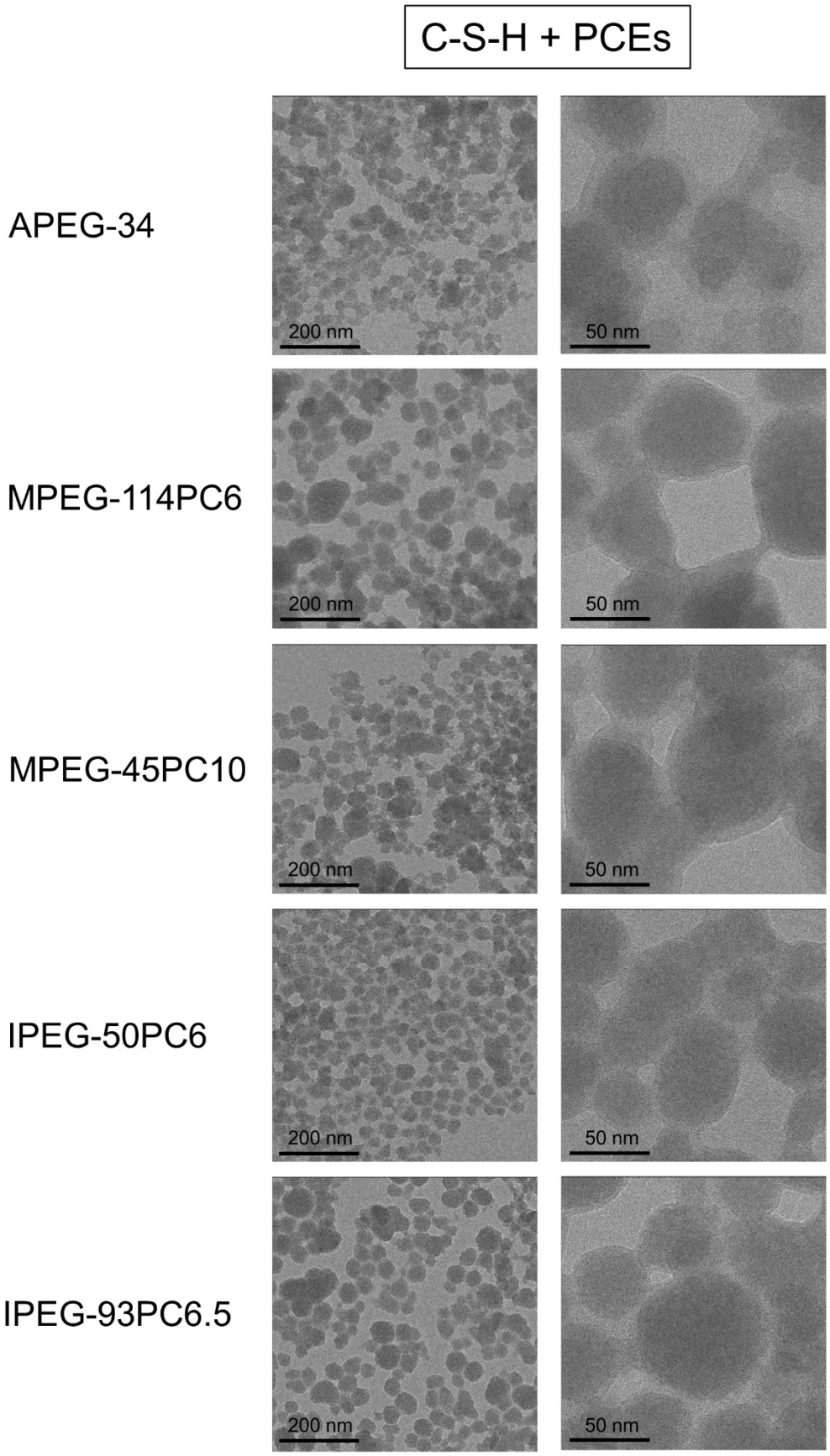

Figure A9: TEM micrographs of C-S-H composites with APEG-34, MPEG-114PC6, MPEG-45PC10, IPEG-50PC6 and IPEG-93PC6.5. Magnifications: 30k (left column) and 120k (right column).

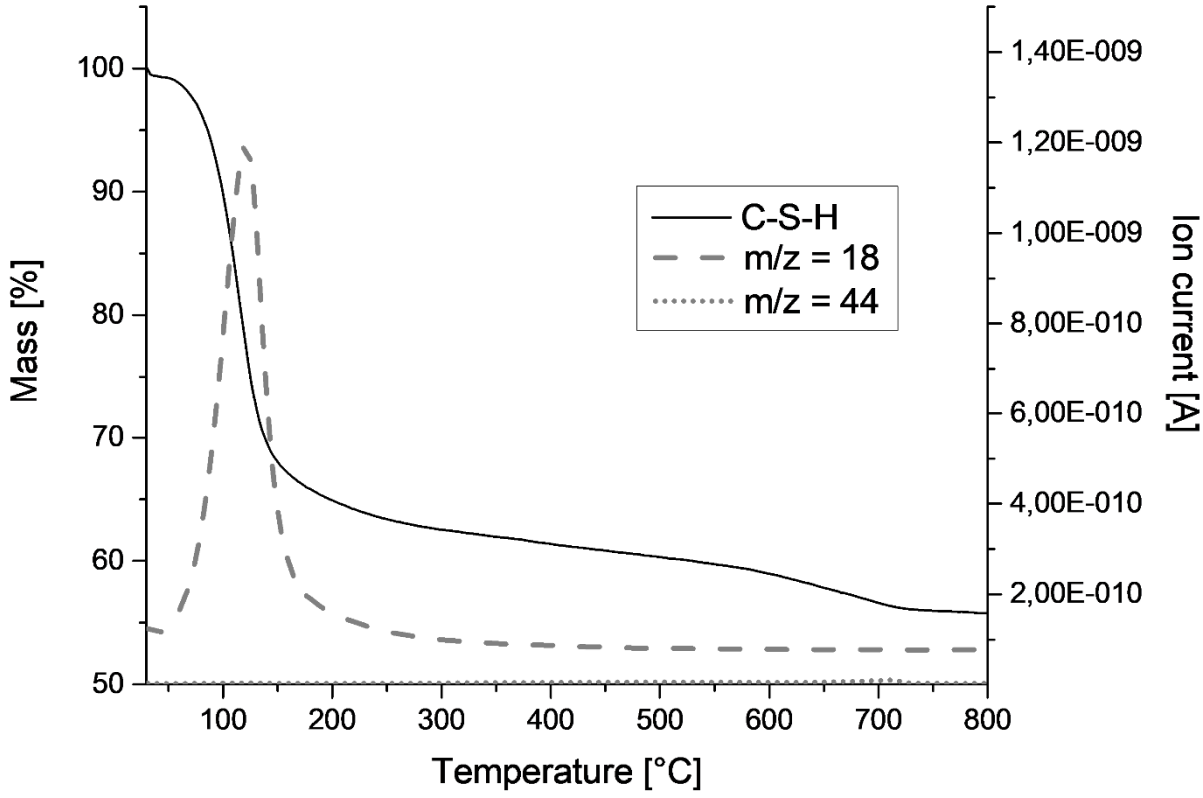

Figure A10: TG-MS spectrum of pure C-S-H.

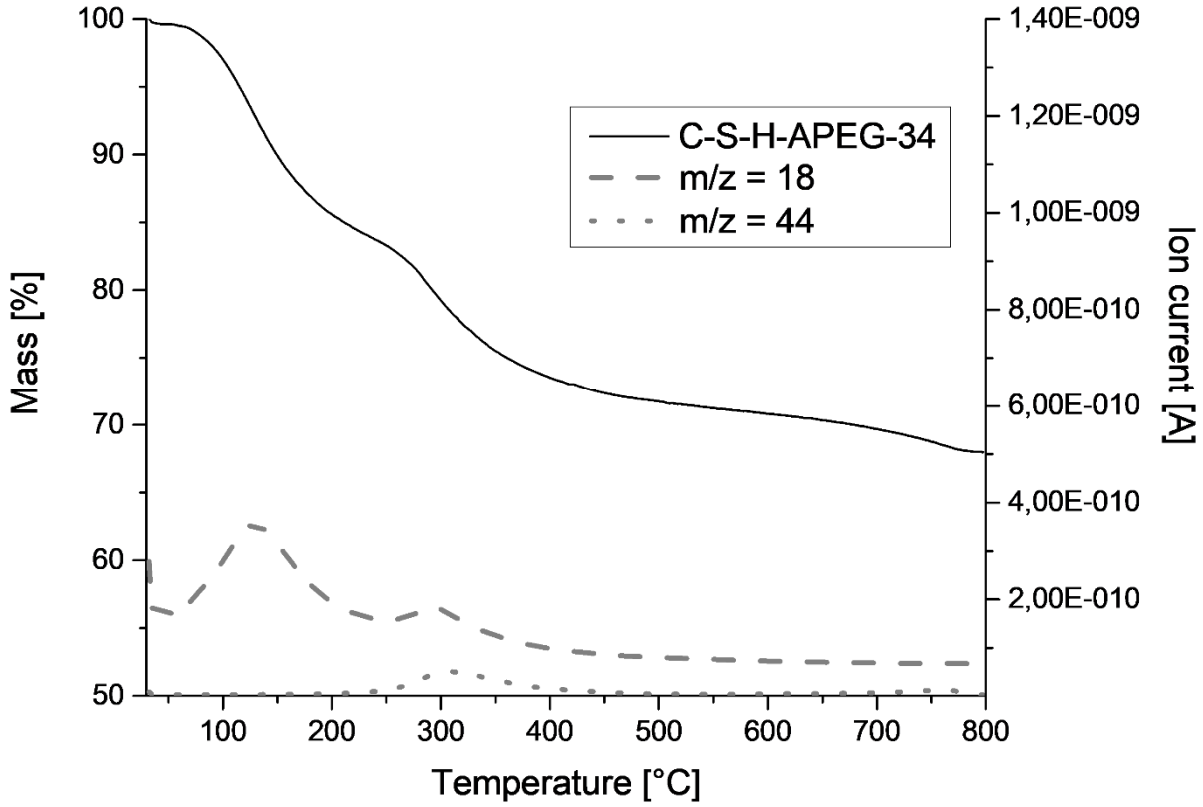

Figure A11: TG-MS spectrum of C-S-H-APEG-34 nanocomposite.

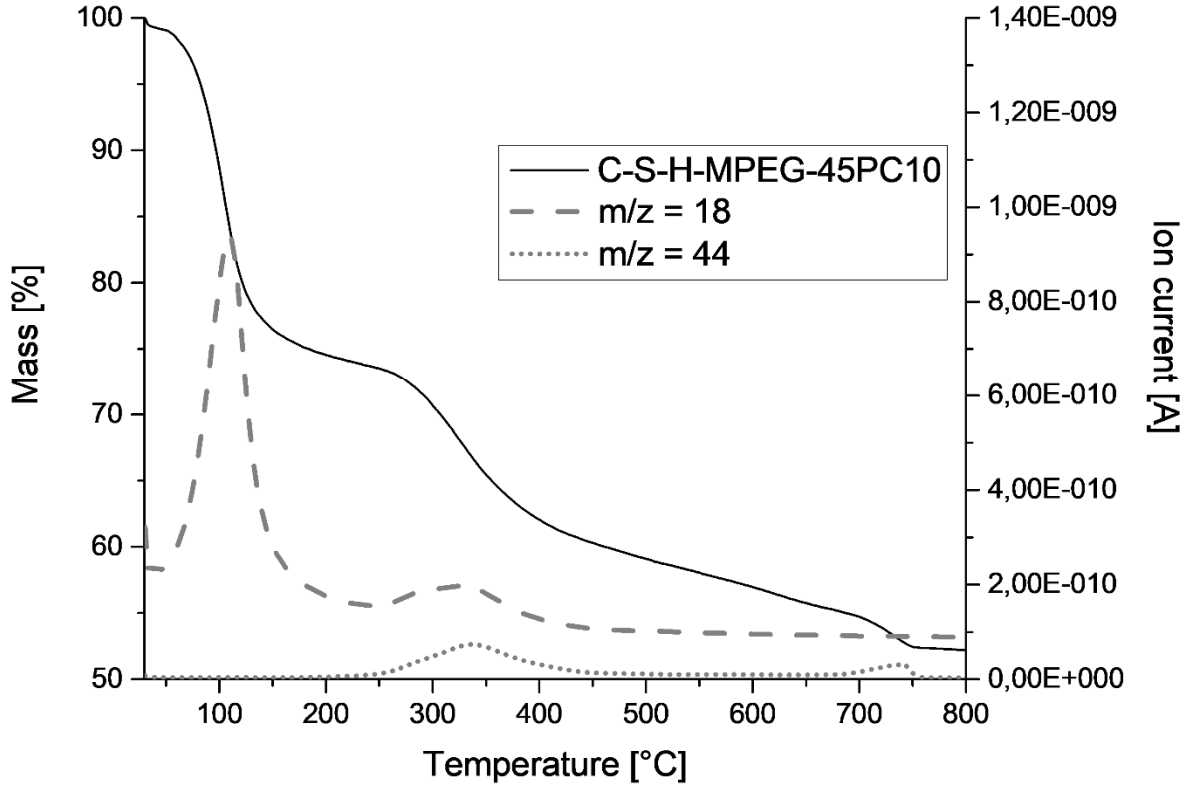

Figure A11: TG-MS spectrum of C-S-H-MPEG-45PC10 nanocomposite.

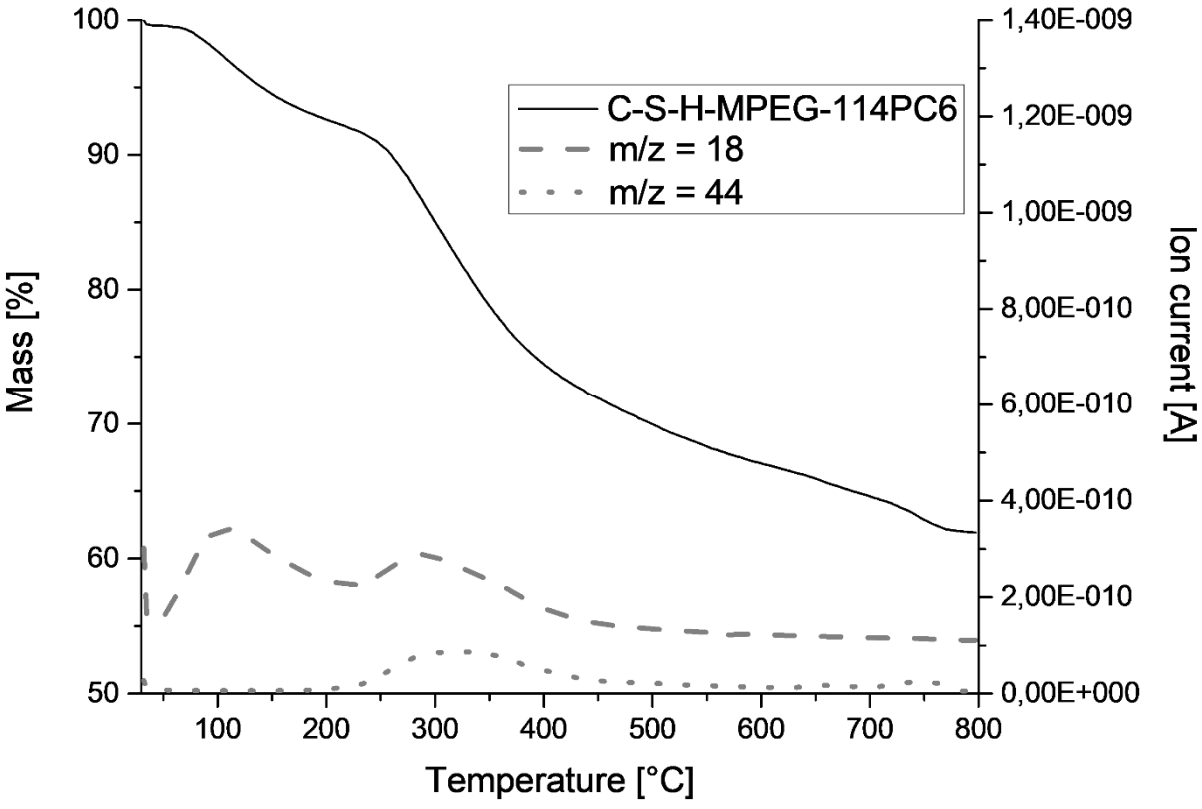

Figure A12: TG-MS spectrum of C-S-H-MPEG-114PC6 nanocomposite.

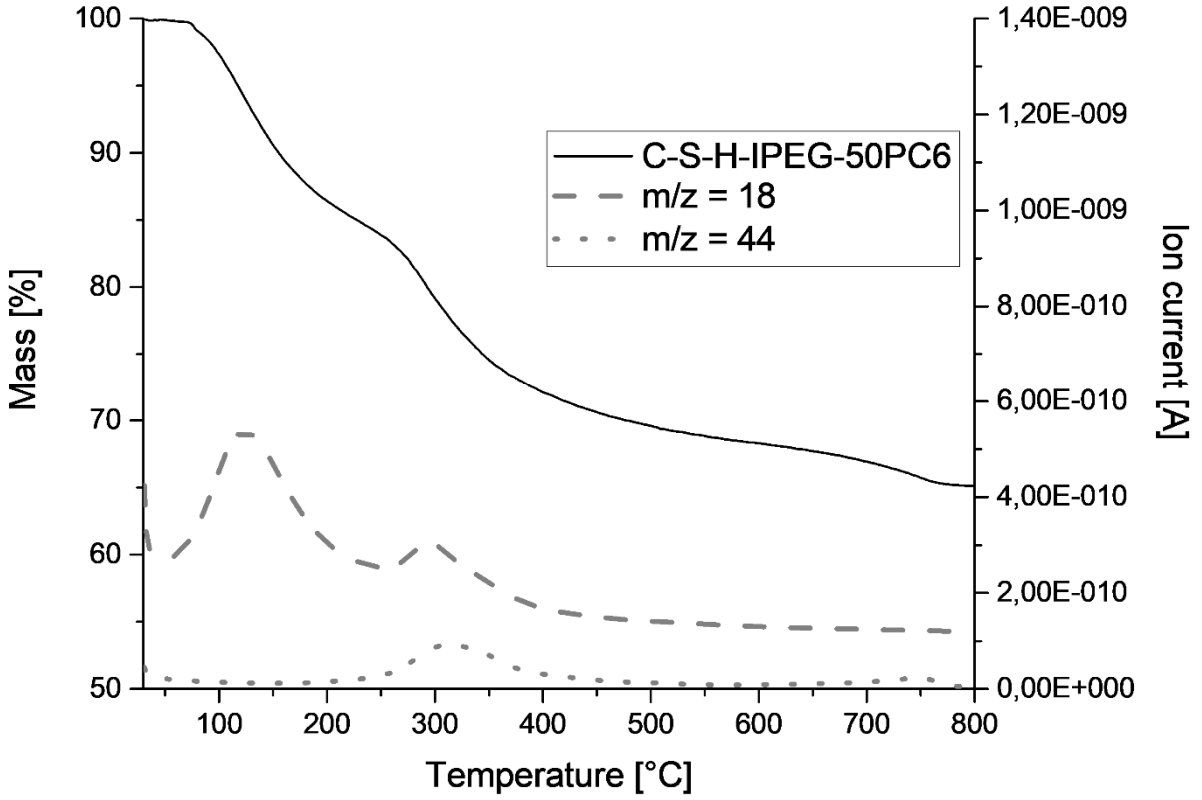

Figure A13: TG-MS spectrum of C-S-H-IPEG-50PC6 nanocomposite.

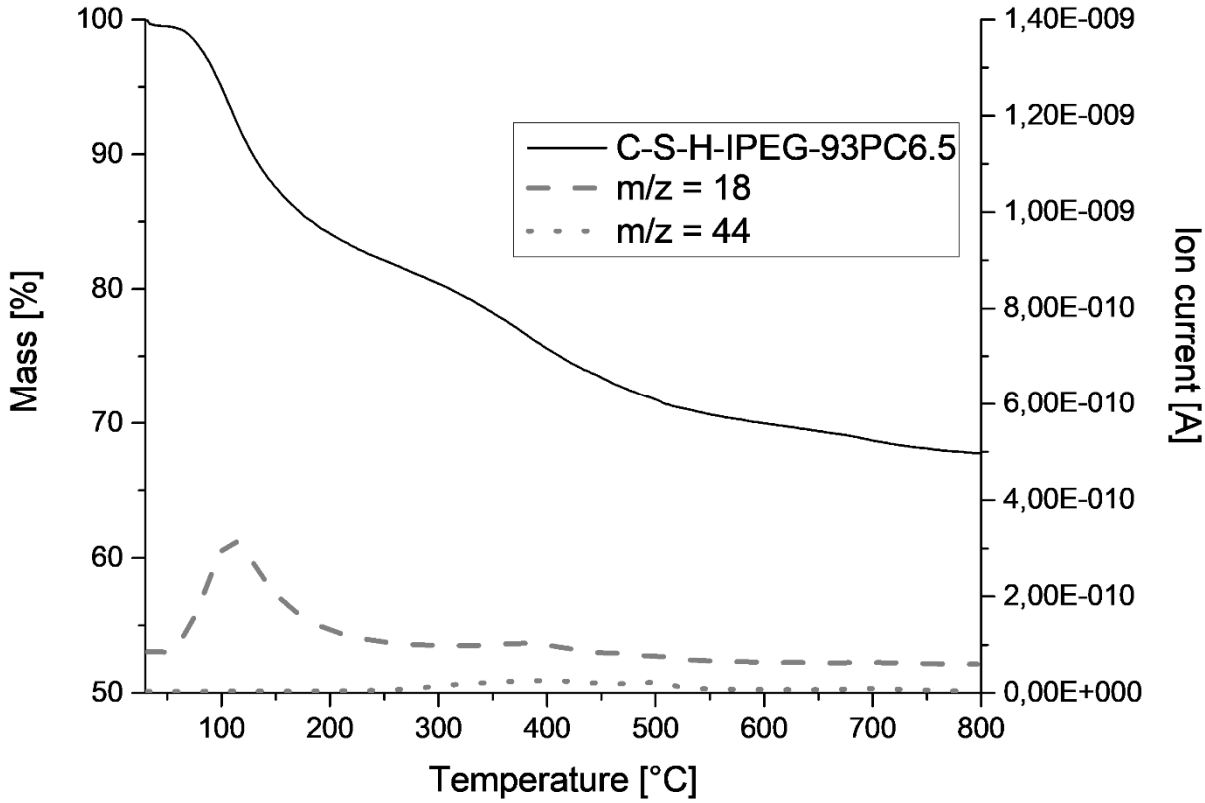

Figure A14: TG-MS spectrum of C-S-H-IPEG-93PC6.5 nanocomposite.

^{29}Si MAS NMR data

Table A1: Peak positions and relative populated areas in % for synthesized C-S-H.

CSH Sample		**Q^0**	**Q^1**	**Q^{2l}**	**Q^2**	**Q^{2v}**	**Q^3**
Pure CSH	ppm	-	-79.30	-82.85	-85.43	-	-
	area [%]	-	**16,1**	**27,6**	**56,3**	**0,0**	**0,0**
CSH-MPEG-114PC6	ppm	-	-79.34	-83.13	-85.47	-87.30	-
	area [%]	-	**9,7**	**26,8**	**52,5**	**10,9**	**0,0**
CSH-MPEG-45PC10	ppm	-	-79.33	-83.00	-85.43	-	-
	area [%]	-	**16,7**	**26,4**	**56,9**	-	**0,0**
CSH-IPEG-50PC6	ppm	-76.14	-79.29	-83.01	-85.39	-87.91	-90.28
	area [%]	**3,2**	**26,6**	**21,0**	**42,2**	**7,0**	**3,2**
CSH-IPEG-93PC6.5	ppm	-	-79.18	-83.76	-85.01	-87.26	-92.28
	area [%]	-	**31,2**	**16,2**	**33,6**	**12,8**	**6,2**